Validation of pressure measuring setup for microscopic tube flow: glaucoma drainage implant application

By Tabitha Hui Ting Teo

Submitted to the graduate degree program in Mechanical Engineering and the Graduate Faculty of the University of Kansas in partial fulfillment of the requirements for the degree of Master of Science.

_____

Co - Chairperson: Dr. Ronald L. Dougherty

_____

Co - Chairperson: Dr. Sara E. Wilson

_____

Committee Member: Dr. Huazhen Fang

_____

Committee Member: Dr. Paul M. Munden

Date Defended: December 1, 2017

The Thesis Committee for Tabitha Hui Ting Teo

certifies that this is the approved version of the following thesis:

VALIDATION OF PRESSURE MEASURING SETUP FOR MICROSCOPIC TUBE FLOW: GLAUCOMA DRAINAGE IMPLANT APPLICATION

_____

Co - Chairperson: Dr. Ronald L. Dougherty

_____

Co - Chairperson: Dr. Sara E. Wilson

Date approved: _____

## ABSTRACT

Current glaucoma drainage implants (GDIs) are unable to provide consistent and long-term post-operative (post-op) intraocular pressure (IOP) control. Valved glaucoma drainage implants (VGDIs) and intra-operative (intra-op) non-valved glaucoma drainage implant (NVGDI) surgical interventions, which were developed in efforts to ensure immediate post-op IOP control, have not been able to provide consistent and long-term post-op IOP control.

A novel method was developed by Dr. Paul Munden, involving the insertion of a degradable cylindrical insert into the tube of the GDI. The idea is that this degradable insert would provide sufficient temporary aqueous humor (AH) flow resistance through the tube in the immediate post-op stage. The flow resistance created by the insert would reduce over time as the insert degrades while scar tissue grows around the tube and provides natural flow resistance. With the success of this modification, the NVGDI would be able to provide both consistent and long-term IOP control.

The primary hypothesis of this research is that an insert placed in a NVGDI tube, will provide flow resistance that is similar to that predicted by Hagen-Poiseuille (H-P) theory. Prior to testing the hypothesis, thorough validation experimental trials were performed by this author, demonstrating that two duplicate setups, which were developed for this research, corresponded well with each other. These validation trials also showed that the pumps and pressure transducers in the setups could accurately measure flow and pressure drop in a consistent manner. Additionally, an anti-microbial cleaning protocol was developed and implemented, ensuring long-term, accurate and consistent pressure measurements through microtubes.

With the verified setups, an experimental study was performed to test the primary hypothesis. This study compared the experimental pressure loss ($\Delta P$) through GDI-like tubes with theory. To the author's knowledge, there has not been any published research comparing experimental GDI results with relevant theoretical data, neither has there been published research measuring long-term (i.e., 5-30 days) *in vitro* $\Delta P$ through GDI tubes. The main objectives of the experimental study were to determine the effect of tube inner diameter (ID) on single tube flow resistance, the effect of annulus size on annular tube flow resistance, and the ability of the setups to measure and maintain consistent annular flow resistance over time.

Single open tube flow trials were performed using microtubes with inner diameters (IDs) of 50 μm and 75 μm in order to determine the effect of tube ID on single tube flow resistance. There was a 1% - 30% difference between the average theoretical and experimental $\Delta P$s for the 50 μm tube trials and a 57% difference for the 75 μm tube trial. Accounting for flow rate and/or length variations in comparison with their respective nominal values, the theory-to-experiment differences were as low as -0.4% and 37% for the 50 and 75 μm tubes, respectively.

Annular flow trials were performed using stainless steel hypodermic tubes of different IDs and nichrome wire inserts of different outer diameters (ODs) in order to determine the effect of annulus size on annular tube flow resistance. It was found experimentally and theoretically that an increase in effective diameter ($D_{eff}$), which is a function of the tube's inner diameter and the insert's outer diameter for annular flow, causes a decrease in $\Delta P$. The differences between theoretical and experimental $\Delta P$s for the annular flow samples were small when $D_{eff}$ was small enough to provide clinically relevant

experimental $\Delta P$ values (i.e., 5-20 mm Hg). The results of the experimental study also showed that the developed test system can accurately maintain constant flow rate and measure $\Delta P$ across GDI-like tubes for more than 20 days. This time period matches the immediate post-op period wherein IOP needs to be controlled until scar tissue has grown sufficiently over the GDI to maintain a reasonable IOP level.

Many glaucoma patients have previously undergone, or will undergo, cataract surgery and/or retinal reattachment surgery. These patients, who have had both VGDI surgery and cataract and/or retinal reattachment surgery, will have residual ocular viscosurgical devices (OVDs) and/or silicone oil left in the eye, which can flow through the implanted VGDI. Therefore, VGDI flow trials were performed using these setups to determine the $\Delta P$ effects on the VGDI when OVDs and silicone oil flow through the VGDI. From these trials, it was observed that the flow of OVDs and silicone oil in a VGDI caused a significant spike in $\Delta P$. It was also observed that emulsified silicone oil caused a much higher $\Delta P$ spike as compared to the $\Delta P$ spike caused by silicone oil flowing through the GDI valve, even though the pure silicone oil took longer to pass through the valve.

For future work, it is recommended that more thorough research be performed to develop the best mathematical model for predicting $\Delta P$ through the annulus of a GDI with a degradable insert. Annular flow trials with stiff tubes and inserts should be performed for periods longer than 30 days as a benchmark for comparison when Baerveldt Glaucoma Implant (BGI) tubes and degradable inserts are tested in the future. It is also recommended that the influence of barometric pressure on the flow rate and pressure within the tubes be further investigated. Future work should be done to examine the use, impact and designability of degradable inserts, and investigate the possibility of drug eluding inserts.

## ACKNOWLEDGEMENT

First, I would like to thank Dr. Ronald Dougherty (my co-advisor and co-committee chair) for all his guidance, involvement and support throughout this research. He has been a wonderful mentor and has always been supportive and helpful in my academic and career pursuits. I would also like to extend my gratitude to Dr. Sara Wilson (my co-advisor and co-committee chair) and Dr. Sara Kieweg (former co-advisor) for their guidance and involvement in this research. I am also very grateful to Dr. Paul Munden for giving me the opportunity to work on this project and for all his guidance in this research.

Additionally, I want to thank Dr. Paulette Spencer for her guidance and help in writing an R03 NIH proposal for this research, Dr. Charles Ye for training me on the operation of the Micro-XCT microscope, and Dr. Prajna Dhar for providing me access to the Leica microscope in her lab. I would also like to thank Ajay Ramani for paving the way and training me on the setup, Jian Qian who supplied me with degradable materials and sodium azide, Aishik Chakraborty and Saba Ghazvini for helping me with operating the Leica microscope.

I would like to thank the Department of Mechanical Engineering (ME) at the University of Kansas. I would, especially, like to thank the ME staff who have helped me throughout this research: Al Syvongsay, Jason Habiger, Kathryn Maisch, Ann Armstrong, Josie Nixon, and Stephanie Moore.

Last but not least, I would like to thank my family for always supporting me, all my friends for being there for me, and most importantly, God for loving me and leading me every step of the way.

*This thesis is dedicated to*

*My parents, who always love and support me;*

*My sister, Natalie, who brightens up my life;*

*My best friend, Nick, who never gives up on me.*

## TABLE OF CONTENTS

## LIST OF FIGURES

## LIST OF TABLES

## NOMENCLATURE

| Symbol | Description |
|---|---|
| $A_f$ | Flow area of cylindrical tube sample; used in the NIH R03 proposal in App. H ($\mu m^2$) |
| $D$ | Tube diameter (m or μm) |
| $D_{eff}$ | Effective annulus diameter (m or μm) |
| $D_i$ | Outer diameter of the insert, which is the inner diameter of the annulus (m or μm) |
| $D_o$ | Inner diameter of a single tube, or outer diameter of the annulus (m or μm) |
| $L$ | Length of tube or insert under consideration (m or mm) |
| $P_{avgbar}$ | Average barometric pressure over the length of the trial (mm Hg) |
| $P_{bar}$ | Barometric pressure (mm Hg) |
| $P_{invbar}$ | Mirrored (inverted) barometric pressure (mm Hg) |
| $\Delta P$ | Pressure differential across tube or annulus length (mm Hg) |
| $\Delta P_{c\_avg}$ | Cumulative average of the pressure differential across tube or annulus length over several trials (mm Hg) |
| $\Delta P_f$ | Final differential pressure across tube or annulus length (mm Hg) |
| $\Delta P_{f\text{-}i}$ | Final differential pressure across tube or annulus length minus the initial differential pressure across tube or annulus length (mm Hg) |
| $\Delta P_i$ | Initial differential pressure across tube or annulus length (mm Hg) |
| $\Delta P_{i\text{-}f}$ | Initial differential pressure across tube or annulus length minus the final differential pressure across tube or annulus length (mm Hg) |

| | |
|---|---|
| $\Delta P_p$ | Differential pressure across tube or annulus length as measured by the pumps (mm Hg) |
| $\Delta P_{p\text{-}t}$ | Differential pressure across tube or annulus length measured by the pumps minus that of the transducers (mm Hg) |
| $\Delta P_{p2}$ | Differential pressure across tube or annulus length as measured by Pump 2 (mm Hg) |
| $\Delta P_{p2\text{-}t1}$ | Differential pressure measured by Pump 2 minus that of Transducer 1 (mm Hg) |
| $\Delta P_{smp1\text{-}2}$ | Differential pressure across tube or annulus length for Sample 1 minus that of Sample 2 (mm Hg) |
| $\Delta P_{stp2\text{-}1}$ | Differential pressure across tube or annulus length for Setup 2 minus that of Setup 1 (mm Hg) |
| $\Delta P_t$ | Differential pressure across tube or annulus length as measured by the transducers (mm Hg) |
| $\Delta P_{t1}$ | Differential pressure across tube or annulus length as measured by Transducer 1 (mm Hg) |
| $\Delta P_{t3}$ | Differential pressure across tube or annulus length as measured by Transducer 3 (mm Hg) |
| $\Delta P_{t1\text{-}3}$ | Differential pressure measured by Transducer 1 minus that of Transducer 3 (mm Hg) |
| $Q$ | Fluid flow rate ($m^3$/s or µl/min) |
| $Q_i$ | Input fluid flow rate ($m^3$/s or µl/min) |
| $Q_{i\text{-}o}$ | Percentage error between the input and output fluid flow rates: $Q_{i\text{-}o} = [(Q_i - Q_o) / Q_o] \times 100$ |
| $Q_o$ | Output fluid flow rate ($m^3$/s or µl/min) |
| $Q_1$ | Fluid flow rate in Setup 1 ($m^3$/s or µl/min) |

| | |
|---|---|
| $Q_2$ | Fluid flow rate in Setup 2 ($m^3$/s or µl/min) |
| $Q_{2-1}$ | Average fluid flow rate measured in Setup 2 minus that of Setup 1 ($m^3$/s or µl/min) |
| Re | Reynolds number |
| $T$ | Temperature (°C) |
| $T_{atm}$ | Atmospheric temperature (°C) |
| $t$ | Time (second, minute, hour or day) |
| $t_{a-c}$ | Percentage error between the actual and calculated time of the experimental trial: $t_{a-c} = [(t_{act} - t_{calc}) / t_{calc}] \times 100$ |
| $t_{act}$ | Actual time of the experimental trial (hour or day) |
| $t_{calc}$ | Calculated time of the experimental trial (hour or day) |
| $t_{ovd}$ | Time for OVD to pass through AGV (minutes) |
| $t_{so}$ | Approximate time for silicone oil to pass through AGV (hour) |
| $t_{vo}$ | Time at which the AGV valve opened (hour) |
| $V$ | Volume (µl) |
| $V_f$ | Flow velocity in the tube or annulus; used in the NIH R03 proposal in App. H (m/s) |
| $V_o$ | Output voltage (Volt or mVolt) |
| $v$ | Fluid velocity in the tube or annulus (m/s) |

| **Greek** | **Description** |
|---|---|

| | |
|---|---|
| $\alpha$ | Significance level of the 2-sided equality test. Probability of rejecting the null hypothesis; used in the NIH R03 proposal in App. H (m/s) |
| $\beta$ | Probability of accepting the null hypothesis in a 2-sided equality test; used in the NIH R03 proposal in App. H (m/s) |
| $\mu$ | Fluid dynamic viscosity (Pa.s) |
| $\rho$ | Fluid density ($kg/m^3$) |
| $\tau$ | Total period of proposed trial (minutes); used in the NIH R03 proposal in App. H (m/s) |

## ABBREVIATIONS

| Abbreviation | Description |
|---|---|
| AGV | Ahmed glaucoma valve |
| ALT | Argon laser trabeculoplasty |
| AH | Aqueous humor |
| IBER | Institute for Bioengineering Research |
| BGI | Baerveldt glaucoma implant |
| BJO | British Journal of Ophthalmology |
| CFD | Computational fluid dynamics |
| DI | Deionized water |
| G | Gauge |
| GDI | Glaucoma drainage implant |
| H-P | Hagen-Poiseuille |
| ID | Inner diameter |
| Intra-op | Intra-operative |
| IOP | Intraocular pressure |
| LTP | Laser trabeculoplasty |
| MIGS | Micro or minimally invasive glaucoma surgery |

| | |
|---|---|
| $NaN_3$ | Sodium azide |
| NEI | National Eye Institute |
| NIAMS | The National Institute of Arthritis and Musculoskeletal and Skin Diseases |
| NIBIB | National Institute of Biomedical Imaging and Bioengineering |
| NIH | National Institutes of Health |
| NVGDI | Non-valved glaucoma drainage implant |
| OD | Outer diameter |
| OVD | Ocular viscosurgical device |
| PEEK | Polyether-ether-ketone |
| Post-op | Post-operative |
| Pre-op | Pre-operative |
| SLT | Selective laser trabeculoplasty |
| SDS | Safety data sheet |
| SS | Stainless steel |
| UPS | Uninterrupted power supply |
| VGDI | Valved glaucoma drainage implant |
| VSD | Methyl deactivated fused silica |

# Chapter 1: Thesis Introduction

Chapter 1 covers an introduction to glaucoma and current glaucoma treatments available. The chapter describes the shortcomings of current GDIs in providing effective and consistent IOP control for glaucoma patients, as well as the proposed type of modification for improving the effectiveness of GDIs.

## 1.1. Overview and Objectives

Glaucoma is one of the leading causes of blindness in the world [1,2]. It is a complex disease that results in damage to the optic nerve and is often characterized by high eye fluid pressure known as the intraocular pressure (IOP). To alleviate the effects of glaucoma, glaucoma treatments focus on reducing IOP levels. Glaucoma drainage implant (GDI) surgery is a common treatment for patients with chronic glaucoma. GDI surgery is more often used to manage severe or resistant glaucoma as an alternative to more conservative treatments such as medical (drug) treatments, laser trabeculoplasty or trabeculectomy [3].

Among the common GDIs used, the Baerveldt Glaucoma Implant (BGI) has shown success in reducing long-term IOP levels. However, the BGI is unable to provide initial flow resistance immediately after surgery. This can cause the IOP to fall to dangerous levels below the nominal IOP range (10 - 22 mm Hg), resulting in vision-threatening complications. Intra-operative (intra-op) modifications to the BGI have been developed in order to resolve this issue, but none have shown to have been able to provide consistent IOP control or eliminate hypotony-related complications that occur during the immediate post-operative (post-op) period of 4 - 6 weeks [4-8].

The overall purpose of this project is to investigate a new modification to the BGI, which would improve its effectiveness (effective in providing consistent IOP control) by providing

temporary immediate post-op flow resistance. This modification to the BGI involves placing a degradable cylindrical insert of appropriate length and diameter in the BGI tube. This insert would provide temporary flow resistance immediately after surgery. It is thought that the insert would provide the needed flow resistance during the first 4 - 6 weeks after surgery wherein the natural resistance provided by scar tissue is absent.

***The primary hypothesis of this research is that an insert, placed in a NVGDI-like tube, will provide flow resistance which can be modeled by the Hagen-Poiseuille (H-P) theory.*** An experimental study performed to test this hypothesis, comparing experimental pressure loss in NVGDI-like tubes with theory, is described in Chapter 3. This thesis also covers initial stages of the study, which involved troubleshooting and validating the two identical experimental setups which are designed for independent verification of data quality and repeatability. The initial study for verification and validation of the setups is described in Chapter 2.

Additional flow studies are also included in Chapter 4. Preliminary flow trials using actual BGI tubes were performed in order to investigate the pressure and flow effects of placing degradable or non-degradable inserts in BGI tubes. Another follow-up study, involving valved glaucoma drainage implants (VGDIs), was also performed to determine the effects of ocular viscosurgical devices (OVDs) and silicone oil on flow and pressure in VGDI tubes.

## 1.2. Glaucoma and Current Treatments

Glaucoma is a complex disease of the eye that results in damage of the optic nerve and the loss of vision. Glaucoma affects more than 70 million people worldwide and is one of the leading causes of irreversible blindness in the world [1,2]. Studies have shown that the projected number of glaucoma patients worldwide will reach 111.8 million by the year 2040 [9].

Damage to the optic nerve is often due to the elevation of the eye's fluid pressure, known as the intraocular pressure (IOP) [1]. In a healthy eye, the aqueous humor (AH) flows out of the eye through the trabecular meshwork as shown in Fig. 1.1 [10]. The IOP and AH flow rate of a healthy eye range from 10 to 22 mm Hg and 1.1 to 4.2 μl/min, respectively [11,12].

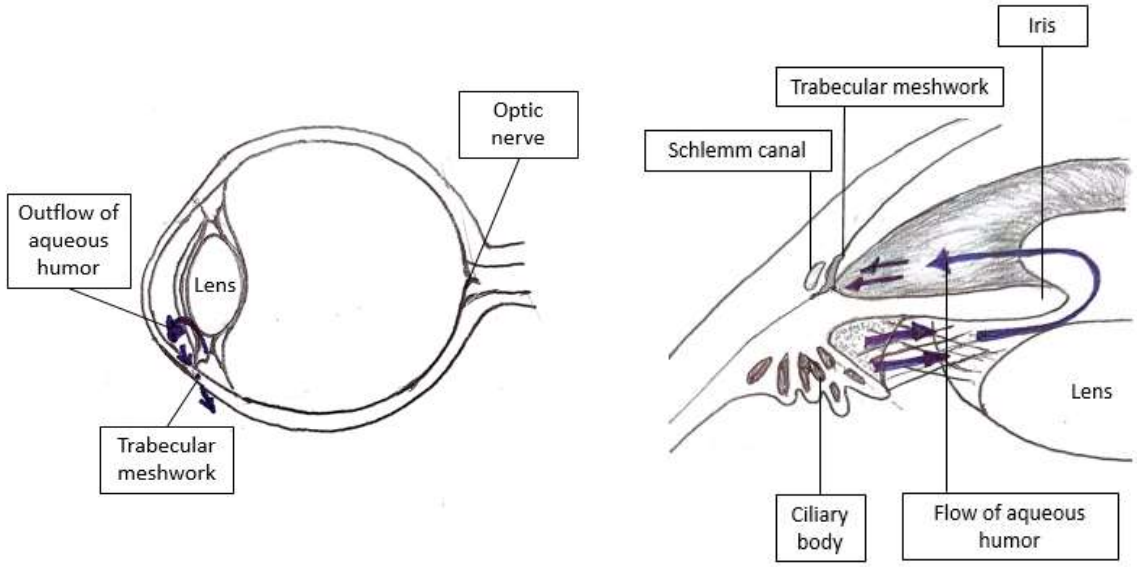


Fig. 1.1: Illustration of normal AH outflow [left] and magnified view of AH outflow through the trabecular meshwork [right]

The eye of a glaucoma patient is unable to maintain a normal outflow of AH caused by the narrowing or complete occlusion of the AH drainage canals, leading to a rise in IOP above the nominal range [13]. This excessive increase in IOP creates mechanical stress on the posterior section of the eye, damaging the optic nerve which is located there, as shown in Fig. 1.2.

The optic nerve connects the retina to the brain, and carries visual information from the eye to the brain. The retina is the light-sensitive lining located at the back of the eye that receives the light entering the eye [10]. Damage to the optic nerve disrupts the relay of information from the retina to the brain, and is termed vision loss.

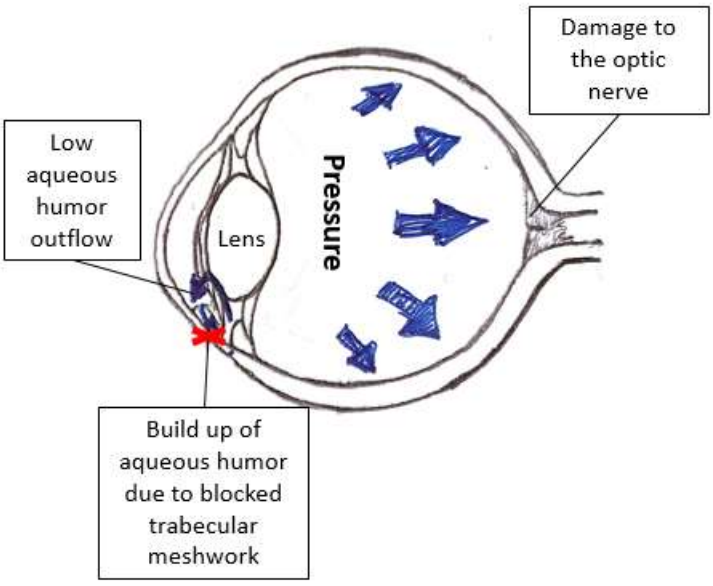


Fig. 1.2: Damage to the optic nerve due to elevated IOP levels caused by glaucoma

### 1.1.1. Overview of Glaucoma Treatment

Reduction in IOP has proven to be the only reliable method for treating glaucoma [1]. There are several types of glaucoma treatment, including medical treatment, conventional surgical treatment (trabeculectomy and glaucoma drainage implants), laser trabeculoplasty, and micro-invasive glaucoma surgery (MIGS).

***Drug Treatment***

Medical (oral or topical drug) treatment is currently the most common initial therapy prescribed by ophthalmologists to lower IOP [14]. Prostaglandin analogs are the most commonly prescribed eye drops for initial lowering of IOP. Prostaglandin analogs reduce IOP levels by increasing the trabecular AH outflow [14]. Other medical agents are beta-blockers, alpha-adrenergic agonists, parasympathomimetic agents, carbonic anhydrase inhibitors, and hyperosmotic agents that lower IOP by increasing trabecular outflow or decreasing AH production [14].

***Laser Trabeculoplasty (LTP)***

Laser trabeculoplasty (LTP) is a common initial therapy for patients who are unable to use or respond to medical treatment [14]. LTP is minimally invasive laser therapy that assists in regulating AH outflow by applying a laser beam to the trabecular meshwork. The laser reduces the AH flow resistance of the trabecular meshwork. There exist two types of LTP procedures: selective laser trabeculoplasty (SLT) and argon laser trabeculoplasty (ALT). ALT uses argon-ion lasers, and SLT uses frequency doubled neodymium: yttrium-aluminum-garnet lasers [14].

***Trabeculectomy***

The primary purpose of a trabeculectomy is to increase AH outflow by creating new openings for AH outflow. Trabeculectomy is a surgical procedure that involves cutting a small window in the sclera to allow fluid to exit the eye as shown in Fig. 1.3. This small window is then covered with a thin layer of the conjunctiva (transparent layer that covers the sclera) [15].

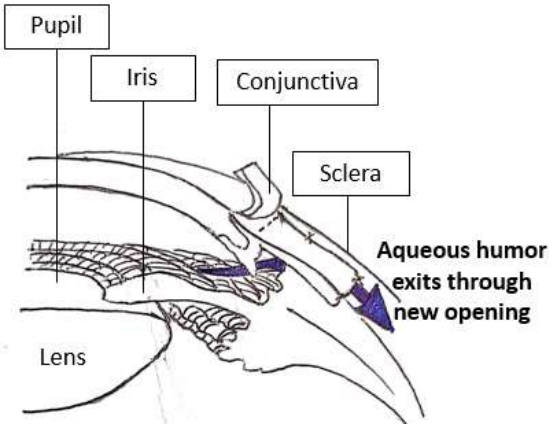


Fig. 1.3: New opening created for AH outflow by trabeculectomy

***Glaucoma Drainage Implants (GDIs)***

GDIs, also known as aqueous shunts, are devices that are implanted in the eyes of glaucoma patients in order to improve IOP control. These devices function to provide an alternate pathway

for the AH to flows out of the eye. GDIs fundamentally consist of a tube that drains aqueous fluid out of the eye. AH flows through the tube to a plate that is mounted on the eye. The plate provides the appropriate flow resistance after scar tissue has grown over the plate. Sizes of the plates range from approximately 135 $mm^2$ to 350 $mm^2$ [16], and the length of the GDI tube is approximately 12 mm [17]. The implant is sewn on the eye as shown in Fig. 1.4.

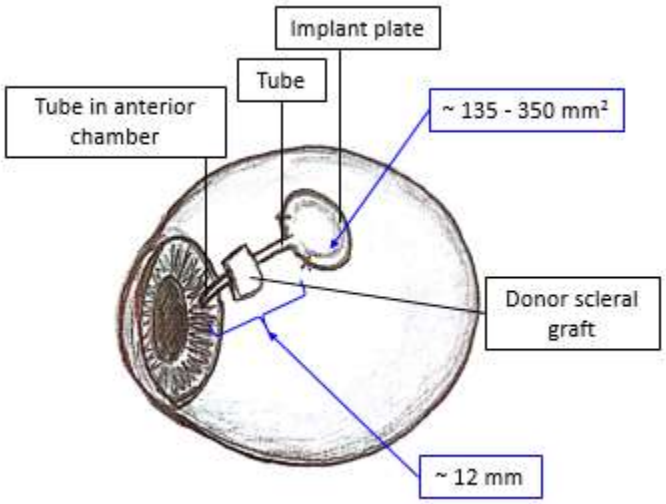


Fig. 1.4: Location of GDI on the eye

***Trabeculectomy versus Glaucoma Drainage Implants (GDIs)***

Trabeculectomy has been considered as the "gold standard" of glaucoma procedures and, in the past, was often prescribed after medical treatments had failed [15]. However, over the past 22 years, the popularity of trabeculectomies has declined [15]. Recently, there has been an increase in the number of GDI procedures and a decrease in trabeculectomy procedures [18]. From 1994 to 2012, the number of trabeculectomies performed has decreased by approximately 77%, but the number of GDI surgeries has increased by 410% [19].

Among the reasons for this decline in the number of trabeculectomy procedures and increase in number of GDI procedures is the greater long-term effectiveness of the GDI as

compared to that of the trabeculectomy. A landmark comparative study demonstrated that GDIs are better at maintaining IOP in glaucoma patients [18]. The study also reported fewer complications and higher success rates of reducing IOP with GDIs as compared to those of trabeculectomies. The failure rate among trabeculectomy patients was more than three times that of the tube shunt patient group [18].

Another study by Kaplan *et al.* [20] that compared the cost-effectiveness of BGIs versus medication and trabeculectomies demonstrated the superiority of GDIs over these other two common glaucoma treatments. GDIs have a higher cost-effectiveness despite costing up to $3904 more than medical treatment and $2203 more than a trabeculectomy [20]. Cost-effectiveness was calculated in units of cost per QALY (quality-adjusted life-year) which considered the cost of the treatment in comparison to the failure and complication rates of the treatment [20].

***Micro or Minimally Invasive Glaucoma Surgeries (MIGS)***

MIGS is a group of newer minimally penetrating glaucoma procedures that is less invasive as compared to conventional glaucoma drainage surgeries such as trabeculectomies and GDI surgery. MIGS include micro-shunt or stent procedures, minimally invasive trabecular ablation, and cyclodestructive procedures [14].

MIGS have been shown to be safer and cause fewer hypotony-related complications or infections due to their less-invasive nature. MIGS are currently a trending area of development in the field of glaucoma treatment [21, 22]. The main limitation of MIGS is that MIGS are less effective in lowering the IOP as compared to traditional drainage surgeries such as GDIs and trabeculectomies [23]. Therefore, MIGS are often done in combination with other conventional surgeries such as cataract surgery or trabeculectomies [23].

The two most established micro-shunts are the Ex-PRESS mini-glaucoma shunt by Alcon and the iStent trabecular microbypass stent by Glaukos. The ExPRESS is almost 3 mm long, is made of biocompatible stainless steel (SS), and has a 400 μm external diameter and a 50 μm lumen diameter (shown in Fig. 1.5) [24].

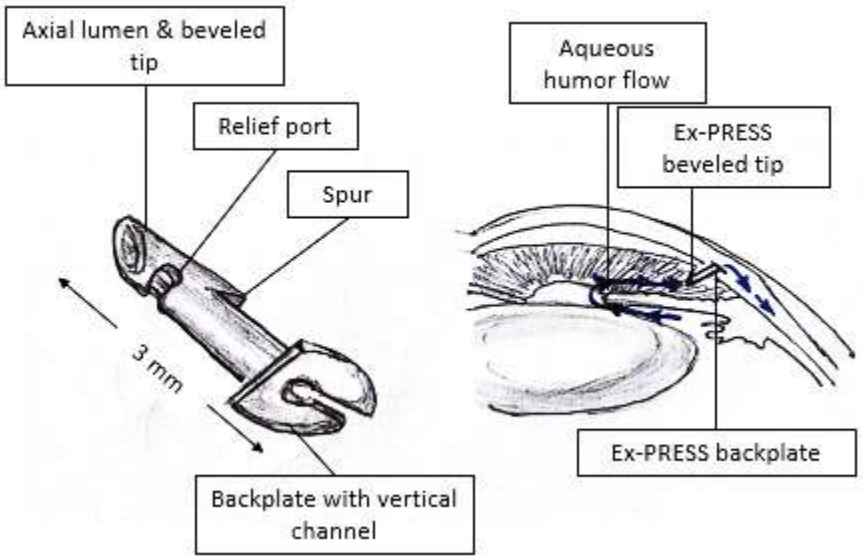


Fig. 1.5: Enlarged image of the Ex-PRESS shunt by Alcon [left] and an illustration of the Ex-PRESS shunt implanted in the eye [right] (adapted from Refs. 25 and 26)

The Ex-PRESS shunts AH from the anterior chamber of the eye to the subconjunctival reservoir [24]. It is commonly implanted in conjunction with a trabeculectomy [24]. The iStent is a titanium stent with a ridge (spur) as shown in the left image of Fig. 1.6. The iStent directly shunts aqueous humor from the anterior chamber, bypassing the trabecular meshwork, and going into Schlemm's canal [22]. The iStent is implanted in the eye as shown in Fig. 1.6. It is often combined with cataract surgery to reduce the IOP of the cataract patient [22].

The Trabectome by NeoMedix (or ab interno trabeculectomy) is a minimally invasive surgical device that ablates part of the trabecular meshwrk and Schlemm canal using a high-frequency electrocautery device, allowing more AH outflow [14, 27].

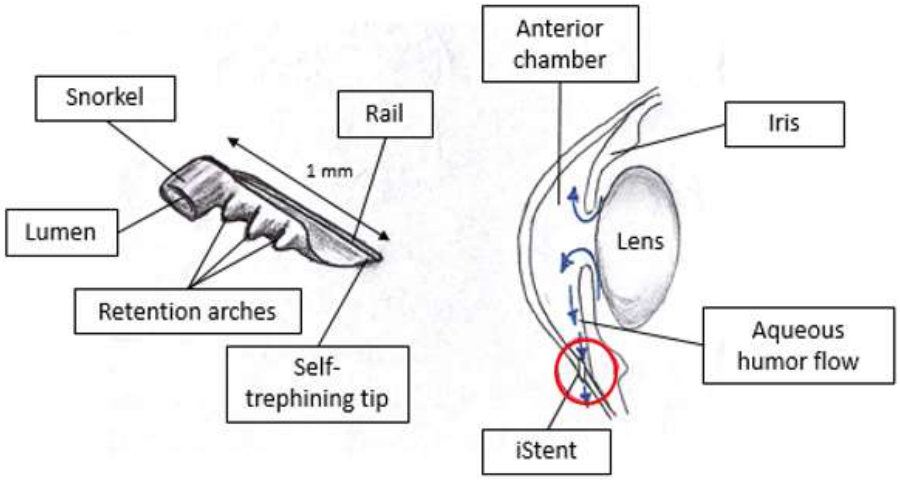


Fig. 1.6: Enlarged image of the iStent by Glaukos [left] and illustration of an iStent implanted in the eye [right] (adapted from Ref. 28)

There is also a group of procedures called cyclodestructive procedures. Cyclodestructive procedures involve the ablation of part of the ciliary body that produces aqueous humor in the eye [29]. The different modes of cyclodestruction include cryotherapy, diathermy, laser and ultrasound [29-32]. The most common is cyclophotocoagulation which uses a diode laser [29].

### 1.1.2. Non-Valved and Valved Glaucoma Drainage Implants (GDIs)

Currently, there are two main types of GDIs: valved GDIs (VGDIs) and non-valved GDIs (NVGDIs). The early GDI designs did not have valves (NVGDs), and were developed with the sole purpose of draining AH out of the eye [3]. It was discovered that NVGDIs did not provide sufficient IOP resistance in the 4- to 6-week post-op stage, resulting in hypotony-related complications. Hypotony is the phenomenon where the IOP falls below the nominal range (IOP < 10 mm Hg) and can cause serious vision-threatening complications [11]. It was only later that VGDIs were developed to resolve this issue of immediate post-op hypotony [3].

Among the commonly used GDIs are the valved Ahmed glaucoma valve (AGV) and the

non-valved Baerveldt glaucoma implant (BGI), shown in Fig. 1.7 [33].

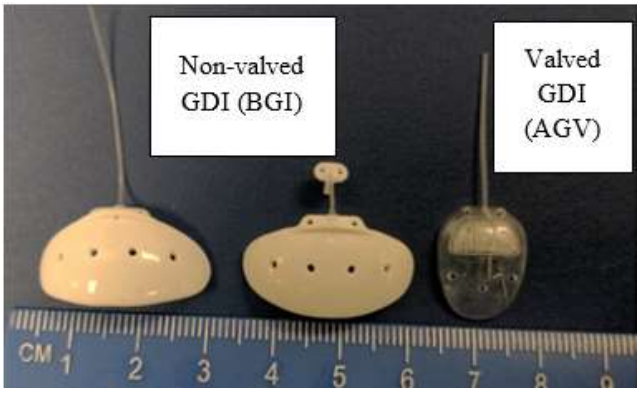


Fig. 1.7: Examples of non-valved and valved GDIs

***Baerveldt Glaucoma Implant (BGI)***

The BGI, by Advanced Medical Optics, Inc., is one of the most commonly used NVGDIs. The design of the BGI is simple, consisting of an end plate for securing the implant on the eye ball and a silicone tube with an ID of approximately 0.30 mm to shunt AH out from the eye (Fig. 1.7). The implant end plate is fabricated out of barium impregnated silicone. This rounded plate has a surface area ranging from 250 $mm^2$ to 350 $mm^2$ and has several fenestrations that allow the growth of tissue fibers on the plate [34].

***Ahmed Glaucoma Valve (AGV)***

The AGV, by New World Medical, is among the most used VGDIs. It has a polypropylene or silicone end plate that is scarab shaped (Fig. 1.7). Similar to the BGI, the AGV silicone models have fenestrations to encourage tissue growth [34]. The AGV is designed to reduce immediate post-op hypotony and other post-op complications by providing sufficient flow restriction to prevent the IOP from falling below 8 to 12 mm Hg [34].

***Comparison of BGI and AGV***

The Ahmed versus Baerveldt study is a landmark study that compared the performance of

BGIs and AGVs in 238 patients after five years [33]. In this study, it was found that BGIs had a lower failure rate of 40% as compared to AGVs with a failure rate of 53% [33].

The study also reported that BGIs had more hypotony-related complications immediately after surgery [33]. This was because BGIs provide little to no initial AH flow resistance, causing excessive AH outflow and a sudden decrease in IOP immediately after surgery. Only approximately four to six weeks after surgery did IOP levels stabilize as scar tissue formed around the episcleral plate of the BGI, providing the necessary flow resistance [35, 36]. In an effort to provide initial post-op AH resistance, many intra-op modifications to BGIs have been developed.

These methods include a two-stage surgical method [7], tube occlusion with a non-absorbable stent suture [4, 37], injection of viscoelatic solution into the anterior chamber of the eye [5] and external ligation of the tube with an absorbable suture and tube fenestrations [38-40]. Although these methods provide relatively adequate early post-op IOP control, they are unable to lower IOP immediately after surgery (lowers IOP after approximately one week). Also, they are not able to provide consistent IOP control during the early post-op weeks (IOP decreases initially but increases again after approximately one month) [6, 8]. Additionally, these methods have not eliminated the occurrence of post-op complications, which are reported to range from 19% to 71.8% [4-8].

### 1.3. New Method of Improving BGI Immediate Post-Operative IOP Control

A relatively new method to improve IOP control immediately after NVGDI surgery (specifically applied to BGIs) has been used by Dr. Paul Munden, formerly an ophthalmologist at the University of Kansas Medical Center, now at the Oklahoma City Veterans Association Medical Center. Should this method be successfully demonstrated in the next few years, the BGI will be able to provide consistent initial IOP control, which has not been achieved with valves or intra-op

modifications.

This method involves placing a degradable insert into the BGI tube prior to surgery in order to provide temporary resistance in the immediate post-op period. The method is illustrated in Fig. 1.8. The idea is that this degradable insert will provide the proper temporary AH flow resistance through the BGI tube. As the insert degrades and reduces in size, tube flow resistance would decrease while scar tissue forms over the BGI plate, providing long-term IOP control.

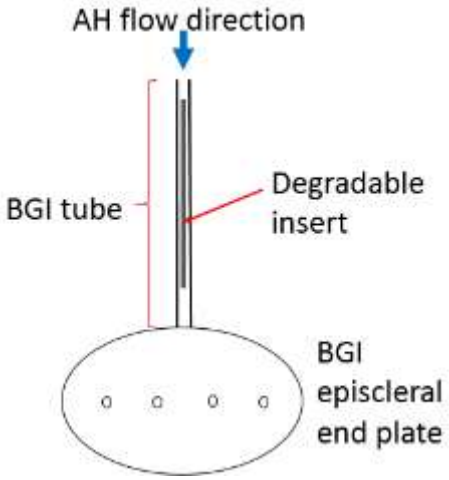


Fig. 1.8: Configuration of degradable insert in BGI tube

Preliminary data have demonstrated that this degradable insert technique may be able to provide the desired IOP control during the immediate post-op period and decrease the occurrence of hypotony-related complications, unlike current intra-op modifications [41]. With the success of this modification, the long-term effectiveness of GDIs can be improved. This modification combines the advantages of a NVGDI and a VGDI, providing long-term IOP control as well as immediate and consistent post-op IOP control. This technique also provides a platform for future research to develop a drug-delivery system that reduces the growth of post-op scar tissue, as recommended by Hong *et al.* in their review of GDIs [3].

## Chapter 2: Setup, Experimental Methods and Setup Validation

This chapter discusses details of the two identical experimental setups (Setups 1 and 2) developed for this study, and explains the verification and validation procedures used to determine the accuracy of the data obtained using the setups.

The following summarizes each section of Chapter 2:

- Section 2.1: Describes the experimental setups.
- Section 2.2: Describes the modifications made by this author to the initial setups.
- Section 2.3: Provides an overview of the preliminary validation trials performed by Ramani who first developed the experimental setups. These trials included single tube flow (50 μm and 75 μm ID microtubes) and annular flow (BGI tubes with degradable inserts) trials [42].
- Section 2.4: Describes the single tube flow trials performed with 50 μm and 75 μm microtubes to determine the repeatability of results in Section 2.3 after modifications were made to the setups. Concludes that both setups maintain consistent pressures for two to three hours.
- Section 2.5: Describes 2-hour and 20-hour annular flow trials performed with stiff hypodermic tubes and nichrome wire inserts. The purpose of these trials was to eliminate the influence of other variables in the experiment and enable accurate benchmarking of the setups. It was found that pressure increased over time without an apparent cause, even though the same sample, procedures and flow conditions were used.
- Section 2.6: Describes verification of the test system (pumps and transducers) to ensure that the pressure increase observed in Section 2.5 was not due to systemic error. Pressure

and flow rate measurements of the pump from Setup 1 were compared with those of the pump from Setup 2. The flow rate measurements of the pump in Setup 2 were also compared with those of a syringe pump. The pressure results measured by the transducer from Setup 1 were compared with those of a third transducer purchased from a different manufacturer. The pressure and flow results of these pumps and transducers corresponded well with one another. These validation trials demonstrated that the pressure increase observed in Section 2.5 was not caused by an error in the system. Therefore, it was very likely caused by microbial growth.

- Section 2.7: Describes the antimicrobial cleaning and sterilization protocol that was developed to prevent the increase in pressure over time. The protocol was effective and resulted in steady and constant pressure measurements for more than 20 days.

- Section 2.8: Compares pressure fluctuations obtained after the antimicrobial protocol as a function of barometric pressure. Some flow trials had pressure data that matched the fluctuations of barometric pressure but some matched the fluctuations of the mirrored (inverted) barometric pressure.

## 2.1. Experimental Setup

Two duplicate experimental setups were developed by Ramani [42] and later modified by this author to increase the accuracy and reliability of pressure measurements. These setups simulate the flow of AH through BGI tubes at the nominal flow rate of AH production (~2.5 µl/min) in the human eye and measure the $\Delta P$ in the tube. Each setup consists of a precision pneumatic pump (0 - 50 µl/min, ± 0.05 µl/min; CorSolutions, Ithaca, NY), a bottle containing deionized (DI) water, microfluidic tubing and connections, a pressure transducer (0 - 130 mm Hg, ± 0.2 mm Hg; Omega Engineering, Norwalk, CT), a data logger (Omega Engineering, Norwalk, CT), and a test

section [43]. The test section is in a temperature-controlled incubator (±2°F; Miller Manufacturing, Glencoe, MN) as shown in Fig. 2.1. The overall benchtop setup with all of its components is shown in Fig. 2.2. The layout of the components inside the incubator is shown in Fig. 2.3.

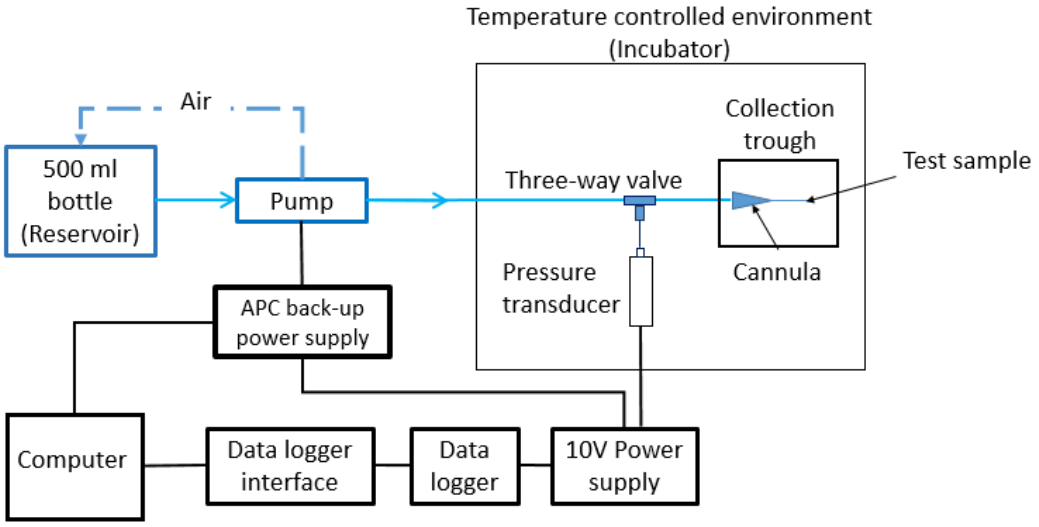


Fig. 2.1: Schematic of experimental setup

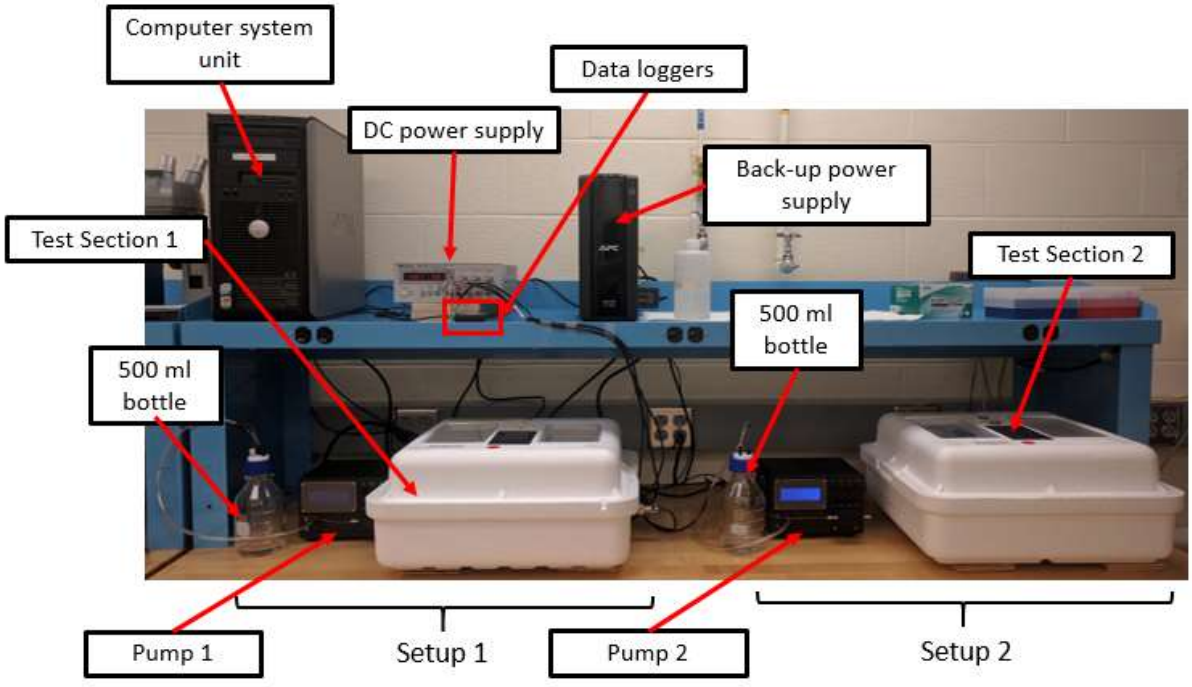


Fig. 2.2: Overall benchtop experimental setup

The two setups are connected to a computer, a 20V DC power supply (Hewlett-Packard, Palo Alto, CA), and a back-up power supply unit (Schneider Electric, West Kingston, RI). A list of the major components in the setup and their specifications can be found in App. A.1.

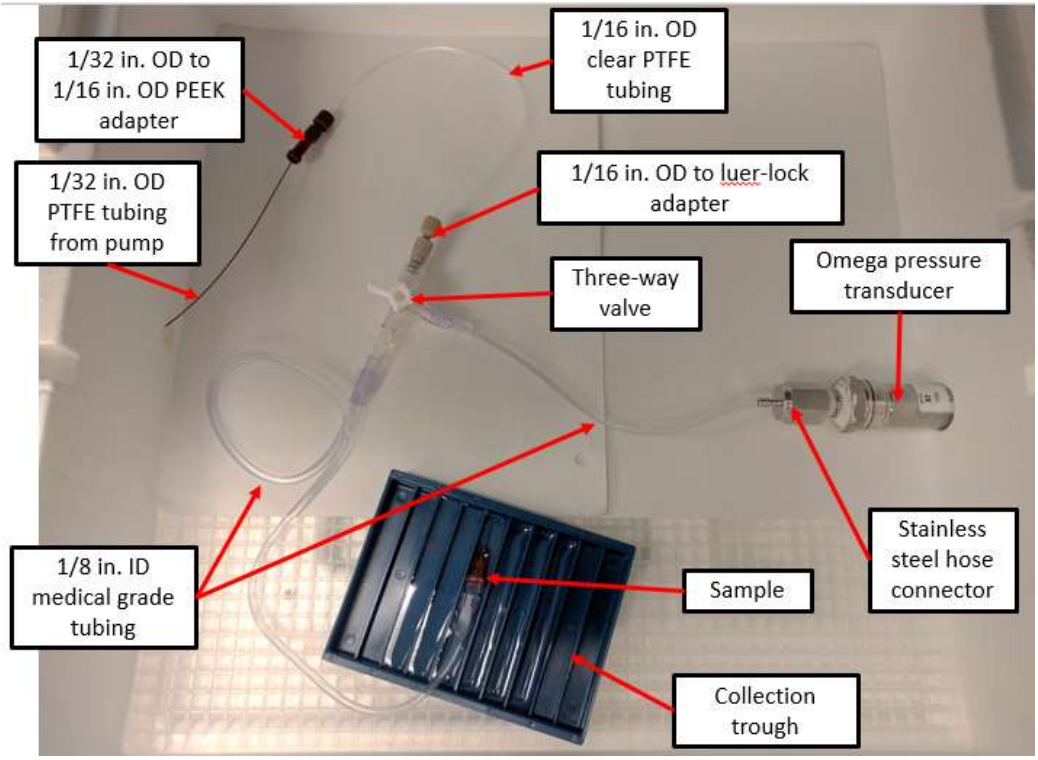


Fig. 2.3: Layout inside the incubator

## 2.2. Modifications Made to the Experimental Setups

***Research question:*** *Could the experimental setups that were previously developed by Ramani [42] measure pressure within a GDI-like tube reliably and accurately?*

Initially, the lengths of the connecting tubes and the configuration of the connections were different in both setups. To standardize the configurations of both setups, the lengths of the tubes were changed to be the same. It was also discovered that there was an error in the conversion calculation performed by Ramani when converting the voltage readings of the pressure transducers to pressure (volts-to-pressure).

Another issue that arose was that the initial setups were unable to control or maintain the surrounding temperature of the test sample. Additionally, the setups experienced several issues such as: fluid leaking out of the tube connections, and the loss of experimental pressure data due to electric power trips that occurred when the engineering building (Learned Hall) was being renovated. In order to solve the issues mentioned, the following modifications were made to the setups:

2.2.1. the voltage-to-pressure conversion equation was corrected (refer to App. A.2),

2.2.2. a back-up power supply unit (Schneider Electric, West Kingston, RI) was implemented,

2.2.3. temperature-controlled test sections: incubators (Miller Manufacturing, Glencoe, MN) were installed,

2.2.4. SS hose connectors were used to link the pressure transducers to the three-way valves (Swagelok Kansas City, Lenexa, KS), and

2.2.5. polyether-ether-ketone (PEEK) connectors were implemented to link the pumps to the three-way valves (IDEX Health & Science, Oak Harbor, WA).

### 2.2.1. Voltage-to-Pressure Conversion

Previously, Ramani used Eq. (2.1) to convert the pressure transducers' voltage readings (mV) to pressure (psi).

$$V_o = 40.002\ \Delta P - 0.0237 \tag{2.1}$$

where $V_o$ is the output voltage measured by the transducer (mV) and $\Delta P$ is the output differential pressure (psi). Equation (2.1) was obtained by plotting a linear best fit curve of $V_o$ against $\Delta P$ (Fig. 2.4) based on the calibration data provided by the manufacturer [Omega, Inc.] (Table 2.1).

However, it was discovered that Ramani had not been using Eq. (2.1) correctly. When

using Eq. (2.1) to convert the transducer voltage to pressure, instead of substituting the transducer's measured output voltage value into '$V_o$', Ramani had substituted the transducer's output voltage value into '$\Delta P$', and took the '$V_o$' result of Eq. (2.1) as $\Delta P$. This caused the magnitude of the $\Delta P$ to be higher than the actual measured $\Delta P$. This created an error of up to 124 mm Hg for a $\Delta P$ reading of 206.7 mm Hg and an error of 18.7 mm Hg for a pressure reading of 50 mm Hg.

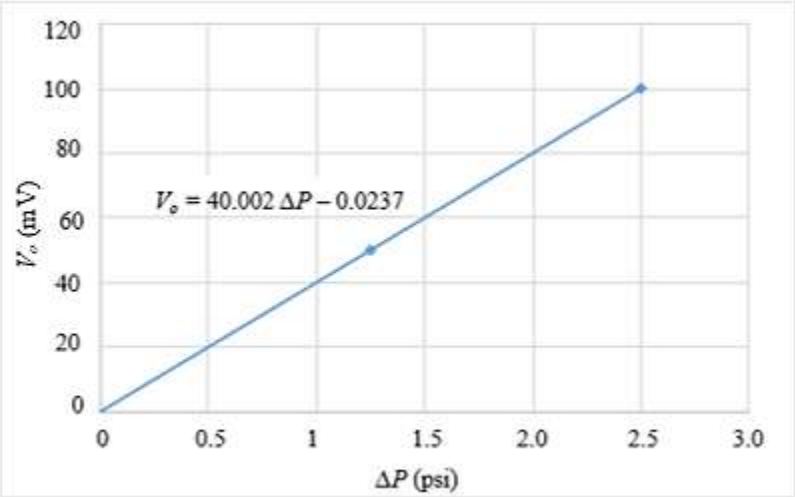


Fig. 2.4: Plot of transducer voltage reading [$V_o$] against differential pressure [$\Delta P$] using the calibration data provided by the manufacturer (reproduced from Ref. 42)

Table 2.1: Example pressure and voltage calibration data provided by manufacturer (Omega) – Transducer 1 (reproduced from Ref. 42)

| Pressure, $\Delta P$ (psi) | Voltage, $V_o$ (mV) |
|---|---|
| 0 | -0.023 |
| 1.25 | 49.977 |
| 2.5 | 99.981 |
| 1.25 | 49.974 |
| 0 | -0.025 |

To prevent the incorrect use of the equation, plots of $\Delta P$ (psi) against $V_o$ (V) were produced using the calibration data provided by the manufacturer for both transducers (Transducers 1 and 2,

respectively). The linear best fit equations were obtained [Eq. (2.2) for Transducer 1 and Eq. (2.3) for Transducer 2]. Refer to App. A.2 for more details.

$$\Delta P = 24.985 V_o - 0.0006 \tag{2.2}$$

$$\Delta P = 24.999 V_o + 0.0006 \tag{2.3}$$

where $\Delta P$ is the output differential pressure (psi) and $V_o$ is the output voltage measured by the transducer (V).

### 2.2.2. Back-Up Power Supply Unit

A Back-UPS XS 1500 uninterruptible power supply (UPS) was purchased from Schneider Electric to overcome the Learned Hall electric power trip issue that caused data to be lost. The UPS unit would also provide protection from other types of power surges. The UPS was connected to the computer, the 20V DC power supply, and the two precision pneumatic pumps. This ensured that power was continually supplied to the pumps, computer and data loggers even when there was no main building power supply. The input and output voltages of the UPS are AC 120V. It has a maximum run time of 2 hours and 8 mins at minimum load (50 Watts), 13 minutes at half load (432.5 Watts), and 4 minutes at full load (865 Watts). It also has ten output connectors. The specifications of the UPS are listed in App. A.3. The normal load on the UPS is 96 Watts and has an estimated run time of 1 hour and 11 minutes.

### 2.2.3. Temperature-Controlled Test Section: Incubator

In order to maintain the environment at the test sample, two Little Giant Still Air Egg Incubators (Model 9300) by Miller Manufacturing were purchased. The incubators are made of Styrofoam. Each incubator has a built-in digital electronic thermostat with an LCD screen that displays temperature and humidity. Each incubator is 19 in. by 19 in. by 9 in., and the input voltage

is 120V AC. The specifications for the incubators are provided in App. A.4.

### 2.2.4. SS Hose Connectors (Transducer-to-Valve Connection)

To solve the issue of fluid leaking at the transducer connection, two Swagelok hose connectors (Part number: SS-2-HC-7-4) were purchased, one for each setup [44]. The initial rubber-caulk connector was replaced with the new Swagelok hose connector in order to provide a more reliable water-tight fitting. The Swagelok connectors are made from 316 SS as shown in Fig. 2.5. One end of each connector is a 1/4 in. female NPT fitting, and the other end is a 1/8 in. inner diameter (ID) hose connector [44].

Fig. 2.5: Swagelok SS hose connector

### 2.2.5. PEEK Tube Connectors (Pump-to-Valve Connection)

In the initial setup, fluid also leaked at the tube connection between the pump and the three-way valve. To resolve this issue, PEEK tube connectors (left image of Fig. 2.6) were purchased from IDEX Health & Science to connect the 1/16 in outer diameter (OD) tube from the pump to the three-way valve. To connect the 1/16 in. OD tube to the valve, a two-part connection involving a 10-32 one-piece conical fingertight connector (Part F-120) and a 10-32 female-to-female luer adapter (Part P-659) [45] are utilized (Fig. 2.6).

Fig. 2.6: 10-32 one-piece conical fingertight connector (left) and a 10-32 female-to-female luer adapter (right)

***Conclusion:*** *The experimental setups previously developed by Ramani could not provide reliable and accurate flow pressure data. Modifications were necessary in order to improve the reliability and accuracy of the setups. The modifications made included correction of the pressure transducers' voltage-to-pressure conversion equation, installation of a back-up power supply (ensuring uninterrupted power), installation of a temperature-control incubator (providing more control of local conditions), and implementation of new leak-proof connectors (i.e., SS hose connectors and PEEK connectors).*

***Next steps:*** *Compare the results of the trials performed by Ramani with the trials performed using the modified experimental setup.*

## 2.3. Preliminary Validations

***Research question:*** *What were the pressure results of the preliminary trials performed by Ramani?*

Preliminary validations were performed by Ramani [42] to determine the ability of the setups to measure reliably around a nominal pressure that was close to the physiological IOP of approximately 15 mm Hg when fluid flow rate was 2.5 µl/min [42]. To obtain initial benchmark pressure data, two-hour experimental trials were performed, measuring fluid pressure through hollow microtubes. Considering experimental restrictions and the theoretical tube parameters

required to achieve the nominal IOP range, 35 mm long 50 µm and 75 µm ID methyl deactivated fused silica (VSD) tubing was used [42].

Procedures for the experimental trials are described in Ramani's thesis [42]. Ramani found that the experimental pressure data for the 50 µm ID tube at 2.5 µl/min were near the upper limit of the theoretical pressure range as shown in Table 2.2. For the 75 µm ID tube at 2.5 µl/min, the experimental pressure data were above the upper limit of the theoretical pressure range (Table 2.2) [42].

Table 2.2: Mean and standard deviation of the time-averaged experimental pressures and theoretical pressure ranges of the 50 µm and 75 µm ID VSD tube trials (reproduced from Ref. 42)

| # of trials | Flow rate with tolerance (µl/min) | Tube internal diameter (microns) | Sample length (mm) | Mean of time-averaged pressure ± std. dev. (mm Hg) | Theoretical pressure range (mm Hg) |
|---|---|---|---|---|---|
| 7 | 2.5 ± 0.125 | 50 ± 4 | 35 | 101.5 ± 3.2 | 48.2 – 103.2 |
| 5 | 2.5 ± 0.125 | 75 ± 4 | 35 | 15.0 ± 0.4 | 9.2 – 16.8 |
| 5 | 1.25 ± 0.0625 | 75 ± 4 | 35 | 8.4 ± 0.2 | 3.7 – 7.6 |

The preliminary annular flow trials that were performed by Ramani were also performed using a test sample with a 29G (gage) steel wire (0.287 mm OD) inserted into a 23G syringe needle (0.34 mm ID). Due to the large flow area, the flow rate was set at 10 µl/min. However, the experimental pressure data was still very low, 2.5 mm Hg to 3.5 mm Hg [42]. Additionally, Ramani carried out short-term and long-term preliminary experimental trials with BGI tubes containing medical grade non-absorbable (prolene) and absorbable suture inserts (monocryl). For the long-term trial with absorbable suture inserts, Ramani performed two 40-day trials with 8 mm long monocryl (poliglecaprone-25) sutures placed in 10-mm long BGI tubes at 2.5 µl/min.

It was found that pressure initially increased over time and decreased after a period of 30 days as shown in Figs. 2.7 and 2.8 [42]. This showed that the sutures increased in size before degrading. Ramani confirmed this by observing the degradation rate of the sutures in glass vials containing distilled water or balanced salt solution (BSS). He found that the diameters of the sutures increased first before decreasing when in contact with water.

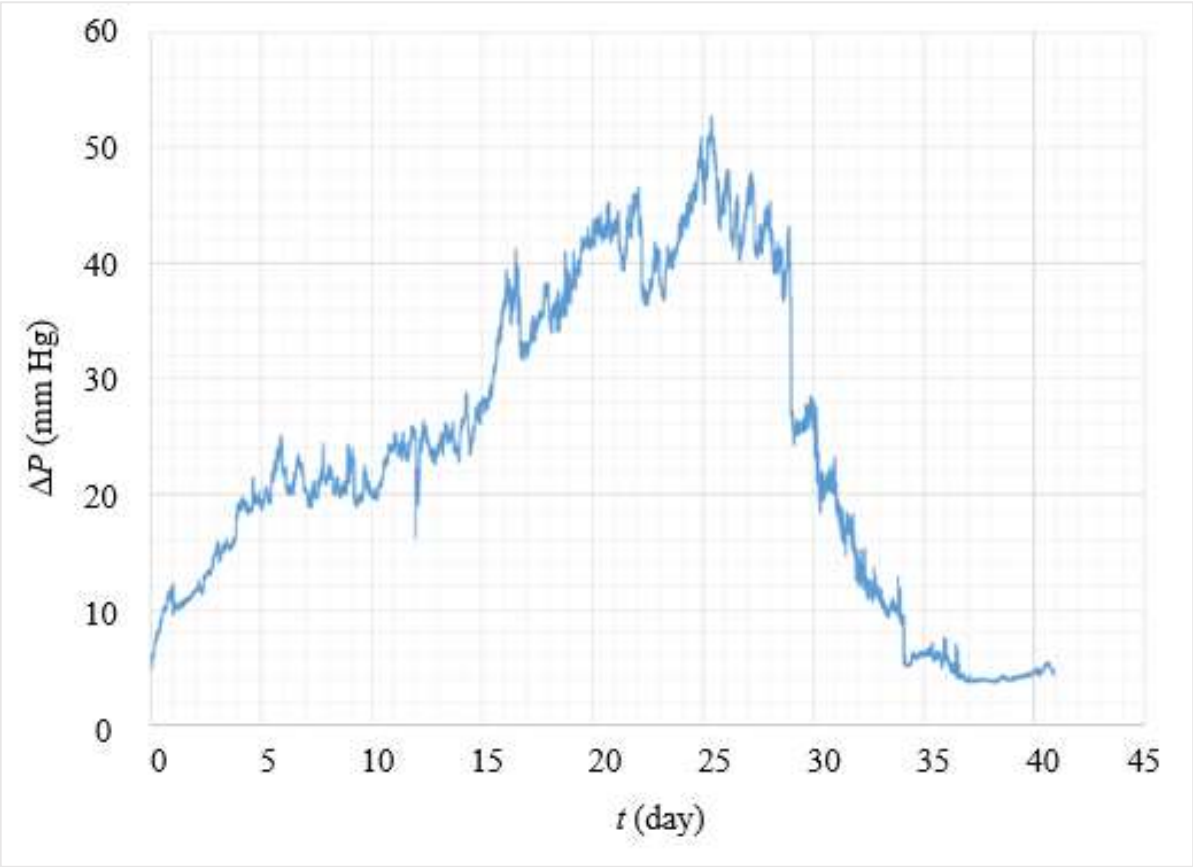


Fig. 2.7: Pressure variations for 8 mm long 3-0 monocryl insert and flow rate of 2.5 μl/min in Setup 1 (reproduced from Ref. 42)

It is important to note that the pressure results obtained by Ramani were affected by the voltage-to-pressure conversion error. Due to the conversion error, the magnitude of measured $\Delta P$ was calculated to be larger (~ 2x) than that of the actual $\Delta P$. Since this error increased the actual magnitude of the measured $\Delta P$ overall, the conversion error could not have caused the variation in

$\Delta P$ over time as observed during the degradable insert trials performed by Ramani (Figs. 2.7 and 2.8) [42]. Thus, the variations in $\Delta P$ observed during those trials were still acceptable indications that the insert changed in size over time.

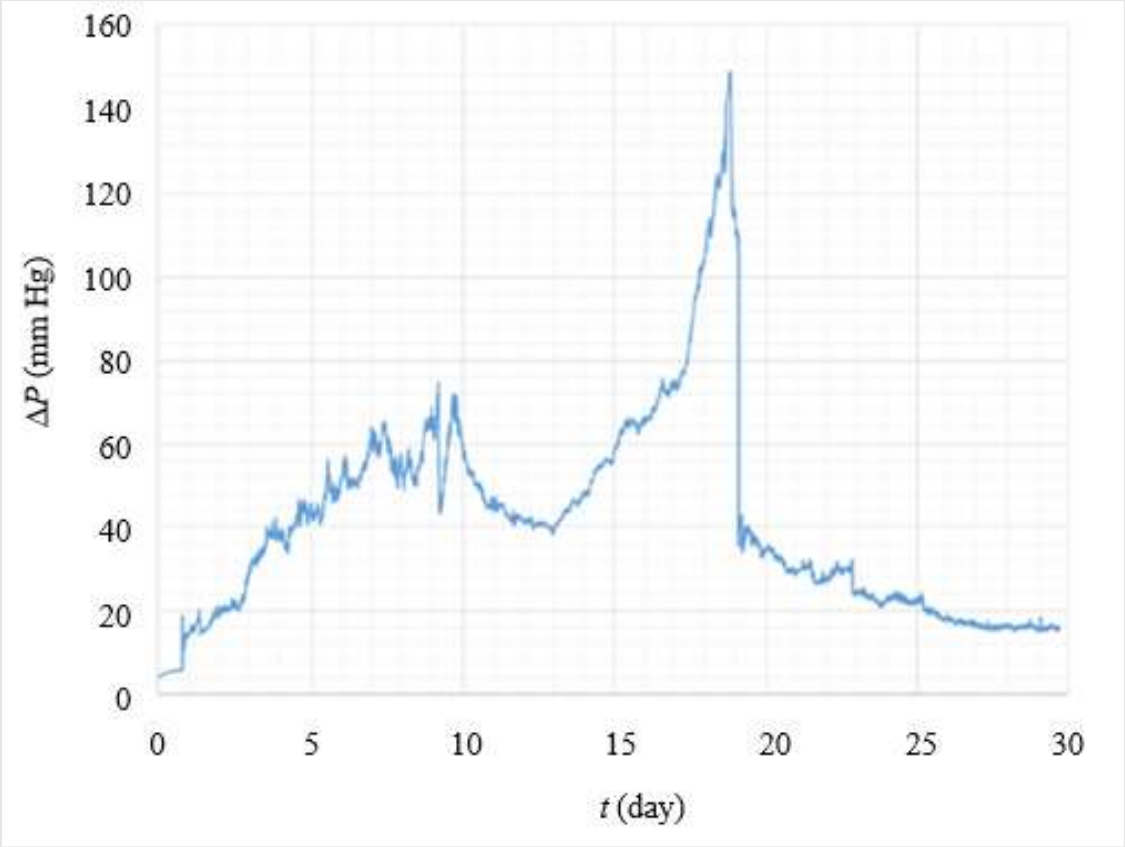


Fig. 2.8: Pressure variations for 8 mm long 3-0 monocryl insert and flow rate of 2.5 µl/min in Setup 2 (reproduced from Ref. 42)

The next course of action (that was performed by this author) was to verify whether the $\Delta P$ trends observed in Figs. 2.7 and 2.8 were caused by the change in size of the suture insert *only*, and not caused by any other variable. This was done by obtaining long-term (30- to 40-day) benchmark data with non-degrading stiff inserts and tubes.

***Conclusion:*** *Ramani performed flow trials involving 50 µm and 75 µm ID VSD tubes and reported $\Delta P$ results that were close to the upper limit of the theoretical $\Delta P$ range. Ramani also performed*

*annular flow trials with BGI tubes and degradable inserts (medical grade sutures). ΔP increased before decreasing after 30 days, demonstrating that the sutures increased in size first before reducing in size.*

***Next steps:*** *Determine if the trials and ΔP results obtained by Ramani could be repeated. Obtain long-term (30- to 40-day) benchmark ΔP data to ensure that the ΔP trends observed by Ramani for the degradable sutures were probably caused by the change in size of the insert and not by any other variable.*

## 2.4. Open Single Tube Flow Validation Trials

***Research question:*** *How will the ΔP results obtained using the modified experimental setups compare to the results obtained by Ramani (50 μm ID VSD tubular flow trials)?*

After modifying the setups, the preliminary open single microtube flow trials that had been done by Ramani, were repeated by the author in the modified setups. This was done in order to ensure that the setups were still able to perform accurate and consistent pressure measurements.

Ten 2- to 3-hour single tube flow trials were performed with ten 50 μm VSD tubes in Setups 1 and 2 (five trials per setup) in order to determine if both setups measured pressures that were relatively close to each other. The samples were 35 mm long. The pumps were primed at 10 μl/min at the start of each trial to remove any undetected air bubbles in the tubes. The flow trial procedures and test sample preparation are described in Apps. B.1 and B.3. The fluid used in these trials was distilled water. The tubular flow trials were performed at a flow rate of 2.5 μl/min and room temperature (25°C). Pressure data were collected at a frequency of 1 Hz for approximately three hours. Table 2.3 summarizes the pressure results obtained from the trials. The pressure plots of the trials are shown in Fig. 2.9.

Table 2.3: Summary of pressure results for the 2- to 3-hour VSD 50 µm tubular flow trial

| Setup | Sample Number | Experimental $\Delta P$ (mm Hg) | |
|---|---|---|---|
| | | Average [a] | Standard Deviation |
| 1 | 1 | 63.60 | 0.62 |
| | 2 | 38.61 | 0.72 |
| | 3 | 47.67 | 0.74 |
| | 4 | 67.87 | 0.20 |
| | 5 | 67.68 | 0.87 |
| | Cumulative average, $\Delta P_{c\_avg}$ [b] | 57.09 | 0.63 |
| 2 | 6 | 63.79 | 0.29 |
| | 7 | 66.32 | 0.84 |
| | 8 | 66.68 | 1.35 |
| | 9 | 45.07 | 0.25 |
| | 10 | 48.69 | 0.42 |
| | Cumulative average, $\Delta P_{c\_avg}$ [c] | 58.10 | 0.63 |

[a] Average experimental $\Delta P$ of each sample over the total length of the trial
[b] Cumulative average of the averages and standard deviations of the experimental $\Delta P$ values of Samples 1 to 5
[c] Cumulative average of the averages and standard deviations of the experimental $\Delta P$ values of Samples 6 to 10

From Table 2.3, it can be seen that the cumulative average $\Delta P$ of the samples in Setups 1 and 2 only had a difference of 1.75% [difference = (Setup 2 $\Delta P_{c\_avg}$ – Setup 1 $\Delta P_{c\_avg}$) / (Average of Setup 2 $\Delta P_{c\_avg}$ and Setup 1 $\Delta P_{c\_avg}$)]. This difference between $\Delta P$ results from both setups is likely caused by slight variations in tube lengths and elevations of the pumps/transducers/samples/test sections. As will be discussed in Section 2.7.1, small variations in

the tube ID, especially when the tube ID is as small as 50 µm and 75 µm, can cause a significant variation in Δ*P*. Given the possible variation of ±4 µm in tube ID (according to Ramani - refer to Table 2.2), the resulting Δ*P* could vary quite significantly. The results also show that both setups can measure consistent pressures for a period of two to three hours with a small cumulative average standard deviation of 0.63 mm Hg.

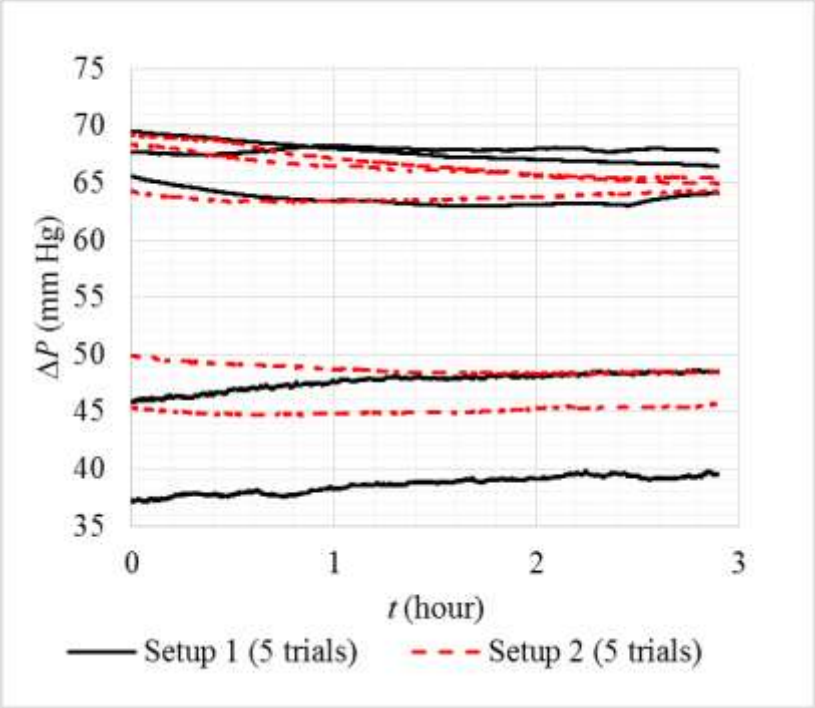


Fig. 2.9: Pressure plot of 2- to 3-hour 50 µm ID VSD microtube trials (*Q* = 2.5 µl/min; 25°C test conditions) [October 5 - November 4, 2015]

Contrary to the Δ*P* results reported by Ramani which showed that the average experimental Δ*P*s were close to the upper limit of the theoretical Δ*P* range (48.2 mm Hg - 103.2 mm Hg as shown in Table 2.2), the average experimental Δ*P* results reported here in Table 2.3 were close to the lower limit of the theoretical range. In addition, the cumulative average Δ*P* values for the 50 µm ID VSD tube trials (as reported in Table 2.3) were half of the average Δ*P* results obtained from the trials performed by Ramani (shown in Table 2.2). This is likely because of the incorrect

voltage-to-pressure conversion equation used by Ramani which increased the magnitude of the actual measured $\Delta P$. For an actual measured $\Delta P$ within the range of 30 to 70 mm Hg, the conversion error would have caused $\Delta P$ to be 16 to 41 mm Hg above the actual measured $\Delta P$.

***Conclusion:*** *The average $\Delta P$ results reported in this section for 50 µm ID VSD tube trials (using the modified setups) are approximately half of the $\Delta P$ results previously reported by Ramani [42]. This was because the $\Delta P$ results reported by Ramani had an error in the voltage-to-pressure conversion equation. The results in this section showed that the setups could measure $\Delta P$ consistently for a period of 2-3 hours and were within the theoretical $\Delta P$ range, but were close to the lower limit of the theoretical range (contrary to the results given by Ramani which showed that $\Delta P$ was close to the upper limit of the theoretical range). The cumulative average pressures measured for the 50 µm ID tubes in Setups 1 and 2 were very close, with a percent difference of only 1.75%.*

***Next steps:*** *Obtain benchmark $\Delta P$ data by performing annular flow trials with stiff tubes and inserts in order to reduce the number of variables that could cause a variation in $\Delta P$.*

### 2.5. Annular Flow Validation Trials with Stiff Tubes and Inserts

***Hypothesis:*** *$\Delta P$ remains constant during flow trials with stiff non-degradable tubes and inserts, since the diameters of the tubes and inserts do not change.*

The overall purpose of the setups is to measure $\Delta P$ across BGI tubes with degradable inserts. In order to reduce the number of variables and allow accurate benchmarking of the setups, trials were performed with stiff metal annular tubes containing stiff non-degradable inserts. Since stiff metal tubes and inserts do not change in size during the trials, it was expected that there would be little to no variation in $\Delta P$. The setups would be validated once they were able to measure $\Delta P$ with

little to no variation during trials with stiff tubes and inserts. Thus, when trials would be later performed with less stiff and degradable samples (which vary in size during the trial), it could be concluded that any variation in $\Delta P$ was not due to issues with the experimental setup, but was really due to the samples being tested. With stiff samples, the diameters of the tubes/inserts could be considered as constant throughout the experimental trial.

### 2.5.1. Two-Hour Annular Flow Validation Trials

***Research question:*** *Would the experimental $\Delta P$ results be relatively similar for each trial when annular flow trials were repeated with similar stiff non-degradable tube-insert samples?*

Short-term two-hour validation trials were performed with 1.5 inch (38.1 mm) long 24G (gage) SS hypodermic tubes (0.381 ± 0.1 mm ID) from Jensen Global and 8 mm long 28G nichrome wire inserts (0.32 ± 0.1 mm OD) from Master of Clouds. The actual measured ranges of the 24G SS tube IDs and 28G nichrome wire ODs were 0.347 mm to 0.362 mm and 0.328 mm to 0.333 mm, respectively. Refer to App. B.6 for the actual measured ranges of the tubes and inserts.

Two samples were prepared. The trial procedures and test sample preparation are described in Apps. B.1 and B.3, respectively. Sodium azide ($NaN_3$) at 0.04% by grams per volume (refer to App. F.1), was added to the DI water that was used as the fluid. $NaN_3$ was added to the DI water to curb any microbial growth in the fluid. Trials were performed with the first sample (Sample 1) in Setup 1 and the second sample (Sample 2) in Setup 2. The trials were repeated two more times. After completing the three trials, the samples were switched between setups. Sample 1 was tested in Setup 2 and Sample 2 was tested in Setup 1. These trials were also repeated two more times. The annular flow trials were performed at a flow rate of 2.5 µl/min and room temperature of 25°C. Pressure data were collected at a frequency of 1 Hz for approximately two hours. Note that the baseline pressure readings (pressure measured without the test sample) were not subtracted from

the measured pressure readings. This was later found to be important for eliminating residual pressure losses that occurred between the pump and the test sample. Refer to Section 3.1.1 for details.

If each setup was consistent in measuring pressure loss across a tube, the average measured pressure data for the second and third trials should be the same or very close (~ ± 2 mm Hg) to the average measured pressure data for the first trial. To verify whether the pump pressure readings corresponded to the transducer pressure readings, the pump pressure data were cross-checked with transducer pressure data. Figures 2.10 and 2.11 are the plots of the pressures measured by the transducers and the pneumatic pumps in Setups 1 and 2 during annular flow trials for Sample 1.

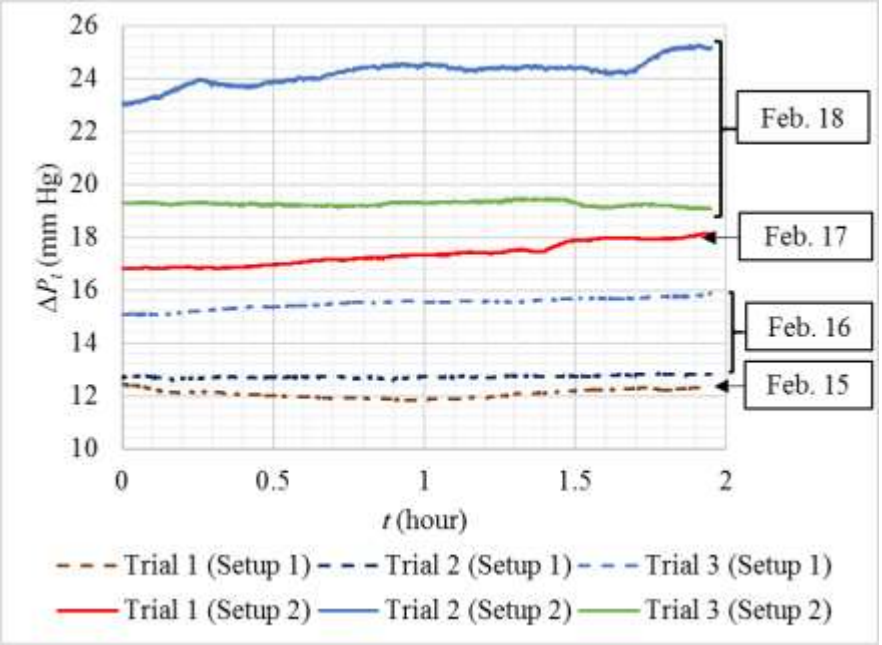


Fig. 2.10: Annular trial pressures for Sample 1 as measured by the transducers, $\Delta P_t$, in Setups 1 and 2 [February 15 - 18, 2016]

It can be seen from Figs. 2.10 and 2.11 that the average measured pressure increased from the first trial to the third, even though the same sample and procedures were used under the same test conditions.

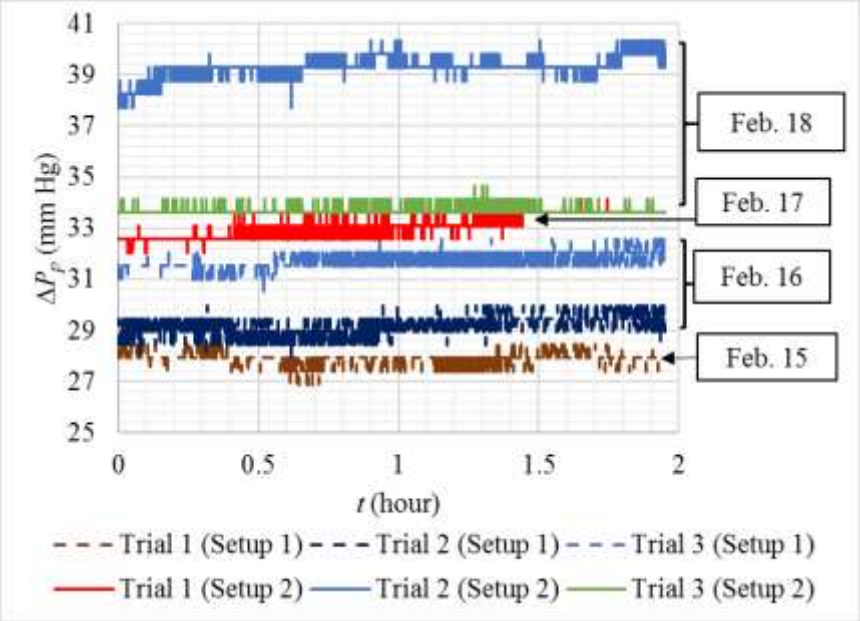


Fig. 2.11: Sample 1 annular trial pressures measured by the pumps, $\Delta P_p$, in Setups 1 and 2 [February 15 - 18, 2016]

Comparing Figs. 2.10 and 2.11, it can be seen that the relative pressure levels of the pumps corresponded with those of the transducers in their respective Setups (i.e., pressure in Trial 1 < Trial 2 < Trial 3). It is also observed that the pressure data measured by the pumps were consistently higher than the pressures measured by the transducers. This is because the pump sensors were located upstream of the pumps (flow source) as compared to the transducers which were located downstream of the pumps in the test section. Additionally, note that, for these flow trials, baseline pressure readings were not taken into account. Therefore, the pressures measured would include any residual pressure loss due to tube resistance between the pumps and the samples, as well as any head losses which were not considered.

Figure 2.12 shows a plot of the differences between the pump and transducer pressures. As given in Fig. 2.12, for Sample 1, the differences between the pressures measured by the pumps and the transducers were relatively consistent (average pump-to-transducer difference of 15.6 mm

Hg ± 0.71 mm Hg). This demonstrated that the experimental pressure trends measured by the pumps matched those of the transducers, with a consistent residual loss between the pumps and the transducers due to their locations (upstream versus downstream) in the setups. Similar trends can be seen for the trials of Sample 2 as shown in Figs. 2.13, 2.14 and 2.15.

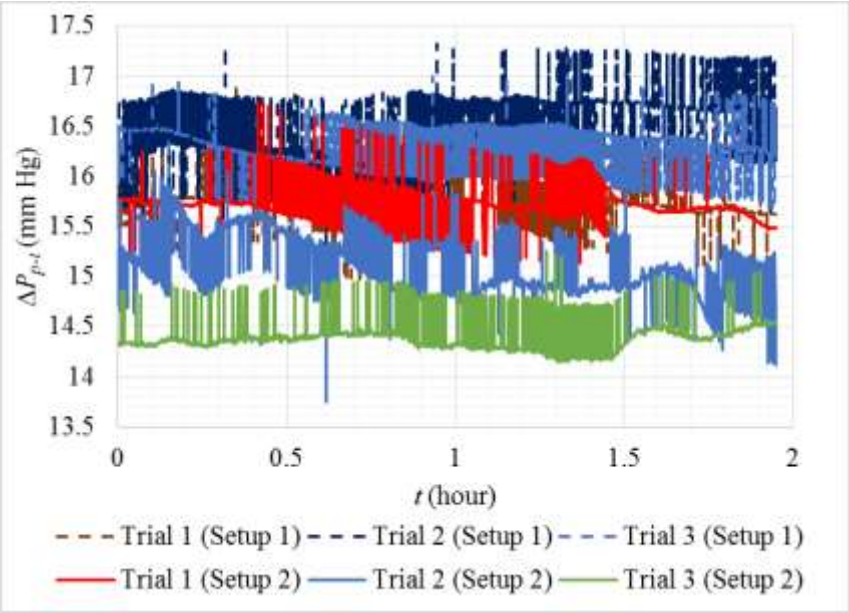


Fig. 2.12: Pressure differences between the transducers and pumps, $\Delta P_{p\text{-}t}$, in their respective setups for Sample 1 [$\Delta P_{p\text{-}t} = \Delta P_p - \Delta P_t$]

From Figs. 2.13 and 2.14, it can be seen that pressure increased as more repetitions were performed from February 19 to 23. Similar to Sample 1, Figs. 2.13 and 2.14 showed that the pressure trends of the pumps followed the pressure trends of the transducers (i.e., pressure in Trial 1 < Trial 2 < Trial 3). This indicated that there was an unaccounted-for effect occurring in the samples/setups. This was further investigated through the procedures described in Sections 2.6 to 2.7.

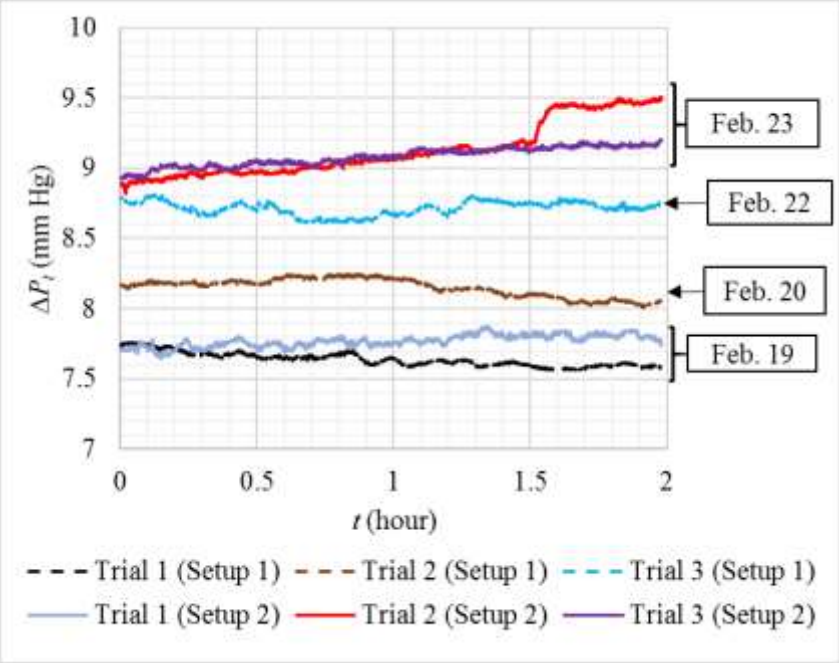


Fig. 2.13: Sample 2 annular trial pressures measured by the transducers, $\Delta P_t$, in Setups 1 and 2 [February 19 - 23, 2016]

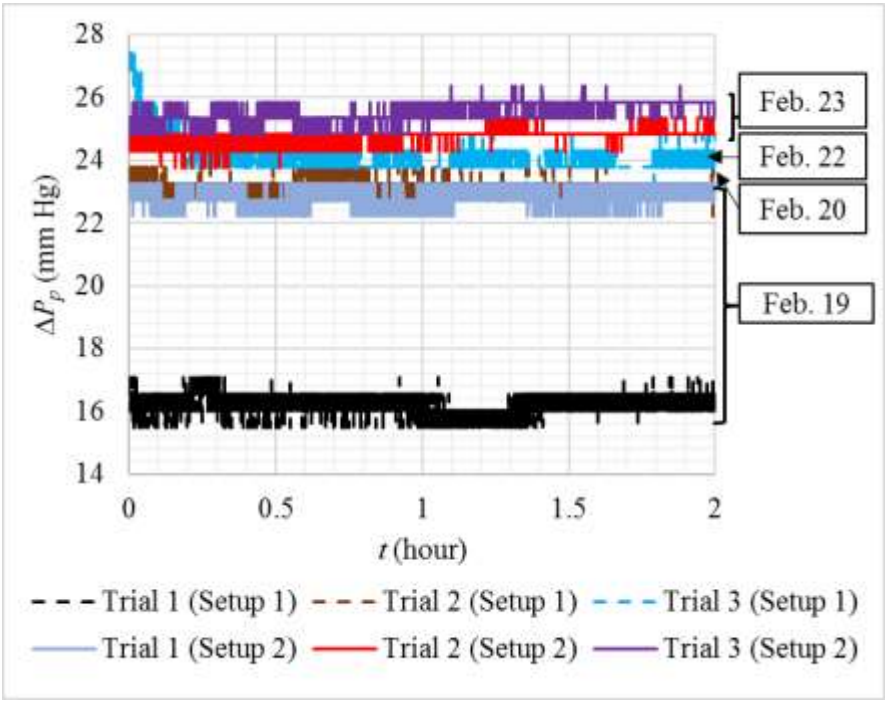


Fig. 2.14: Sample 2 annular trial pressures measured by the pumps, $\Delta P_p$, in Setups 1 and 2 [February 19 - 23, 2016]

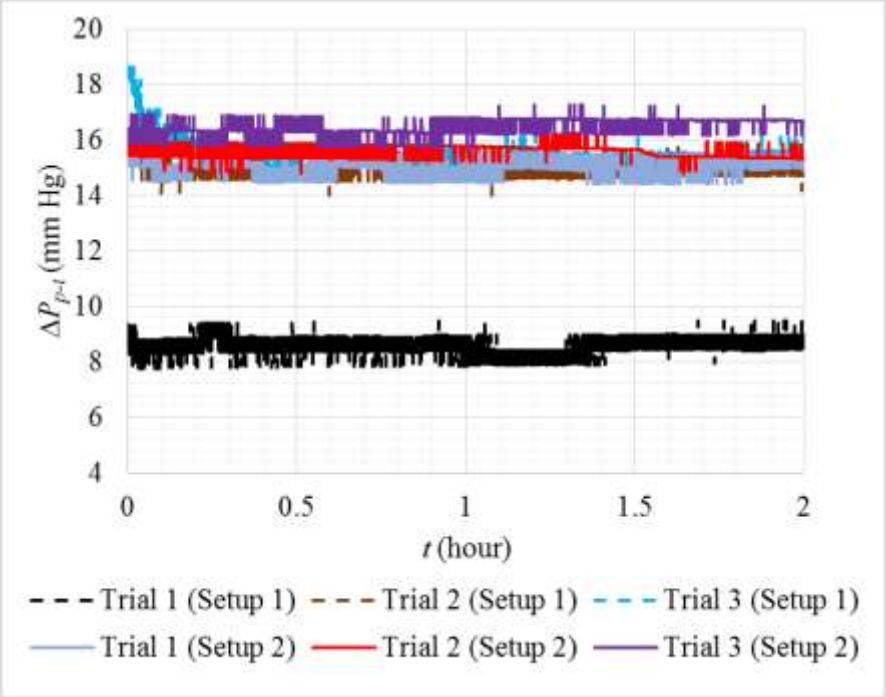


Fig. 2.15: Pressure differences between the transducers and pumps, $\Delta P_{p\text{-}t}$, in their respective setups for Sample 2 [$\Delta P_{p\text{-}t} = \Delta P_p - \Delta P_t$]

Another observation is that the differences between transducer and pump pressures for each trial were relatively consistent except for those of Trial 1 in Setup 1, which was the outlier (shown in Fig. 2.15). This difference may have been caused by an error during the trial procedure or a minor pump system error that was corrected before the other trials were performed.

Table 2.4 summarizes the averages and standard deviations of the measured pump and transducer pressures for Samples 1 and 2. From Table 2.4, it can be seen that $\Delta P$s measured by the transducers and pumps in Setups 1 and 2 for Samples 1 and 2 increased from Trials 1 to 3, except for the pump $\Delta P$ Sample 1 in Setup 2, which decreased from Trials 2 to 3. Sample 1's Setup 2 pump $\Delta P$ decreased from Trials 2 to 3, contrary to its transducer $\Delta P$ measurements, whose $\Delta P$ increased from Trials 2 to 3. This inconsistency may have been the result of a pump system error as well. It was also noted that Trials 2 and 3 for Samples 1 were performed on the same day. Thus

the error could also have been a procedural error that was corrected before the next trials were performed in Setup 2.

Table 2.4: Summary of transducer and pump average pressure measurements for Samples 1 and 2 annular trials

| | Transducer average pressure, $\Delta P_t$ (mm Hg)[a] | | | | Pump average pressure, $\Delta P_p$ (mm Hg)[a] | | | | Difference between transducer and pump pressure, $\Delta P_{p\text{-}t}$ (mm Hg)[b] | | | |
|---|---|---|---|---|---|---|---|---|---|---|---|---|
| Sample | 1 | | 2 | | 1 | | 2 | | 1 | | 2 | |
| Setup | 1 | 2 | 1 | 2 | 1 | 2 | 1 | 2 | 1 | 2 | 1 | 2 |
| Trial 1 | 12.1 | 17.4 | 7.64 | 7.77 | 27.9 | 33.1 | 16.1 | 22.8 | 15.8 | 15.7 | 8.50 | 15.0 |
| Trial 2 | 12.7 | 24.2 | 8.15 | 9.13 | 29.3 | 39.3 | 23.0 | 24.8 | 16.5 | 15.1 | 14.8 | 15.6 |
| Trial 3 | 15.5 | 19.3 | 8.71 | 9.08 | 31.8 | 33.6 | 24.0 | 25.5 | 16.3 | 14.4 | 15.3 | 16.5 |
| Cumulative average, $\Delta P_{c\_avg}$[c] | 13.4 | 20.3 | 8.17 | 8.66 | 27.1 | 35.3 | 21.0 | 24.4 | 16.2 | 15.1 | 12.9 | 15.7 |
| Standard deviation [d] | 1.48 | 2.89 | 0.44 | 0.63 | 2.21 | 2.82 | 3.49 | 1.16 | 0.29 | 0.54 | 3.10 | 0.59 |

[a] Pressure for each trial averaged over the 2-hour period shown in Figs. 2.10, 2.11, 2.13 and 2.14
[b] Difference between transducer pressure and pump pressure averaged over the 2-hour period shown in Figs. 2.12 and 2.15 ($\Delta P_{p\text{-}t} = \Delta P_p - \Delta P_t$)
[c] Cumulative average of $\Delta P_t$, $\Delta P_p$ and $\Delta P_{p\text{-}t}$ over Trials 1, 2 and 3
[d] Standard deviation of $\Delta P_t$, $\Delta P_p$ and $\Delta P_{p\text{-}t}$ over Trials 1, 2 and 3

Again, from Table 2.4 and Fig. 2.15, it can be seen that the differences between the pump and transducer pressures were relatively constant with small standard deviations (Table 2.4: refer to last four columns). The average differences between the pumps and transducers for each trial were within the range of 14.4 to 16.5 mm Hg except for that of Sample 2 during Trial 1 in Setup 1 (8.50 mm Hg). The average difference between the pressures measured by the transducers and their respective pumps excluding that outlier was 15.6 ± 0.67 mm Hg. As mentioned previously,

this difference may have been caused by a minor human or system error that was corrected before the other trials were performed. These results show that the setups were unable to produce consistent pressure measurements.

Table 2.5 compares the cumulative average $\Delta P$ for the annular trials using Samples 1 and 2 in Setups 1 and 2. From Table 2.5, it can be seen that the differences between the pressures measured in Setups 1 and 2 were higher for Sample 1 than they were for Sample 2 as shown by the positive values of $\Delta P_{smp1\text{-}2}$ (refer to last row). This was likely because the initial pressure for Sample 2 at the beginning of the flow trial was lower than that of Sample 1 (the average pressure in Trial 1). Although both samples were assembled with a 24G tube and a 28G nichrome wire insert, manufacturing tolerances likely caused a variation in the tubing and insert diameters. A larger tube inner diameter (ID) and/or a smaller insert outer diameter (OD) would have resulted in a larger flow area in Sample 2 than in Sample 1, resulting in Sample 2's lower average pressure (Table 2.5).

Table 2.5: Comparison among cumulative average pressures for the annular trials with Samples 1 and 2 in Setups 1 and 2

| | Transducer's $\Delta P_{c\_avg}$ (mm Hg)[a] | | Pump's $\Delta P_{c\_avg}$ (mm Hg)[a] | |
|---|---|---|---|---|
| | Setup 1 | Setup 2 | Setup 1 | Setup 2 |
| Sample 1 | 13.4 | 20.3 | 27.1 | 35.3 |
| Sample 2 | 8.17 | 8.66 | 21 | 24.4 |
| Difference between Samples 1 and 2, $\Delta P_{smp1\text{-}2}$ [b] | 5.23 | 11.64 | 6.1 | 10.9 |

[a] Cumulative average of $\Delta P_t$ or $\Delta P_p$ over Trials 1, 2 and 3

[b] $\Delta P_{smp1\text{-}2}$ = (Sample 1's $P_{c\_avg}$) – (Sample 2's $P_{c\_avg}$)

Again, from Table 2.4, the flow pressures were not relatively constant throughout the trials.

Note that, although baseline pressure readings (pressure measured without the test sample) were not subtracted from the measured pressure readings, this is not the cause for the inconsistency in pressure readings, since the baseline pressure is merely a result of tube resistance and head loss, which were not altered during the trials.

***Conclusion:*** *$\Delta P$ results increased over the course of the annular flow trials even though the same stiff non-degradable tube-insert samples were used under the same test conditions. Both pump and transducer pressure readings confirmed this trend, showing the same $\Delta P$ increase.*

***Next steps:*** *Perform more long-term (more than 2 hours) annular flow trials with the same tube-insert sample combinations in order to determine if this $\Delta P$ increase occurs during a continuous trial. This is to observe this trend of increasing $\Delta P$ over an extended uninterrupted trial.*

### 2.5.2. 20-Hour Annular Flow Validation Trials

***Research question:*** *Does the increase in $\Delta P$ that was observed in Section 2.5.1 occur during a continuous more-than-2-hour annular flow trial? Will the presence/absence of a temperature-controlled environment (incubator) affect the increase in $\Delta P$?*

Eight 20-hour trials were performed in Setups 1 and 2 in order to further investigate the pressure-rise-with-time issue. Two new samples were prepared. The testing procedure and sample setup are explained in Apps. B.1 and B.3. A 0.2% $NaN_3$ solution was used as the test fluid. The concentration of $NaN_3$ was increased from 0.04% to 0.2% in an attempt to address the issue of increasing $\Delta P$ that was observed during the 2-hour trials, assuming that this issue might be caused by microbial growth within the tubes. Two trials were performed for each sample in each setup, making a total of eight separate trials. With these trials, the effect of having an incubator was also tested. Similar to the 2-hour validation trials, baseline pressure data were not subtracted from the

measured pressure data. The incubator was used in Setup 1, but not in Setup 2. Experimental pressures are shown in Fig. 2.16; and the pressure data is summarized in Table 2.6.

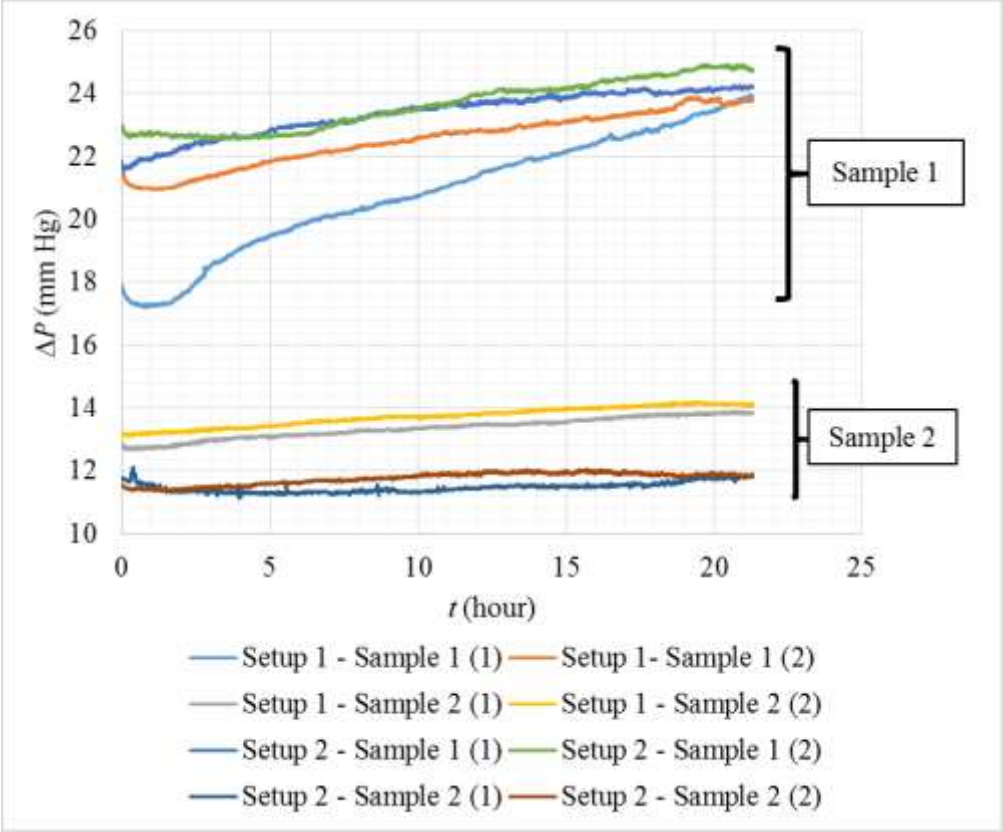


Fig. 2.16: Repeated 20-hour annular trial pressures for Samples 1 and 2 [March 30 - April 5, 2016] (note: Samples 1 and 2 here are not the same as Samples 1 and 2 in Figs. 2.10 and 2.13)

A gradual increase was observed from the first hour to the end of the experiment as shown in Fig. 2.16. From Table 2.6, the differences between the initial and final pressures of Sample 1 were consistently higher than those of Sample 2. It can also be observed that the presence/absence of the incubator did not appear to be the cause of the increase in pressure over time. Pressure still rose over time in both setups, although Setup 1 had an incubator and Setup 2 did not. Note that the average and initial pressures were consistently higher in the second trial for each combination of setup and sample, except for Sample 2 in Setup 2, wherein for the second trial, the initial pressure was slightly lower than the average pressure.

Table 2.6: Summary of pressure results of Samples 1 and 2 in Setups 1 and 2

| Sample | Setup | 1 (Incubator) | | 2 (No Incubator) | |
|---|---|---|---|---|---|
| | Trial | 1 | 2 | 1 | 2 |
| 1 | Date [a] | 30-Mar. | 31-Mar. | 1-Apr. | 2-Mar. |
| | Average $\Delta P$ (mm Hg)[b] | 20.85 | 22.53 | 23.36 | 23.63 |
| | Standard deviation of $\Delta P$ (mm Hg)[c] | 1.88 | 0.85 | 0.70 | 0.80 |
| | Initial $\Delta P$, $\Delta P_i$ (mm Hg) | 17.88 | 21.81 | 21.85 | 23.01 |
| | Final $\Delta P$, $\Delta P_f$ (mm Hg) | 23.89 | 23.76 | 24.20 | 24.73 |
| | Difference between $\Delta P_i$ and $\Delta P_f$, $\Delta P_{f-i}$ (mm Hg)[d] | 6.01 | 1.95 | 2.35 | 1.72 |
| 2 | Date [a] | 1-Apr. | 2-Apr. | 30-Mar. | 31-Mar. |
| | Average $\Delta P$ (mm Hg)[b] | 13.36 | 13.72 | 11.47 | 11.76 |
| | Standard deviation of $\Delta P$ (mm Hg)[c] | 0.33 | 0.31 | 0.16 | 0.19 |
| | Initial $\Delta P$, $\Delta P_i$ (mm Hg) | 12.84 | 13.14 | 11.80 | 11.53 |
| | Final $\Delta P$, $\Delta P_f$ (mm Hg) | 13.85 | 14.10 | 11.82 | 11.87 |
| | Difference between $\Delta P_i$ and $\Delta P_f$, $\Delta P_{f-i}$ (mm Hg)[d] | 1.00 | 0.96 | 0.02 | 0.34 |

[a] Day and month in the year 2016

[b] Pressure averaged over the 20-hour period shown in Fig. 2.16

[c] Standard deviation of pressure data over the 20-hour period shown in Fig. 2.16

[d] Difference between initial and final pressures ($\Delta P_{f-i} = \Delta P_f - \Delta P_i$)

Similar to the 2-hour trials (Section 2.5.1), the differences between the average pressures measured in the setups were higher for Sample 1 than for Sample 2 because the initial pressure for Sample 1 was higher. This was probably because the flow area of Sample 1 was smaller than that of Sample 2.

It was hypothesized that the increase in pressure observed in both the 2-hour and 20-hour trials could have been due to systemic problems of the pump or the transducer. Perhaps calibration errors or inconsistent output flow rates by the pumps. Another hypothesis was that, although the concentration of $NaN_3$ was increased, it was insufficient to prevent microbial growth from occurring in the tubes and in the sample. It was also possible that mineral deposition was occurring in the sections of the tubes between the pumps and the samples.

In order to determine the cause of this continuous rise in pressure, further experimental validation trials were performed in order to test the reliability of the pneumatic pumps in measuring pressure and flow rate, as well as the accuracy of the pressure transducers in measuring pressure in the test sample.

***Conclusion:*** *There was an obvious $\Delta P$ increase from the beginning to the end of each 20-hour flow trial. The presence/absence of a temperature-controlled incubator did not show a measurable effect on this increase in $\Delta P$. In addition, increasing $NaN_3$ concentration did not resolve the issue.*

***Next steps:*** *Perform validation flow trials to determine if the continuous increase in $\Delta P$ is caused by systemic error (faulty pump and/or pressure transducer) or by microbial growth in the tubing. Reduce $NaN_3$ concentration back to 0.04%, since higher concentrations of $NaN_3$ can be hazardous for the user.*

### 2.6. Further Validation of Pressure and Flow Rate Measurements

***Hypothesis:*** *The pump and pressure transducer measurements (flow rate and pressure) are accurate and reliable. The pump and transducer measurements will correspond with each other and with the measurements of other comparable fluid flow and pressure-measuring devices.*

As mentioned in Section 2.5, more extensive validation trials were performed on the pressure transducers and the pumps in both setups in order to determine if the pressure measurement error discussed in Section 2.5 was caused by errors in the pumps or transducers. Fundamentally, the pressure/flow rate measurements of the pumps/transducers were cross-checked between setups (Setup 1 versus Setup 2) and between each other (pump versus transducer measurements). If the flow measurements of the devices matched well between devices, the system would be deemed to be accurate, and system error was not the cause of the continuous rise in pressure measurement described in Section 2.5.

### 2.6.1. Verification of Pump Pressure and Flow Rate Measurement Accuracy

The pumps are microfluidic pneumatic precision pumps by CorSolutions that can pump fluid at flow rates between 0 and 50 μl/min (± 0.125 μl/min). The pumps can be run in two modes: flow mode (0 - 50 μl/min) and pressure mode (0 - 1 bar) [46].

In Section 2.5.1, it was verified that the pumps corresponded well with the transducers in their respective setups. However, it was not verified whether the pumps' internal pressure-measuring systems were accurate. Each pump contains a microprocessor, a compressor regulation system that pressurizes the air in the bottle in order to pump fluid, and an in-line flow sensor that measures the actual flow rate of the fluid leaving the bottle [46]. The microprocessor sends commands to the pressure regulation system which pressurizes the fluid in the bottle according to the flow sensor readings [46]. Since Pump 1's output flow rates/pressures are based on Pump 1's internal flow rate and pressure measurements, it was vital to ensure that this internal measuring system was reliable.

To verify the accuracy of Pump 1's flow rate and pressure measurements, Pump 1 was placed in series with Pump 2 as shown in Fig. 2.17. Pump 2 pumped fluid from the bottle to the

test section, and Pump 1 functioned as the flow sensor measuring the flow rate of the fluid coming from Pump 2. The pressure measured by Pump 1 was compared with the pressure measured by the transducer in Setup 1. The flow rate measured by Pump 1 was compared with the flow rate measured by Pump 2.

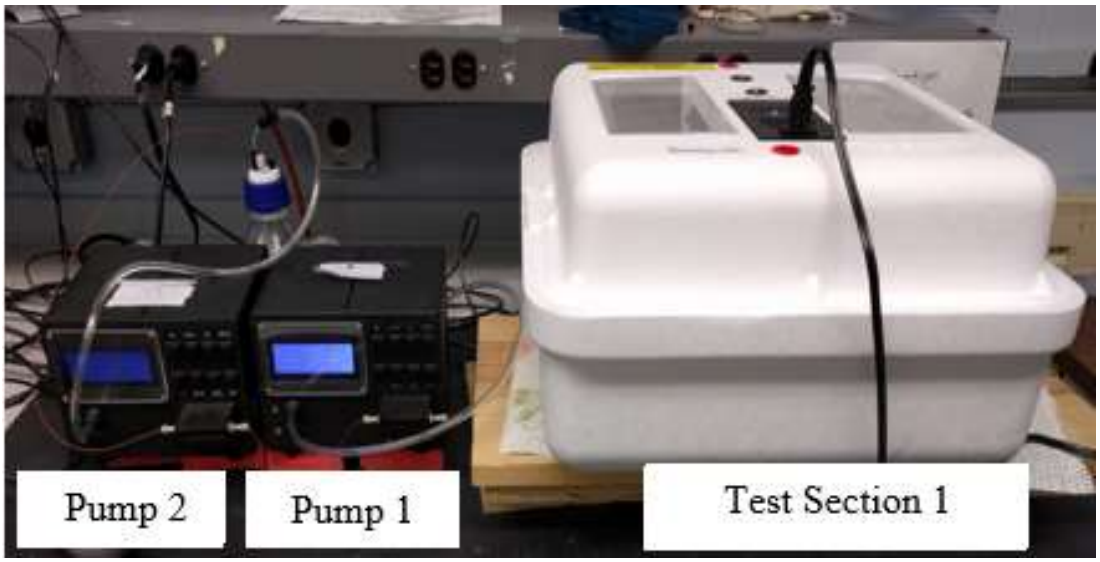


Fig. 2.17: Setup of pump in-line pressure-measurement check

Approximately 18-hour annular flow trials were performed using 1.5 inch (38.1 mm) long 24G SS tubes with 28G SS inserts. The test sample preparation and trial procedures are described in Apps. B.1 and B.3. A 0.04% $NaN_3$ solution was the fluid used in these trials. SS inserts were used instead of the 28G nichrome inserts used in Section 2.5 in order to investigate the effect of tube/insert material on the pressure drop through the tubes.

To evaluate the accuracy of the pumps' pressure measurements, Pump 2's pressure plots were compared with Transducer 1's pressure plots as described in Section 2.6.1(a). To evaluate the accuracy of pumps' flow rate measurements, Pump 1's flow rates were compared with those of Pump 2 as described in Section 2.6.1(b).

### a) ***Pressure Measurement Verification (Pump versus Transducer)***

***Research question:*** *Will the pressure measurements of the pneumatic pumps correspond with those of the pressure transducers connected to them?*

The experimental pressure plots of Transducer 1 (transducer in Setup 1) and Pump 2 are shown in Figs. 2.18 and 2.19, respectively. From Figs. 2.18 and 2.19, the same gradual pressure increase over time is observed. The pressure trends of the transducer and the pump corresponded well with each other. The difference between the transducer and pump pressures were calculated and plotted as shown in Fig. 2.20. Table 2.7 summarizes the averages and standard deviations of Transducer 1's and Pump 1's pressure data.

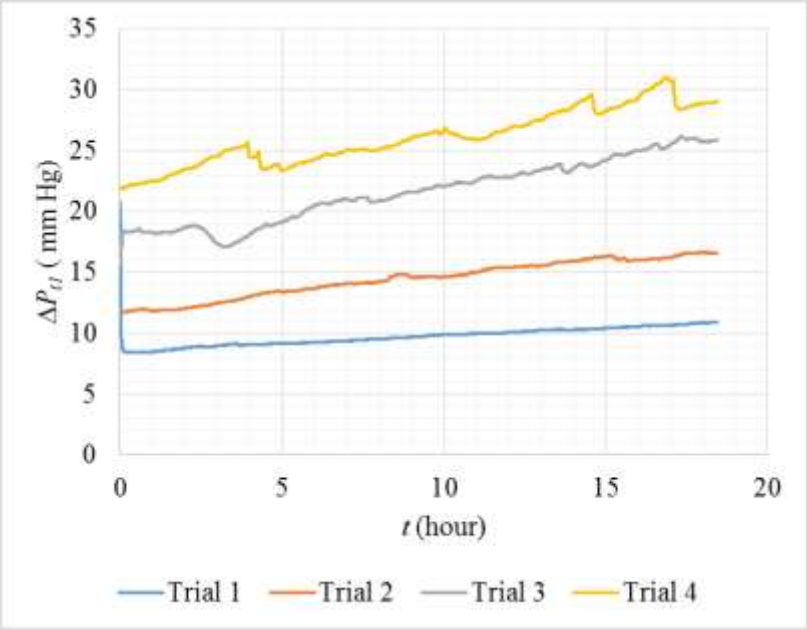


Fig. 2.18: Transducer 1 pressure plot for annular trials in Setup 1, $\Delta P_{t1}$ [October 26 - 29, 2016]

From Table 2.7 and Fig. 2.20, it can be seen that the average difference between the transducer pressure and the pump pressure were relatively constant throughout all four trials with a very small average standard deviation of 0.19 mm Hg. Pump 2's pressure trends matched well with the Transducer 1's pressure trends.

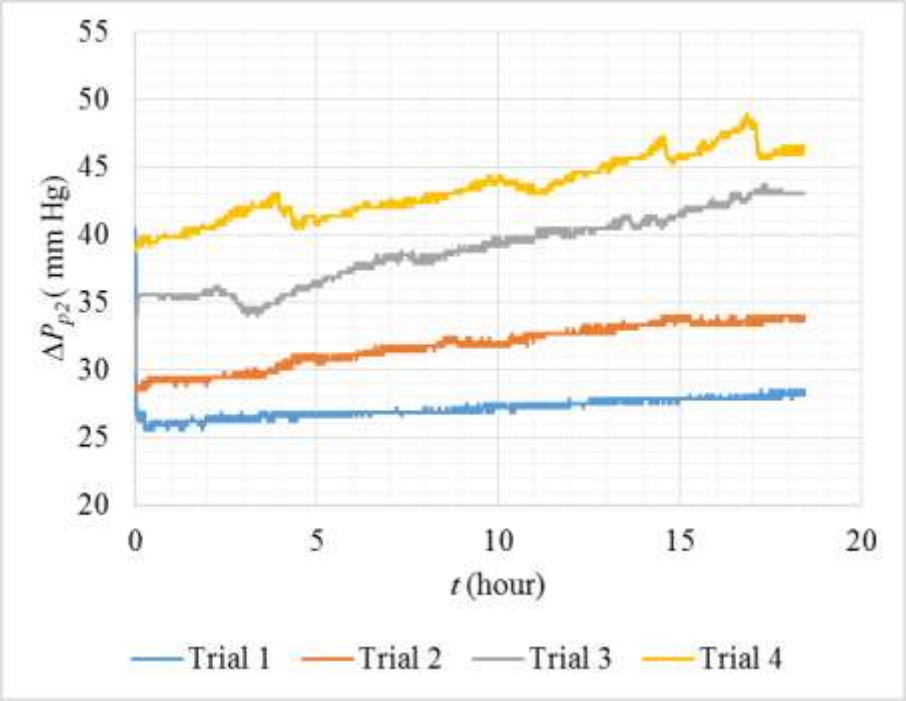


Fig. 2.19: Pump 2 pressure plot for annular trials in Setup 1, $\Delta P_{p2}$ [October 26 - 29, 2016]

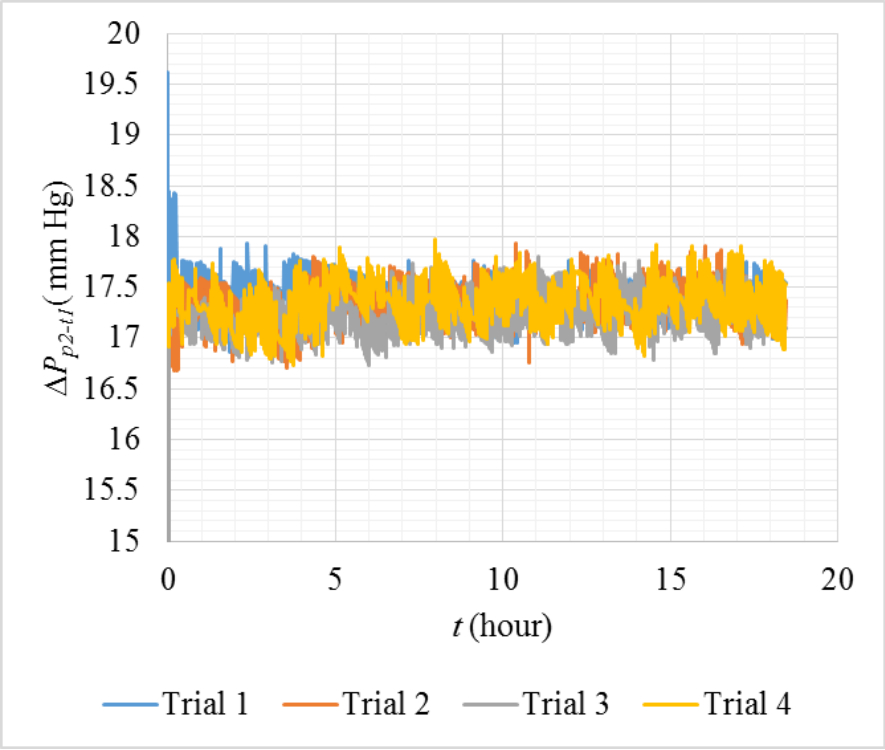


Fig. 2.20: Plot of difference between Transducer 1 and Pump 2 $\Delta P$, $\Delta P_{p2\text{-}t1}$ ($\Delta P_{p2\text{-}t1} = \Delta P_{p2} - \Delta P_{t1}$)

Table 2.7: Averages and standard deviations of Transducer 1 and Pump 1 pressure data

| Trial Number | Average $\Delta P$ (mm Hg) | | |
|---|---|---|---|
| | Transducer 1, $\Delta P_{t1}$ | Pump 2, $\Delta P_{p2}$ | Difference, $\Delta P_{p2\text{-}t1}$ [c] |
| 1 | $9.70^{a} \pm 0.72^{b}$ | $27.09^{a} \pm 0.70^{b}$ | $17.39^{a} \pm 0.17^{b}$ |
| 2 | $14.43^{a} \pm 1.51^{b}$ | $31.76^{a} \pm 1.57^{b}$ | $17.33^{a} \pm 0.18^{b}$ |
| 3 | $21.60^{a} \pm 2.60^{b}$ | $38.81^{a} \pm 2.66^{b}$ | $17.21^{a} \pm 0.20^{b}$ |
| 4 | $26.06^{a} \pm 2.26^{b}$ | $43.40^{a} \pm 2.28^{b}$ | $17.34^{a} \pm 0.20^{b}$ |
| Cumulative Average | $17.95^{d} \pm 1.77^{e}$ | $35.27^{d} \pm 1.80^{e}$ | $17.32^{d} \pm 0.19^{e}$ |

[a] Average $\Delta P$ over the 18 hour period shown in Figs. 2.18 and 2.19
[b] Standard deviation of $\Delta P$ over the 18 hour period shown in Figs. 2.18 and 2.19
[c] Difference between transducer pressure and pump pressure averaged over 18 hour period shown in Fig. 2.20 ($\Delta P_{p2\text{-}t1} = \Delta P_{p2} - \Delta P_{t1}$)
[d] Cumulative average of the average $\Delta P$s over Trials 1, 2, 3 and 4
[e] Average standard deviation of the $\Delta P$s over Trials 1, 2, 3 and 4

From Table 2.7, it can be seen that the pressure data measured by Pump 2 were consistently higher than the pressures measured by Transducer 1. As mentioned in Section 2.5.1, this is because the pump sensor is located upstream of the test section as compared to the transducer that is located downstream at the test section; and the pressure measured by the pump may include additional pressure loss due to tube resistance and head loss. The differences between the pressure readings of Transducer 1 and Pump 2 were consistently at an average of 17.32 mm Hg with small average standard deviation of 0.19 mm Hg. In general, the pressure measured by the Pump 2 and the Transducer 1 match well with each other.

***Conclusion:*** *The $\Delta P$ measurements from the pump matched well with the $\Delta P$ measurements of the connected pressure transducer.*

***Next steps:*** *Perform flow trials to validate the accuracy of the pumps' flow rate measurements since the pumping mechanisms of the pumps are dependent on their respective internal flow sensors. Externally measure the output flow rate of the pneumatic pumps by placing the pumps in-line during a flow trial [where one pump measures the output flow rate of the other pump].*

***b) Flow Rate Measurement Verification (Pump 1 versus Pump 2)***

***Research question:*** *Will the flow rate measurements of the two pneumatic pumps correspond with each other when placed in-line?*

The flow rate measured by Pump 1 was compared with that of Pump 2. Pump 1 functioned as a second flow rate measuring device, and Pump 2 pumped fluid out of the bottle to the test section and measured flow rate. Figures 2.21 and 2.22 show the flow rates measured by Pump 1 and Pump 2, respectively. Since the flow rate was set at 2.5 μl/min, both pump flow rate readings should have remained constant at 2.5 μl/min for all four trials. This constancy in flow rate can be observed in Figs. 2.21 and 2.22.

It is noted in Fig. 2.21, that there was a slight drop in flow rate in the period of 15 hours and 20 hours for Trial 2. This drop was not seen in the Pump 2 data of Fig. 2.22. This slight variation of Pump 1's flow rate reading was minor and was probably due to a small error in the pump system or someone bumping into the system at the time. The test setups are very sensitive. Slight movements of the systems could affect the readings of the pumps/transducers. In Table 2.8, it can be seen that the average differences between the flow rate readings of Pumps 1 and 2 were very close, with only a 0.02 μl/min difference.

The average flow rate measured by Pump 1 (2.49 μl/min) was only slightly lower than that of Pump 2 (2.50 μl/min); but overall the flow rates were the same with a very small average

standard deviation of 0.02 mm Hg. Therefore, it was concluded that the flow rate measurements of Pumps 1 and 2 were consistently in agreement with each other.

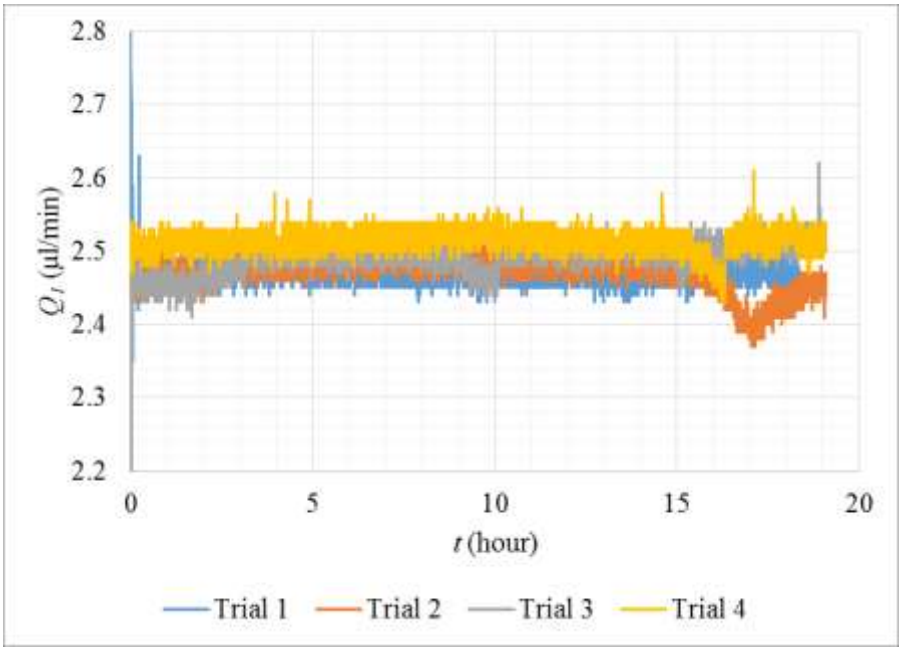


Fig. 2.21: Pump 1 flow rate, $Q_1$, for annular trials in Setup 1. Pump 1 as flow sensor [October 26 - 29, 2016]

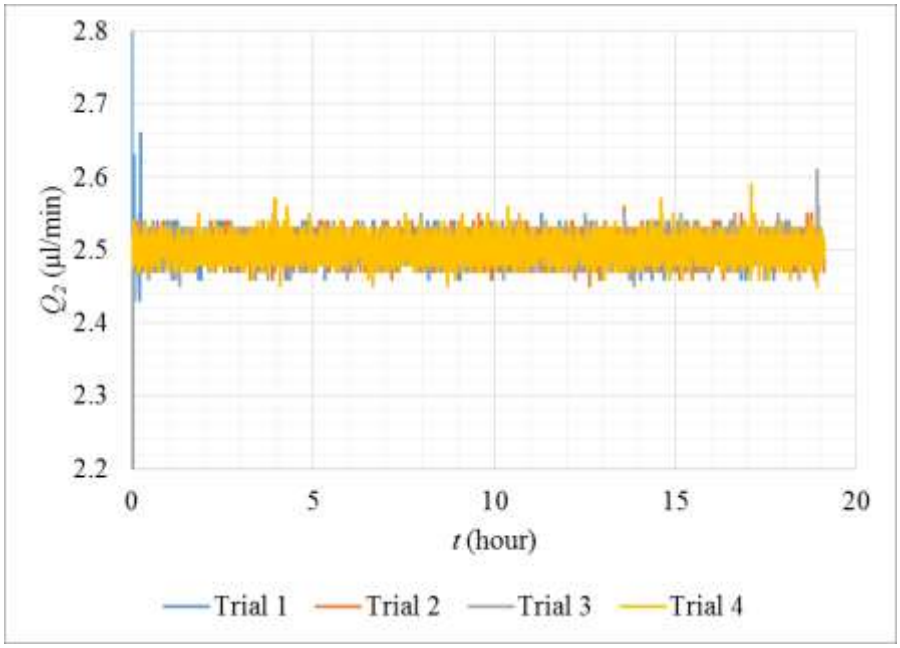


Fig. 2.22: Pump 2 flow rate for annular trial in Setup 1. Pump 2 as pump [October 26 - 29, 2016]

Table 2.8: Averages and standard deviations of flow rates measured by Pumps 1 and 2

| Trial Number | Pump 1 flow rate, $Q_1$ [Flow sensor] (µl/min)[a] | Pump 2 flow rate, $Q_2$ [Pump] (µl/min)[a] | Difference in flow rate, $Q_{2-1}$ (µl/min)[c] |
|---|---|---|---|
| Trial 1 | $2.47^a \pm 0.01^b$ | $2.50^a \pm 0.02^b$ | 0.03 |
| Trial 2 | $2.47^a \pm 0.02^b$ | $2.50^a \pm 0.01^b$ | 0.03 |
| Trial 3 | $2.49^a \pm 0.03^b$ | $2.50^a \pm 0.02^b$ | 0.01 |
| Trial 4 | $2.51^a \pm 0.02^b$ | $2.50^a \pm 0.01^b$ | -0.01 |
| Cumulative Average | $2.49^c \pm 0.02^d$ | $2.50^c \pm 0.02^d$ | $0.02^e$ |

[a] Average $Q$ over the 18 hour period shown in Figs. 2.21 and 2.22
[b] Standard deviation of $Q$ over the 18 hour period shown in Figs. 2.21 and 2.22
[c] Difference between $Q_1$ and $Q_2$ averaged over the 18 hour period shown in Figs. 2.21 and 2.22 ($Q_{2-1} = Q_2 - Q_1$)
[d] Average standard deviation of $Q_1$ or $Q_2$ over Trials 1, 2, 3 and 4
[e] Average of the absolute values of $Q_{2-1}$ over Trials 1, 2, 3 and 4

***Conclusion:*** *The flow rate measurements of Pump 1 matched these of Pump 2 with very small variation (difference between average measured flow rate of Pumps 1 and 2 was 0.02 µl/min).*

***Next steps:*** *Perform trials to rule out the possibility that there was a consistent system issue with both pumps' internal flow sensors due to a manufacturing problem. This was done by comparing the flow measurements of the pneumatic pumps with the output flow rate of a different type of pump (syringe pump).*

### 2.6.2. Pneumatic Pump Check Against Syringe Pump

***Research question:*** *Will the flow rate measurements of the pneumatic pumps correspond with the output flow rate of a syringe pump? Is there a consistent manufacturing issue with the pneumatic pump flow sensors?*

Further trials were performed to cross-check the measurements of the pneumatic pumps with a syringe pump in order to fully rule out the possibility that there was a system issue that existed in both pneumatic pumps. Unlike the pneumatic pumps, the syringe pump does not function based on a feedback loop. Fluid is pushed out of the syringe at a set rate via a small step angle stepping motor that drives a precision lead screw and pusher block against the piston of a syringe [47]. A kdScientific syringe pump (Legato 100) was used, which could deliver 2.5 μl/min with a ± 0.05 μl/min accuracy for a 100 ml syringe [47].

Specifications of the kdScientific syringe pump are given in App. C.1. The accuracy or accuracies of the pneumatic pumps' measurements was checked by comparing the flow rate measurements of the two different pumping mechanisms. If the measurements matched well, it would be concluded that the pneumatic pump system was accurate.

The syringe used for these trials was a 5 ml BD Plasti-Pak syringe (BD Medical). This syringe was chosen because it did not leak and produced flow rates that matched the calculated flow rates from measuring the output volume and the time taken to remove 2 ml of fluid from the syringe. (Time taken to remove volume in syringe = volume in syringe / flow rate.) Table D.2.1a, D.2.1b, D.2.2a and D.2.2b were used for recording the input parameters (input flow rate and syringe volume) and output parameters (output volume and infusion time) of the syringe pump. The syringe pump and the pneumatic pump (Pump 2) were placed in-line as shown in Fig. 2.23.

The syringe pump dispensed fluid through the tube of the pneumatic pump's flow sensor and into the test section. A total of six trials were performed at the set flow rate of 15 μl/min (3 trials) and 30 μl/min (3 trials), using the same test procedures as described in App. B.1. No test samples were used in these trials. The syringe was filled with 2 ml of 0.04% $NaN_3$ solution. Table 2.9 compares the input parameters of the syringe and the actual output parameters measured.

Figure 2.24 shows the flow rate measured by the pneumatic pump flow sensor.

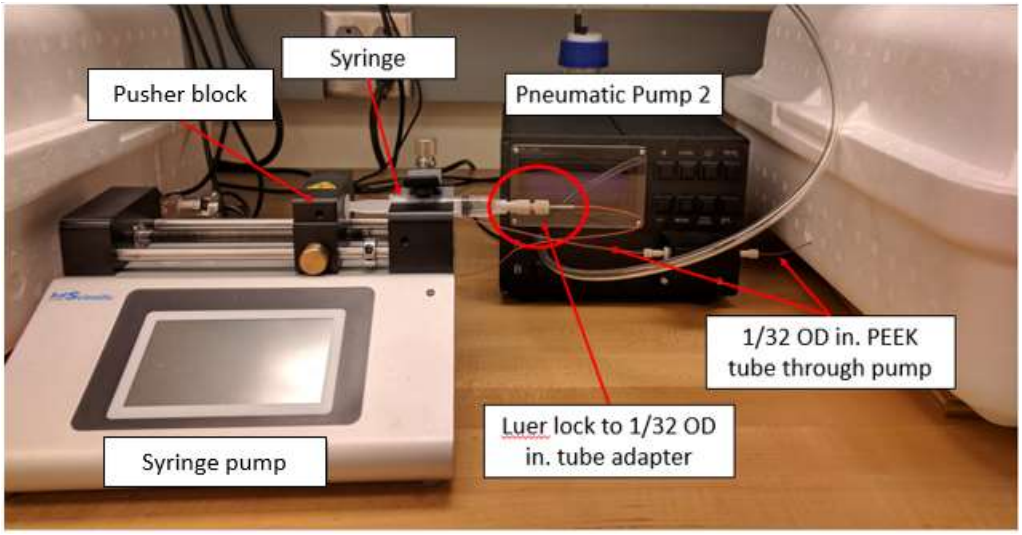


Fig. 2.23: Syringe pump and pneumatic pump placed in-line

Table 2.9: Averages of the input flow parameters (syringe pump) compared with the measured output flow parameters (pneumatic pump flow sensor) for all trials at input flow rates of 15 µl/min and 30 µl/min

| Input flow rate, $Q_i$ (µl/min) | 15 | 30 |
|---|---|---|
| Volume in syringe, $V$ (ml) | 2.0 | 2.0 |
| Average measured output flow rate, $Q_o$ (µl/min)[a] | 14.57 | 28.41 |
| Percentage error between $Q_i$ and $Q_o$, $Q_{i\text{-}o}$ [b] | 3% | 6% |
| Calculated infusion time, $t_{calc}$ (hour)[c] | 2.22 | 1.11 |
| Actual infusion time, $t_{act}$ (hour)[d] | 2.32 | 1.16 |
| Percentage error between $t_{act}$ and $t_{calc}$, $t_{a\text{-}c}$ [e] | 4.4% | 4.4% |

[a] Average $Q_o$ over three trials at each $Q_i$ setting measured by the pneumatic pump. $Q_o$ of each trial was averaged over 0.15 - 1.1 hours and 0.3 - 2.2 hours for $Q_i$ at 15 and 30 µl/min, respectively

[b] $Q_{i\text{-}o} = [(Q_i - Q_o) / Q_o] \times 100$

[c] $t_{calc}$ (hour) = $V$ (µl) / $Q_i$ (µl/hour)

[d] Average $t_{act}$ of the three trials at each $Q_i$ setting. $t_{act}$ was taken to be the period from the beginning of the trial to the time when the $Q_o$ fell to 0.2 µl/min

[e] $t_{a\text{-}c} = [(t_{act} - t_{calc}) / t_{calc}] \times 100$

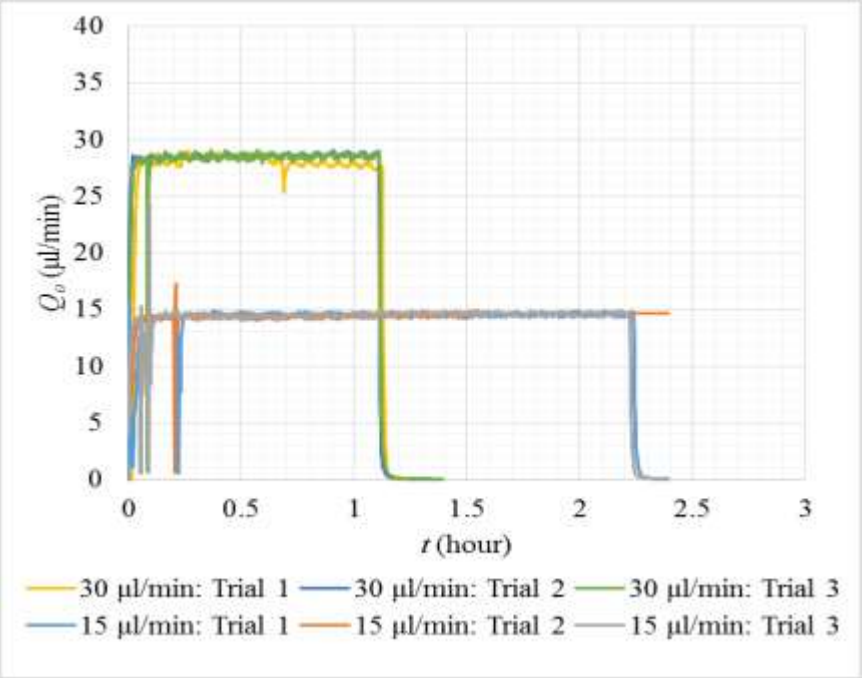


Fig. 2.24: Plot of output flow rates ($Q_o$) of syringe pump for fluid volume of 2 ml in a BD plastic syringe when set at flow rates 15 µl/min and 30 µl/min (measured with pneumatic pump)

It can be seen that the flow rate measured by the pneumatic pump corresponded with the input parameters of the syringe pump with small errors of at most 6% (Fig. 2.24 and Table 2.9). Based on calculations, the time it takes to completely infuse 2 ml of fluid from the syringe at a flow rate of 15 µl/min and 30 µl/min is 2.2 hours and 1.1 hours, respectively. The actual infusion time was only 4.4% different from the expected infusion time. Therefore, the flow rate measured by the pneumatic pump corresponded well with the output flow rate of the syringe pump with a difference of less than 6%. Refer to Table D.2.1a, D.2.1b, D.2.2a and D.2.2b for more details.

***Conclusion:*** *The flow rate measurements of the pneumatic pump corresponded well the output flow rate of the syringe pump within less than 6% difference. Therefore, the pneumatic pumps' internal flow sensors are accurate within 6% when measuring flow rate of the syringe pump.*

***Next steps:*** *After verifying that the pump flow rate measurements of the pneumatic pumps were*

*accurate within less than 6% error, the next task was to verify the accuracy of the pressure transducers. This task involved comparing the pressure readings of the transducers with another transducer from a different manufacturer.*

### 2.6.3. Verification of Transducer Pressure Measurement Accuracy

***Research question:*** *Can the pressure transducers used in the experimental setups accurately and reliably measure the differential pressure in a GDI-like tube? Will the pressure measurements of the transducers in the setups (Transducer 1 or 2) match the pressure measurements of a different type of transducer (Transducer 3) when measuring the differential pressure in the same sample?*

The transducers in the setups are Omega transducers (PX429-2.5GV) that can measure fluid pressures in the ranges of 0 to 2.5 psi (0 - 130 mm Hg). In Section 2.6.1, it was determined that the transducer pressure readings corresponded with the pump readings. However, to completely verify that the transducers were measuring pressure accurately, the readings of the Omega transducers were compared with the readings of another transducer from a different manufacturer. The third transducer was purchased from Dwyer. Unlike the Omega transducer, the Dwyer pressure transducer was current output instead of voltage output. Therefore, a current input data logger was purchased from Omega. Specifications of the Dwyer transducer and the Omega current input data logger are in Apps. C.2 and C.3.

For these trials, four 2-hour single open tube trials were performed with two 25 mm long 50 μm ID VSD tubes (2 trials per sample). The test procedures and test sample preparation are described in Apps. B.1 and B.3. A 0.04% $NaN_3$ solution was used in these trials.

The Dwyer transducer (Transducer 3) was placed in-line with the Omega transducer in Setup 1 (Transducer 1) as shown in Fig. 2.25. This was to ensure that the two transducers measured

the pressure difference at relatively the same point.

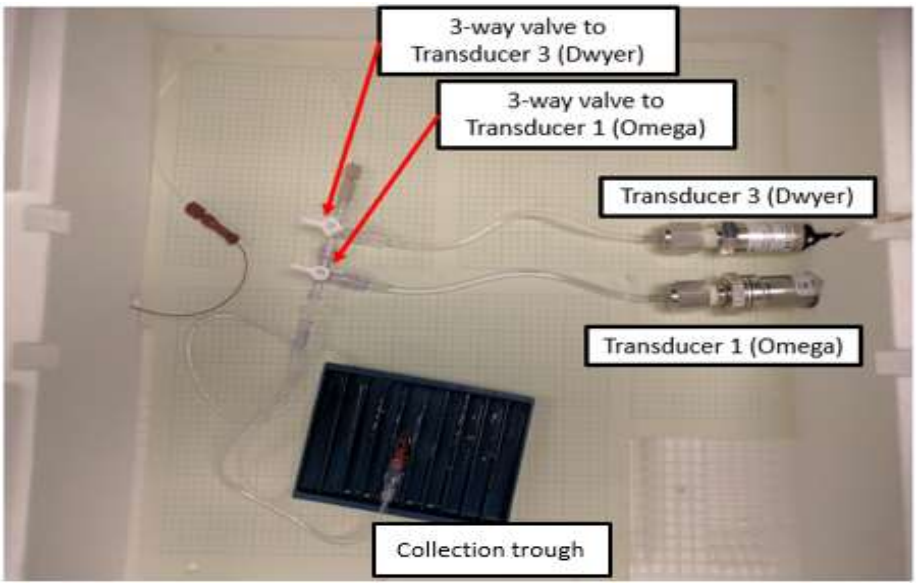


Fig. 2.25: Transducer 1 (Omega) placed in-line with Transducer 3 (Dwyer) in Setup 1

The pressure plot of the Omega transducer and the Dwyer transducer for the four trials is shown in Figs. 2.26 and 2.27, respectively. From looking at Figs. 2.26 and 2.27, it can be seen that the pressure trend of Transducer 1 corresponds with the pressure trend of Transducer 3. To determine if both transducers were reporting the same pressure trend, the differences between the pressures measured by Transducer 1 and Transducer 3 at each data point were calculated and plotted in Fig. 2.28. The comparison between the averages and standard deviations of the pressures measured by Transducers 1 and 3 are listed in Table 2.10.

It can be seen in Table 2.10 that the average of the differences between Transducer 1 and Transducer 3 is 1.26 mm Hg. The differences between the pressures are also relatively constant at each data point, with a small average standard deviation of 0.13 mm Hg. The pressure measurements of Transducer 1 (Omega) and Transducer 3 (Dwyer) match. Therefore, the Omega transducers measure pressure accurately. Pressure transducer system error is not the cause for the

inconsistency in pressure measurement found in Sections 2.5.1 and 2.5.2.

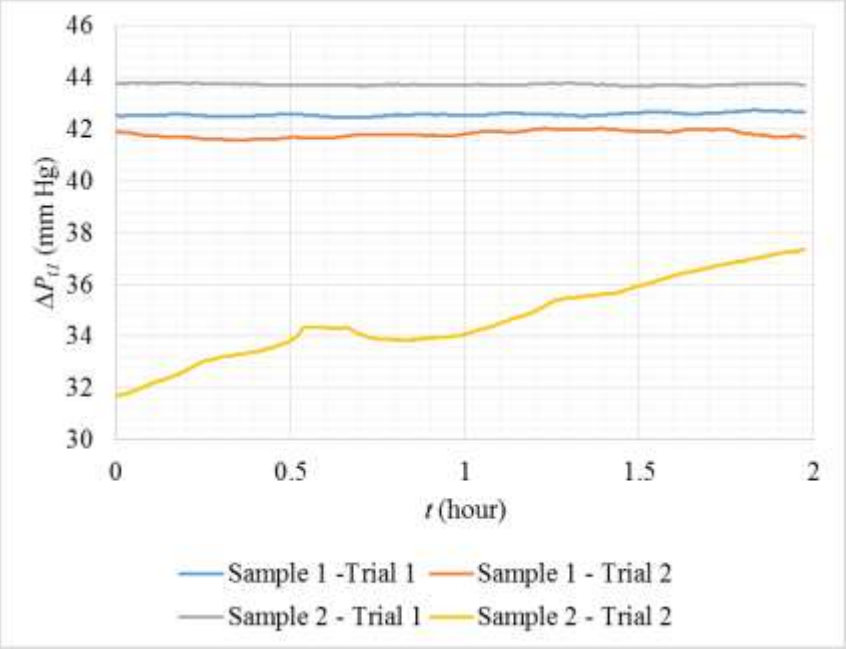


Fig. 2.26: Transducer 1 (Omega) pressures for Samples 1 and 2 in trials with 50 μm ID VSD tubing [May 30 - 31, 2017]

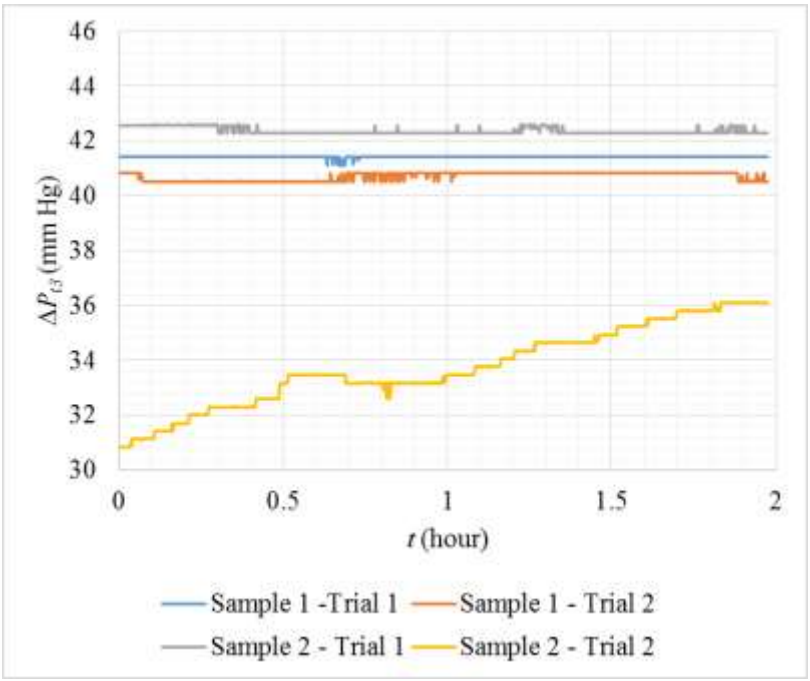


Fig. 2.27: Transducer 3 (Dwyer) pressures for Samples 1 and 2 in trials with 50 μm ID VSD tubing [May 30 - 31, 2017]

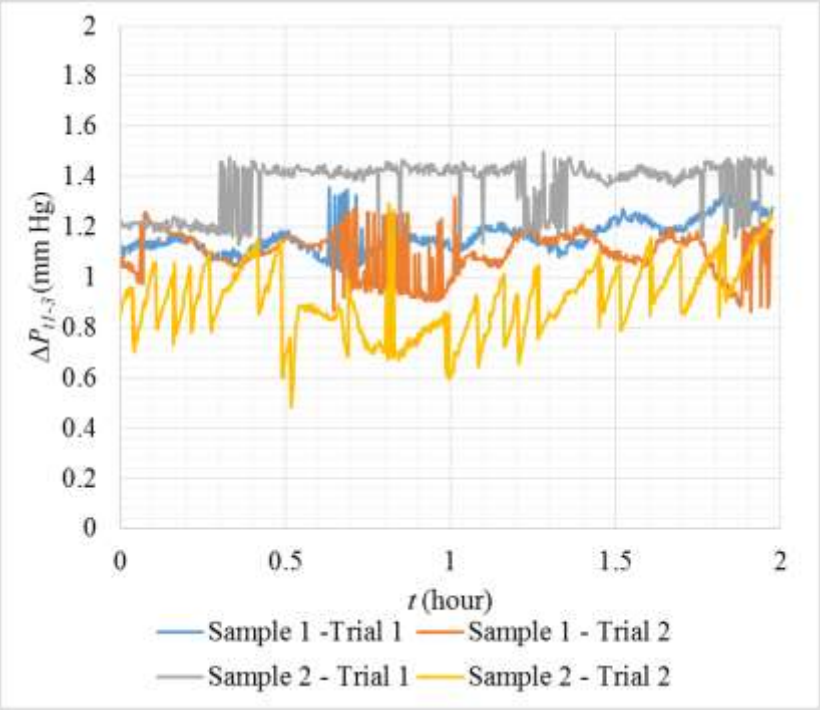


Fig. 2.28: Pressure difference between Transducers 1 (Omega) and 3 (Dwyer) for trials with 50 µm ID VSD tubing [May 30 - 31, 2017]

Table 2.10: Comparison of averages and standard deviations of pressures measured by Transducers 1 and 3 for trials with 50 µm ID VSD tubing

| Sample Number | Trial Number | $\Delta P$ (mm Hg) | | |
|---|---|---|---|---|
| | | Transducer 1, $\Delta Pt_1$ | Transducer 3, $\Delta Pt_3$ | Difference, $\Delta P_{t1-3}$ [c] |
| 1 | 1 | $42.91^{a} \pm 0.22^{b}$ | $41.66^{a} \pm 0.22^{b}$ | $1.25^{a} \pm 0.08^{b}$ |
| | 2 | $45.02^{a} \pm 1.98^{b}$ | $43.79^{a} \pm 1.91^{b}$ | $1.24^{a} \pm 0.14^{b}$ |
| 2 | 1 | $44.01^{a} \pm 0.19^{b}$ | $42.69^{a} \pm 0.23^{b}$ | $1.32^{a} \pm 0.09^{b}$ |
| | 2 | $38.35^{a} \pm 3.15^{b}$ | $37.13^{a} \pm 3.05^{b}$ | $1.22^{a} \pm 0.19^{b}$ |
| Cumulative Average | | $42.57^{d} \pm 1.39^{e}$ | $41.32^{d} \pm 1.35^{e}$ | $1.26^{d} \pm 0.13^{e}$ |

[a] Average $\Delta P$ over the period of 0-2 hours

[b] Standard deviation of $\Delta P$ over the period of 0-2 hours

[c] Difference between $\Delta Pt_1$ and $\Delta Pt_3$ at each data point ($\Delta P_{t1-3} = \Delta P_{t1} - \Delta P_{t3}$)

[d] Average of $\Delta P_{t1}$, $\Delta P_{t3}$ or $\Delta P_{t1-3}$ over the four trials

[e] Average standard deviation of $\Delta P_{t1}$, $\Delta P_{t3}$ or $\Delta P_{t1-3}$ over the four trials

***Conclusion:*** *The pressure measurements of Transducer 1 (voltage output) correspond with the pressure measurements of Transducer 3 (current output). Therefore, the transducers used in the setups can reliably and accurately measure differential pressures in GDI-like tubes. Based upon measurements, it can be concluded that the issue of continuously increasing* $\Delta P$ *was not caused by systemic issues with the pumps or transducers, but likely caused by deposition of particles in the tubes as a result of microbial growth.*

***Next steps:*** *Perform flow trials to determine if this* $\Delta P$ *increase was caused by microbial growth.*

### 2.6.4. Conclusion after Pressure and Flow Rate Measurement Validation

After comparing the pressures measured by the pumps and the pressures measured by the transducers, it was determined that the pump and the transducer pressure results from both setups matched well with each other (Section 2.4). To determine if the pumps correlated with one another, the pressure measurements of the pumps in Setups 1 and 2 were compared. The pressures measured by both pumps for the same sample corresponded well with each other (Section 2.6.1).

Based on the test comparing measurements of pneumatic Pump 2 and a syringe pump, it was found that the pressure data between the pneumatic pump and the syringe pump compared reasonably well (Section 2.6.2). Therefore, it can be concluded that the pneumatic pumps provide accurate flow rate measurements. The accuracy of the transducers (manufacturer: Omega) in Setups 1 and 2 were also compared and validated with a third transducer from a different manufacturer (Dwyer) (Section 2.6.3). It was found that the pressure readings of the Omega transducers matched well with the Dwyer transducer.

Therefore, it was concluded that the continuous increase in pressure reading during long-term trials was not due to systemic errors in the transducers or the pumps. This rise in pressure

was hypothesized to be caused by particle deposition or bacterial growth somewhere along the pump lines or within the sample where the cross-sectional diameter is smallest (less than 1/32 in. = 0.80 mm). Increasing $NaN_3$ concentration did not help in resolving the issue of increasing $\Delta P$. The next course of action was to investigate whether this issue was caused by microbial growth.

## 2.7. Investigating the Effect of Microbial Growth on $\Delta P$

After determining that systemic errors in the pumps and transducers were not the cause for the continuously increasing $\Delta P$ during the trials with stiff non-degradable tubes and inserts, the next course of action was to determine if this issue was truly caused by microbial growth.

### 2.7.1. Micro-CT Imaging to Investigate the Possibility of Microbial Deposits

***Research question:*** *Was the continuous $\Delta P$ increase during flow trials caused by microbial growth?*

In an effort to investigate this possibility of microbial growth in the tubes, micro-CT scans were taken of samples before and after trials in order to determine if deposits in the tubes or on the inserts could be detected through comparison of the scans. Two 10-day flow trials with 50 μm and 75 μm ID VSD tubes were performed before any cleaning or sterilization was done on the setups. The trials were performed at a flow rate of 2.5 μl/min and at 25°C. The test procedures and test sample preparation are described in App. B.1. A 0.04% $NaN_3$ solution was the fluid used in these trials. The $\Delta P$ results for the flow trials are shown in Fig. 2.29.

As observed in Fig. 2.29, the $\Delta P$ results did not remain constant over the 10-day trials, varying up to 50 mm Hg and 200 mm Hg (differences between maximum and minimum values) for the 50 μm and 75 μm samples, respectively. Contrary to theory, the 75 μm sample showed a larger increase in $\Delta P$ as compared to the 50 μm sample. Therefore, micro-CT scans were taken of the 75 μm ID VSD tube sample after the 10-day trial to determine if deposits could be seen in the

tube sample. Micro-CT scans were taken using the Xradia MicroXCT-400 tomographic X-ray microscope and are shown in Fig. 2.30 (±1.5 μm accuracy). More details about the MicroXCT are given in Section 3.1.3, and more examples of micro-CT scans are shown in App. E.

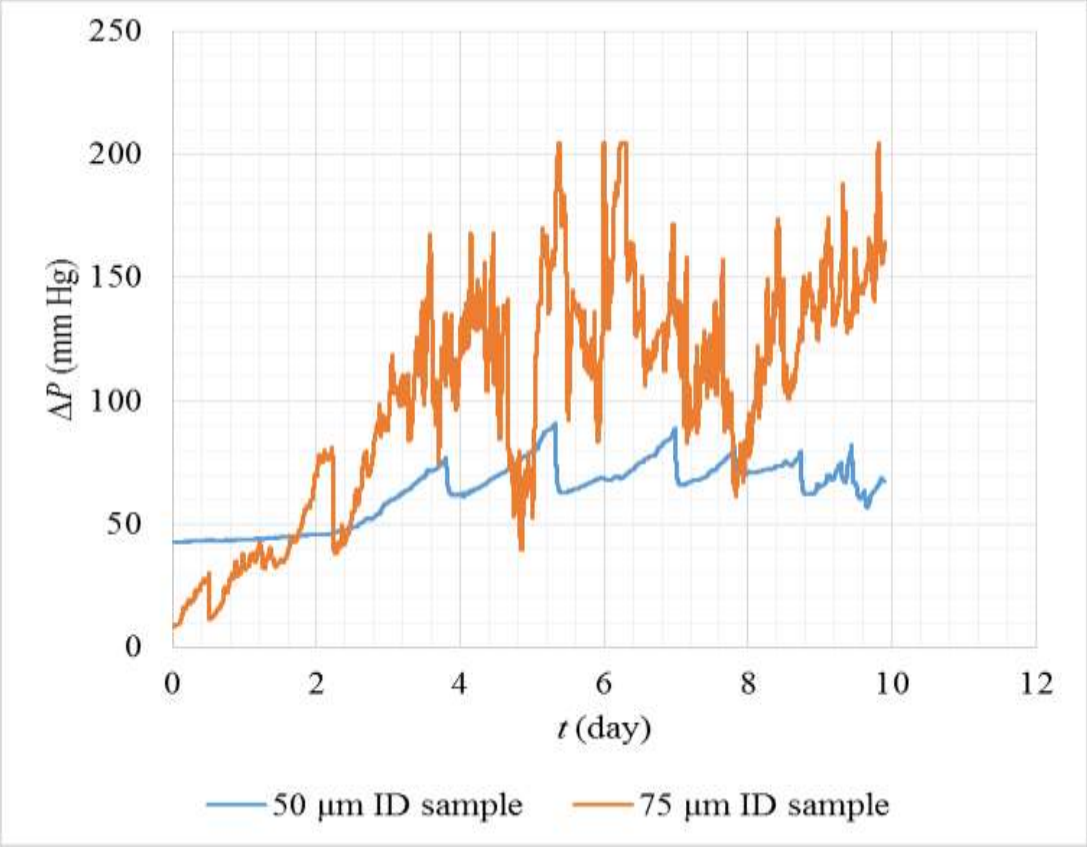


Fig. 2.29: Pressure plots for 10-day 50 μm and 75 μm ID VSD tube flow trials [December 21 - 31, 2016]

From Fig. 2.30, it appears that there were no deposits on the inner wall of the 75 μm tube. The tube appeared smooth and relatively uniform. This observation implies that microbial growth was not the cause for the large increase in Δ*P*. However, it was still possible that flow-restricting-deposits were present in the tubes, but that the density was too low to be shown on the micro-CT scans. The density of the deposits could have been approximately that of air, creating relatively little contrast between the air in the tube and the deposits. Thus, it would not show on the scans.

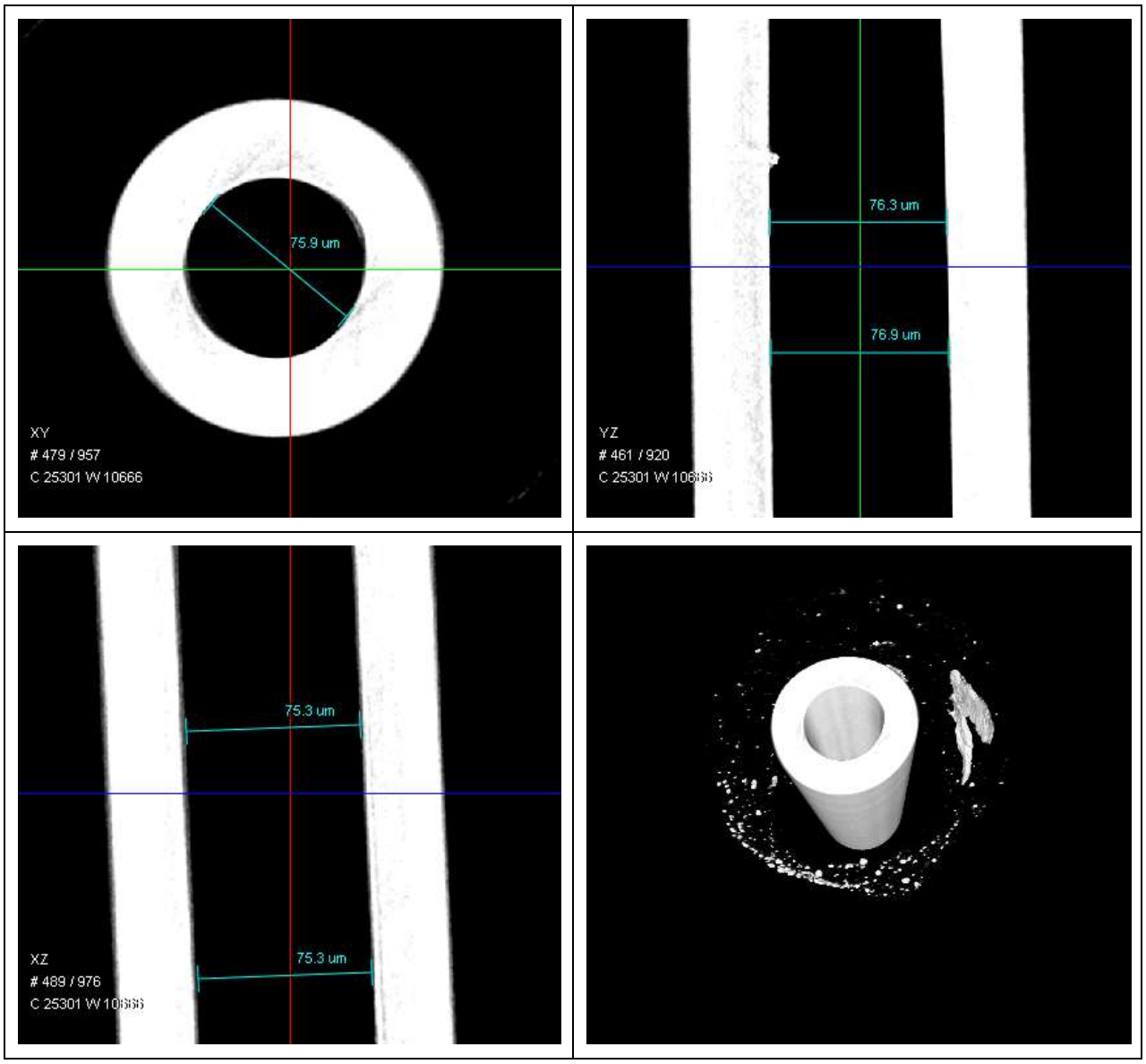


Fig. 2.30: Micro-CT images in the X-Y plane [top left], Y-Z plane [top right], X-Z plane [bottom left], and three-dimensions [bottom right] of the 75 µm VSD tube sample after the 10-day trial to test for microbial growth (magnification: 40x) [January 30, 2017]

Another flow trial was performed to further investigate the possibility of microbial deposits on the sample by comparing micro-CT scans of a sample before and after the trial. This time, an annular flow trial was performed using a 24G SS tube with 28G nichrome wire insert; and micro-CT scans were taken of the sample before and after the trial. The testing procedure and sample setup are explained in App. B.1. The trial was performed at the flow rate of 2.5 µl/min and room

temperature (25°C), using 0.04% $NaN_3$ solution. The $\Delta P$ plot of the trial is shown in Fig. 2.31. The micro-CT images of the sample before and after the trial are shown in Figs. 2.32 and 2.33, respectively. The scans were taken at approximately the same location along the tube and insert before and after the trial.

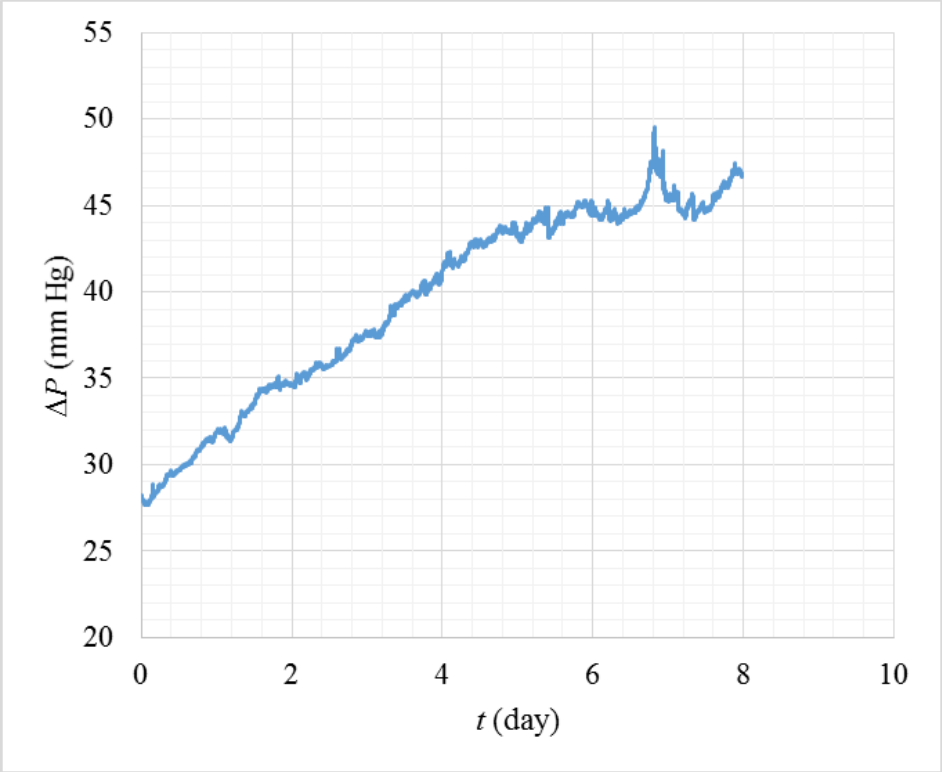


Fig. 2.31: Annular trial pressure with 24G tube and 28G insert ($Q$ = 2.5 µl/min; 25°C test conditions) [December 6 - 15, 2016]

The micro-CT images taken before the trial (Fig. 2.32) appear to have more flow area compared to those taken after the trial (Fig. 2.33), which should have caused a decrease in $\Delta P$ instead of the increase shown in Fig. 2.31. This flow area appearance was probably because the contrast of the image taken before the trial (Fig. 2.32) was not adjusted during post-processing, whereas the contrast of the image taken after the trial (Fig. 2.33) was adjusted to show more clearly the tube-insert walls.

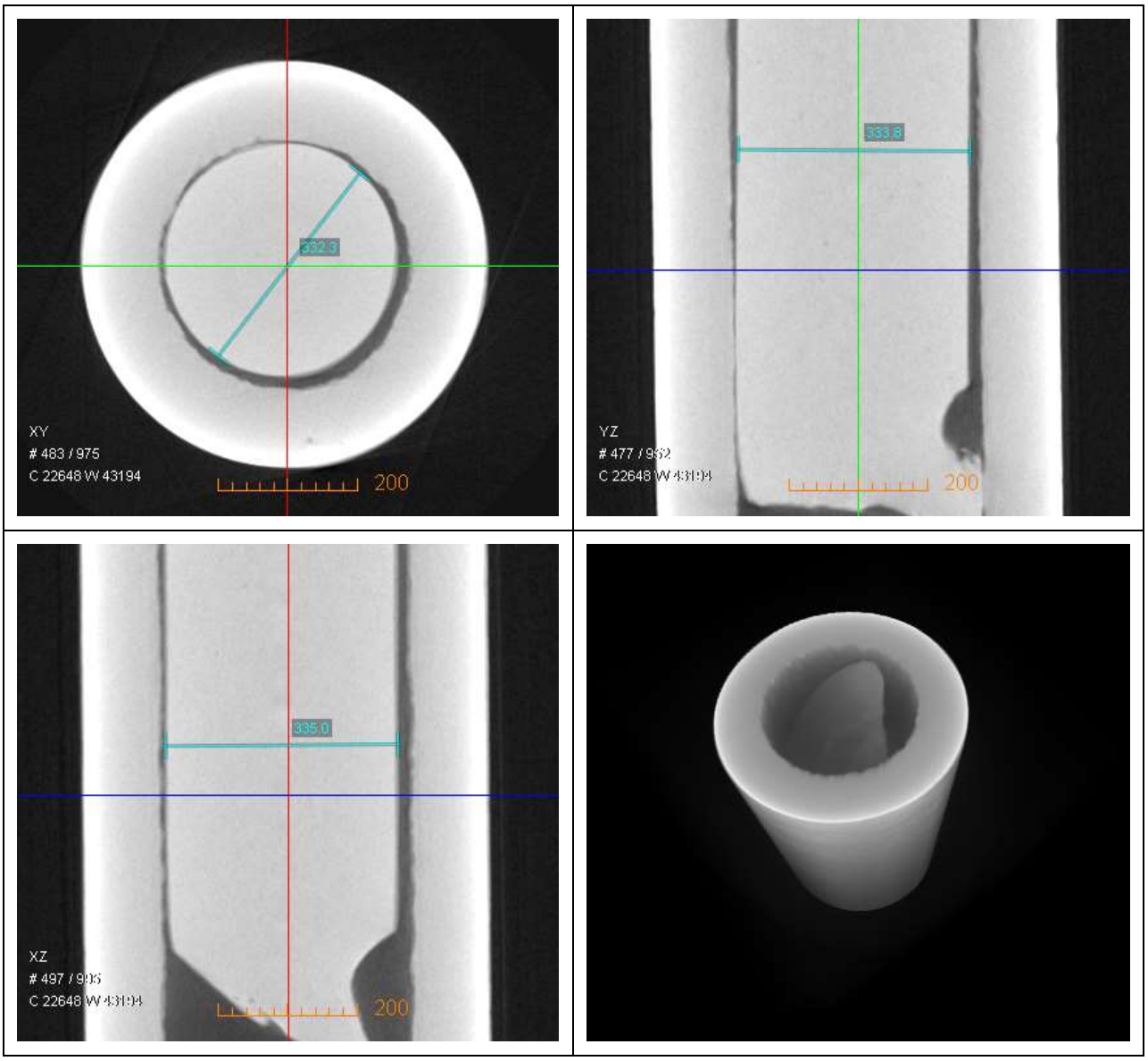


Fig. 2.32: Micro-CT images in the X-Y plane [top left], Y-Z plane [top right], X-Z plane [bottom left], and three-dimensions [bottom right] of the 24G-tube-28G-insert sample before the trial (magnification: 20x) [December 2, 2016]

It can be seen from Figs. 2.32 and 2.33, that there were no observable deposits on the surface of the tube wall or insert, neither before nor after the trial. This could have been because the densities of the deposits in the tubes were similar to that of air. Thus, the deposits would not be observed on the micro-CT scans. It is also possible that microbial growth did not create deposits that clog up the tubes, but merely increased the viscosity of the fluid flowing through the tubes.

Even though microbial deposits were not found, a thorough cleaning and sterilization antimicrobial protocol was developed and implemented in an effort to resolve the issue of continuously increasing $\Delta P$ which could be caused by microbial growth.

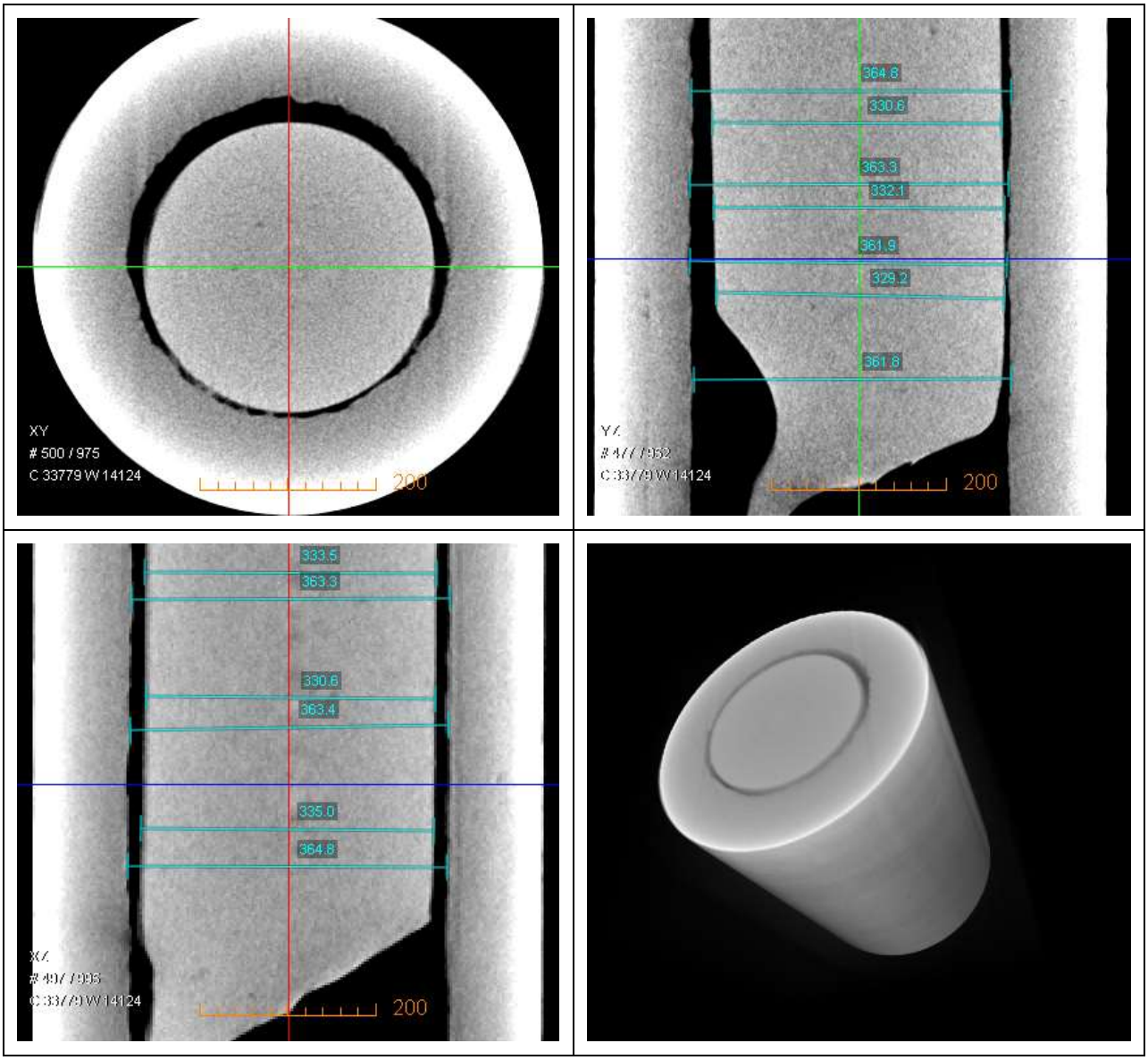


Fig. 2.33: Micro-CT images in the X-Y plane [top left], Y-Z plane [top right], X-Z plane [bottom left], and three-dimensions [bottom right] of the 24G-tube-28G-insert sample after the trial (magnification: 20x) [December 19, 2016]

***Conclusion:*** *There were no observable microbial deposits in the tubes after flow trials. There is a possibility that the cause of the continuous $\Delta P$ increase was not microbial growth. It is also*

*possible that the deposits were merely not observable on the micro-CT scans due to having a similar density as that of air.*

***Next steps:*** *Determine whether a final thorough cleaning and sterilization of the experimental system would resolve the issue of continuous increase in* $\Delta P$.

### 2.7.2. Flow Trial Results after Implementation of the Antimicrobial Protocol

***Research question:*** *Will an antimicrobial cleaning protocol resolve the issue of continuously increasing* $\Delta P$ *and enable the setups to provide accurate, reliable and relatively constant long-term* $\Delta P$ *measurements?*

An antimicrobial protocol was developed and implemented in an effort to resolve this issue of continuously increasing $\Delta P$. The $\Delta P$ results were analyzed. To show that the experimental setup is reliable in obtaining pressure measurements, $\Delta P$ results should be constant for more than 10 days when non-degradable stiff tubes are used.

This antimicrobial protocol involved sterilizing the glass bottles, and flushing the pumps with bleach solution, isopropyl alcohol (IPA) and sodium azide ($NaN_3$) solution. The protocol is described in Appendices F.1 and F.2. After the antimicrobial protocol, five 10-day single tube flow trials with 50 μm ID VSD tubes were performed. The first three trials were performed in the months of February and March of 2017. The last two were performed in September of 2017. The results are shown in Table 2.11 and Fig. 2.34.

From Fig. 2.34 and Table 2.11, it can be seen that the differences between the initial and final $\Delta P$s were no larger than 4.00 mm Hg, even though the flow trials were 10 days long. Unlike the $\Delta P$ plots shown in Fig. 2.29, the $\Delta P$ plots for the trials after cleaning and sterilization (Fig.

2.34) remained relatively constant with standard deviations of less than or equal to 1.60 mm Hg (Table 2.11).

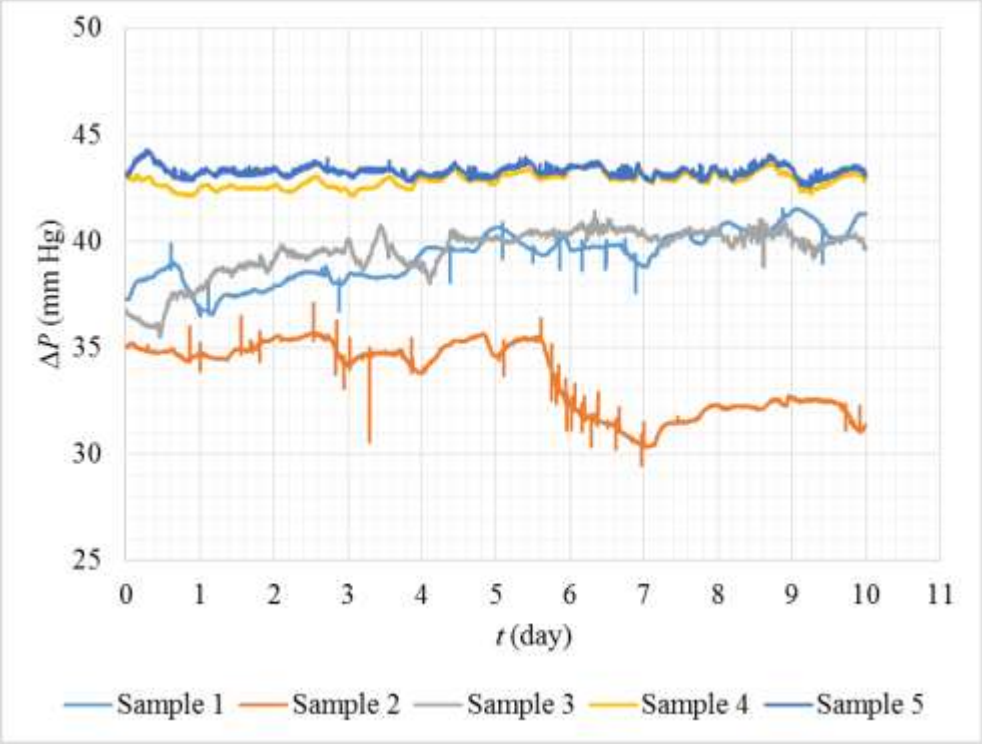


Fig. 2.34: Five 10-day trials with 50 µm ID VSD tubes [February 21 - September 16, 2017]

Table 2.11: Summary of experimental Δ*P* results of the five 10-day 50 µm ID VSD tube trials with cleaning and sterilization protocol

| Sample | 1 | 2 | 3 | 4 | 5 |
|---|---|---|---|---|---|
| Trial Start Date | 2/21/2017 | 3/13/2017 | 3/20/2017 | 9/6/2017 | 9/6/2017 |
| Experimental Δ*P* (mm Hg)[a] | 39.26 ± 1.17 | 33.66 ± 1.60 | 39.50 ± 1.13 | 42.94 ± 0.34 | 43.35 ± 0.26 |
| Difference between initial and final Δ*P*, $\Delta P_{f\text{-}i}$ (mm Hg)[b] | 4.00 | -3.67 | 3.03 | -0.16 | -0.07 |

[a] Average pressure ± standard deviation over the 10-day period shown in Fig. 2.34

[b] Difference between initial and final pressures ($\Delta P_{f\text{-}i} = \Delta P_f - \Delta P_i$)

These results demonstrated that the cleaning and sterilization protocol developed was effective in curbing the continuously increasing $\Delta P$ measurement issue that was likely caused by microbial growth. This issue of microbial growth, and the cleaning and sterilization protocol, is further discussed in Section 3.8.4. In Section 2.8, it is shown that steady $\Delta P$ measurements up to 25 days in length could be obtained after the antimicrobial protocol was implemented.

***Conclusion:*** *The antimicrobial protocol was effective in resolving the issue of continuously increasing $\Delta P$. Thus, microbial growth was very likely the cause of the continuously increasing experimental $\Delta P$ results for fluids flowing in small tubing.*

***Next steps:*** *Implement this antimicrobial protocol before future trials.*

## 2.8. Comparing Long-Term $\Delta P$ Results with Atmospheric Conditions

***Research question:*** *Why do the flow trials that were performed at the same time have similar $\Delta P$ variations? Are there variables which are affected by changes in barometric pressure or other ambient conditions?*

The two trials using Samples 4 and 5 were performed two days longer than the other samples of Table 2.10 and Fig. 2.34; from September 6 to September 18, 2017. The trials were started at the same time in two different setups (Sample 4 was in Setup 1 and Sample 5 was in Setup 2). It was observed that the trials of Samples 4 and 5 exhibited similar $\Delta P$ variations (Fig. 2.34). Since the trials were performed simultaneously, these very similar $\Delta P$ variations could possibly be caused by external atmospheric conditions, specifically barometric pressure. In order to test this hypothesis, the hourly barometric pressure, atmospheric temperature and humidity from September 6 to September 18, 2017 were taken from the "Personal Weather Stations" website [48], then plotted with the trial pressures as shown in Figs. 2.35, 2.36 and 2.37. As can be observed in

these figures, the ambient condition variations during the 13 days were not similar to the pressure variations of Samples 4 and 5.

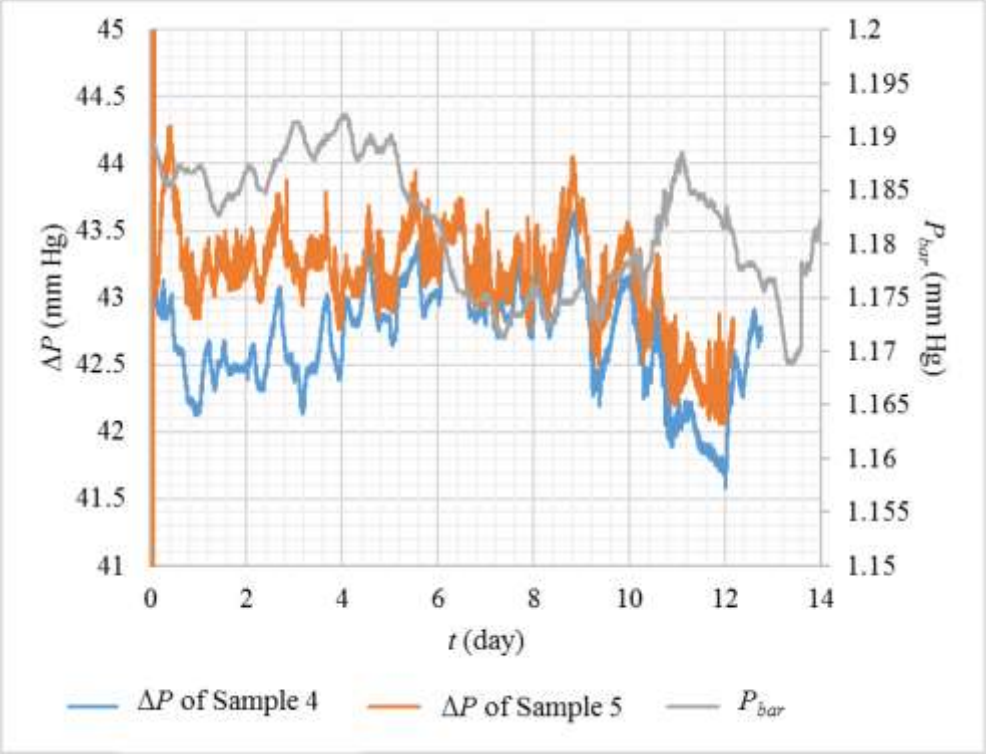


Fig. 2.35: Samples 4's and 5's pressure and barometric pressure, $P_{bar}$ [September 6 - 18, 2017]

When the barometric pressure was directly compared to the pressures of Samples 4 and 5, there was no observable similarity between the pressure variations and the barometric pressure variation (Fig. 2.35). However, when the barometric pressure was mirrored about the average barometric pressure ('inverted'), a similar shape was observed between the measured/experimental pressures and the barometric pressure (refer to Figs. 2.38, 2.39 and 2.40). The 'inverted' barometric pressure was calculated as:

$$P_{invbar} = P_{bar} - 2(P_{bar} - P_{avgbar}) \tag{2.4}$$

where, $P_{invbar}$ is the inverted barometric pressure (mm Hg), $P_{bar}$ is the barometric pressure (mm Hg), and $P_{avgbar}$ is the average barometric pressure over the length of the trial (mm Hg).

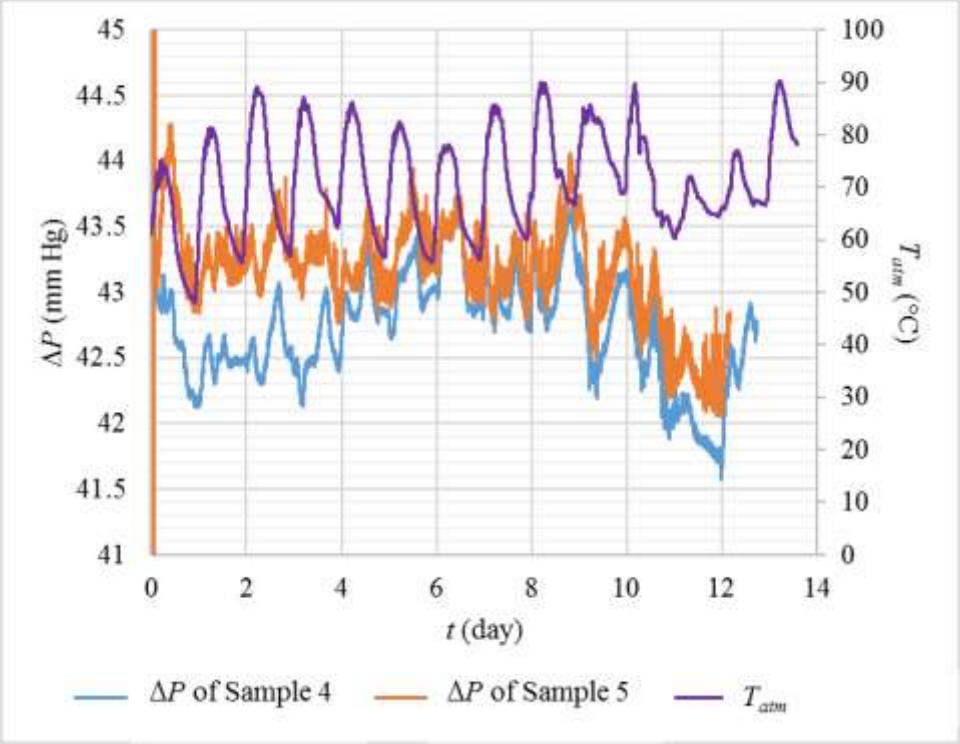


Fig. 2.36: Samples 4's and 5's pressure and atmospheric temperature, $T_{atm}$ [September 6 - 18, 2017]

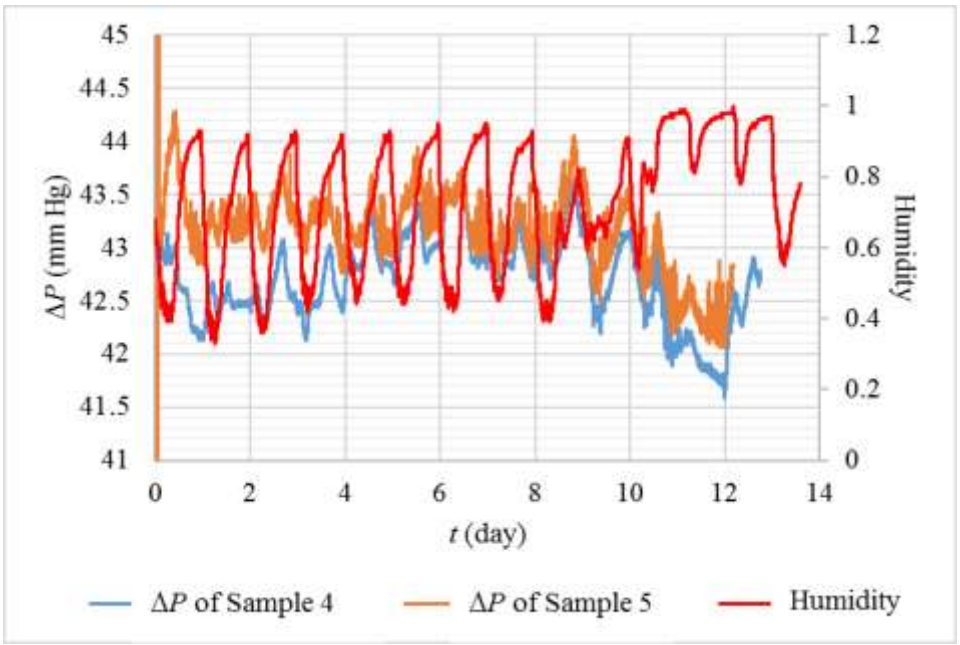


Fig. 2.37: Samples 4's and 5's pressure and atmospheric humidity [September 6 - 18, 2017]

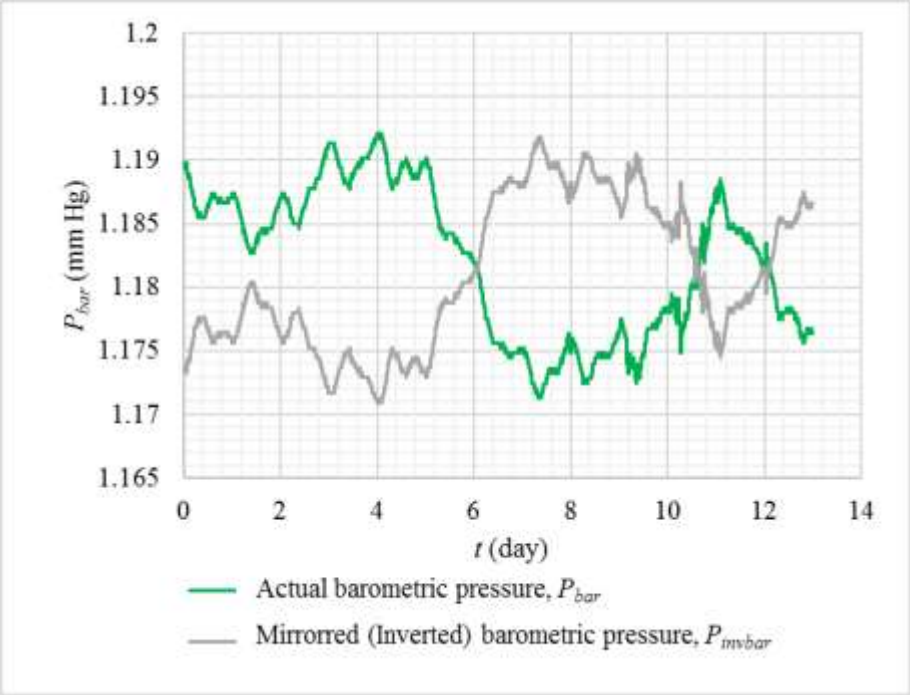


Fig. 2.38: Actual barometric pressure, $P_{bar}$, and the mirrored ('inverted') barometric pressure, $P_{invbar}$ [September 6 - 18, 2017]

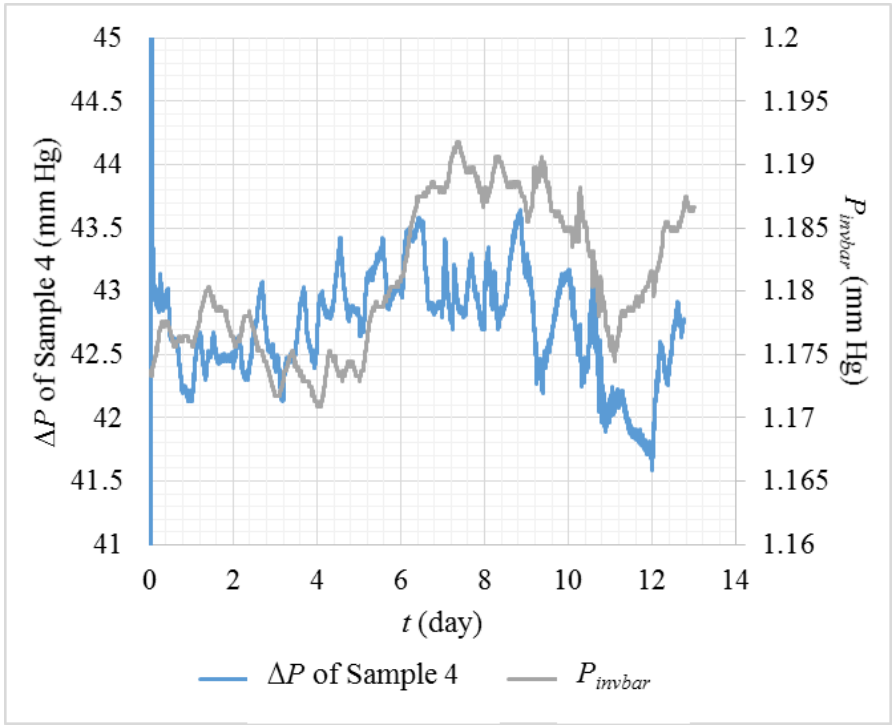


Fig. 2.39: Sample 4's $\Delta P$ and the mirrored ('inverted') barometric pressure, $P_{invbar}$ [September 6 - 18, 2017]

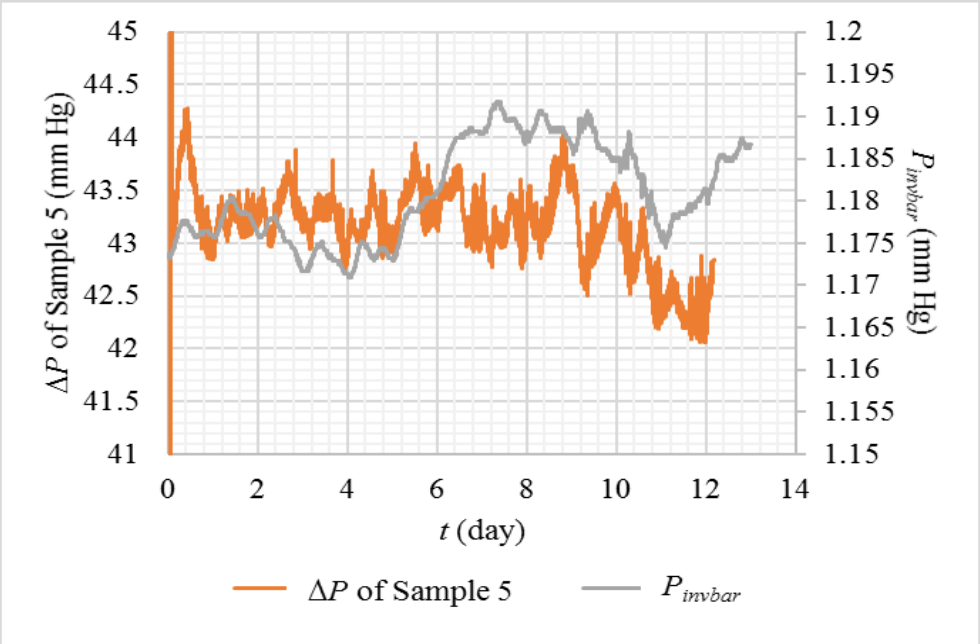


Fig. 2.40: Sample 5's $\Delta P$ and the mirrored ('inverted') barometric pressure, $P_{invbar}$ [September 6 - 18, 2017]

It is possible that barometric pressure did affect the pressure, since the output flow rate of the pneumatic pumps is dependent on the internal flow sensor of the pump. The pressure was indirectly affected by the variation in flow rate measurement by the pump. Being a closed loop system, the pump's flow sensor measured differential pressure or flow rate across it in order to determine and maintain the output flow rate (2.5 µl/min). However, the flow rate measurement made by the flow sensor may be inversely affected by the variation in surrounding pressure which in turn, affected the resulting pressures in the samples [49]. Therefore, the variation in barometric pressure may have been the cause of the $\Delta P$ modulation of Samples 4 and 5.

To further investigate this phenomenon, the trials of Samples 4 and 5 were repeated with two new 50 µm ID VSD samples, Samples 6 and 7. The trials began on September 25, 2017 and ended on October 20, 2017. The same sample preparation, flow conditions and trial procedures that were used for Samples 4 and 5 were used for Samples 6 and 7. The pressure results of these

samples were compared with the barometric pressure and the mirrored (inverted) barometric pressure, similar to the comparisons for Samples 4 and 5. Shown in Fig. 2.41 are Sample 6's and 7's pressure data compared with the actual barometric pressure.

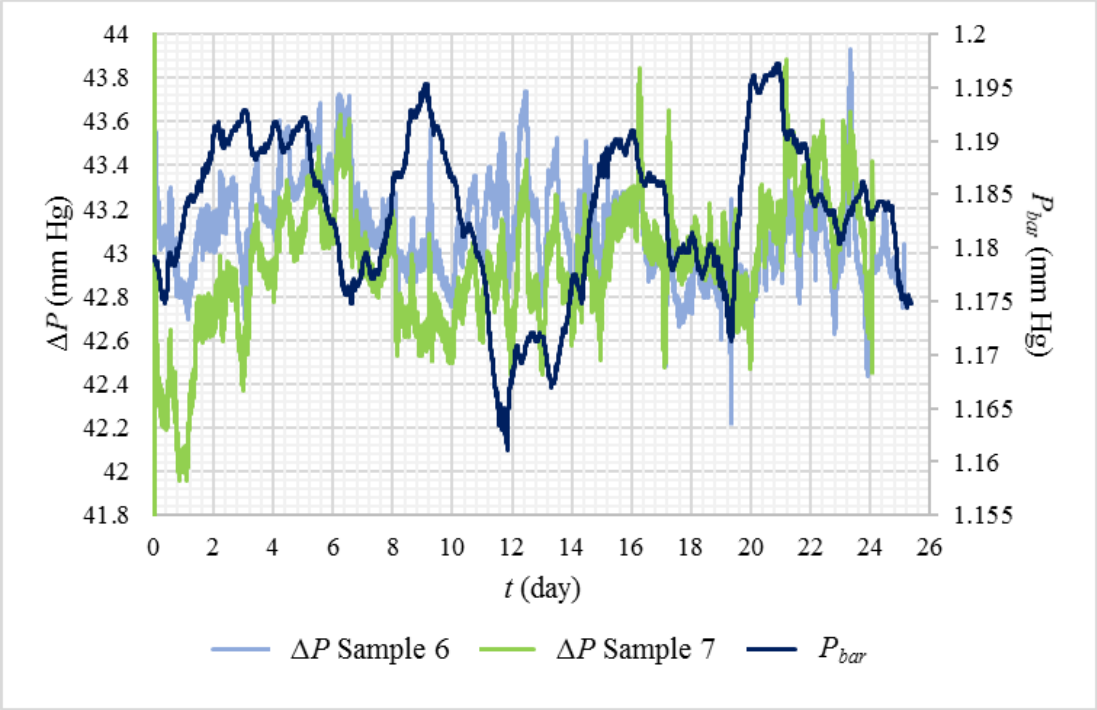


Fig. 2.41: Comparison among pressures of Samples 6 and 7 and barometric pressure, $P_{bar}$ [September 25 - October 20, 2017]

Similar to the trials of Samples 4 and 5, the pressure trends remained relatively constant for 25 days. Sample 6's and 7's average pressures were 43.1 ± 0.23 mm Hg and 42.9 ± 0.29 mm Hg, respectively. From Fig. 2.41, it can be seen that the $\Delta P$ variations of Samples 6 and 7 were very similar. It can also be seen that $\Delta P$ variations practically matched the trend in $P_{bar}$ variation during the first 8 days and between day 15 and 25, but not between day 9 and day 14. The trials were then compared with the mirrored or 'inverted' barometric pressure (Fig. 2.42).

Unlike Samples 4 and 5, it can be seen from Fig. 2.42 that the 'inverted' barometric pressure did not match the $\Delta P$ variations of Samples 6 and 7 as well as the actual barometric

pressure. Therefore, it is uncertain as to whether barometric pressure is the cause of the variation in $\Delta P$ results. However, the similar variations for Samples 4 and 5, and for Samples 6 and 7, show that there could be an underlying influence of barometric pressure. In order to better understand the influence of barometric pressure on flow trial pressure, the barometric lab pressure should be collected and compared with the modulating $\Delta P$ trial data.

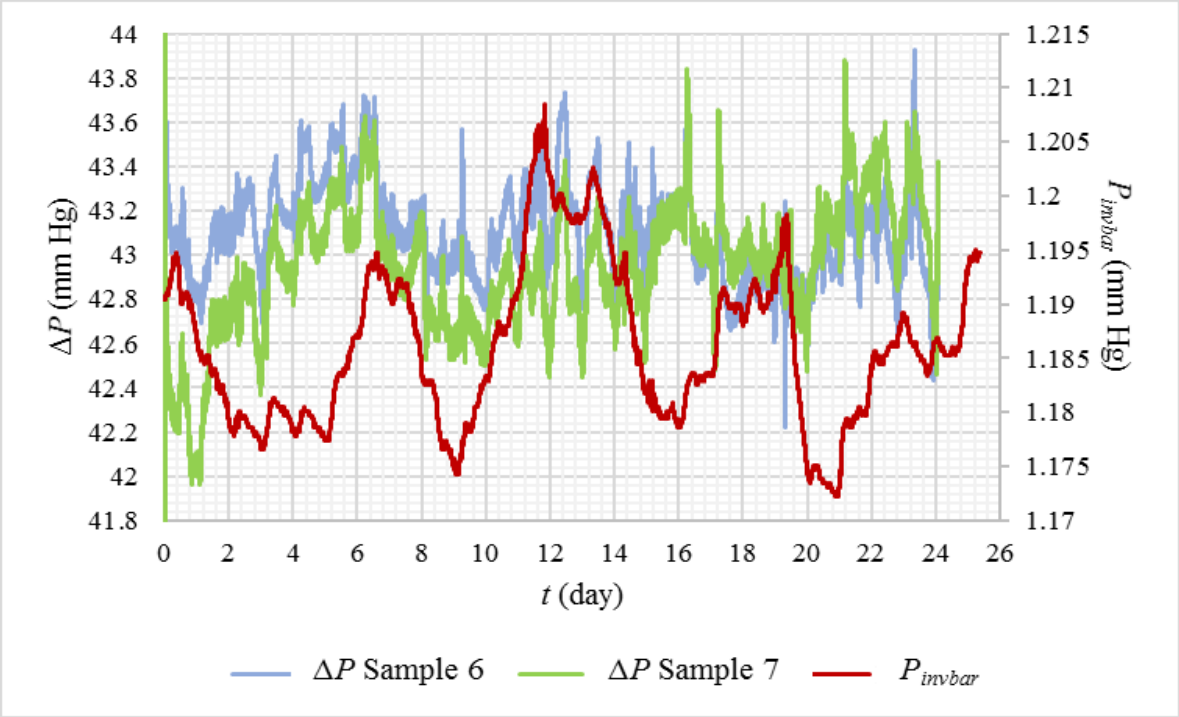


Fig. 2.42: Comparison among pressures of Samples 6 and 7 and the mirrored ('inverted') barometric pressure, $P_{invbar}$ [September 25 - October 20, 2017]

***Conclusion:*** *Some similarities were found between the flow trials' $\Delta P$ with that of barometric pressure and/or the 'inverted' barometric pressure. These findings were inconclusive since the barometric pressures used for comparison were taken outside the lab and not in the the lab where the trials were performed. Therefore, the lab barometric pressure should be recorded and compared with the experimental pressure variations.*

***Recommended next steps:*** *It is recommended that the ambient pressure in the lab itself be*

*collected and compared with trial $\Delta P$ results in order to see if ambient pressure is related to the small variations in trial $\Delta P$.*

## 2.9. Summary of the Setup, Experimental Methods and Setup Validation

In Section 2.1, the components and design of the experimental setup were described. These setups simulate the flow of AH through BGI tubes at low flow rates and pressures. The setups were first developed by Ramani and later modified by this author for improved accuracy and reliability.

Section 2.2 described the modifications of the original setup that were made by this author, including the addition of a back-up power supply unit, a temperature-controlled incubator, and water-tight connectors. Section 2.3 provided an overview of the preliminary validation trials that were performed by Ramani [42] using the setups that he developed (prior to the modifications made by this author). From these trials, he found that the experimental pressure data for the open single tube flow trials with 50 μm and 75 μm ID tubes (50 μm: 101.5 mm Hg; 75 μm: 15.0 mm Hg) were near the upper limit of the theoretical pressure range (50 μm: 103.2 mm Hg; 75 μm: 16.8 mm Hg). Ramani also found that there was a gradual increase in pressure during the trials with absorbable suture inserts in BGI tubes. However, these results were affected by a voltage-to-pressure conversion error that he made.

Short-term trials with 50 μm ID VSD tubes (that were done previously by Ramani [42]) were repeated using the modified setups, and the pressure results were analyzed (Section 2.4). This was done to ensure that the setups were still able to perform accurate and consistent pressure measurements after the modifications were made. These trials demonstrated that Setups 1 and 2 measured consistent pressures for two to three hours with small standard deviations (Setup 1: 0.63 mm Hg; Setup 2: 0.63 mm Hg).

In order to simulate fluid flow in a BGI tube containing an insert, eliminate the influence of other variables in the experiment, and enable accurate benchmarking of the setups, annular flow trials were performed with stiff hypodermic tubes and nichrome wire inserts (Section 2.5). Two hour trials were performed with 24G (gage) hypodermic tubes and 28G nichrome wire inserts. From these trials, it was found that the average differential pressure across the 28G tubes ($\Delta P$), increased with each repeated trial, even though the same sample and procedures were used. It was verified that this $\Delta P$ increase was not due to a measurement error of the pressure transducers, because the transducers' pressure measurements (Transducers 1 and 2) corresponded well with their respective pneumatic pumps' pressure measurements (Pumps 1 and 2).

In order to confirm this occurrence of increasing $\Delta P$, 20 hour annular flow trials were performed with the same sample combination as for the 2 hour trials (24G hypodermic tubes and 28G nichrome inserts). From these trials, it was confirmed that $\Delta P$ increased from the beginning to the end of the trial for each respective sample. It was hypothesized that this increase in $\Delta P$ could have been due to systemic errors or particle build-up in the tubing connecting the pump and the sample. In order to determine whether this continuous $\Delta P$ increase was caused by systemic error (from the pumps or transducers), more extensive system validation trials were performed as described in Section 2.6.

First, the pumps' internal pressure-measuring systems needed to be verified since each pump's output flow rate/pressure is based on the pump's internal flow rate and pressure measurements (Section 2.6.1). This was done by performing annular flow trials with the pump from Setup 1 (Pump 1) placed in-line with the pump from Setup 2 (Pump 2). Pump 2 pumped fluid through the tubes, and Pump 1 functioned as an external flow sensor to validate the flow rate of Pump 2.

In order to ensure that Pump 2's pressure measurements were reliable, Pump 2's pressure data were compared with those of Transducer 1's (Transducer 1 was located downstream of Pump 2 and measured pressure in the same tube). The pressure measurements of Pump 2 matched well with the pressure measurements of Transducer 1 (average difference between $\Delta P$ measured by Pump 2 and Transducer 1 of 17.32 mm ± 0.19 mm Hg). Thus, Pump 2's measurements were reliable. It was found that the flow rate measurements of both Pumps 1 and 2 matched well with each other (average absolute difference in flow rate of 0.02 µl/min). The flow pressures measured by Pump 2 also compared well with those of Transducer 1. Therefore, the pumps' internal pressure-measuring systems were found to be reliable and were not the cause for the increase in $\Delta P$.

Although the flow rate measurements of both pumps corresponded well with one another, more validation trials were performed in order to ensure that the flow rate measurements of the pneumatic pumps (Pumps 1 and 2) were still accurate when cross-checked with a different type of pump from a different manufacturer. The flow rate measurements of the pumps were compared with those of a syringe pump from a different manufacturer; and it was found that the pneumatic pump flow rate measurements matched well with the syringe pump's flow rate output and settings (percentage error between input and output flow rates of less than 6%) [details in Section 2.6.2].

To fully verify that the pressure transducers were measuring pressure accurately, one of the transducers (Transducer 1) was compared with a third transducer from a different manufacturer (Transducer 3) (Section 2.6.3). Transducers 1 and 2 are voltage output pressure transducers, whereas Transducer 3 is a current output pressure transducer. Transducers 1 and 3 were placed in-line, measuring the pressure of the same sample at almost the same point. It was found that the pressure readings of Transducers 1 and 3 matched well with a consistent average difference of

1.26 ± 0.13 mm Hg. Therefore, the pressure transducers used in the setups (Transducer 1 and 2) were measuring pressure accurately. Based on all of this extensive testing, it was determined that the continuous increase in Δ*P* was very likely caused by microbial growth or mineral deposition.

In an effort to prevent Δ*P* from increasing over time, an antimicrobial cleaning and sterilization protocol was developed. It involved flushing of the system with 10% bleach solution, isopropyl alcohol (IPA), and DI water, and sterilization of the glass bottles. After performing this antimicrobial protocol, it was found that steady and constant Δ*P* measurements could be obtained (Δ*P* did not increase over time) for more than 10 days when performing trials with 50 μm ID VSD tubing. Section 2.7 compares the Δ*P* results with and without the antimicrobial protocol.

When analyzing the steady and constant long-term Δ*P* data, it was discovered that the small Δ*P* fluctuations (less than ±1.6 mm Hg) of two 50 μm ID VSD tube trials performed at the same time followed a similar trend (Samples 4 and 5). It was hypothesized that this could be caused by fluctuations in the surrounding pressure (barometric pressure, temperature or humidity). These Δ*P* results were compared with the barometric pressure, temperature and humidity reported by the PWS Weather website (Lawrence, Kansas weather [48]) during the period of the trials (Section 2.8). For the two samples (Samples 4 and 5) that were tested simultaneously, the trials' Δ*P* data did not correspond with variations in barometric pressure. However, when the Δ*P* results were compared with the mirrored (inverted) barometric pressure variation, a similar trend was observed between the Δ*P* results and barometric pressure for some of the recorded data. The Δ*P* data of these trials did not correspond with atmospheric temperature and humidity.

A second set of 50 μm ID VSD tube flow trials was performed for 25 days, and the Δ*P* results were compared with barometric pressure (Samples 6 and 7). Contrary to Samples 4 and 5, it was found that the Δ*P* trends resembled the barometric pressure trend more closely than the

inverted barometric pressure trend. This inconsistency was probably because the barometric pressure obtained was not the actual ambient pressure in the lab. In order to determine the true influence of barometric pressure on the trials, the barometric pressure in the lab should be collected and compared with the modulating $\Delta P$ trial results.

## Chapter 3: Experimental System for Rigorous Study of Flow through GDIs

In this chapter, the primary hypothesis of this study is investigated. The primary hypothesis states that the experimental differential pressures ($\Delta P$) in BGI-like tubes that are measured in the experimental setups correspond well with theoretical $\Delta P$ predictions. Therefore, the experimental pressures measured in the setups were cross-checked with theoretical pressure loss calculations to confirm the accuracy of the pressures measured by the setups. Section 3.1 describes the theoretical calculations used to validate the experimental $\Delta P$ measured as well as the measurement methods used to obtain precise diameter measurements for more accurate theoretical calculations.

A paper that was submitted to the British Journal of Ophthalmology (BJO) on September 27, 2017 is included in this chapter (Sections 3.2 to 3.7). The authors were Teo, Ramani, Munden, Wilson, Kieweg, and Dougherty. In this paper, tubular and annular flow trials were performed with stiff non-degradable inserts, and the experimental $\Delta P$ results were compared with theory (Hagen-Poiseuille). The paper consisted of the following main sections:

3.2. Cover Page

3.3. Abstract

3.4. Introduction

3.5. Materials and Methods

3.6. Results

3.7. Discussion

Additional information that could not be included in the submitted paper is added in Section 3.1 and 3.8.

## 3.1. Theoretical Pressure Loss Calculations and Precise Diameter Measurements

Section 3.1 describes in detail the fundamental pressure loss calculations and diameter measurement methods used. The theoretical calculations used to predict the $\Delta P$ for tubular and annular flow are described in Sections 3.1.1 and 3.1.2. The calculations are based on the Hagen-Poiseuille theory for flow through a single open tube and flow through an annulus [50].

Section 3.1.3 describes the methods/equipment explored for obtaining more precise measurements of the tube IDs and the insert ODs, since it was noted that small changes in tube and insert diameters could cause significant changes in $\Delta P$. The LEICA materials analysis microscope and the Xradia MicroXCT tomographic X-ray microscope were explored. Ultimately, the MicroXCT microscope was the most suitable for this application. It can take very precise measurements (± 0.2 μm) and images of the microscopic tubes and inserts.

### 3.1.1. Tubular Flow Theoretical Pressure Loss Calculations

The pressure measured in the single open VSD tube trials were cross-checked with the Hagen-Poiseuille law for flow through a single open tube. Since the experimental trials were performed with deionized (DI) water at room temperature (25°C), the flow properties of water at room temperature were used (i.e., density and dynamic viscosity of water) [51]. The Reynolds number is calculated as follows:

$$\mathrm{Re} = \frac{\rho v D_o}{\mu} = \frac{4 \rho Q}{\pi \mu D_o} \tag{3.1}$$

where Re = Reynolds number, $\rho$ = density of water (1000 kg/m$^3$), $v$ = flow velocity (m/s) [$v = 4Q/(\pi D_o^2)$], $D_o$ = tube inner diameter (m), $\mu$ = dynamic viscosity of water (0.0008904 Pa-s at 25°C), and $Q$ = flow rate (m$^3$/s).

Table 3.1 lists the Reynolds numbers calculated for water flow through tubes with $D_o$ = 45

μm to 85 μm at a flow rate of 2.5 μl/min (at room temperature). The VSD tubes used in this study had nominal $D_o$'s of 50 μm and 75 μm. It can be seen in Table 3.1, in that the highest Reynolds number achieved in this study was no more than 1.32 (Re < 2100 for laminar flow) [50]. The flow is fully developed after moving ~0.1$D_o$ along the tube [50]. Therefore, pressure loss through the tube was calculated using the Hagen-Poiseuille (H-P) equation for laminar fully-developed flow through a single open tube with smooth walls (negligible surface roughness) [50]. The H-P equation for a single open tube is as follows [50]:

$$\Delta P = \frac{128 Q \mu L}{\pi D_o^4} \tag{3.2}$$

where $L$ = length of tube (m).

Note that before December 2016, trials were performed with 35 mm long VSD tubes according to Ramani's tube sample preparation procedures [42]. After December 2016, the single open tubular trials were performed with 25 mm long tubes. This was because shorter 24G hypodermic tubes were purchased (1.0 inch long tubes), eliminating the need for a longer VSD which was initially necessary to ensure that glue did not flow back and block the tube entrance [42]. Pressure loss through a tube was calculated for different $D_o$'s at both $L$ = 25 mm and 35 mm using Eq. (3.2) (Table 3.1). It can be observed from Table 3.1 that just a 5 μm decrease in $D_o$ from 50 μm to 45 μm can cause a significant increase in $\Delta P$ (up to 33 mm Hg for a 35 mm long tube).

The theoretical tube pressure losses calculated for the 50 μm and 75 μm tubes were compared with the experimental tube pressure losses measured during the trials. As explained in App. B.1, at the beginning of each trial, pressure was measured and logged for approximately 30 minutes without attaching the test sample. This measurement yielded a baseline pressure.

At the end of a trial, the average baseline pressure was subtracted from the pressure

measured after the sample had been attached to the test section. This was done in order to eliminate the residual pressure losses that occurred between the pump and the test sample. These residual pressure losses were caused by:

- frictional losses in the tubes between the pump and the test sample,
- sudden/angled flow area expansion/contraction at the connections,
- head loss due to height difference between the pump and test sample.

Table 3.1: Theoretical pressures calculated from the H-P equation for open single tube flow with different $D_o$'s ($Q$ = 2.5 μl/min; $\mu$ = 0.0008904 Pa-s; $L$ = 25 mm and 35 mm)

| $D_o$ (μm) | $v$ (m/s) | Re | $\Delta P$ for $L$ = 25 mm | | $\Delta P$ for $L$ = 35 mm | |
|---|---|---|---|---|---|---|
| | | | Pa | mm Hg | Pa | mm Hg |
| 45.0 | 0.02620 | 1.32 | 12901.9 | 69.1 | 9215.6 | 96.8 |
| 50.0 | 0.02122 | 1.19 | 8464.9 | 45.4 | 6046.4 | 63.5 |
| 55.0 | 0.01754 | 1.09 | 5781.6 | 31.0 | 4129.7 | 43.4 |
| 60.0 | 0.01474 | 0.99 | 4082.2 | 21.9 | 2915.9 | 30.6 |
| 65.0 | 0.01256 | 0.92 | 2963.8 | 15.9 | 2117.0 | 22.2 |
| 70.0 | 0.01083 | 0.85 | 2203.5 | 11.8 | 1573.9 | 16.5 |
| 75.0 | 0.00943 | 0.79 | 1672.1 | 9.0 | 1194.3 | 12.5 |
| 80.0 | 0.00829 | 0.74 | 1291.6 | 6.9 | 922.6 | 9.7 |
| 85.0 | 0.00734 | 0.70 | 1013.5 | 5.4 | 723.9 | 7.6 |

The average measured experimental pressure minus the average residual (baseline) pressure was the actual pressure loss at the test sample region. This pressure loss was compared with the theoretical pressures calculated using the H-P equation based on the test parameters.

### 3.1.2. Annular Flow Theoretical Pressure Loss Calculations

To calculate the theoretical pressure loss when an insert was placed in the GDI tube, the modified H-P equation for a tube with an annulus was used. In order to use this equation, the same flow criteria as that of the single open tubular flow trial had to be met. Therefore, the Reynolds number was calculated. Reynolds number for flow through an annulus was calculated as follows:

$$\mathrm{Re} = \frac{\rho\, v\, D_{eff}}{\mu} = \frac{4\,\rho\, Q}{\mu\,\pi\, D_{eff}} \tag{3.3}$$

where $v$ = annular flow velocity (m/s) [$Q = (v\,\pi\, D_{eff}{}^2)\,/\,4$]; and $D_{eff}$ was calculated as follows [50]:

$$D_{eff}{}^4 = D_o{}^4 - D_i{}^4 - \frac{\left(D_o^2 - D_i^2\right)^2}{\ln\left(\frac{D_o}{D_i}\right)} \tag{3.4}$$

Table 3.2 lists the Reynolds number calculated for an annulus with a fixed outer diameter, $D_o$ of 300 μm. This value was chosen because the ID of a BGI tube is approximately 300 μm [29]. From Table 3.2, it can be seen that the Reynolds number is below 0.215 when $\Delta P$ is within the clinically relevant range (5 - 25 mm Hg). Therefore, the flow is laminar and fully developed after moving ~0.1$D_o$ along the tube [50]. Notice also that for annular flow, the Reynolds number decreases as effective diameter increases.

Since the flow is fully developed and laminar, the modified H-P equation is used to calculate pressure loss through the tube annulus. The equation is as follows [50]:

$$\Delta P = \frac{128 Q\,\mu\, L}{\pi D_{eff}{}^4} \tag{3.5}$$

From Table 3.2, it is noted that an insert with an OD between 270 μm and 280 μm, placed in the BGI tube, should create the necessary pressure for maintaining healthy IOP levels (8 - 22

mm Hg). Notice also that a 5 μm change in $D_i$ causes a large change in $\Delta P$ (up to 40 mm Hg difference) especially when $D_{eff}$ falls below 50 μm. Relationships between these parameters are further discussed in Sections 3.6 and 3.7.

Table 3.2: Theoretical pressures calculated from the H-P equation for annular tube flow at different $D_i$'s ($D_o$ = 300 μm; $Q$ = 2.5 μl/min; $\mu$ = 0.0008904 Pa-s; $L$ = 8 mm; $T$ = 25°C)

| $D_o$ (μm) | $D_i$ (μm) | $D_{eff}$ (μm) | $v$ (m/s) | Re | $\Delta P$ for $L$ = 8 mm | |
|---|---|---|---|---|---|---|
| | | | | | Pa | mm Hg |
| 300.0 | 285.0 | 33.9 | 0.00605 | 0.2300 | 9186.8 | 68.9 |
| 300.0 | 280.0 | 41.9 | 0.00457 | 0.2154 | 3909.0 | 29.3 |
| 300.0 | 275.0 | 49.5 | 0.00369 | 0.2051 | 2018.7 | 15.1 |
| 300.0 | 270.0 | 56.6 | 0.00310 | 0.1972 | 1178.4 | 8.8 |
| 300.0 | 265.0 | 63.4 | 0.00268 | 0.1910 | 748.6 | 5.6 |
| 300.0 | 260.0 | 69.9 | 0.00237 | 0.1860 | 505.9 | 3.8 |
| 300.0 | 255.0 | 76.2 | 0.00212 | 0.1818 | 358.5 | 2.7 |
| 300.0 | 250.0 | 82.3 | 0.00193 | 0.1783 | 263.7 | 2.0 |
| 300.0 | 245.0 | 88.2 | 0.00177 | 0.1753 | 199.9 | 1.5 |
| 300.0 | 240.0 | 93.9 | 0.00164 | 0.1727 | 155.4 | 1.2 |
| 300.0 | 235.0 | 102.8 | 0.00147 | 0.1705 | 108.3 | 0.8 |

### 3.1.3. Precise Diameter Measurements

Since a small change in $D_{eff}$ could cause a significant change in $\Delta P$, more precise measurements of $D_o$ and $D_i$ were needed in order to ensure a more accurate comparison between theory and experimental pressure data. Additionally, because $\Delta P$ is significantly affected by $D_{eff}$,

any accumulation of small particles on the inner walls of the microtube/annular tube sample could cause a significant change in $\Delta P$. Therefore, better microscopic imaging methods were explored in order to provide more exact measurements of $D_o$ and $D_i$. The following imaging devices were explored:

- Leica DM2500 M materials analysis microscope located in M2SEC Lab 1549, University of Kansas [52], and
- Xradia MicroXCT-400 tomographic X-ray microscope located in Learned Hall Room 1120, University of Kansas (Carl Zeiss X-ray Microscopy, Pleasanton, CA) [53].

***Leica Materials Analysis Microscope***

The Leica microscope was the first micro-imaging option explored. The microscope is located in the Surface Characterization Laboratory (M2SEC 1549) belonging to Dr. Prajna Dhar, Associate Professor in Chemical and Petroleum Engineering. This microscope provided relatively clear imaging of the wire insert and measurements of the wire insert OD with an accuracy between ±1 μm and ±4 μm, depending on the magnification (i.e., 10x, 40x, or 63x). Figure 3.1 shows an example of an image taken of a 28G nichrome wire insert using the Leica microscope. To measure the ID of a SS hypodermic tube, a top transverse view of the tube is taken as shown in Fig. 3.2. However, it was difficult to obtain measurements of the tube IDs smaller than 100 μm.

Measurements were taken by counting the number of pixels and multiplying that number by its pixel-to-length conversion as follows:

- 10x magnification:

  7 pixels = 10 μm; 1 pixel = 10/7 μm = 1.4286 μm
- 40x magnification:

33 pixels = 10 μm; 1 pixel = 10/33 μm = 0.3030 μm

- 63x magnification:

  44 pixels = 10 μm; 1 pixel = 10/44 μm = 0.2273 μm

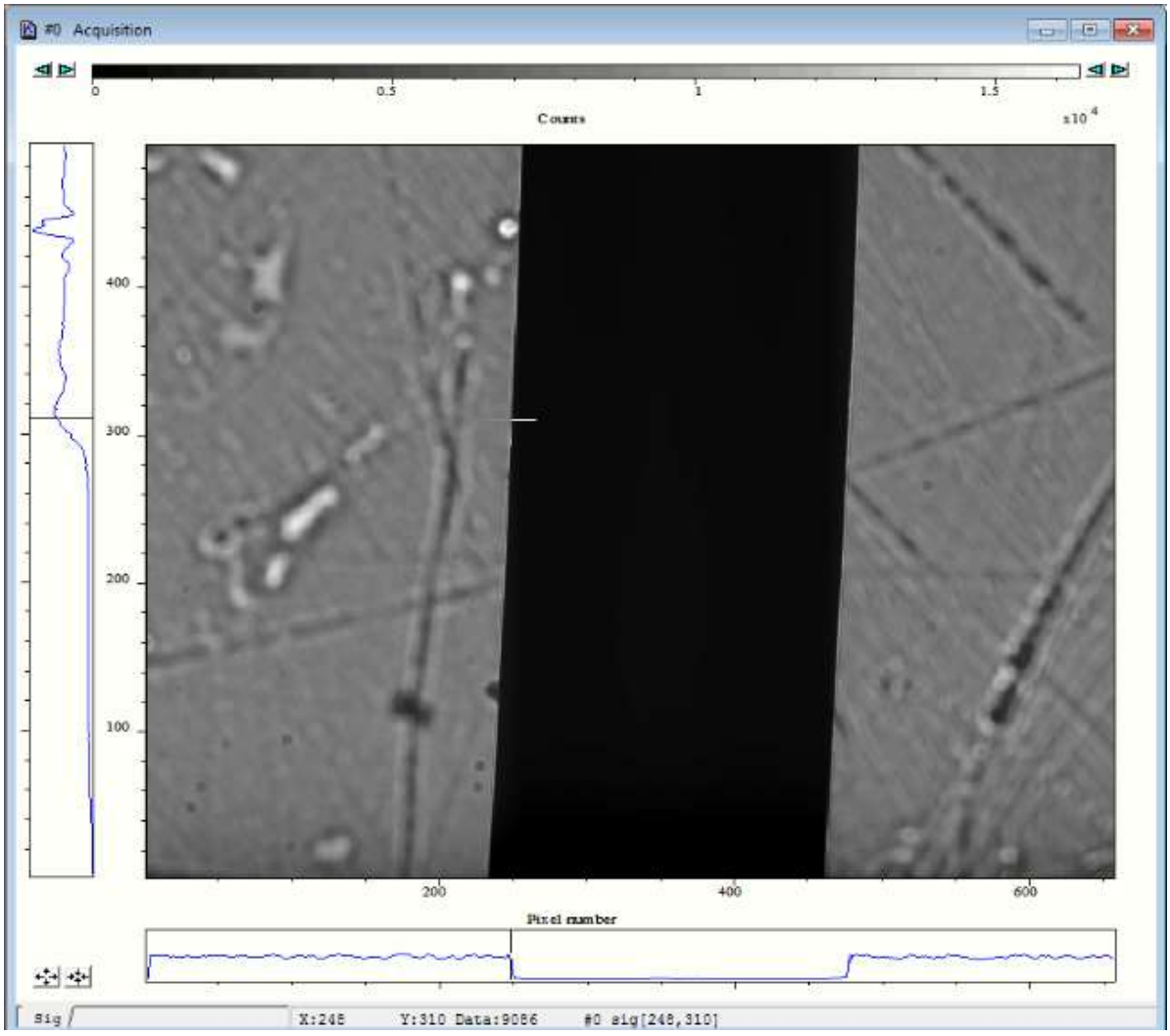


Fig. 3.1: Image of a wire insert taken with the LEICA microscope (magnification: 10x)

A major drawback of the Leica microscope was that it was unable to provide imaging of an insert while it was in a tube. This made it difficult to determine if there were particles depositing on the inner wall of the tube or on the insert, since the insert had to be removed from the tube in order to view it under the Leica microscope. The particles could have fallen off during removal of

the insert. Additionally, due to the microscope's limitation of providing only a 2-dimensional one-sided view, the eccentricity/concentricity of the insert in the tube could not be observed.

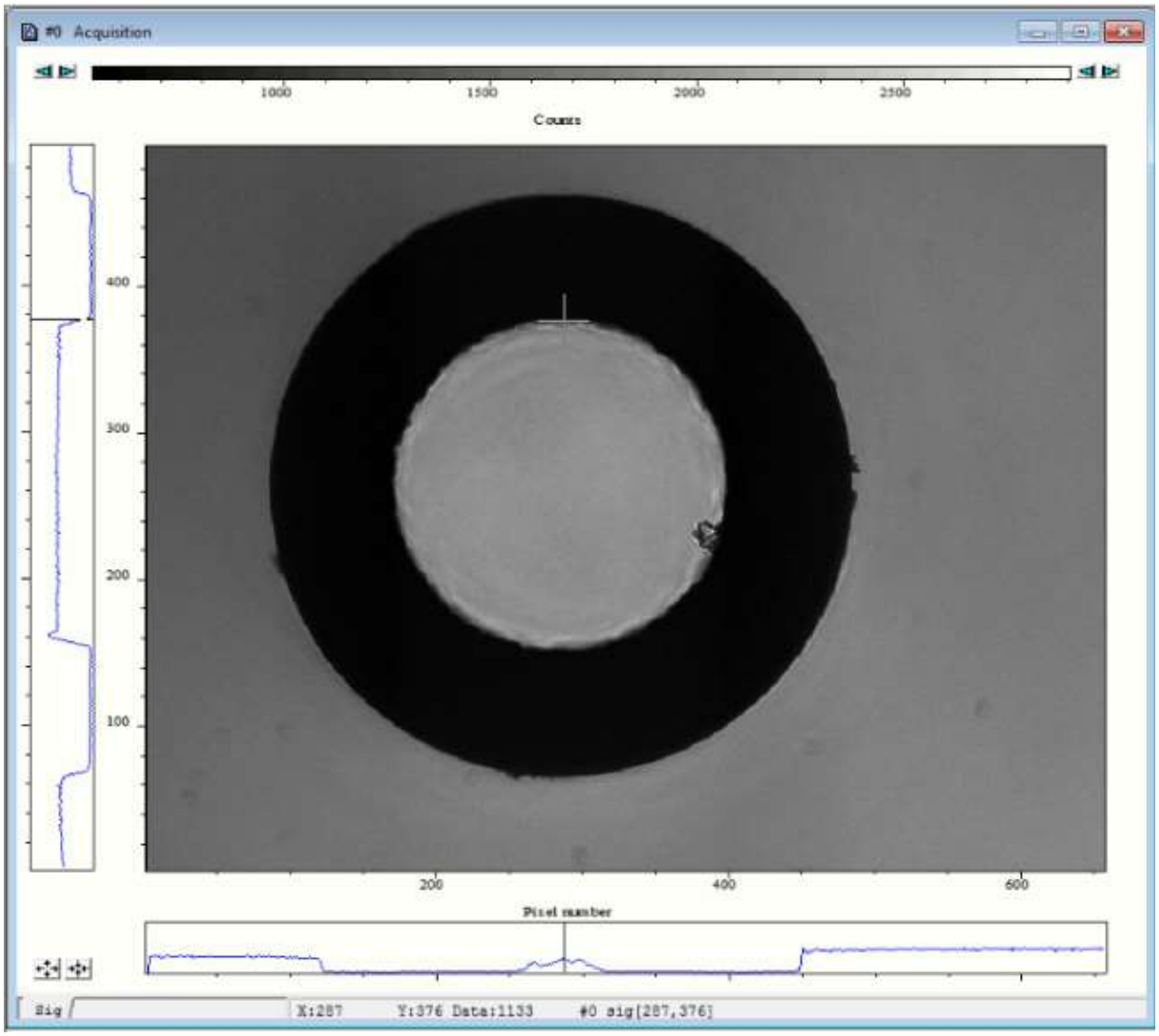


Fig. 3.2: Image of 24G hypodermic tube top, transverse view, taken with the LEICA microscope (magnification: 10x)

***Xradia MicroXCT Tomographic X-Ray Microscope***

The micro-XCT microscope was later used due to its ability to provide non-destructive micro-CT imaging of the tube-insert combination. It provided a 3-dimensional view, allowing the measurement of the tube and insert at different rotation angles. This allowed the diameter

measurements to be more accurate (±1.5 μm). From the micro-CT scans, particle depositions on the insert/tube walls could be seen more clearly. However, note that, if the particles deposited in the sample tubes and on the inserts had densities similar to that of air, the particles would not be visible in the micro-CT scans since there would be insufficient visible contrast between the particles and the air in the tubes.

The microscope is located in one of the Institute of Bioengineering Research (IBER) laboratories, University of Kansas (Learned Hall 1120). The main contact person for usage of the microXCT microscope is Dr. Qiang (Charles) Ye, Director of the IBER laboratories. Training from Dr. Ye was required before using the microXCT microscope. The rates and procedures for using the microXCT are described in App. E.1.

Theoretical pressures that were calculated from the micro-CT diameter measurements were compared with the pressures measured from the experimental flow trials described in Section 2.9. The micro-CT images of the samples used in the trials described in Section 2.9 are shown in Apps. E.2 and E.3.

The microXCT microscope was also very useful for measuring the inner diameter at the BGI tube-to-plate entrance as shown in Fig. 3.3. This was done because one of Dr. Munden's ideas was to place the degradable suture through the tube-to-plate opening instead of from the other end of the tube. It was suspected that the tube-to-plate entrance was smaller than the ID of the tube. These precise measurements would have been impossible without the use of the microXCT microscope, especially since the tube diameter is very small and the shape of the BGI plate was irregular.

The tube-to-plate opening of the BGI was cut out, as shown in Fig. 3.4, and was

approximately 1 mm by 1 mm. The cut-out sample was placed in the crocodile clip on the microXCT mounting platform for imaging.

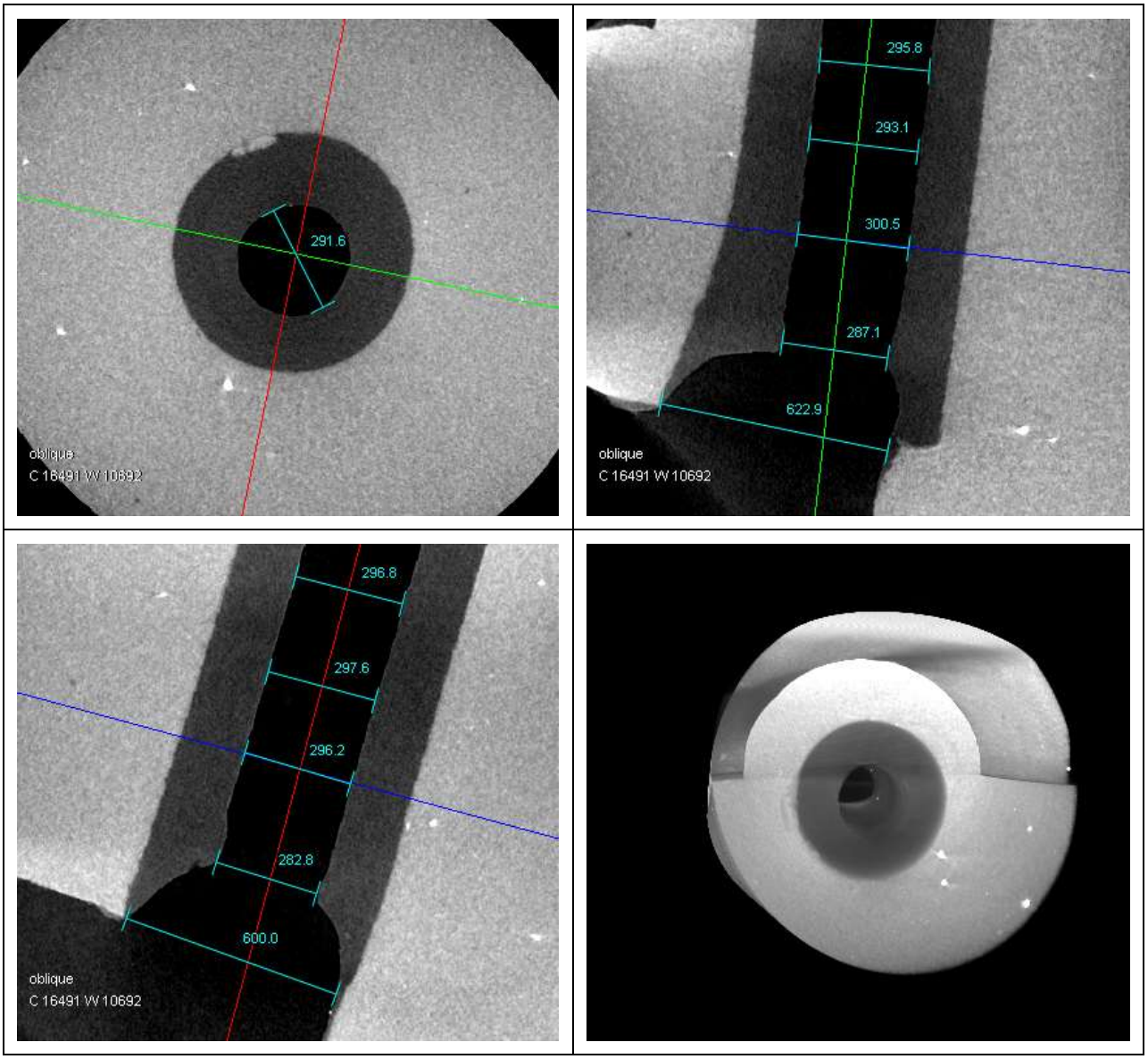


Fig. 3.3: Micro-CT images of the entrance from the silastic tube to the episcleral plate of a BGI sample with ID measurements from the X-Y plane [top left], Y-Z plane [top right] and X-Y plane [bottom left], as well as a three-dimensional view [bottom right] (magnification: 10x) [February 20, 2017]

The average ID of the tube-to-plate opening was measured to be 293.7 ± 5.5 µm which was 11.26 µm smaller than the average BGI tube ID of 0.30 mm as sketched in Fig. 3.4. This could

pose a problem if the diameter of the degradable insert that was placed in the BGI tube was larger than the ID of the tube-to-plate opening. Additionally, considering that some degradable materials expand before degrading, the degradable insert could entirely occlude the tube entrance and cause the BGI to fail.

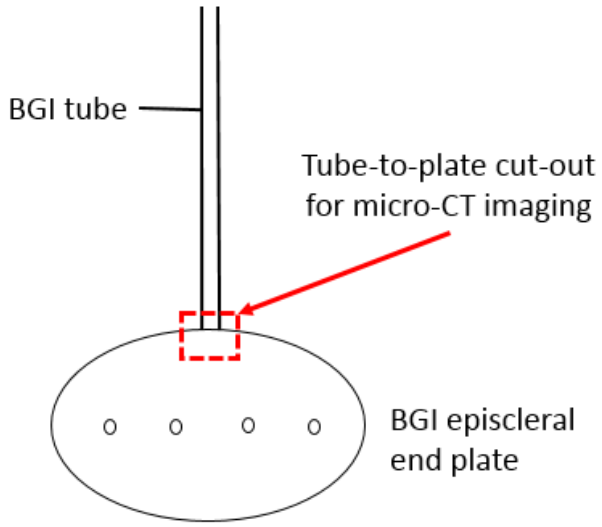


Fig. 3.4: Tube-to-plate cut-out for micro-CT imaging

## 3.2. Cover Page of Submitted Paper

**Experimental system for rigorous study of flow through glaucoma drainage devices**

T H T Teo, A Ramani, P M Munden, S E Wilson, S L Kieweg, R L Dougherty

Department of Mechanical Engineering, University of Kansas, 1530 W 15th Street, 3138 Learned Hall, Lawrence, KS 66045 T H T Teo
Master's Student
Product Development Center [GB-F72], Ford Motor Company, 20901 Oakwood Blvd, Dearborn, MI 48124 A Ramani
AVBOM Analyst
Department of Ophthalmology, University of Kansas Eye Center**,** 7400 State Line Road, Suite 100**,** Prairie Village, KS 66208 P M Munden
Ophthalmologist
Department of Mechanical Engineering, University of Kansas, 1530 W 15th Street, 3138 Learned Hall, Lawrence, KS 66045 S E Wilson
Associate Professor
Department of Mechanical Engineering, University of Kansas, 1530 W 15th Street, 3138 Learned Hall, Lawrence, KS 66045 S L Kieweg
Associate Professor
Department of Mechanical Engineering, University of Kansas, 1530 W 15th Street, 3138 Learned Hall, Lawrence, KS 66045 R L Dougherty
Professor

Correspondence to: S E Wilson, sewilson@ku.edu

**SYNOPSIS**

Pressure measurements for single microtubes and annular microtubes were repeatable and fell within theoretical predictions. Use of annular inserts in non-valved glaucoma drainage devices present an option for providing immediate post-operative intraocular pressure control.

## 3.3. Abstract

Background/Aims: Treatment of elevated intraocular pressure (IOP) for severe glaucoma may require implantation of glaucoma drainage implants (GDIs) to shunt aqueous humor (AH) from the eye to reach the normal physiological IOP range of 10 - 22 mm Hg. We describe an experimental system which measures pressure drop for physiologic flow rates (1.0 - 3.5 μl/min) through non-valved GDI (NVGDI) microtubes for investigating hypotony prevention during the early post-operative NVGDI surgery period. The effect of adding annular inserts to prevent post-operative hypotony is studied.

Methods: Flow trials were performed using VSD (polyether-ether-ketone-sheathed fused silica) microtubes having inner diameters of 50 and 75 μm. Annular flow trials were performed using 24 gage (G) and 30G stainless-steel hypodermic tubes having 26G, 28G, 30G, and 36G nichrome wire inserts.

Results: The pressure measurements for single microtubes were no more than 2 mm Hg outside of theoretical ranges (5 - 45 mm Hg). For instance, the average experimental pressure of a 50.4 μm inner diameter microtube was 35.1 mm Hg, while theory predicted 35.6 - 55.5 mm Hg. For annular flow, pressure measurements were bounded by theory and corresponded with the theoretical trend of increasing pressure for decreasing effective diameter, within the range of 6 - 20 mm Hg.

Conclusions: Results were repeatable and constant over 2-hour to 10-day periods, demonstrating that the experimental system can be used to study the transition from immediate post-operative to long-term IOP control. Annular inserts were found to be effective in increasing pressure and could be used to prevent post-operative hypotony. Future efforts will examine varying annular insert size and using degradable inserts.

## 3.4. Introduction

Glaucoma encompasses a group of conditions that result in intraocular pressure (IOP) related damage to the optic nerve that will reduce vision and, if not treated, may lead to blindness. Normal IOP levels range from 10 - 22 mm Hg and are elevated in patients with glaucoma [11]. When drugs or laser surgery fail to lower the IOP to a safe level, a glaucoma drainage implant (GDI) may be surgically implanted.

There are two main forms of GDIs: valved (VGDI) and non-valved (NVGDI). A fibrous capsule forms around the GDI 2 - 6 weeks after surgery, creating long-term AH outflow resistance for IOP control [3]. VGDIs provide reasonable post-operative IOP control, but poorer long-term control than NVGDIs [10]. NVGDIs offer little resistance to aqueous humor (AH) outflow in the immediate post-operative period, resulting in low IOP (hypotony) [7]. NVGDI modifications to prevent post-operative hypotony have included several intraoperative methods [4, 7, 37-40]. Combinations of these methods (e.g., external tube ligation with an absorbable suture and tube fenestrations) sometimes provide immediate clinical post-operative IOP control. However, *in vivo* studies of these methods report complication rates ranging from 19% - 71.8% [4-8]. An ideal GDI should control immediate post-operative IOP (VGDI-like) with good long-term control (NVGDI-like).

In an initial clinical study by our research group, it was found that the placement of a degradable insert in a NVGDI showed promising results in reducing the risk of early post-operative hypotony [43]. Placing a degradable insert of outer diameter ($D_i$) and length ($L$) in NVGDI tubing should provide sufficient resistance to AH outflow for maintaining acceptable early post-operative IOP. The insert degrades over a clinically relevant period (4-6 weeks) and maintains AH outflow at typical physiologic rates (~2.5 µl/min) until formation of the fibrous capsule around the implant

plate provides consistent physiologic flow and IOP control. While these early clinical results are promising, there is a need for a rigorous experimental assessment of the effects of such inserts on NVGDIs.

Described herein is the development and validation of duplicate experimental setups to measure flow rate and pressure drop across NVGDI tubing. Validation: 1) investigated experimental consistency, within each setup and between setups; and 2) compared experiment with theory. Validated experimental setups enable future systematic *in vitro* evaluation of modified NVGDI performance.

The experimental setups pump deionized (DI) water through GDI-like tubing, simulating AH flow through implanted GDI tubing, while flow is controlled and pressure is monitored. Inflexible SS or VSD tubing is used, and inserts are nichrome wire. In the following, a theoretical model for pressure and flow is introduced; and experimental data is compared with the theoretical model.

Previous studies have measured very short-term *in vitro* pressure across GDI tubing as applied to clinical situations [38-40, 54-57]. The majority of those studies focused on comparing short-term pressure measurements among different types of GDIs and comparing pressures resulting from different NVGDI intraoperative modifications. In this regard, no published research has been found which compares GDI experiments with relevant theory. Similarly, no *in vitro* research on annular flow (GDI tubing with an insert) has been found; nor long-term (e.g., 5-30 day) *in vitro* studies of pressure-flow through GDI-like tubing. It is very important to fill these gaps in research. Thus, based upon these critical needs, our goals are to assess the:

1. effect of inner diameter ($D_o$) on single tube flow resistance. Hagen-Poiseuille (H-P) laminar

flow theory [50] indicates that, as inner diameter decreases, resistance, and therefore pressure drop, increases. Experimental measurements are compared to H-P pressure drop ($\Delta P$) predictions. While the focus is annular flow, this study initially evaluates whether H-P theory (with its assumptions/limitations) can accurately predict our specific tubular experimental results, helping to validate the experimental setup and determine that theory can then be used to assist in developing novel GDI designs.

2. effect of annulus size on annular tube flow resistance. Theory indicates that, as the effective diameter ($D_{eff}$) decreases, flow resistance, and therefore $\Delta P$, increases in a specific repeatable manner. Experimental measurements are compared to H-P-predicted annular flow $\Delta P$; and results are used to assess accuracy as applied to NVGDIs. This is critical for future work, helping to explore the viability of an annular insert for reducing flow and maintaining reasonable IOP during the 30-day post-operative period.
3. ability to maintain consistent annular flow resistance over time. It is expected that resistance and $\Delta P$ across single and annular NGVDD-like tubing remains constant over time. The results presented demonstrate that the experimental setup is appropriate for assessing long-term flow measurements in glaucoma-related settings.

## 3.5. Materials and Methods

The analytical model assumes the fluid to be incompressible and Newtonian, as well as being fully developed laminar flow throughout a smooth-walled tube or annulus. For 2.5 µl/min flow in a 50 µm $D_o$ open tube or $D_{eff}$ [see Eq. (3.6)] annular tube, the computed velocity and Reynolds number ($\mathrm{Re} = \rho v D/\mu$, $D = D_{eff}$ or $D_o$) are 0.021 m/s and 1.18, respectively. Since Re is well below the 2100 break-point for laminar flow [50] and is fully developed after moving ~$0.1D_o$ along the tube [50], theoretical pressures can be modeled using the analytical H-P solution [50]:

$$\Delta P = 128(Q)(\mu)(L) / (\pi D_{eff}^4) \tag{3.6}$$

where

$$D_{eff}^4 = D_o^4 - D_i^4 - (D_o^2 - D_i^2)^2 / \ln(D_o/D_i) \tag{3.7}$$

Here, $\Delta P$ is the differential pressure along a length $L$ tube, $Q$ is the flow rate, and $\mu$ is the fluid dynamic viscosity. $D_o$ and $D_i$ are the outer and inner diameters, respectively, of the tube's annulus. For non-annular tubes, $D_i = 0$, and $D_{eff} = D_o$ [50]. For this case, a single tube of $D_o$ = 60 - 90 µm with $Q$ = 2.5 µl/min should give $\Delta P$ in the clinically relevant range of 5 - 25 mm Hg (Fig. 3.5); and annular tube $D_{eff}$ should range from 45 - 70 µm.

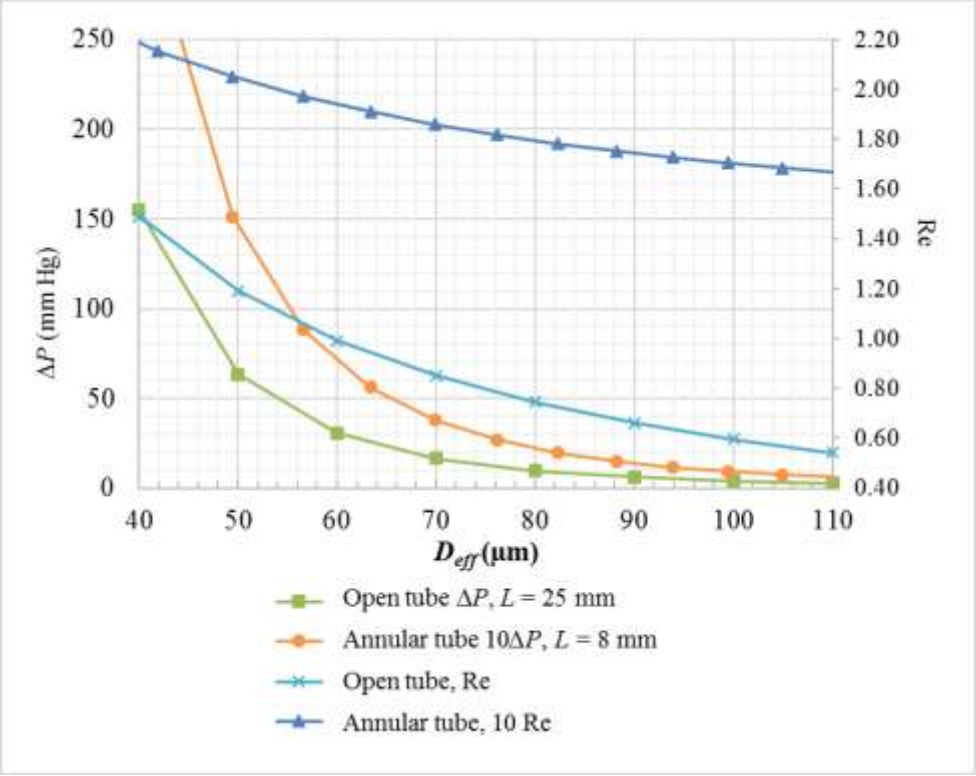


Fig. 3.5: Theoretical $\Delta P$ and Re variations as $D_{eff}$ changes (annular $D_o$ = 350 µm, $D_i$ varies)

### 3.5.1. Experimental Setup

Two identical microflow pressure- and flow-measuring setups were developed (Fig. 3.6).

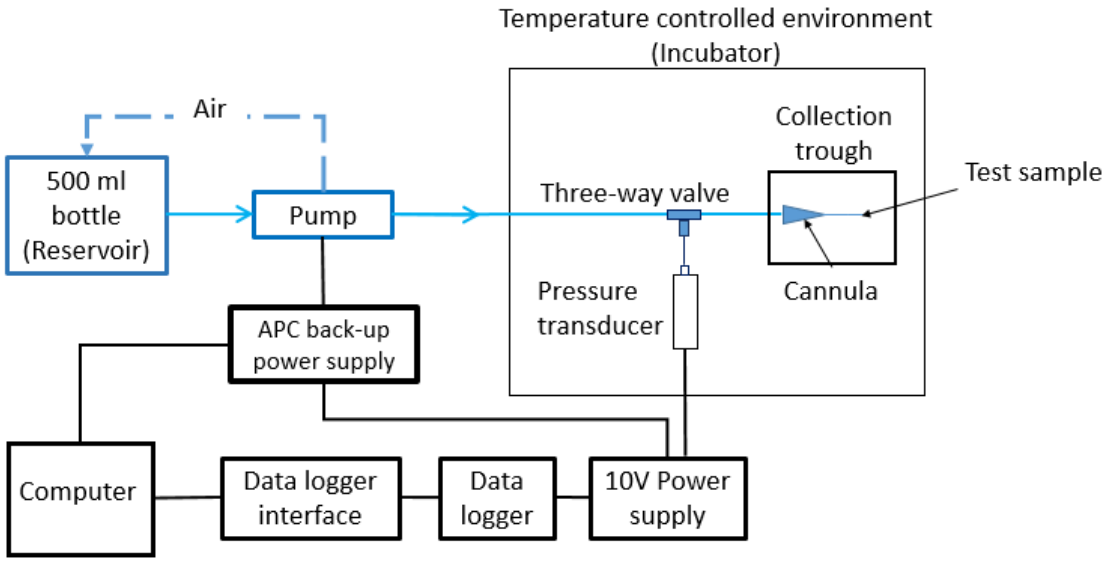


Fig. 3.6: Schematic of microflow pressure and flow rate measurement test setup

The two setups were used to validate each other, which then allowed simultaneously performing separate trials. Each setup consisted of a precision pneumatic pump (0 - 50 µl/min, ±0.05 µl/min; CorSolutions, Ithaca, NY-US), a bottle containing deionized (DI) water, microfluidic tubing and connections, a pressure transducer (0 - 130 mm Hg, ±0.2 mm Hg; Omega Engineering, Norwalk, CT-US), a data logger (Omega Engineering, Norwalk, CT-US), and a test sample [43]. The test sample was located in a temperature-controlled incubator (±1°C; Miller Manufacturing, Glencoe, MN-US).

Trials were run using various tubing configurations. A typical trial pumped DI water at the nominal human AH rate of 2.5 µl/min, and measured the accompanying pressure across test sample tubing. Manufactured GDI tube lengths are 7 - 32 mm, with typical implanted lengths being from 7 - 20 mm.

### 3.5.2. Experimental Trial Procedure

***Open Single Tube Flow Trials***

For single open tube tests, 2 - 3 hour long flow trials were performed to validate the setups' abilities to measure pressures across the microtube test samples [42]. To test setup repeatability in open single tube trials, 10 trials were performed using 35 mm long VSD microtubes with $D_o$ = 50 µm (five trials) and 75 µm (five trials) (Fig. 3.7). These are robust inert tubes with smooth wall surfaces having precise inner diameters within ±3 µm of nominal (per manufacturer) [58]. Each 35 mm long VSD microtube was placed in a 24G SS hypodermic dispensing tip at the test section (Fig. 3.6); and pressure was logged at 0.1 Hz. Follow-on tests were then done (Fig. 3.7) with tubing whose sizes were determined with micro-CT scans (±0.2 µm) to improve comparison with theoretical predictions. To test the long-term pressure measurement consistency of the setups, these trials were done with 25 mm long 50 µm (3 samples) and 75 µm (1 sample) VSD tubes for 10 days and 2 days, respectively.

***Annular Flow Trials***

For annular tubing tests, three hour trials were performed using combinations of 23G, 24G, and 30G SS hypodermic tubes with 26G, 28G, 30G, and 36G nichrome inserts (8 mm long). These tests were performed to determine the ability of the two setups to provide accurate initial annular flow and pressure data for tubes with various annuli, and to investigate trends in the difference between theory and experiment. Prior to each test, any bubbles were flushed from the setups. After each trial, the sample was dried and micro-CT imaged to accurately measure sample $D_i$ and $D_o$.

## 3.6. Results

### 3.6.1. Open Single Tube Flow Trials with VSD Microtubes

Figure 3.7 shows the initial ten trial runs' results (solid lines), five with nominal $D_o$ = 50 µm and five with nominal $D_o$ = 75 µm (not micro-CT imaged, so $D_o$'s were ±3 µm) [20]. The high pressures shown within the first hour of Fig. 3.7 were from priming the pumps at 10 µl/min,

flushing any bubbles. As shown, after reducing flow rate to 2.5 µl/min, data leveled out to become relatively consistent.

The experimental $\Delta P$ was averaged over the 2 - 3 hour acquisition time of Fig. 3.7. The average experimental $\Delta P$ ranges for the 50 and 75 µm $D_o$ tubes were 44.8 - 67.2 (±9.3) and 8.0 - 8.5 (±0.1) mm Hg, respectively. Accounting for variations in $D_o$, $Q$, and $L$, the initial average measured steady-state pressures (solid lines) were typically close to, or within, the limits of the theoretical pressure ranges (Table 3.3). As previously stated, additional test runs were performed wherein the tubing diameters were micro-CT scanned. Results from this set of runs are also shown in Fig. 3.7 (dashed lines).

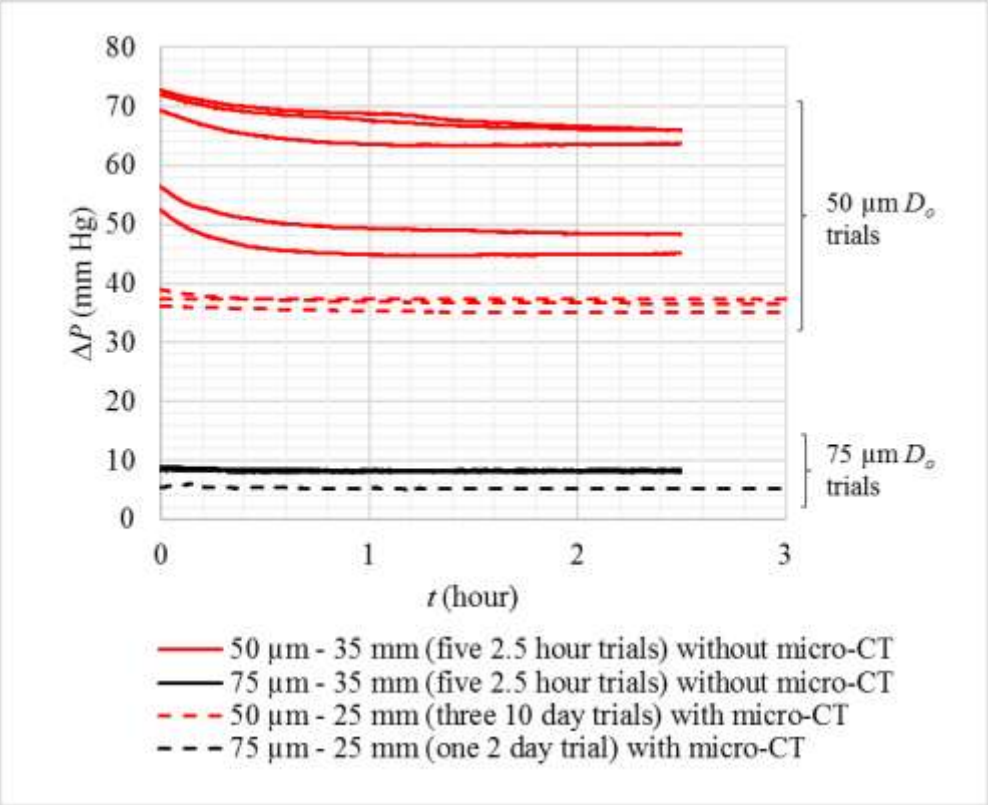


Fig. 3.7: Experimental pressure results of VSD microtube flow for 50 and 75 µm $D_o$'s ($Q$ = 2.5 µl/min; 25°C test conditions). Note that dashed lines are essentially constant from 3 hours through the applicable 2-day or 10-day period.

Table 3.3: Comparison of experimental results (Fig. 3.7) with theoretical predictions using various $D_i$ and $D_o$ combinations for single open tube and annular trials. This table is sorted from smallest to largest $D_{eff}$ , first for open tubes, then for annuli

| Tube-Insert Sample | Diameter | | | $\Delta P$ (mm Hg)[d] | | |
|---|---|---|---|---|---|---|
| | $D_o$ (μm) (min to max) | $D_i$ (μm) (min to max) | $D_{eff}$ (μm) (min to max) | Theory (Range)[b] (H-P) | Experimental Average ± Standard Deviation | Difference (Range)[b,c] |
| No Insert | 50.1 (49.3 to 50.7) | 0.0 | 50.1 (49.3 to 50.7) | 45.0 (39.1 to 52.4) | 39.3 ± 1.17[e] | 15% (-0.4% to 33%) |
| No Insert | 50.4 (48.6 to 51.9) | 0.0 | 50.4 (48.6 to 51.9) | 43.9 (35.6 to 55.5) | 33.7 ± 1.60[e] | 30% (6% to 65%) |
| No Insert | 51.7 (50.9 to 52.8) | 0.0 | 51.7 (50.9 to 52.8) | 39.7 (33.5 to 46.1) | 39.5 ± 1.13[e] | 1% (-15% to 17%) |
| No Insert | 75.9 (75.3 to 76.9) | 0.0 | 75.9 (75.3 to 76.9) | 8.5 (7.4 to 9.6) | 5.4 ± 0.65[f] | 57% (37% to 78%) |
| 30G-36G | 165.0 (162.6 to 167.3) | 136.7 (134 to 138.8) | 46.2 (40.6 to 52.2) | 19.9 (10.2 to 39.5) | 15.0 ± 0.10[a] | 33% (-32% to 164%) |
| 23G-26G | 437.3 (432.9 to 438.7) | 411.5 (411.1 to 411.8) | 55.8 (48.0 to 58.7) | 9.3 (6.3 to 20.3) | 8.8 ± 0.04[a] | 6% (-22% to 109%) |
| 24G-28G | 358.8 (355.5 to 362.0) | 330.7 (328.2 to 332.5) | 56.5 (48.6 to 64.9) | 8.9 (4.2 to 19.2) | 9.6 ± 0.09[a] | -7% (-34% to 20%) |
| 24G-30G | 351.8 (346.9 to 358.2) | 265.1 (262.5 to 268.5) | 128.0 (118.6 to 138.0) | 0.34 (0.21 to 0.54) | 0.24 ± 0.01[a] | 41% (4% to 83%) |
| 23G-28G | 437.3 (428.4 to 444.3) | 336.1 (333.2 to 340.7) | 152.1 (163.3 to 136.4) | 0.17 (0.11 to 0.31) | 0.37 ± 0.01[a] | -54% (-71% to -16%) |

[a] Averaged over data acquisition time between 0.5 and 2.5 hours; accuracy of experimental pressure measurement is ±0.2 mm Hg; $L$ = 8 mm

[b] Range is for variation in $Q$ (±0.125 μl/min), $L$ (±1 mm), $D_i$ and $D_o$ (minimum to maximum values of columns 2 to 3)

[c] Difference = (Theoretical – Experimental) / Experimental

[d] $Q$ = 2.5 μl/min, and $\mu$ = 0.00089 Pa-s (25°C)

[e] 10 day average; experimental pressure measurement accuracy is ±0.2 mm Hg; $L$ = 25 mm

[f] 2 day average; experimental pressure measurement accuracy is ±0.2 mm Hg; $L$ = 25 mm

The average experimental pressures and tube $D_o$'s of the three 50 and the 75 μm microtubes are listed in the first four rows of Table 3.3. For the micro-CT'd tube diameters of 50.1, 50.4, 51.7 and 75.9 μm, the standard deviations of the experimental $\Delta P$'s were 1.16, 1.59, 1.15 and 0.65 mm Hg, respectively, demonstrating that the setups can provide consistent pressure measurements over long-term periods of 2 - 10 days.

### 3.6.2. Annular Flow Trials for Hypodermic SS Tubes with Nichrome Inserts

Since the most important effort of this paper is to investigate the effects of adding inserts to NVGDI-like tubing and determine the degree of pressure stability/repeatability, we next show annular flow trial results (tubes with cylindrical inserts). Figure 3.8, along with Table 3.3 (last five rows), shows experimental pressure results for annular flow in 23G, 24G and 30G tubes with 8 mm long 26G, 28G, 30G and 36G nichrome inserts.

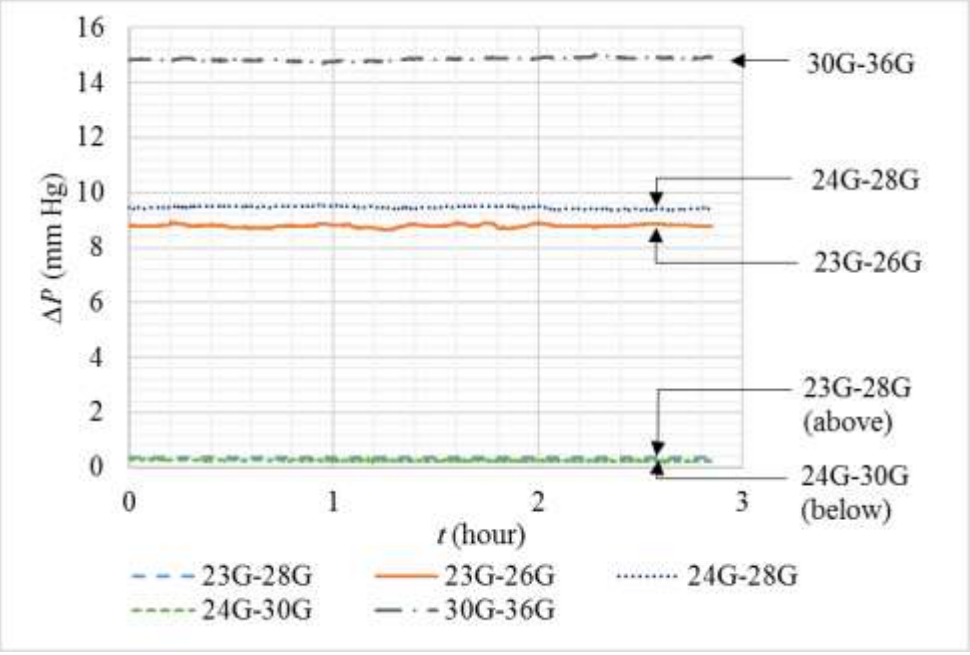


Fig. 3.8: Experimental pressure results of annular flow in 23G, 24G and 30G SS hypodermic tubes with 26G, 28G, 30G and 36G nichrome inserts ($Q$ = 2.5 μl/min; $L$ = 8 mm; 25°C test conditions)

## 3.7. Discussion

Both experimentally and theoretically, when $D_{eff}$ increases, $\Delta P$ decreases. This can be observed by comparing Table 3.3's 'experimental average' and 'theory' columns with the '$D_{eff}$' column.

### 3.7.1. Open Single Tube Flow Trials with VSD Microtubes

A tube with a nominal $D_o$ and $L$ may vary within manufacturer's tolerance ranges; and $Q$ was measured within transducer tolerance range. Therefore, theoretical $\Delta P$ predictions could vary substantially.

With fluid properties at room temperature (25°C), the combination of variations in tube $D_o$ (50 ± 3 μm or 75 ± 3 μm), $Q$ (2.5 ± 0.125 μl/min), and $L$ (35 ± 1 mm), the calculated theoretical $\Delta P$ ranges in the 50 μm and 75 μm $D_o$ tubes were 46.4 - 87.7 mm Hg and 9.9 - 15.9 mm Hg, respectively. Since the solid line data in Fig. 3.7 did not have micro-CT scanned diameters, these theoretical ranges apply. The nominal 50 μm data fell within its theoretical range. The nominal 75 μm data fell about 1 mm Hg below its theoretical range. Knowing that tube $D_o$ had the greatest impact on $\Delta P$, which was obvious from it being fourth power in Eq. (3.6) ($D_{eff} = D_o$, $D_i = 0$), a small extra variation for the 75 μm tubes could yield a 1 mm Hg mismatch, along with impact of ±0.2 mm Hg transducer measurement error. The possible variations listed, coupled with fourth power dependence on diameter, demonstrate that meaningful comparison with data required accurate knowledge of each tube sample's experimental diameter, preferably within ±1 μm. Thus, the next samples run and shown in Fig. 3.7 (dashed lines) were micro-CT scanned.

Micro-CT scans were made at only a few locations along the length of each tube; so, when making theoretical calculations, the micro-CT scanned segments were taken as representative of the whole tube length. These measured diameters were used to calculate theoretical $\Delta P$ in Table

3.3. Variations in $Q$ and $L$ were also included in theoretical predictions. From Table 3.3, there was a 1% - 30% difference between average theoretical and experimental pressures for 50 μm tube trials and a 57% difference for the 75 μm tube trial. Note that, if we account for flow rate and/or length error ranges in comparison with their nominal values, theory-to-experiment differences could be as low as -0.4% and 37% for 50 and 75 μm tubes, respectively (shown in the "Range" values of Table 3.3's column 7). Note that the 37% difference was due to a 2 mm Hg difference for a 7 mm Hg value. So, the measurement/theoretical magnitudes were relatively close, and therefore, the difference could be from low-impact sources. Experimental pressures could have been lower than theoretical pressures due to expansion of VSD tubes as internal fluid pressure was exerted on them. Future experiments will be performed to investigate potential cause(s).

### 3.7.2. Annular Flow Trials for Hypodermic SS Tubes with Nichrome Inserts

For Table 3.3's rows 5 - 7, experimental $\Delta P$s were relatively close to theoretical $\Delta P$s and were within the theoretical range that accounted for variation in $Q$, $L$, $D_o$ and $D_i$. The difference between theoretical and experimental $\Delta P$ was small when $D_{eff}$ was small enough to produce a clinically relevant experimental $\Delta P$ (30G-36G, 24G-28G and 23G-26G samples). When $D_{eff}$ was large enough that the experimental $\Delta P$ was very low (24G-30G and 23G-28G; Table 3.3's rows 8-9), the experimental/theoretical comparison was poor. This is understandable, since pressure transducer error was ± 0.2 mm Hg; and these two samples' experimental $\Delta P$s ranged over 0.2-0.4 mm Hg.

### 3.7.3. Overall Experimental Verification

These experiments were designed to provide benchmark validation measurements and confirmation of theoretical application to the setups. Thus, if the experimental setup needed modification or theory needed revision, comparison between the two should provide direction for

that modification or revision.

Results presented have demonstrated that the current test system can accurately maintain constant flow rate and measure pressure drop across tubing similar to that used in GDIs. In addition, the current experimental setup can take consistent long-term (e.g., 10 days) pressure drop data which compares well with theoretical predictions.

These results support the examination of NVGDI modifications (e.g., degrading inserts) that have potential for consistently controlling post-operative IOP while scar tissue growth covers the implant to take long-term IOP control. Future work will examine the use, impact and designability of degradable inserts, and then investigate the added possibility of drug eluding inserts.

Acknowledgements: Micro-CT scans made possible by KU's Institute of Bioengineering Research (IBER).

Funding: Partial support provided by KU Medical Center (KUMC) Eye Center.

## 3.8. Additional Information

This section includes supporting material that could not be included in the submitted paper due to length restrictions.

### 3.8.1. Theoretical Analysis for Single Tube Flow

For the case of $D_i$ = zero, Fig. 3.9 gives H-P predictions for variation of $D_o$ while maintaining the flow rate ($Q$) and tube length ($L$) at 2.5 µl/min and either 25 or 35 mm. This $D_o$ variation yields $\Delta P$ values within an order of magnitude above and below clinically relevant pressures; and it is apparent that even ±3 µm in $D_o$ has a potentially significant effect on the pressure, especially at smaller $D_o$'s, causing pressure changes up to ± 20 mm Hg (Table 3.4). Note

that, from Fig. 3.9, $D_o$ between 60 and 90 µm gives pressures in the clinically relevant range of 5-25 mm Hg for 25 mm long tubes.

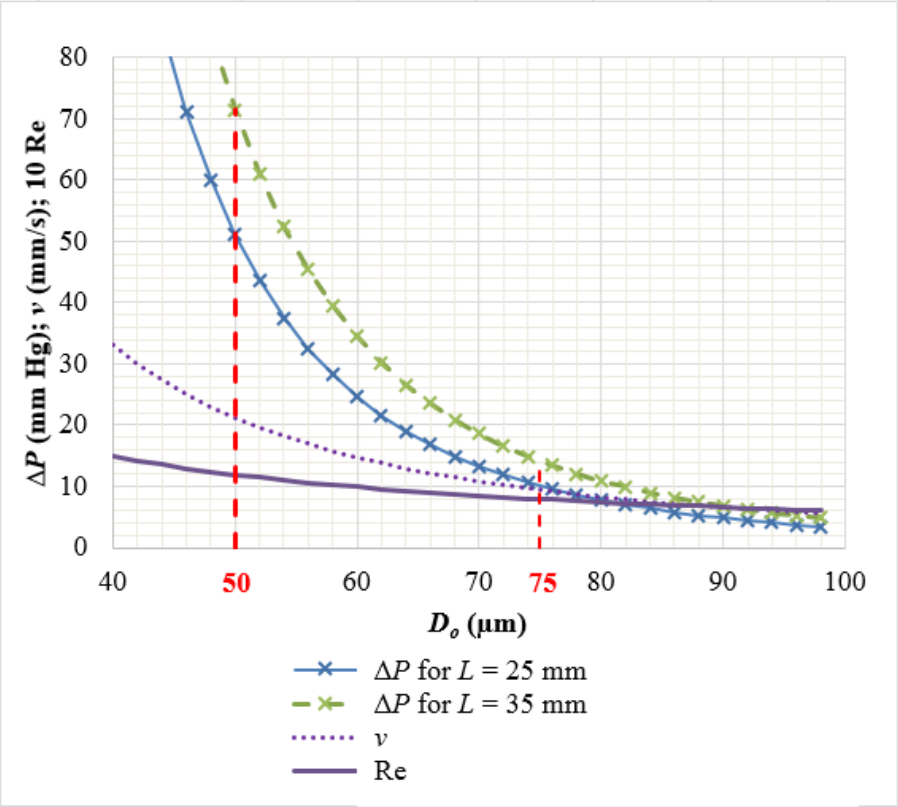


Fig. 3.9: Theoretical pressure loss, velocity, and Reynolds number for flow through single tubes with different $D_o$'s ($Q$ = 2.5 µl/min; properties at 25°C)

Due to the fact that a tube with a nominal inner diameter ($D_o$) and length ($L$) may vary within the manufacturer's tolerance ranges, and that flow rate ($Q$) was measured within the tolerance range of the flow meter (± 0.2 mm Hg), theoretical pressure predictions can vary over a significant range. Table 3.4 shows the theoretical effect of varying each parameter individually, as well as in combination. As can be seen in Table 3.4, tube $D_o$ had the greatest impact, which was obvious from it being a fourth power term in Eq. (3.6), when $D_{eff} = D_o$ ($D_i$ = 0). Thus, Table 3.4, coupled with the results previously examined in Fig. 3.7, demonstrated the possible theoretical variations and showed that a meaningful comparison with data required having relatively accurate

knowledge of the experimental diameter for each experimental tube sample, preferably with a ±1 μm measurement technique.

Table 3.4: Theoretical and experimental pressure ranges for microtube trials. This table illustrates the effects of variation in $D_o$, $Q$, and $L$ on theoretical $\Delta P$. Experimental $\Delta P$ of the 2.5-hour trials with 50 μm and 75 μm tube $D_o$s from Fig. 3.7 is compared to the theoretical $\Delta P$, assuming that there are variations in all three parameters

| Nominal Values: Flow Rate ($Q$) = 2.5 μl/min; Length ($L$) = 35 mm<br>Dynamic Viscosity ($\mu$) = 0.00089 Pa.s (at 25°C) | | | | |
|---|---|---|---|---|
| 50 μm Exp. Results (mm Hg): 44.8 – 67.2[a] (± 9.3)[b]<br>75 μm Exp. Results (mm Hg): 8.0 – 8.5[a] (± 0.1)[b] | | | | |
| $D_o$ Variation (μm) | $Q$ Variation (μl/min) | $L$ Variation (mm) | $D_o$: 50 μm Theoretical $\Delta P$ Range (mm Hg) | $D_o$: 75 μm Theoretical $\Delta P$ Range (mm Hg) |
| ± 3 | ± 0 | ± 0 | 50.3 – 81.3 | 10.7 – 14.8 |
| ± 0 | ± 0.125 | ± 0 | 60.3 – 66.7 | 11.9 – 13.5 |
| ± 0 | ± 0 | ± 1 | 61.7 – 65.3 | 12.2 – 12.9 |
| ± 3 | ± 0.125 | ± 1 | 46.4 – 87.8 | 9.9 – 15.9 |

[a] Averaged over the 2 - 3 hour data acquisition time period; accuracy of experimental pressure measurement is ± 0.2 mm Hg

[b] Standard Deviation (mm Hg)

Table 3.4 also shows a comparison of the initial experimental data with theoretical predictions that include possible variations in tube diameter, tube length and flow rate. Accounting for these variations, the initial average measured steady-state pressures were found to be somewhat below the theoretical pressure ranges, but typically close to, or within, the lower limits of the pressure ranges.

### 3.8.2. Example Micro-CT Scans

Examples of the micro-CT scans for a 75 μm VSD tube are shown in Fig. 3.10; and scans for a 24G SS tube with a 28G nichrome insert are shown in Fig. 3.11.

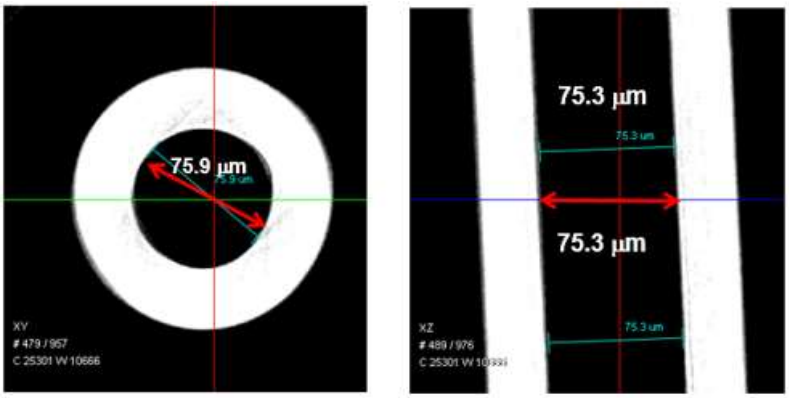


Fig. 3.10: Example micro-CT image of the cross-section of a nominal 75 µm $D_o$ VSD microtube in the (a) X-Y plane and (b) X-Z plane

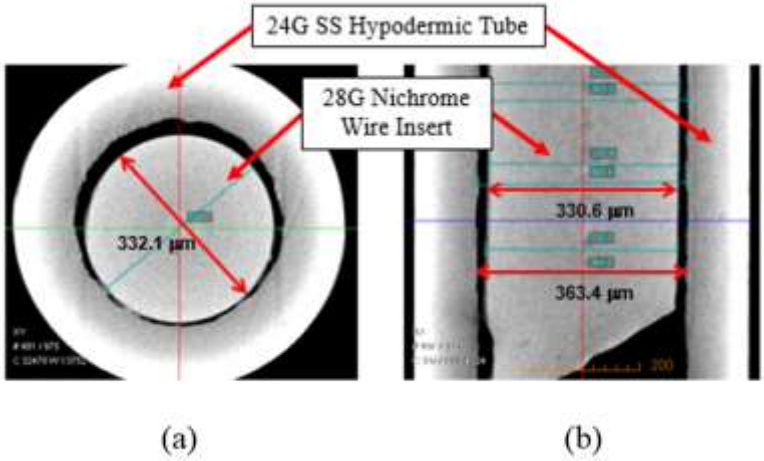


Fig. 3.11: Example micro-CT image of the cross-section of a 24G SS hypodermic tube with a 28G nichrome wire insert in the (a) X-Y plane and (b) X-Z plane

From Fig. 3.11, it is seen that the 28G nichrome wire insert is not concentric with the 24G SS tube. This non-concentricity could be one of the factors affecting $\Delta P$ that cannot be estimated with the conventional H-P theory. Refer to App. E.2 for the micro-CT images of the three 50 µm and one 75 µm VSD tubes, for which experimental pressure results are shown in Fig. 3.7. For the micro-CT scans of the annular tube-insert samples (experimental ΔP results are shown in Fig. 3.8), refer to App. E.3.

### 3.8.3. Additional Annular Flow Δ*P* Data

The annular flow trials discussed in the paper were repeated with new samples. The samples were labelled as shown in Table 3.5 during testing to allow differentiation of the samples. Note that the samples labelled A1, B1, C01, D1, and E1 were for the five samples that were discussed in the submitted paper; and A2, B2, C02, D2 and E2 were for the repeated samples. The Δ*P* plots for all ten trials are shown in Fig. 3.12. Table 3.5 lists the experimental results and the measurements of the samples for all ten trials. Refer to App. E.3 for the micro-CT images of the samples.

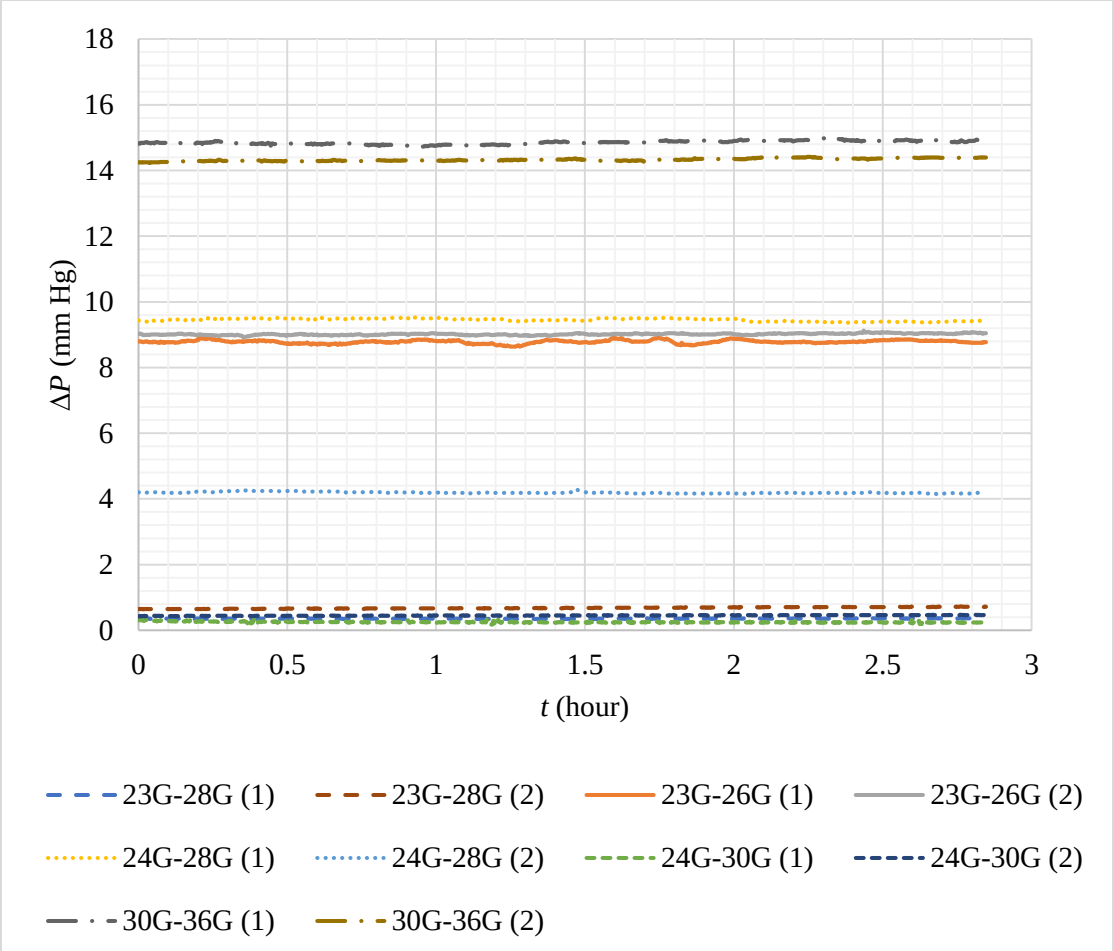


Fig. 3.12: Δ*P* results of all annular trials with varying $D_o$ and $D_i$, including the repeated trials

Table 3.5: Annular trial $D_i$ and $D_o$ measurements and their respective theoretical $\Delta P$ ranges and average experimental $\Delta P$s with indication of whether micro-CT imaging was done on the samples

| Sample Label | Micro-CT Done[a] | SS Tube | | Nichrome Insert | | Theoretical $\Delta P$ range (mm Hg)[c] | Average ± Standard Deviation of Experimental $\Delta P$ (mm Hg) |
|---|---|---|---|---|---|---|---|
| | | Gauge | $D_o$ (μm)[b] | Gauge | $D_i$ (μm)[b] | | |
| A1 | Yes | 23G | 437.3 | 28G | 336.1 | 0.14 – 0.20 | 0.37 ± 0.01 |
| B1 | Yes | 23G | 436.0 | 26G | 411.5 | 9.07 – 12.90 | 8.78 ± 0.04 |
| C01 | Yes | 24G | 358.8 | 28G | 330.7 | 7.39 – 10.50 | 9.59 ± 0.09 |
| D1 | Yes | 24G | 351.8 | 30G | 265.1 | 0.28 – 0.40 | 0.24 ± 0.01 |
| E1 | Yes | 30G | 165.0 | 36G | 136.7 | 16.53 – 23.49 | 14.98 ± 0.10 |
| A2 | Yes | 23G | 434.0 | 28G | 334.5 | 0.15 – 0.21 | 0.81 ± 0.06 |
| B2 | No | 23G | - | 26G | - | - | 9.04 ± 0.02 |
| C02 | Yes | 24G | 364.5 | 28G | 328.5 | 3.50 – 4.97 | 4.14 ± 0.03 |
| D2 | No | 24G | - | 30G | - | - | 0.50 ± 0.02 |
| E2 | No | 30G | - | 36G | - | - | 14.45 ± 0.04 |

[a] Indicates whether micro-CT images were taken of the sample (Yes/No)

[b] Average diameters measured from micro-CT images

[c] Theoretical pressure range calculated using H-P theory with average measured $D_o$ and $D_i$, $Q$ = 2.5 μl/min, $L$ = 25 mm, and $\mu$ = 0.00089 Pa-s (25°C); Range is for variation in $Q$ (±0.125 μl/min) and $L$ (±1 mm)

### 3.8.4. Long-Term Results

To the authors' knowledge, long-term (e.g., 5 to 30 day) results have not been presented in the literature. Typically, *in vitro* runs that are less than a few hours long have been presented by past researchers [38]. Initially, when long-term runs were made on the current experimental setup, pressure drop across the test specimen rose dramatically over 7- to 21-day trials. Figure 3.13

shows an example 10-day run with the dramatic increase in pressure drop (curve label: without cleaning and sterilization).

Though not repeatable [precisely], the general trend of increasing $\Delta P$ over time was observed in multiple trials. It was postulated that microbial growth in the very small flow areas (tubing or annuli) could be responsible for the increase in $\Delta P$ over time: thus the escalating pressure which was not repeatable because the microbial growth was not consistent for the various runs. To counteract microbial growth and clean out impurities, a cleaning and sterilization protocol was developed. The three clean trials shown in Fig. 3.13 are the same three 10-day 50 µm VSD tube sample flow trials shown in Fig. 3.7.

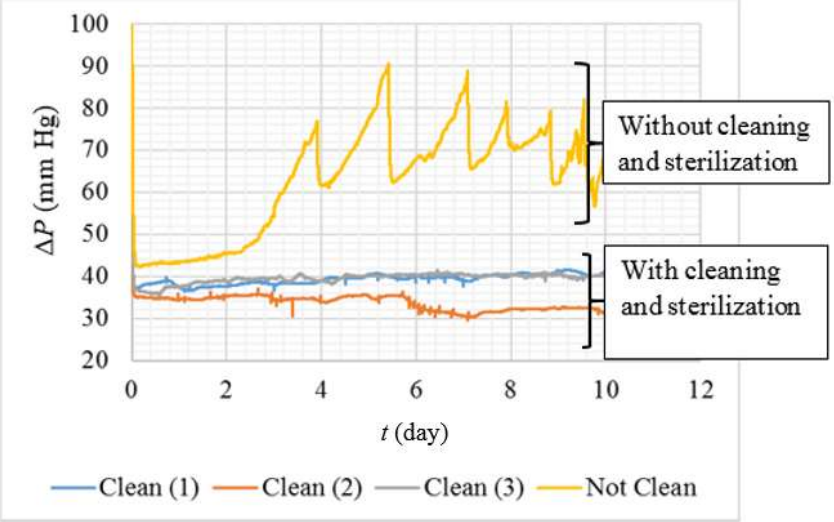


Fig. 3.13: Comparison among long-term pressure results for 50 µm tubes with and without cleaning and sterilization procedure ($Q$ = 2.5 µl/min; $L$ = 25 mm; 25°C test conditions) [February 21 - March 30, 2017]

***Cleaning and Sterilization Protocol***

A 10 % bleach solution was pumped through the tubing delivery lines for several hours (~24 hours), followed by isopropyl alcohol, before flushing the system with DI water alone. The reservoir was then autoclaved and sodium azide ($NaN_3$) was added to the DI water (0.04% $NaN_3$)

before performing long-term testing. The process of making the bleach solution and the $NaN_3$ solution is described in App. F.1. The anti-microbial protocol is described in more detail in App. F.2.

The full protocol was implemented on February 17, 2017. Therefore, it is important to note that trials performed before February 17, 2017 may have been affected by bacterial growth or particle depositions. However, trials performed with newly prepared samples (samples that had not been used in any prior trials) and that were shorter than 5 hours, were assumed to be unaffected by bacterial growth.

The results which were recorded following this anti-microbial process are also shown in Fig. 3.13. These results appear to confirm that, in testing systems, bacteria may grow and impede extremely small (< 75 μm) tubular and/or channel flows. At this point, it is also postulated that the eye's immunological systems safeguard against such growth - - although it could be that some cases of glaucoma might be caused by similar microbial growth in the eye's flow system. This issue will be further investigated in the future.

# Chapter 4: Additional Experimental Data

Chapter 4 discusses additional trials that were performed using the experimental setups. The following summarizes each section of Chapter 4:

- 4.1: Preliminary trials were performed with BGI tubes having degradable and non-degradable inserts in order to determine their effects on tube pressure.
- 4.2: Trials were performed using Ahmed glaucoma valves (AGVs), which are a type of valved-GDI (VGDI). These AGV trials were performed to investigate the effect of ocular viscosurgical devices (OVDs) and silicone oil on the AGV tube pressure.

## 4.1. Preliminary Trials with BGI Tubes

After performing trials with stiff inserts and stiff tubes, preliminary trials were carried out with BGI tubes. These trials were performed to observe the long-term (~20 day) pressure modulations in BGI tubes with stiff and non-stiff inserts, and determine if the stiffness of the inserts affected the pressure loss in the BGI tubes. These trials were also performed to determine if the same error of increasing $\Delta P$, that was manifested when stiff metal inserts and tubes were used (Section 2.4.1), occurs when BGI tubes are used instead.

It is important to note that all of the trials presented in Section 4.1 were performed before the anti-microbial protocol was developed. The results obtained during these trials may not reflect the actual pressure modulations caused by the inserts in the BGI tubes. These pressure variations may have been compromised by bacterial growth or particle depositions within the tubes.

### 4.1.1. Long-Term BGI Trials with Stiff Metal Inserts

***Research question:*** *Will experimental $\Delta P$ remain constant and fall within the theoretical $\Delta P$ range when stiff metal inserts are placed in flexible BGI tubes?*

Two 19-day trials were performed, one with a 28G nichrome wire insert (~ 0.32 mm OD) and the other with a 29G kanthal wire insert (~ 0.286 mm OD). Both inserts were 8 mm long and the flow rate for the trials was 2.5 µl/min. The inserts were placed in 10 mm long BGI tubes as described in App. B.4. The flow trials were carried out in Setup 2 as described in App. B.1. Table 4.1 summarizes the theoretical and experimental $\Delta P$ results. The pressure plots for the annular flow trials with the 29G kanthal and 28G nichrome inserts in BGI tubes are shown in Fig. 4.1.

Table 4.1: Summary of theoretical and experimental $\Delta P$ results for 19-day trials with 28G nylon and 29G kanthal inserts in BGI tubes

| **Insert type** | **28G nichrome** | **29G kanthal** |
|---|---|---|
| Insert OD range, $D_i$ (mm)[a] | 0.315 - 0.323 | 0.279 - 0.292 |
| BGI tube ID range, $D_o$ (mm)[a] | 0.344 - 0.352 | 0.344 - 0.352 |
| Theoretical $D_{eff}$ range (mm) | 0.045 - 0.069 | 0.088 - 0.113 |
| Theoretical $\Delta P$ range (mm)[b] | 3.35 - 26.0 | 0.46 - 1.80 |
| Average experimental $\Delta P$ (mm Hg)[c] | 20.74 ± 0.93[d] | 0.33 ± 0.023[d] |
| Initial experimental $\Delta P$, $\Delta P_i$ (mm Hg) | 18.5 | 0.34 |
| Final experimental $\Delta P$, $\Delta P_f$ (mm Hg) | 21.9 | 0.36 |

[a] Measured range of diameters (refer to App. B.5)
[b] Range is for variation in $Q$ (±0.125 µl/min), $L$ (±1 mm), $D_i$ and $D_o$ (minimum to maximum values)
[c] Average experimental $\Delta P$ over 0 to 19 days
[d] Standard deviation of the experimental $\Delta P$ over 0 to 19 days

From Fig. 4.1 and Table 4.1, it can be seen that the average experimental $\Delta P$ was within the theoretical $\Delta P$ range for the 28G nichrome trial. The experimental $\Delta P$ for the 29G kanthal trial was 0.13 mm Hg below the theoretical range. This was probably because $\Delta P$ for the 29G kanthal trial was 0.33 mm Hg when the pressure transducer measurement error is ± 0.2 mm Hg.

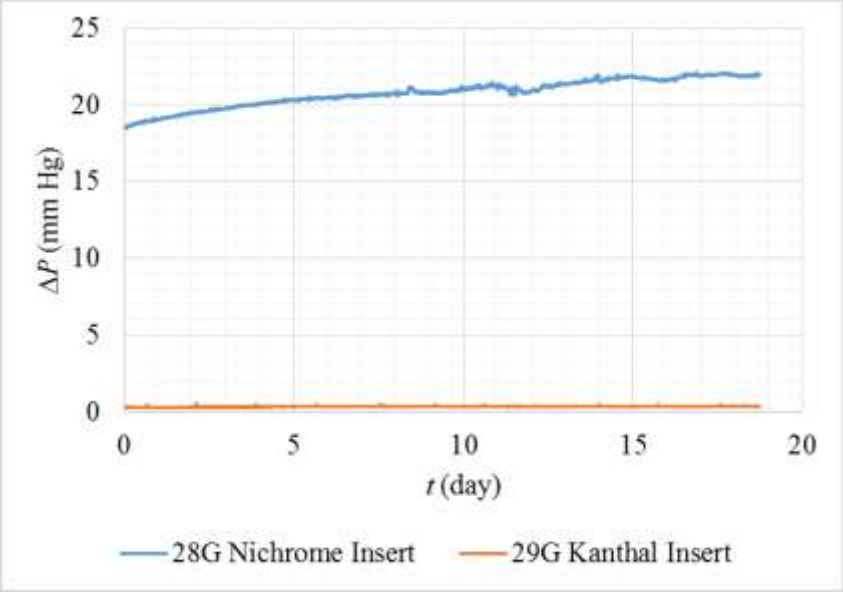


Fig. 4.1: Pressure plot of 19-day annular trials with 28G nichrome insert and 29G kanthal inserts in BGI tubes ($Q$ = 2.5 µl/min; $L$ = 8 mm; 25°C conditions) [July 21 - August 10, 2016]

From Fig. 4.1 and Table 4.1, it can also be seen that the nichrome insert created a higher pressure loss in the BGI tube as compared to that of the kanthal insert. It is noted from Eq. (3.4) and Eq. (3.5) that a larger $D_i$ would result in a smaller $D_{eff}$, followed by a larger $\Delta P$. Therefore, this difference in $\Delta P$ is expected since the 28G nichrome insert OD ($D_i$ = 0.315 mm - 0.323 mm) was greater than the 29G kanthal insert OD ($D_i$ = 0.279 mm - 0.292 mm). Refer to App. B.6 for more information on the tube/insert diameters.

It was also observed that the 29G kanthal insert's $\Delta P$ remained relatively constant at 0.33 mm Hg with a standard deviation of 0.023 mm Hg after five hours (Table 4.1). However, it can be seen from Fig. 4.1 that the issue of $\Delta P$ increasing over time (as described in Section 2.4.1) occurs only during the flow trial with the 28G nichrome insert. This issue has since been deduced to be a result of contamination (microbial growth) that can be resolved through sterilization. During the flow trial with the 28G nichrome insert, $\Delta P$ increased by 3.4 mm Hg, from 18.5 to 21.9 mm Hg.

It is possible that this increase in $\Delta P$ observed in the 28G nichrome trial did not occur in the 29G kanthal trial because the ratio of $D_o$ to $D_i$ for the 29G trial was larger compared to that for the 28G trial. Therefore, this caused $D_{eff}$ to be larger and $\Delta P$ to be lower for the 29G trial compared to the 28G trial. With a larger $D_{eff}$, there is less resistance to flow. Thus, small particles present in the tubes are probably less likely to cause blockage in the tubes and have less of an effect on $\Delta P$.

***Conclusion:*** *For the 28G nichrome trial, the average experimental $\Delta P$ was within the theoretical $\Delta P$ range, but $\Delta P$ increased continuously over time. For the 29G kanthal trial, the average experimental $\Delta P$ was slightly lower than theory but remained relatively constant throughout the trial. The continuous increase in $\Delta P$ for the 28G nichrome trial was probably due to microbial growth. The issue of microbial growth was resolved after these trials had been performed (refer to Section 2.7). Increasing $\Delta P$ was not observed for the 29G kanthal trial, most likely because, compared to the 28G nichrome trial, the $D_{eff}$ for the 29G kanthal trial was large enough that a small amount of microbial growth did not cause significant flow resistance.*

### 4.1.2. BGI Trials with Flexible Inserts

Preliminary flow trials with flexible non-degradable and degradable inserts in BGI tubes were performed. These flow trials were carried out with flexible inserts in BGI tubes, since the overall goal of this study is to determine the pressure effects of placing degradable inserts (which are not stiff) in BGI tubes.

***Non-Degradable Flexible Inserts***

***Research question:*** *Will experimental $\Delta P$ remain constant and fall within the theoretical $\Delta P$ range when non-degradable flexible inserts are placed in flexible BGI tubes?*

The non-degradable soft/flexible inserts used were (a) 0.30 mm OD nylon monofilaments

and (b) 3-0 medical grade polypropylene sutures (commercially known as prolene). Refer to App. B.6 for specifications of the nylon monofilament and the 3-0 prolene suture.

a. Nylon insert in BGI tube trials

A single sample was prepared, which was composed of an 8 mm long 28G nylon insert placed in a 10 mm long BGI tube. Four 48-hour repeated trials were performed in Setup 1 with this sample. The sample was labelled as Sample 0. These trials were performed to investigate the effect of placing a flexible insert in a BGI tube. These trials also helped to determine if the presence of a temperature controlled environment (achieved by running trials in an operating incubator) had an effect on the issue of continuously increasing $\Delta P$ during the trial, which was described in Section 2.1.4. The first trial was performed in open air at room conditions without a temperature controlled incubator. The second through fourth trials were performed with the incubator set at 37°C ± 2°C (body temperature). The sample was prepared as described in App. B.4; and the flow trials were carried out as described in App. B.1. The average $\Delta P$ over the 48 hours and standard deviation for Trials 1 through 4 are shown in Table 4.2. The pressure plots for the four trials are shown in Fig. 4.2.

It can be seen from Fig. 4.2 and Table 4.2 that, although Trials 2 to 4 were performed using the same sample under the same experimental conditions, $\Delta P$ still varied rather significantly from trial to trial. The average $\Delta P$ in Trial 2 (with incubator) was higher than that for Trial 1 (no incubator). This increase in $\Delta P$ could be attributed to either the presence of the incubator or the same cause as for the issue observed in Section 2.1.4. It is noted that nylon has a tendency to absorb water. Therefore, it is possible that the nylon swelled and caused an increase in flow resistance, resulting in an increase in $\Delta P$. However, because these trials were performed before the sterilization, this increase in $\Delta P$ could also have been due to microbial growth as discussed in

Section 2.7. It can also be seen from Table 4.2, that the average experimental $\Delta P$ of the trials was much greater than the theoretical $\Delta P$ range, which could also be attributed to the increase in size of the nylon insert, since $\Delta P$ was large at the beginning of the trial, before there was time for microbial growth.

Table 4.2: Summary of the four repeated theoretical and experimental $\Delta P$ results for 48-hour trials with 28G nylon inserts in BGI tubes (Sample 0)

| Trial number | 1 | 2 | 3 | 4 |
|---|---|---|---|---|
| Incubator | Absent | Present | Present | Present |
| Temperature | ~25°C | 37°C | 37°C | 37°C |
| Theoretical $D_{eff}$ range (mm)[a] | 0.071 - 0.088 | | | |
| Theoretical $\Delta P$ range (mm Hg)[b] | 1.23 - 4.17 | 0.96 - 2.93 | | |
| Average experimental $\Delta P$ (mm Hg) | 18.2 | 19.3 | 13.1 | 16.4 |
| Standard deviation of experimental $\Delta P$ (mm Hg) | 1.34 | 2.18 | 1.40 | 2.23 |

[a] Minimum to maximum $D_i$ and $D_o$ values: 28G nylon insert (0.300 - 0.305 mm) and BGI tube (0.344 - 0.352 mm) [refer to App. B.6]
[b] Range is for variation in $Q$ (±0.125 µl/min), $L$ (±1 mm), $D_i$ and $D_o$ (minimum to maximum values); refer to Table 4.1 for BGI tube ID range

The dynamic viscosity of water, $\mu$, decreases as temperature increases: $\mu$ = 0.0008904 Pa-s at room temperature (25°C); $\mu$ = 0.0006913 Pa-s at body temperature (37°C). According to Eq. (3.4), $\Delta P$ decreases as $\mu$ decreases. Therefore, due to viscosity alone, $\Delta P$ in Trial 1 should be lower than $\Delta P$ in Trials 2, 3 and 4. However from Fig. 4.2, the average $\Delta P$ of Trial 1 is higher than those of Trial 3 and 4, but lower than that of Trial 2.

Additionally, given that Trials 2, 3 and 4 were performed with the same sample under the same conditions, the average $\Delta P$ values of all three trials should be relatively equal. However, there were large differences among the average $\Delta P$s of Trials 2, 3, and 4 (difference up to 6.2 mm

Hg, per Table 4.2). Based on these trial results, it does not appear that temperature or other environmental factors gave rise to the issue of continuously increasing $\Delta P$ that was described in Section 2.1.4.

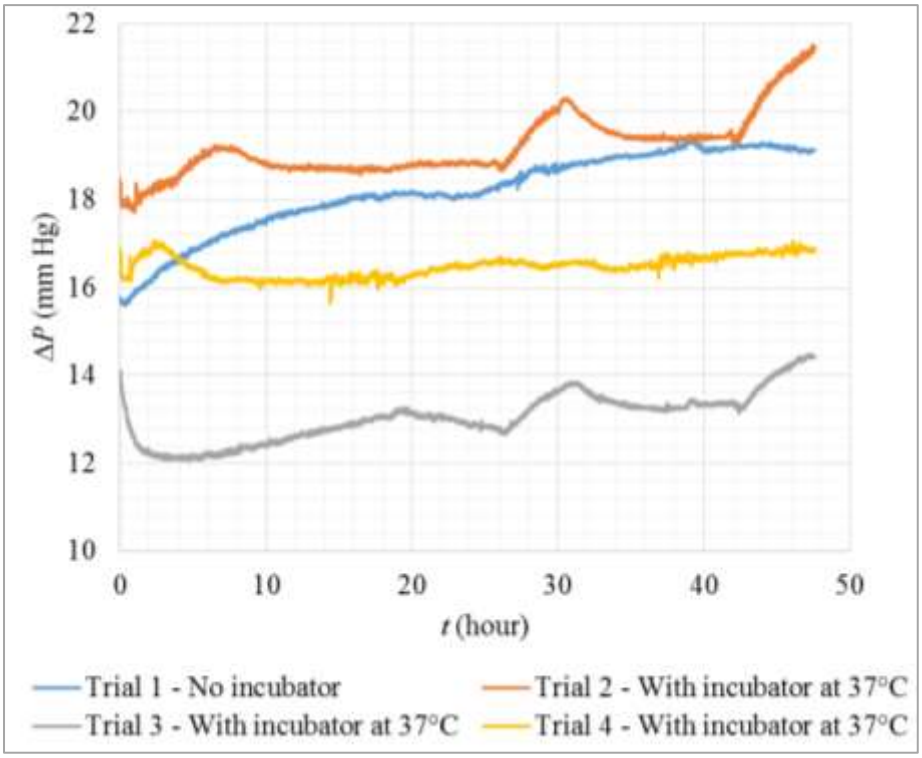


Fig. 4.2: Pressures for four 48-hour annular trials with 28G nylon-insert-in-BGI-tube Sample 0 ($Q$ = 2.5 µl/min; $L$ = 8 mm) [April 29 - May 24, 2016]

Another set of 48-hour trials was performed with three 8 mm long 28G nylon inserts that were placed in three 10 mm long BGI tubes. The three samples were prepared as described in App. B.4; and the trials were carried out in Setup 2 as described in App. B.1. The ODs of all three inserts were measured with a micrometer prior to running the flow trials. The flow trials were carried out at a flow rate of 2.5 µl/min and temperature of 37°C in Setup 1. The pressure plots for the three samples are shown in Fig. 4.3.

The ODs of Samples 1, 2 and 3 were 0.300 mm, 0.303 mm and 0.300 mm, respectively.

Although the ODs of the samples appeared to be relatively close with only a 3 µm difference, the large change in $\Delta P$ (up to 12 mm Hg) among the samples indicates that the micrometer measurements may not have been accurate enough. As mentioned in Section 2.7.2, even a 5 µm change in insert OD can change the $\Delta P$ by 40 mm Hg. However, it must be noted that these pressure results may not have been accurate as well, since these trials were performed before the anti-microbial protocol was implemented and could have been affected by bacterial growth. The average $\Delta P$ and standard deviation of $\Delta P$ over 48 hours for Samples 1 to 3 are shown in Table 4.3.

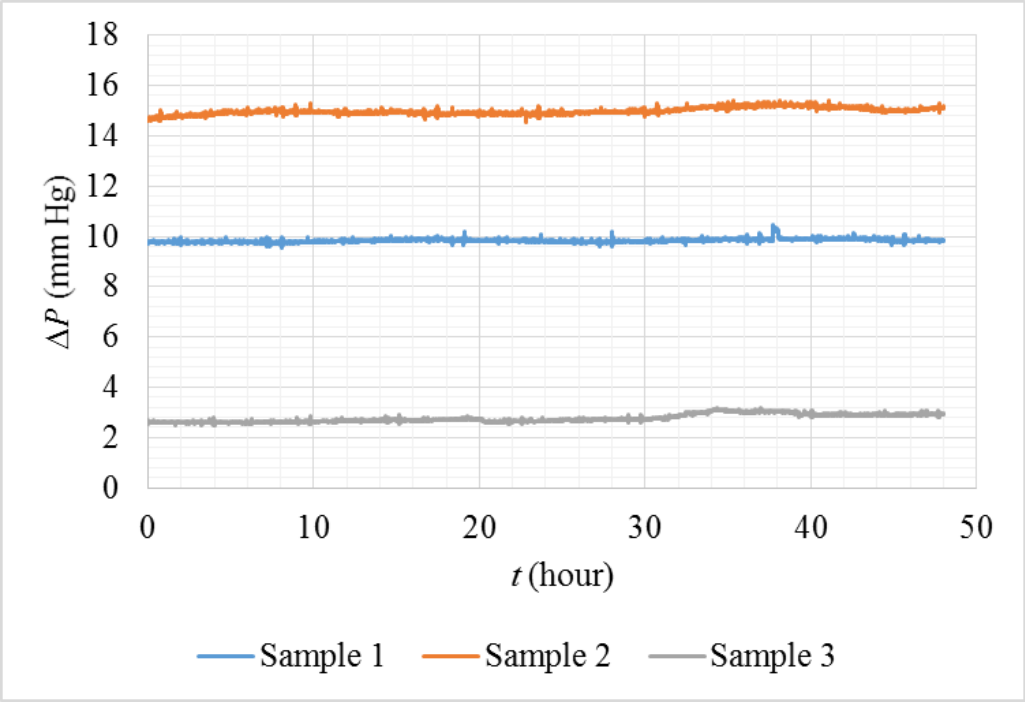


Fig. 4.3: Pressures for 48-hour annular trials for three 28G nylon-wire-in-BGI-tube samples ($Q$ = 2.5 µl/min; $L$ = 8 mm; 37°C conditions) [April 29 - July 21, 2016]

From Table 4.3, it can be seen that the experimental $\Delta P$ values do not fall within the theoretical $\Delta P$ ranges. It is possible that the nylon absorbed water and increased in size, causing $\Delta P$ to be higher. It is also possible for the experimental $\Delta P$ to be larger than theoretical $\Delta P$ due to the presence of microbes in the tubing, resulting in a $\Delta P$ increase.

Table 4.3: Summary of theoretical and experimental Δ*P* results for 48-hour trials with 28G nylon inserts in BGI tubes (Samples 1 to 3)

| Nylon sample number | 1 | 2 | 3 |
|---|---|---|---|
| Measured insert OD range, $D_i$ (mm) | 0.300 - 0.305 | 0.297 - 0.307 | 0.297 - 0.302 |
| Theoretical $D_{eff}$ range (mm) | 0.071 - 0.088 | 0.069 - 0.092 | 0.075 - 0.092 |
| Theoretical Δ*P* range (mm Hg)[a] | 0. 957 - 2.93 | 0.813 - 3.42 | 0.813 - 2.36 |
| Experimental Δ*P* (mm Hg) | 9.84 ± 0.064[b] | 15.0 ± 0.123[b] | 2.77 ± 0.151[b] |

[a] Range is for variation in $Q$ (±0.125 µl/min), $L$ (±1 mm), $D_i$ and $D_o$ (minimum to maximum values) at 37°C conditions; Refer to Table 4.1 for BGI tube ID range
[b] Average ± standard deviation of experimental Δ*P* (mm Hg)

From Fig. 4.3, it can also be seen that the Δ*P* of each sample remained relatively constant over the 48 hour period, with small standard deviations of no more than 0.151 mm Hg. The constant Δ*P* results imply that the 28G nylon samples did not swell significantly enough to cause an increase in Δ*P*. This occurrence is contrary to the results of Sample 0 as shown in Fig. 4.2 and Table 4.2. It is uncertain as to why Δ*P* was constant for Samples 1, 2 and 3, but not for Sample 0, even though the experimental procedures were the same for all samples and trials. It is possible that microbial growth had a greater effect on Sample 0's Δ*P* results because the sample was used repeatedly four times. Since all trials were 48 hours long, Sample 0 was exposed to microbes at least four times longer than Samples 1, 2 and 3.

***Conclusion:*** *The experimental Δ*P*s for all of the trials did not match with theory. This inconsistency with theory could have been caused by the presence of microbes in the tubes. It can also be seen that Δ*P* for Sample 0 varied significantly with standard deviations up to 2.23 mm Hg, even though Trials 2 to 4 were performed under the same test conditions. However, for Samples 1, 2, and 3, Δ*P* remained constant with a maximum standard deviation of 0.151 mm Hg. It is*

*possible that ΔP was inconsistent for Sample 0 because it was exposed to microbes at least four times longer than Samples 1, 2 and 3. Since the inserts were flexible, there was also the possibility that the insert of Sample 0 was crammed into the tube, whereas the inserts in Samples 1, 2 and 3 were stretched out.*

b. 3-0 prolene suture in BGI tube trials

For the prolene suture trials, three 8 mm 3-0 prolene sutures were placed in three 10 mm BGI tubes. Similar to the 28G nylon trials, the three samples were prepared as described in App. B.4; and the flow trials were carried out in Setup 2 as described in App. B.1. The three flow trials were carried out at a flow rate of 2.5 µl/min and room temperature (25°C). The pressure plots from the trials are shown in Fig. 4.4. The average Δ*P*s and standard deviations are listed in Table 4.4. For these trials, the ODs of each sample insert were not measured prior to the experiment.

Table 4.4: Average Δ*P* and standard deviation over 20 hours for trials with 3-0 prolene suture inserts in BGI tubes (Samples 1 to 3)

| 3-0 prolene sample number | 1 | 2 | 3 |
|---|---|---|---|
| Insert OD range, $D_i$ (mm)[a] | 0.241 - 0.246 | | |
| Theoretical $D_{eff}$ range (mm) | 0.153 - 0.139 | | |
| Theoretical Δ*P* range (mm Hg)[b] | 0.14 - 0.29 | | |
| Experimental Δ*P* (mm Hg)[c] | 0.190 ± 0.020 | 0.626 ± 0.042 | 7.74 ± 0.16 |

[a] Minimum to maximum $D_i$ and $D_o$ values: 28G nylon insert (0.241 - 0.246 mm) and BGI tube (0.344 - 0.352 mm) [refer to App. B.6]
[b] Range is for variation in $Q$ (±0.125 µl/min), $L$ (±1 mm), $D_i$ and $D_o$ (minimum to maximum values); refer to Table 4.1 for BGI tube ID range
[c] Average ± standard deviation of experimental Δ*P* (mm Hg)

From Table 4.4 and Fig. 4.4, it is noted that, although the prolene samples were taken from the same suture spool, the average Δ*P* values varied significantly. This variation could be due to

differences in suture OD. Although the manufacturer labels the 3-0 prolene suture OD to be 0.20 mm, the actual measured OD of the 3-0 prolene sutures ranged from 0.241 mm to 0.246 mm. Additionally, since the prolene inserts were flexible, there was the possibility that some inserts were more crammed into the tubes and others more stretched out, resulting in a variation in pressure results.

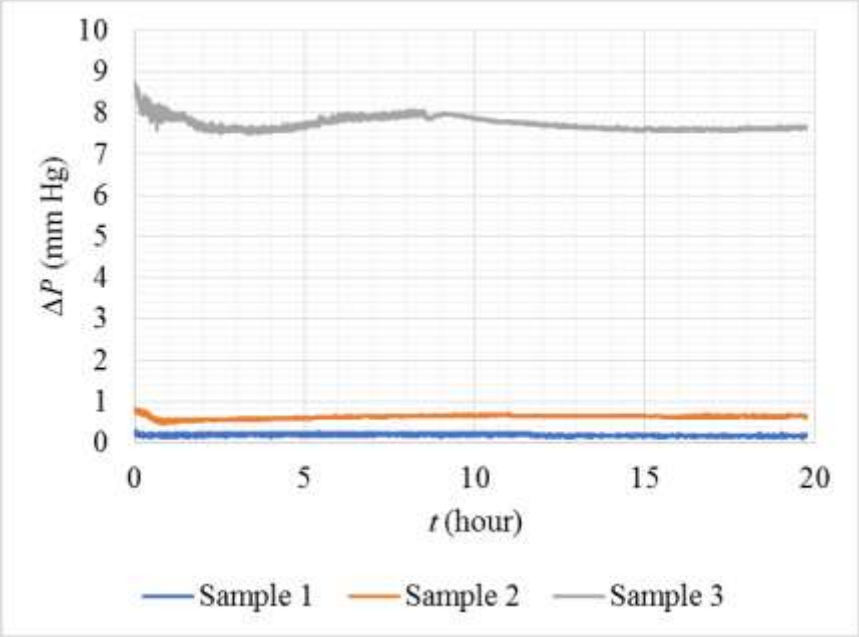


Fig. 4.4: Pressures of 20-hour annular trials with 3-0 prolene inserts in BGI tubes ($Q$ = 2.5 µl/min; $L$ = 8 mm; 25°C conditions) [September 20 - October 3, 2015]

This large variation in average $\Delta P$ could also be caused by a buildup of small particles or bacteria inside the BGI tubes. Notice from Fig. 4.4 that $\Delta P$ is highest for Samples 3 and lowest for Sample 1. Sample 1 was tested first followed by Samples 2 and 3. Therefore, it is possible that there were residual particles or microbes remaining in the pump tubing or in the connecting tubing, which flowed into the BGI tubes, restricting flow and creating a greater $\Delta P$.

***Conclusion:*** *The experimental $\Delta P$ for Sample 1 matched with theory, but the experimental $\Delta P$s for Samples 2 and 3 did not. There was a large variation in average experimental $\Delta P$ even though*

*the samples were cut from the same suture spool. This large variation could be attributed to the buildup of microbes or small particles in the tubes.*

***Next steps:*** *Perform trials with degradable inserts to study the effect of insert degradation on the tube pressure.*

***Degradable Inserts***

***Research question:*** *What is the pressure effect of placing degradable inserts in BGI tubes? Do the experimental* $\Delta P$*s fall within the theoretical ranges?*

After testing with non-degradable inserts, trials were performed with degradable inserts in order to study the effects of insert degradation on the pressure in the tube. The degradable inserts were medical grade poliglecaprone sutures (commercially known as monocryl) and polylactic-co-glycolic acid (PLGA) fibers that were fabricated by Jian Qian, a post-doc in the Berkland Lab. The PLGA fibers were chosen for testing initially because the degradation rate and the OD of the fibers could be manipulated by Qian. Note that the accuracy of fabricating the fibers to get a specific OD value was very low. In order to overcome this, the fibers were cut and measured manually with a microscope (measured at more than 6 different points along the fiber). The fibers with the desired range of OD measurements were chosen. Refer to App. B.6 for specifications of monocryl and PLGA.

a. 3-0 monocryl inserts in BGI tube trials

Three 17-hour trials and one 12-day trial were performed. There were four separate samples of 10 mm long BGI tubes with 8 mm long 3-0 monocryl suture inserts (refer to App. B.4 for sample preparation procedures). The test procedures are described in App. B.1. The trials were performed at a flow rate of 2.5 µl/min and at room temperature (25°C) in Setup 2. Poliglecaprone

(monocryl) is a synthetic absorbable monofilament that swells first before degrading after being in contact with a fluid [59]. Starting with an OD of approximately 0.20 mm, the 3-0 monocryl suture expands to about 0.30 mm OD when it is submerged in water before beginning to degrade [59]. The pressure plots of the annular trials are shown in Figs. 4.5 and 4.6. Table 4.5 summarizes the theoretical and experimental pressure results from the four trials.

From Fig. 4.5, Fig. 4.6, and Table 4.5, it can be seen that $\Delta P$ continuously increased over time for all four samples. This increase in $\Delta P$ could be due to the increase in size of the monocryl insert before degradation. However, the increase could also be caused by the growth of bacteria in the tubes, since these trials were performed before the antimicrobial protocol was implemented.

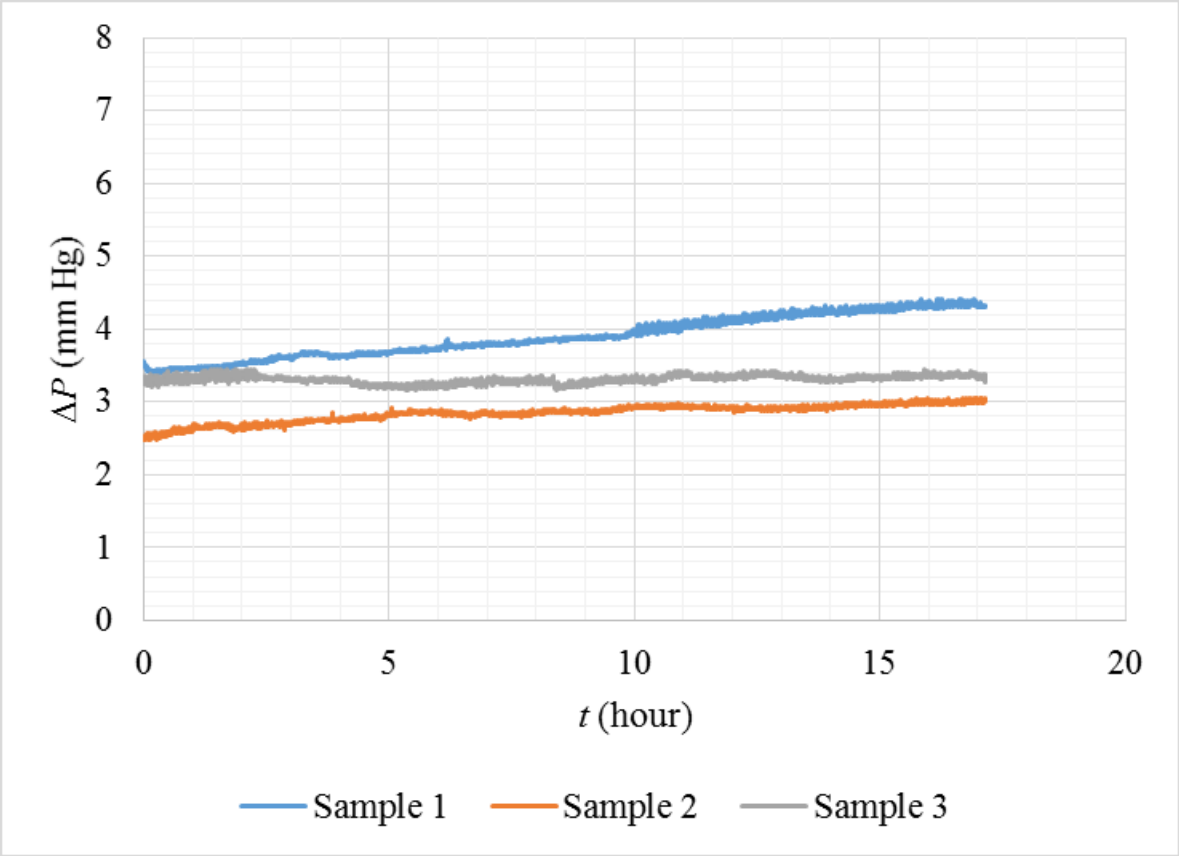


Fig. 4.5: Pressures of 17-hour annular trials with 3-0 Monocryl inserts in BGI tubes ($Q$ = 2.5 µl/min; $L$ = 8 mm; 37°C conditions) [October 23 - 29, 2016]

Table 4.5: Summary of theoretical and experimental $\Delta P$ results for 17-hour trials with 3-0 monocryl inserts in BGI tubes

| Length of trial | 17 hours | | | 12 days |
|---|---|---|---|---|
| 3-0 monocryl sample number | 1 | 2 | 3 | 4 |
| Measured insert OD range, $D_i$ (mm)[a] | 0.269 - 0.279 | 0.269 - 0.279 | 0.277 - 0.287 | 0.269 - 0.279 |
| Theoretical $D_{eff}$ range (mm) | 0.103 - 0.124 | 0.103 - 0.124 | 0.094 - 0.115 | 0.103 - 0.124 |
| Theoretical $\Delta P$ range (mm Hg)[b] | 0.32 - 0.94 | 0.32 - 0.94 | 0.43 - 1.38 | 0.32 - 0.94 |
| Initial experimental $\Delta P$,$\Delta P_i$ (mm Hg) | 3.54 | 2.51 | 3.26 | 7.32 |
| Final experimental $\Delta P$, $\Delta P_f$ (mm Hg)[c] | 4.30 | 3.02 | 3.37 | 8.45 |
| Difference between $\Delta P_f$ and $\Delta P_i$, $\Delta P_{f\text{-}i}$ (mm Hg)[c] | 0.76 | 0.51 | 0.11 | 1.13 |

[a] Measured with micrometer (resolution: 0.0001 in.)

[b] Range is for variation in $Q$ (±0.125 µl/min), $L$ (±1 mm), $D_i$ and $D_o$ (minimum to maximum values): refer to Table 4.1 for BGI tube ID range

[c] $\Delta P$ value at end of the experimental trial (17 hours or 12 days)

[d] $\Delta P_{f\text{-}i} = \Delta P_f - \Delta P_i$

From Table 4.5, it can be seen that the $\Delta P_i$s were above the range of the theoretically predicted $\Delta P$s. These discrepancies could be due to the presence of bacteria in the flow lines. Additionally, the $D_i$ measurements, made with a micrometer, may not have been accurate or sensitive enough to properly predict the theoretical $\Delta P$. It was possible that the experimental $\Delta P$s were larger than theoretical $\Delta P$s because the monocryl inserts swelled as they absorbed water.

***Conclusion:*** *The experimental ΔPs for all of the trials were above the range of the theoretical ΔP. It can be seen that there was a continuous rise in ΔP over time which could have been due to the swelling of the monocryl before degradation. These occurrences could also have been caused by the growth of bacteria in the tubes.*

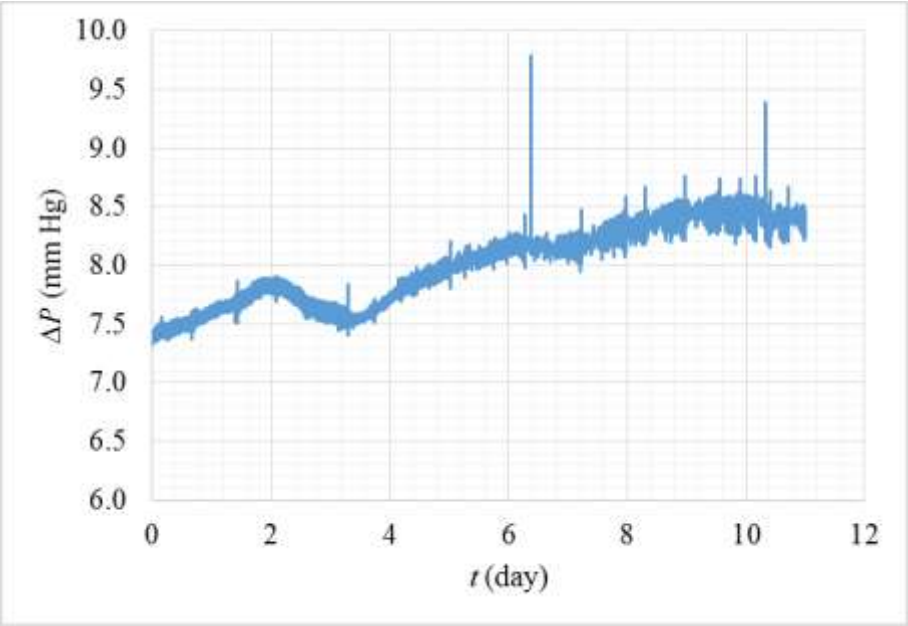


Fig. 4.6: Pressure for 12-day flow trial with a 3-0 monocryl insert in BGI tube sample ($Q$ = 2.5 µl/min; $L$ = 8 mm; 37°C conditions) [July 21 - August 10, 2016]

b. PLGA inserts in BGI tubes

Four 8 mm long samples of PLGA fibers were cut from an approximately 2 m long PLGA fiber, and the ODs of the fibers were measured with a micrometer. The measurements are listed in Table 4.6. Each PLGA fiber was placed in a 10 mm long BGI tube. The samples were prepared as described in App. B.4. Four 4.6-day annular flow trials were performed with each sample at a flow rate of 2.5 µl/min and at a temperature of 37°C. These trials were performed at body temperature because the degradation rate of PLGA is greater at higher temperatures. The trial procedures were carried out as described in App. B.1.

Samples 2 and 3 were tested in Setup 1, while samples 1 and 4 were tested in Setup 2. Although the trials were performed in different setups, there is no reason to believe that the difference in setups affected the $\Delta P$ results, since both setups had been verified to correspond well with each other (refer to Chapter 2). Figure 4.7 shows the pressure plots from the four 5-day PLGA trials. Table 4.6 summarizes the theoretical and experimental $\Delta P$ values for the trials.

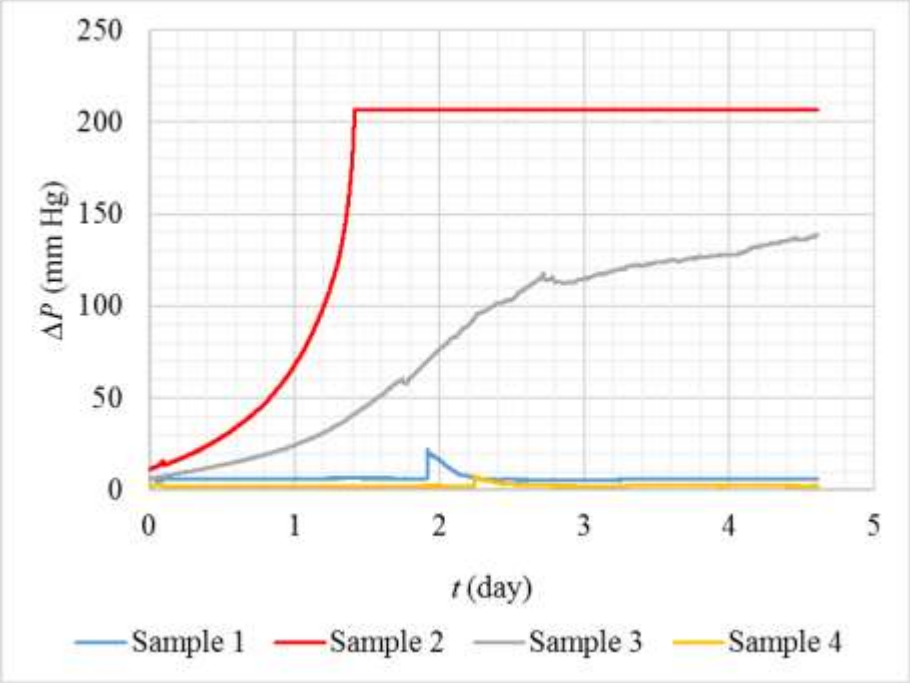


Fig. 4.7: Pressures of 4.6-day annular trials with PLGA inserts in BGI tubes ($Q$ = 2.5 µl/min; $L$ = 8 mm; 37°C conditions) [May 27 - August 22, 2016]

From Fig. 4.7 and Table 4.6, it can be seen that $\Delta P$ increased the most for Samples 2 and 3, and increased the least for Samples 1 and 4 ($\Delta P$ remained relatively constant). A possible reason for the little to no increase in $\Delta P$ for Samples 1 and 4 is that the initial $\Delta P$s for these two samples were smallest, implying that $D_{eff}$ was high, causing very little effect on $\Delta P$ when the inserts expanded before degradation. However, based on the insert OD measurements, the largest $\Delta P$ should be for Sample 4. It is possible that the micrometer measurements were not accurate, thus causing this inconsistency between theoretical and experimental $\Delta P$. In addition, the results of

these trials may have been affected by growth of bacteria or deposition of small particles in the tubing.

Table 4.6: Summary of theoretical and experimental $\Delta P$ results for four 4.6-day trials with PLGA inserts in BGI tubes

| PLGA sample number | 1 | 2 | 3 | 4 |
|---|---|---|---|---|
| Measured insert OD range, $D_i$ (mm) | 0.254 - 0.264 | 0.264 - 0.274 | 0.272 - 0.290 | 0.297 - 0.302 |
| Theoretical $D_{eff}$ range (mm) | 0.120 - 0.140 | 0.109 - 0.129 | 0.0903 - 0.121 | 0.0752 - 0.0921 |
| Theoretical $\Delta P$ range (mm Hg)[a] | 0.15 -0.28 | 0.21 - 0.41 | 0.28 - 0.88 | 0.81 - 1.83 |
| Initial experimental $\Delta P$, $\Delta P_i$ (mm Hg) | 5.73 | 11.28 | 5.96 | 1.05 |
| Final experimental $\Delta P$, $\Delta P_f$ (mm Hg)[b] | 6.04 | 206.71 | 138.45 | 2.24 |
| Difference between $\Delta P_f$ and $\Delta P_i$, $\Delta P_{f\text{-}i}$ (mm Hg)[c] | 0.31 | 195.42 | 132.49 | 1.20 |

[a] Range is for variation in $Q$ (±0.125 µl/min), $L$ (±1 mm), $D_i$ and $D_o$ (minimum to maximum values): Refer to Table 4.1 for BGI tube ID range
[b] $\Delta P$ value at end of the experimental trial
[c] $\Delta P_{f\text{-}i} = \Delta P_f - \Delta P_i$

From Fig. 4.7, $\Delta P$ of Sample 2 rose from 11.28 mm Hg to 206.71 mm Hg. The $\Delta P$ reading remained constant at 206.71 mm Hg because that is the largest reading that the data logger could record. Thus, $\Delta P$ for Sample 2 probably continued to increase beyond what the data logger could read.

Similar to the monocryl trials, the experimental $\Delta P$s obtained for the PLGA trials were above the theoretical $\Delta P$ ranges calculated. Once again, this discrepancy could be due to presence of small particles or bacteria accumulating within the flow lines of the setup (pump to test section) or swelling of the inserts before degradation, causing an increased $\Delta P$ reading.

***Conclusion:*** *The experimental ΔPs for all of the trials were above the theoretical ΔP range. This could have been caused by the presence of microbes in the tubes, as well as swelling or cramming of the inserts in the tubes. There was also a continuous rise in ΔP, especially for Samples 2 and 3. This could have been caused by the increase in size of the PLGA before degradation combined with the presence of microbes in the tubes.*

## 4.2. AGV Experimental Study

Cataracts and glaucoma are the two leading causes of blindness in the world, and often coexist in elderly patients [60]. Viscoelastic solutions, also known as ophthalmic viscosurgical devices (OVD), are used to protect the endothelium of the eye, aid the manipulation of the anterior segment, and maintain the shape of the anterior chamber during cataract surgery [61]. Two commonly used OVDs for cataract surgery are Viscoat and ProVisc (Alcon Laboratories) which are packaged together as DuoVisc (Fig. 4.8). Refer to App. G.4 for the specifications of these OVDs.

Ideally, an OVD should remain in the eye during surgery and be easily aspirated at the end of surgery to prevent post-op IOP elevation [62]. The combination of Viscoat and ProVisc (DuoVisc) combines the advantages of both OVDs for cataract surgery. Viscoat is a dispersive OVD wheras ProVisc is cohesive OVD. Thus, ProVisc clears out of the eye easily while Viscoat takes longer to clear out of the eye [61, 63]. Viscoat has been shown to stay in place in the eye better during surgery as compared to ProVisc [62, 63]. Viscoat is normally used in the early stages of cataract surgery, during capsulorhexis and phacoemulsification, while ProVisc is used for intraocular lens implantation [64].

Retinal detachment is a phenomenon in which the retina of the eye tears and detaches from the choroid as shown in Fig. 4.9. Retinal detachment is a serious problem that can cause blindness

if not managed immediately [65]. Silicone oil is used as an intraocular tamponade after a vitrectomy (surgery to reattach the retina) [66]. A tamponade agent (silicone oil) provides surface tension across the retinal tear to physically prevent fluid flow into the sub-retinal space behind the retina [66]. The silicone oil can be left in the patient's eye permanently or be removed during a second surgery, depending on how badly the silicone oil affects the patient's IOP [66].


Fig. 4.8: DuoVisc viscoelastic system consisting of Viscoat and ProVisc (Alcon)

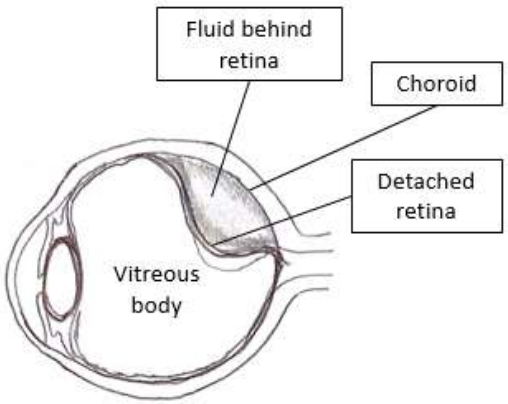


Fig. 4.9: Illustration of detached retina

Many patients who need cataract surgery also have glaucoma [34]. Additionally, secondary glaucoma can develop in patients who have had cataract surgery, and vice versa [34]. Retinal

detachment can also cause complications such as glaucoma, hypotony and cataracts [67]. Additionally, patients who have undergone cataract or glaucoma surgery have a higher risk of a retinal detachment [68].

Considering that many patients who require cataract surgery or retinal reattachment surgery also need glaucoma surgery, patients with this combination of surgeries might have retained silicone oil and/or OVDs that could possibly flow into the patient's GDI and affect the functionality of the GDI (especially a VGDI with a very small flow opening). Compared to the BGI, AGVs have a narrower flow path through the butterfly valve of the AGV. Therefore, the flow of the viscoelastic solution and the silicone oil would probably affect the $\Delta P$ through the AGV more than through the BGI. Thus, it is important to determine the pressure effects on an AGV when OVDs and silicone oil flow through it. The following sections describe the experiments performed by this author in order to examine these effects. However, first, priming of the AGVs were examined (Section 4.2.1).

### 4.2.1. Baseline Fluid Pressure Response in AGVs

***Research question:*** *What is the pressure response of AGVs prior to manually priming the AGV as recommended by the manufacturer?*

New World Medical instructions indicate that an AGV must be examined and primed prior to implantation. Priming is accomplished by injecting approximately 1 cc of sterile water or BSS through the AGV with a blunt 26G hypodermic tube [69]. This is important because a brand new AGV requires an initial opening pressure of approximately 3017 mm Hg to activate the valve [70]; and the eye cannot undergo that high pressure without resulting in blindness. Therefore, six flow trials were performed with six never-primed AGVs in order to observe the $\Delta P$ response before an AGV is primed.

The experimental setups were modified for AGV trials according to the diagram shown in Fig. 4.10. The trough was replaced by a 200-ml beaker filled with 50 ml of DI water. The AGV sample was placed in the beaker and fully submerged in the DI water. A beaker is used for the AGV trials instead of the collection trough used in the BGI trials because full submersion of the AGV sample could not be done in the shallow trough. The setup and procedures of the AGV flow trials are described in Apps. G.1 and G.2. The trials were performed with 0.04% $NaN_3$ solution, at flow rate of 2.5 µl/min and room temperature (25°C). The pressure variations and a summary of the trial pressure results are shown in Fig. 4.11 and Table 4.7, respectively.

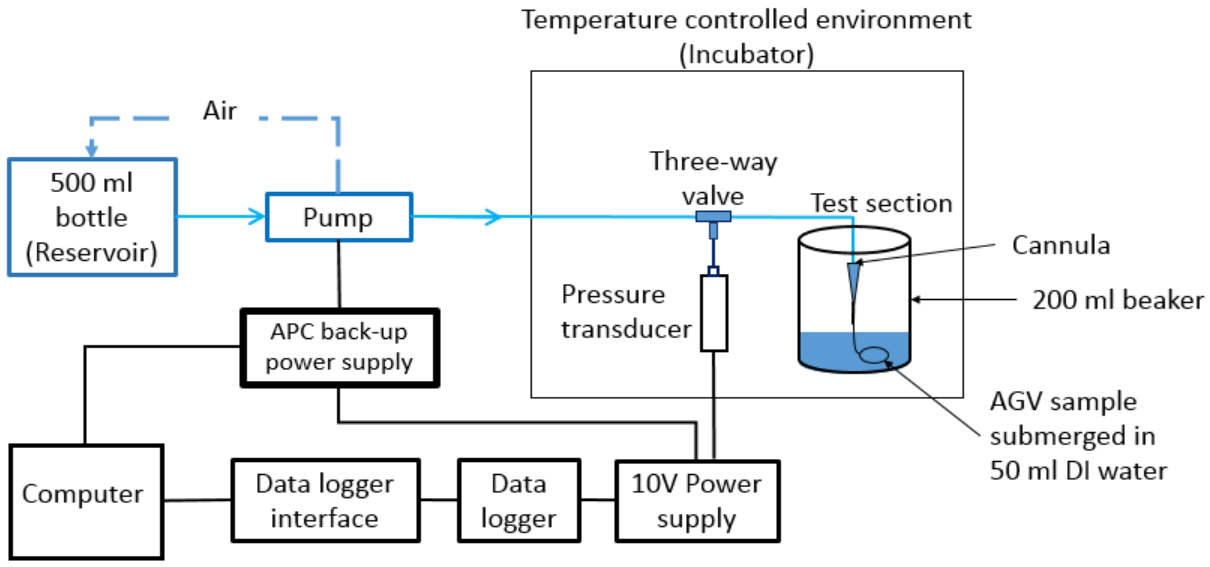


Fig. 4.10: Diagram of modified experimental setup for AGV flow trials

From Fig. 4.11 and Table 4.7, it can be seen that all of the AGV $\Delta P$s reached a maximum value of 206.7 mm Hg and took an average of 2.03 ± 1.42 hours for $\Delta P$ to fall below 206.7 mm Hg, indicating that the valve opened at that time. The average experimental $\Delta P$ of all six samples was 52.70 mm Hg with a standard deviation of 16.34 mm Hg. Although the valves opened, the average $\Delta P$ was still above the IOP range of a healthy eye (10 - 22 mm Hg) [11].

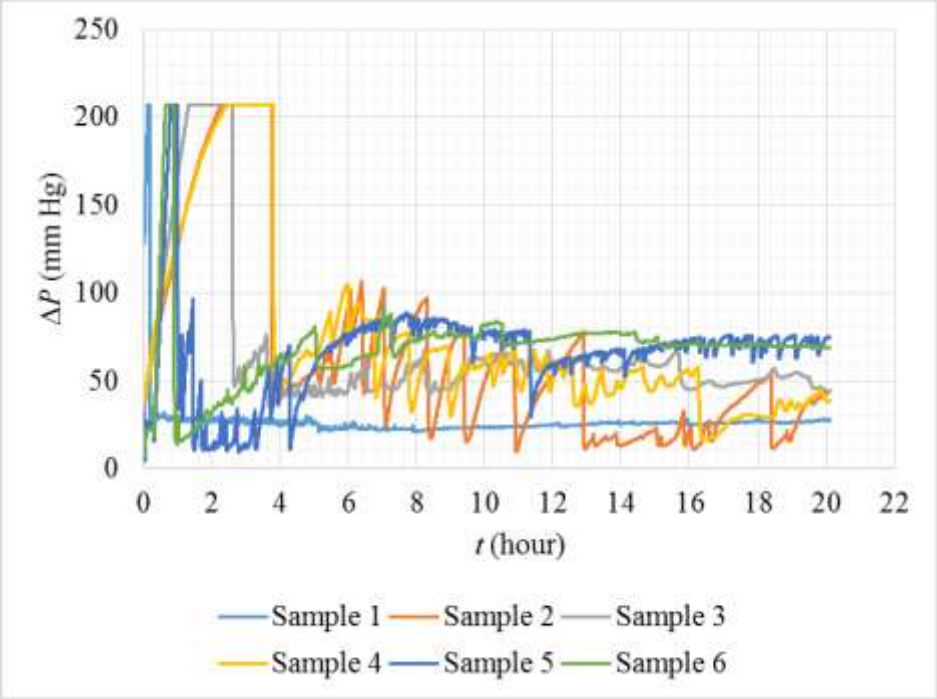


Fig. 4.11: Pressures of six 23-hour AGV trials [February 20 - July 21, 2017]

Table 4.7: Summary of the Δ*P* results of six 23-hour unprimed AGV trials

| AGV sample number | Time valve opened, $t_{vo}$ (hour)[a] | Average experimental Δ*P* after valve opened (mm Hg)[b] |
|---|---|---|
| 1 | 0.18 | 24.63 ± 1.65 |
| 2 | 3.74 | 42.80 ± 24.69 |
| 3 | 2.60 | 53.53 ± 6.72 |
| 4 | 3.79 | 52.01 ± 18.09 |
| 5 | 0.99 | 71.54 ± 8.47 |
| 6 | 0.88 | 71.70 ± 5.83 |
| **Average[c]** | 2.03 ± 1.42[c] | 52.70 ± 16.34[d] |

[a] $t_{vo}$ = time at which Δ*P* < 206.7 mm Hg, after achieving maximum Δ*P* value of 206.7 mm Hg
[b] Average ± standard deviation of experimental Δ*P* between 5 and 23 hours for each sample
[c] Average ± standard deviation of $t_{vo}$ for the six flow trials
[d] Average ± standard deviation of experimental Δ*P* between 5 and 23 hours for the six flow trials

The maximum pressure that can be measured and recorded by the experimental setup is 206.7 mm Hg. Therefore, it is uncertain as to the actual maximum $\Delta P$ value that was reached before the valve opened. The average $\Delta P$ of the AGVs after each valve opened did not fall within the nominal IOP range, as indicated by New World Medical, because these AGVs were not manually primed prior to the tests, as instructed by the manufacturer. Therefore, it can be seen that without priming the AGVs prior to the trials, $\Delta P$ values reached extreme levels above the nominal IOP range. Results showing the importance of priming AGVs prior to implantation are discussed further in Sections 4.2.2 and 4.2.3.

***Conclusion:*** *It was observed that the AGV tube pressure increased to extreme levels above the nominal IOP range of 10 - 22 mm Hg when it was not primed, which would be severely detrimental to the eye. Therefore, these tests verify that it is important to prime the AGV prior to implantation in the eye.*

### 4.2.2. Fluid Pressure Response in AGVs with OVDs

***Research Question:*** *What is the pressure effect of ocular viscosurgical devices (OVDs) on AGVs?*

In order to determine how the $\Delta P$ in an AGV would respond when OVDs flow through it, six 15-hour trials were performed with six AGVs and OVDs manually injected in AGV tubes. Three trials were performed with Viscoat and three with ProVisc. The setup and trial procedures are described in Apps. G.1 and G.2. The trials were performed with 0.04% $NaN_3$ solution, at flow rate of 2.5 µl/min and room temperature (25°C). Table 4.8 shows the summary of pressure results for the 15-hour flow trials. The pressures for the six trials are shown in Figs. 4.12 and 4.13. Figure 4.13 is a magnified version of Fig. 4.12. From Table 4.8 and Fig. 4.12, it can be seen that the time taken for Viscoat to exit from the AGV was longer than the time taken for ProVisc to clear out of the AGV. These results were expected due to the dispersive characteristics of Viscoat and agree

with the findings of Yoshino *et al.* [71].

Table 4.8: Summary of the $\Delta P$ results for six 15-hour AGV trials with OVDs (three with Viscoat and three with ProVisc)

| AGV sample | Time for OVD to pass through AGV, $t_{ovd}$ (minutes)[a] | Maximum $\Delta P$ (mm Hg) | Average experimental $\Delta P$ (mm Hg) | | |
|---|---|---|---|---|---|
| | | | Initial, $\Delta P_i$ [b] | Final, $\Delta P_f$ [c] | Difference, $\Delta P_f - \Delta P_i$ |
| Viscoat - Sample 1 | 74 | 172.95 | 12.12 ± 0.33 | 13.11 ± 0.59 | 0.99 |
| Viscoat - Sample 2 | 31 | 79.51 | 8.07 ± 0.56 | 8.99 ± 0.39 | 0.92 |
| Viscoat - Sample 3 | 43 | 118.98 | 8.75 ± 0.46 | 7.06 ± 1.64 | -1.70 |
| **Viscoat – Average[d]** | 49 ± 18 | 123.81 ± 38.30 | 9.90 ± 1.57 | 9.65 ± 1.77 | 1.20 ± 0.35[e] |
| ProVisc - Sample 1 | 28 | 80.65 | 8.60 ± 0.17 | 9.44 ± 0.72 | 0.84 |
| ProVisc - Sample 2 | 30 | 78.91 | 3.90 ± 4.93 | 16.65 ± 3.75 | 12.75 |
| ProVisc - Sample 3 | 29 | 95.7 | 19.22 ± 8.94 | 14.07 ± 3.40 | -5.15 |
| **ProVisc – Average[f]** | 29 ± 1 | 85.10 ± 7.55 | 10.57 ± 6.41 | 13.39 ± 2.98 | 6.24 ± 4.92[g] |

[a] $t_{ovd}$ = Approximate time after $\Delta P$ peak (determined by looking at plot)

[b] Average ± standard deviation of experimental $\Delta P$s before OVD was injected into the AGV tube

[c] Average ± standard deviation of experimental $\Delta P$s from $t_{ovd}$ to the end of flow trial (15 hours)

[d] Overall average ± standard deviation of $t_{ovd}$, maximum $\Delta P$, $\Delta P_i$, $\Delta P_f$ and $\Delta P_f - \Delta P_i$ for the Viscoat trials

[e] Average ± standard deviation for the absolute values of $\Delta P_f - \Delta P_i$ for all three Viscoat trials

[f] Overall average ± standard deviation of $t_{ovd}$, maximum $\Delta P$, $\Delta P_i$, $\Delta P_f$ and $\Delta P_f - \Delta P_i$ for the ProVisc trials

[g] Average ± standard deviation for the absolute values of $\Delta P_f - \Delta P_i$ for all three ProVisc trials

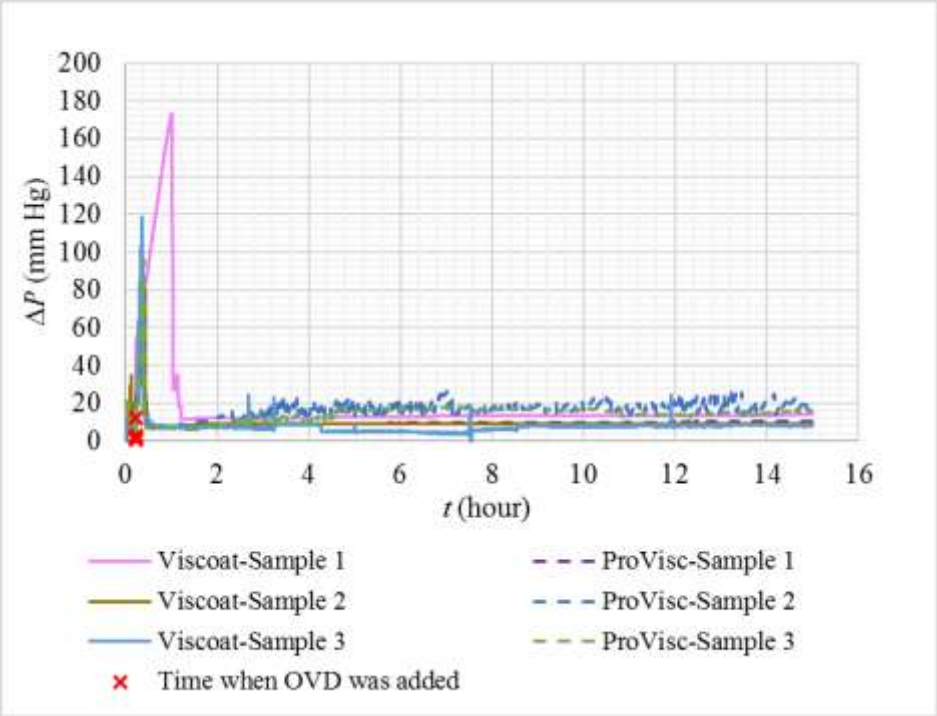


Fig. 4.12: Pressures for 15-hour AGV trials with the addition of Viscoat and Provisc

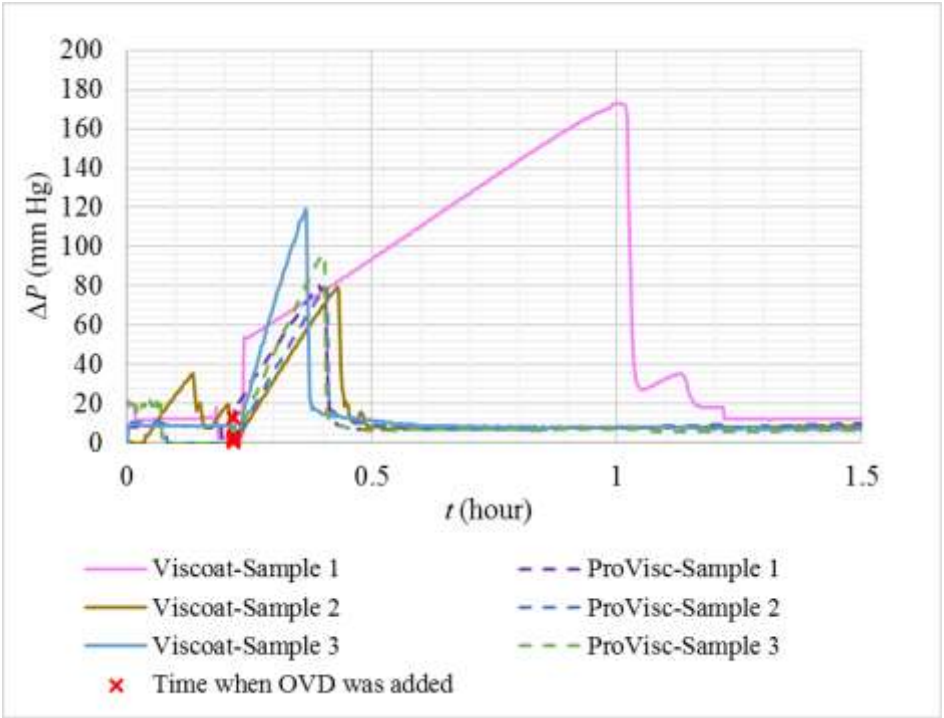


Fig. 4.13: First 1.5 hours of the 15-hour AGV trials with the addition of Viscoat and Provisc (magnified version of Fig. 4.12)

Yoshino *et al.* investigated residual OVDs in the eye after phacoemulsification and discovered that ProVisc completely disappeared from the anterior chamber after the quantitative procedure, whereas a residual layer of Viscoat remained on the corneal endothelium ($0.74 \pm 0.16$ μm thick) [71].

From Table 4.8 and Fig. 4.12, it can be seen that the maximum $\Delta P$ caused by Viscoat was generally higher than the $\Delta P$ caused by ProVisc [63]. This was contrary to theory since Viscoat has a lower molecular weight than ProVisc. Theoretically, with a lower molecular weight, Viscoat should not create a large increase in $\Delta P$ when it passes through the valve [63]. However, these results agree with the findings of Rainer *et al.* [64]. Rainer *et al.* compared the effects of using Viscoat and DuoVisc on post-op IOP and found that Viscoat caused a significant increase in IOP and more IOP spikes during the early post-op period [64]. In that study, Viscoat was used in the early stage of cataract surgery and ProVisc was used only during intraocular lens implantation [64]. It is possible that this significant IOP increase was because it took longer for Viscoat to flow out of the AGV than for ProVisc. The extended outflow time could have created a greater flow resistance, resulting in higher $\Delta P$. It was also noted that the differences between $\Delta P_f$ ($\Delta P$ after the spike) and $\Delta P_i$ ($\Delta P$ before the OVD was injected) for the Viscoat trials were relatively small. This showed that there was little change between the average $\Delta P$ before and after the OVD passed through the valve.

It can be seen that $\Delta P_f - \Delta P_i$ results for all three ProVisc samples were inconsistent. It can be seen from Table 4.8, that there was a significant increase from $\Delta P_i$ to $\Delta P_f$ for ProVisc Sample 2, but a significant decrease from $\Delta P_i$ to $\Delta P_f$ for ProVisc Sample 3. For ProVisc Sample 1, there was no significant increase from $\Delta P_i$ to $\Delta P_f$. Therefore, it is inconclusive as to whether ProVisc significantly affected the operation of the AGV. More experimental trials are necessary in order to

obtain more conclusive results.

From Fig. 4.13, it can be seen that the peak $\Delta P$ for Viscoat Sample 1 was significantly higher than those of the other two Viscoat samples. This large difference may be due to human error in standardizing the quantity of Viscoat injected into the AGV tube. The quantity of Viscoat injected into the AGV tube was difficult to standardize since only a very small amount (~0.07 $cm^3$) was needed to fill the AGV tube; and it was more difficult to control the amount of Viscoat injected into the tube, due to its higher dynamic viscosity, as compared to the dynamic viscosity of ProVisc.

Also, from Table 4.8, note that the $\Delta P_i$s for all six samples were within the nominal IOP range of 5 to 25 mm Hg. This was because all of the AGV samples tested in these trials were primed prior to performing the trials. Therefore, it is vital to prime AGVs before implanting them on the eye.

***Conclusion:*** *Viscoat caused a larger increase in $\Delta P$ than ProVisc. Viscoat also took longer to flow through the AGV. The trials showed that OVDs in AGVs could cause a significant increase in IOP levels and take a significant amount of time to pass through the valve.*

### 4.2.3. Fluid Pressure Response in AGVs with Silicone Oil

***Research question:*** *What is the pressure effect of silicone oil on AGVs?*

Four 15-hour flow trials were performed in order to test the pressure effect on AGVs when silicone oil flows through them. Three of the trials were performed with pure silicone oil (~0.07 $cm^3$) and one trial with emulsified silicone oil. The emulsified silicone oil was prepared by adding 1 ml of silicone oil to 1 ml of DI water in a 5 ml centrifuge tube, and mixing the combination for approximately 1 minute. Mixing was manually done by vigorously shaking the centrifuge tube for approximately 1 minute. Emulsified silicone oil was used to more closely simulate the actual flow

of silicone oil through the AGV when in the eye. It has been reported that silicone oil emulsifies in the eye several months after post-op: 1% after 1 month, 85% after 6 months and 100% after 12 months [72]. Therefore, due to the tendency to emulsify, it is more likely that small droplets of silicone oil in the AH flows through the AGV instead of a single large droplet of silicone oil.

The setup and trial procedures are described in Apps. G.1 and G.2. The trials were performed with 0.04% $NaN_3$ solution, at a flow rate of 2.5 µl/min and room temperature (25°C). Table 4.9 summarizes the results of the AGV trials with silicone oil. Figure 4.14 shows the pressure plots of the four 15-hour AGV trials with silicone oil; and Fig. 4.15 is an expanded version of Fig. 4.14, showing only the first 0.8 hour.

Table 4.9: Summary of the $\Delta P$ results for 15-hour AGV trials with silicone oil (three with pure silicone oil and one with emulsified silicone oil)

| AGV sample | Approximate time for silicone oil to pass through AGV, $t_{so}$ (hour)[a] | Maximum $\Delta P$ (mm Hg) | Average experimental $\Delta P$ (mm Hg) | | |
|---|---|---|---|---|---|
| | | | Initial, $\Delta P_i$ [b] | Final, $\Delta P_f$ [c] | Difference, $\Delta P_f - \Delta P_i$ |
| 1 (Pure) | 3.45 | 39.19 | 7.47 ± 0.19 | 10.35 ± 0.21 | 2.88 |
| 2 (Pure) | 11.48 | 32.57 | 9.15 ± 0.30 | 13.97 ±0.30 | 4.82 |
| 3 (Pure) | 2.25 | 34.71 | 10.58 ± 1.97 | 10.07 ± 0.47 | -0.52 |
| **Average[d]** | 5.73 ± 4.10 | 35.49 ± 2.76 | 9.07 ± 1.27 | 11.46 ± 1.78 | 2.74 ± 1.76[e] |
| 4 (Emulsified) | 0.53 | 51.81 | 12.33 ± 2.32 | 14.95 ± 0.67 | 2.62 |

[a] Time at which $\Delta P$ began to be relatively constant (standard deviation ≤ ±1 mm Hg) minus the time at which silicone oil was injected into the AGV tube
[b] Average ± standard deviation of experimental $\Delta P$ before injecting silicone oil into AGV tube
[c] Average ± standard deviation of experimental $\Delta P$ from $t_{so}$ to the end of flow trial (15 hours)
[d] Overall average ± standard deviation of experimental $\Delta P$s for the three pure silicone oil flow trials
[e] Average ± standard deviation of the absolute $\Delta P_f$ - $\Delta P_i$ values

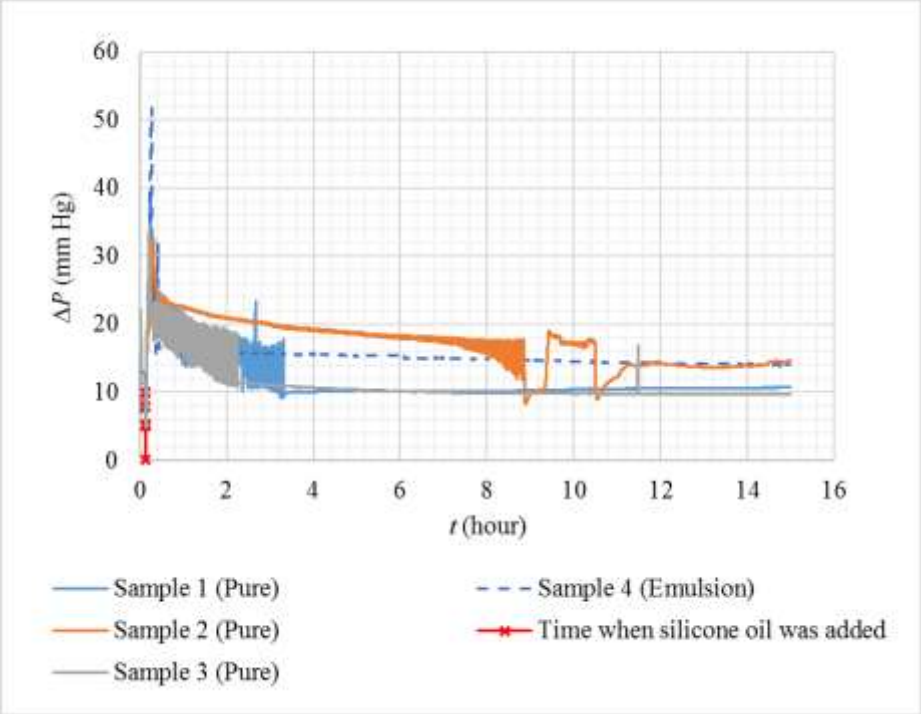


Fig. 4.14: Pressures of the 15-hour AGV trials with the addition of pure silicone oil and a silicone oil emulsion

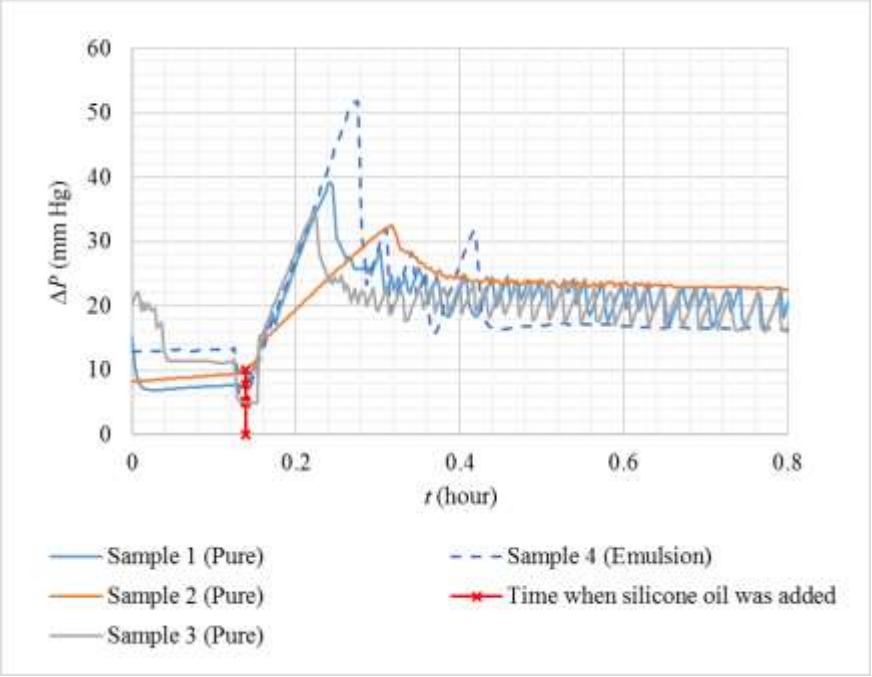


Fig. 4.15: Expanded 0.8-hour plot of the 15-hour AGV trials with the addition of pure silicone oil and silicone oil emulsion (magnified version of Fig. 4.14)

It can be seen from Table 4.9 and Fig. 4.14 that the peak $\Delta P$ in the AGV, caused by the emulsified silicone oil, was significantly higher than the peak $\Delta P$ caused by pure silicone oil. Also, there were two distinct $\Delta P$ peaks for the emulsified silicone oil (Fig. 4.15). It is uncertain as to why emulsified silicone oil had a higher peak $\Delta P$ than that of the pure silicone oil, even though pure silicone oil should have a higher viscosity than emulsified silicone oil. It is noted that there was only one emulsified silicone oil trial. Thus, these findings may not apply to all cases of silicone oil flow through AGV tubes. More emulsified silicone oil trials are necessary in order to investigate this phenomenon.

It can be seen that it took longer for the pure silicone oil to pass through the AGV, with an average time of 5.73 hours, as compared to the emulsified silicone oil's 0.53 hour. This could have been because the pure silicone oil had greater adherence to the walls of the AGV tubes as compared to emulsified silicone oil, causing the pure silicone oil to remain in the tubes longer than the emulsified silicone oil. Again, it is noted that there was only one emulsified silicone oil trial performed. Therefore, these results may not apply to all cases of silicone oil flow through AGV tubes.

From Table 4.9, it can also be seen that, for pure silicone oil Samples 1 and 2, $\Delta P_f$ values were higher than the $\Delta P_i$ values. However, for pure silicone oil Sample 3, $\Delta P_f$ was higher than $\Delta P_i$. More trials are necessary to investigate this phenomenon. It is recommended that a more standardized measurement method be implemented in future experimental trials (refer to Section 4.3 for details).

Once again, note that $\Delta P_i$ values for all four silicone oil samples were within the nominal IOP range. This was because the AGVs used were primed prior to the trials. Therefore, it is very important to prime the AGV before implanting onto the eye.

***Conclusion:*** *Silicone oil caused a significant increase in ΔP. Silicone oil also took longer to pass through the AGV. However, more testing is needed to confirm these findings.*

## 4.3. Summary of the Additional Experimental Trial Results

An increase in Δ*P* over time was observed for both the degradable and non-degradable insert trials. For the preliminary trials with BGI tubes (Section 4.1), the experimental Δ*P*s did not match the theoretical Δ*P* ranges for both degradable and non-degradable insert trials. This discrepancy could have been caused by microbial growth in the tubes since these annular trials were performed prior to the implementation of the anti-microbial protocol. The pressure results for the trials with flexible inserts were inconsistent even though the samples were cut from the same suture spool. This inconsistency in pressure results may have been because some of the inserts were crammed in the tubes, but others were stretched out. For the non-degradable insert trials, the continuous increase in Δ*P* could have been due to microbial growth. For the degradable insert trials, the continuous increase in Δ*P* could be attributed to the increase in size of the inserts prior to degradation.

AGV flow trials were performed to determine the pressure effects of not manually priming AGVs prior to implantation (Section 4.2.1). The trial results showed that, when AGVs had not been primed, the pressure in the AGV tube increased significantly above the nominal IOP range. However, the pressures of AGVs that were manually primed prior to trials were within the nominal IOP range. Therefore, it is important to prime AGVs prior to implantation.

It was also found that OVDs caused a significant increase in AGV tube pressures and took longer to pass through the AGV. The results showed that Viscoat caused a larger increase in Δ*P* than ProVisc. Viscoat also took longer to flow through the AGV than ProVisc. Silicone oil was found to also cause a significant increase in Δ*P* above the nominal IOP range of 25 mm Hg.

Therefore, it is important to note that OVDs and silicone oil can cause a detrimental increase in IOP if passed through the AGV in the eye.

Comparing the results from the OVD trials with those of the silicone oil trials, it was observed that OVDs caused larger $\Delta P$ spikes as compared to those caused by the silicone oil. It can also be seen that it took approximately the same amount of time for the OVD and the emulsified silicone oil to pass through the AGV. Pure silicone oil took the longest to pass through the AGV as compared to the OVDs and the emulsified silicone oil. However, this was expected due to the pure silicone oil's high viscosity.

As mentioned in Section 4.2.3, a more standardized measurement method should be implemented in future experimental trials. A possible idea is to utilize the kdScientific syringe pump that was used during the experimental setup-validation trials (Section 2.5.2). With this syringe pump, one could set the specific OVD or silicone oil volume that is to be dispensed into the AGV tube. Trial and error would be necessary in order to determine the right pump settings for this application. Additionally, more repeated runs are needed to confirm or deny the results found.

# Chapter 5: Conclusions and Recommendations

This chapter summarizes the conclusions and results of all chapters, as well as discusses recommendations for future studies.

## 5.1. Conclusions

In summary, current GDIs are unable to provide immediate and consistent IOP control. Various attempts, such as the design of valved GDIs and intra-op NVGDI surgical interventions, have resulted in some improvements, but have not been able to provide consistent and immediate post-op IOP control. To resolve this issue, a relatively new method was proposed by Munden [41] in order to provide consistent IOP control in the immediate post-op stage of BGI surgery. With the success of this modification, the BGI will be able to provide immediate and consistent IOP control.

The ultimate goal of this project is to analyze the pressure effects of this modification on the BGI. This thesis covers the study to validate and substantiate the reliability of two microflow pressure-measuring experimental setups designed to evaluate pressure modulations through BGI tubes which include this modification. Benchmark pressure data were obtained by performing single-tube-flow trials with stiff micron-sized VSD tubes, and annular flow trials with stiff SS hypodermic tubes and nichrome wires of different diameters. These trials were performed to test the primary hypothesis of this thesis which states that the experimental pressure loss through tubes with BGI-like IDs will match the theoretically calculated pressure loss using the Hagen-Poisueille theory.

Thorough experimental validation trials were performed in order to verify and validate the accuracy of the experimental setup. The $\Delta P$ results from these validation trials showed that both Setups 1 and 2 corresponded well with each other. When 10 two-hour trials with 50 μm ID VSD were performed (five per setup), the cumulative average pressures measured over the five trials in

both setups were very close with a difference of only 0.91%. The cumulative average pressures measured in Setups 1 and 2 were 57.3 ± 11.3 mm Hg and 57.8 ± 9.1 mm Hg, respectively.

To test for repeatability for flow through annular tubes, annular flow trials with stiff tubes and inserts were performed, repeating the trials with the same two samples three times in both setups. During these trials, it was observed that the $\Delta P$ results were not repeatable even though the same test sample was used each time. It was found that $\Delta P$ increased over time after each trial repetition. For example, the average $\Delta P$ in the first trial performed with Sample 1 on February 15, 2016 was 12.1 mm Hg whereas the $\Delta P$ measured for the last two trials performed on February 18, 2016 were 24.2 mm Hg and 19.3 mm Hg.

However, these trials demonstrated that the pump and the pressure transducer pressure readings agreed with one another. The differences between the $\Delta P$s measured by the pumps and transducers for Sample 1 were constant at an average of 16.2 ± 0.29 mm Hg and 15.1 ± 0.54 mm Hg for Setups 1 and 2, respectively. For Sample 2, the differences between the $\Delta P$s measured by the pumps and transducers were also relatively constant at 12.9 ± 3.10 mm Hg and 15.7 ± 0.59 mm Hg for Setups 1 and 2, respectively.

Eight 20-hour trials were also performed in Setups 1 and 2 with two samples to further investigate this pressure measurement issue. The pressure results showed that there was a gradual increase in $\Delta P$ from the first hour to the end of the experimental trials; and this was observed in all eight trials. Differences of up to 6.01 mm Hg and 1.00 mm Hg between initial $\Delta P$ and final $\Delta P$ for Samples 1 and 2, respectively, were observed. In order to determine if this issue was caused by systematic errors, further experimental validation trials were performed to test the reliability of the pneumatic pumps in measuring pressure and flow rate, as well as the accuracy of the pressure transducers in measuring fluid pressure at the test sample.

The internal flow rate and pressure sensors of the pneumatic pumps were investigated by comparing the measurements of the pumps in-line, measuring pressures for the same sample. It was found that the two pumps' flow rate and pressure readings compared well with each other (±0.02 µl/min; ±0.19 mm Hg). The pneumatic pumps were also cross-checked with a syringe pump, and it was found that the pneumatic pump's flow rate sensors accurately (3% at 15 µl/min and 6% at 30 µl/min) measured the output flow rate of the syringe pump. The pressure transducer readings were cross-checked with the pressure readings of a third transducer from a different manufacturer and type (current output instead of voltage output). After cross-checking the pressure readings of the two types of transducers, it was found that the transducer readings from both types of transducers matched well (±0.13 mm Hg). Therefore, the continuously increasing $\Delta P$ measurements were not caused by systemic error of the pumps or transducers.

Since pump or transducer systemic issues were not causing the continuously rising $\Delta P$ measurements, it was hypothesized that microbial growth might have been causing this issue. A cleaning and sterilization protocol was developed. To test the effectiveness of the protocol, 10-day trials were performed using 50 µm ID VSD tubes. The results showed that the cleaning and sterilization protocol was effective in providing more consistent $\Delta P$ measurements. Before the cleaning and sterilization protocol, pressures increased by as much as 200 mm Hg. However, after implementing the cleaning and sterilization protocol, the pressure results remained constant for long periods (~28 days) with small standard deviations of less than 4 mm Hg.

The verified setup was used to test the primary hypothesis of the study, comparing the experimental pressure loss through GDI-like tubes with theoretical pressure loss calculated using the Hagen-Poiseuille equation. The results of these trials were discussed in a paper submitted to

the BJO. The theoretical pressure loss calculations were done using the tube diameter measurements made with the microXCT microscope.

Single open tube flow trials were performed using VSD microtubes with IDs of 50 μm and 75 μm in order to determine the effect of tube ID on the pressure loss through single tubes having IDs small enough to create Δ*P*s within the clinically relevant range (5 - 25 mm Hg). These trials demonstrated that the experimental pressures fell within the theoretically predicted pressure ranges which accounted for variations in tube length and flow rate from their respective nominal values. Annular flow trials were performed with SS hypodermic tubes having different IDs and nichrome wire inserts of different ODs in order to determine the effect of annulus size (effective diameter, $D_{eff}$) on the pressure. $D_{eff}$ is a function of tube ID ($D_o$) and insert OD ($D_i$). The results demonstrated that the experimental pressures remained within the theoretically predicted pressure range. The difference between the theoretical and experimental Δ*P*s was smaller when $D_{eff}$ was small enough to provide experimental Δ*P*s within the clinically relevant range.

Therefore, the Δ*P* results presented in the BJO paper demonstrated that the current test system can maintain constant flow rate (±0.05 μl/min) and accurately measure pressure across tubes with similar diameters to those used in GDIs (±0.2 mm Hg). The results also show that the two test setups can measure Δ*P* through annular tubes, comparing well with theoretical Δ*P* values that were calculated according to very precise diameter measurements made using micro-CT imaging. The experimental Δ*P* results were well within the theoretical Δ*P* ranges. In addition, the current experimental setups can take consistent long-term (e.g., 10 days) pressure drop data which are within theoretical pressure ranges.

Using the validated setups, trials were performed with AGVs in order to determine the Δ*P* effects when OVDs or silicone oil flows through the AGV in the eye. Preliminary AGV trials

demonstrated the importance of priming the AGV before implantation. The average time taken for the valve of an AGV to open was 2.03 ± 1.42 hours, and the average Δ*P* value for the AGV trials was 52.7 ± 16.34 mm Hg.

Two types of OVDs were used in the trials, Viscoat and ProVisc. It was found that it took longer for Viscoat to pass through the AGV than that for ProVisc. The average times for Viscoat and ProVisc to pass through the AGV were 49 ± 18 minutes and 34 ± 6 minutes, respectively. The trials also showed that Viscoat created, on average, larger Δ*P* spikes (average maximum Δ*P* of 123.8 mm Hg) compared to ProVisc (average maximum ΔP of 93 mm Hg). This observation was contrary to the theoretical assumption that Viscoat would cause a lower Δ*P* spike, but agreed with the findings of Rainer *et al.* [64].

From the silicone oil flow trials, it was observed that the peak Δ*P* caused by the emulsified silicone oil (51.8 mm Hg) was higher than that caused by the pure silicone oil (35.5 mm Hg) when passing through the AGV. It was also noted that it took longer for the pure silicone oil to pass through the AGV with an average time of 5.73 hours as compared to the emulsified silicone oil's with an average time of 0.53 hours. More trials with emulsified silicone oil are needed in order to provide more conclusive data. It was found that OVDs caused a greater spike in Δ*P* (85.1 - 123.8 mm Hg) as compared to silicone oil (35.5 - 51.8 mm Hg), but it took longer for silicone oil to pass through the AGV (29 - 49 minutes) as compared to the time taken for OVDs to pass through the AGV (31 minutes - 11.5 hours).

## 5.2. Recommendations and Future Work

The following are recommendations for future work needed to advance this research:

- Perform long-term annular flow trials with degradable sutures using BSS at body temperature

(37°C) to better simulate the conditions of the body.

- Perform long-term annular flow trials with stiff tubes and inserts for more than 30 days to obtain benchmark $\Delta P$ trend for comparison with annular trials using BGI tubes and degradable inserts.
- Perform more standardized AGV trials to compare the effects of OVDs and silicone oil (especially emulsified silicone oil) on $\Delta P$ in AGVs.
- Obtain a third experimental setup to increase the efficiency of running 20- to 30-day experimental trials by conserving the time required to run the trials.
- Further investigate the effects of barometric pressure/atmospheric temperature/humidity on the small fluctuations of 20- to 30-day $\Delta P$ data in the samples.
- Develop a more precise mathematical model with CFD for predicting $\Delta P$ through the annulus of a GDI having a degradable insert. This is to provide as much information as possible for the design of the degradable insert modification of GDI tubes that was proposed by Dr. Munden. An NIH R03 proposal was submitted on June 15, 2017, proposing how the experimental study and the implementation of CFD could be performed. The proposal is attached in App. H.
- Perform trials using the novel PCL/PEG degradable monofilament that was developed by Dr. Berkland and Dr. Munden in the BGI tube.
- After validating the efficacy of the degradable insert modification, perform *in vivo* trials using animal subjects.

## REFERENCES


[1] Weinreb R.N., Aung T., and Medeiros F.A., *"The Pathophysiology and Treatment of Glaucoma a Review"*. The Journal of the American Medical Association, 2014. **311**(18): pp. 1901-1911.

[2] Susanna R.J., De Moraes C.G., Cioffi G.A., and Ritch R., *"Why Do People (Still) Go Blind from Glaucoma?"*. Translational Vision Science and Technology, 2015. **4**(2): pp. 1.

[3] Hong C.H., Arosemena A., Zurakowski D., and Ayyala R.S., *"Glaucoma Drainage Devices: A Systematic Literature Review and Current Controversies"*. Survey of Ophthalmology, 2005. **50**(1): pp. 48-60.

[4] Kansal S., Moster M.R., Kim D., Schmidt C.M., Jr., Wilson R.P., and Katz L.J., *"Effectiveness of Nonocclusive Ligature and Fenestration Used in Baerveldt Aqueous Shunts for Early Postoperative Intraocular Pressure Control"*. Journal of Glaucoma, 2002. **11**(1): pp. 65-70.

[5] Marchini G., Ceruti P., Vizzari G., Toscani M., Amantea C., Tosi R., and Marchetti P., *"Long-Term Outcomes of a Modified Technique Using the Baerveldt Glaucoma Implant for the Treatment of Refractory Glaucoma"*. Journal of Glaucoma, 2016. **25**(12): pp. 952-958.

[6] Emerick G.T., Gedde S.J., and Budenz D.L., *"Tube Fenestrations in Baerveldt Glaucoma Implant Surgery: 1-Year Results Compared with Standard Implant Surgery"*. Journal of Glaucoma. **11**(4): pp. 340-346.

[7] Tong L., Frazao K., LaBree L., and Varma R., *"Intraocular Pressure Control and Complications with Two-Stage Insertion of the Baerveldt Implant"*. Ophthalmology, 2003. **110**(2): pp. 353-358.

[8] Trible J.R. and Brown D.B., *"Occlusive Ligature and Standardized Fenestration of a Baerveldt Tube with and without Antimetabolites for Early Postoperative Intraocular Pressure Control"*. Ophthalmology, 1998. **105**(12): pp. 2243-2250.

[9] Tham Y.C., Li X., Wong T.Y., Quigley H.A., Aung T., and Cheng C.Y., *"Global Prevalence of Glaucoma and Projections of Glaucoma Burden through 2040: A Systematic Review and Meta-Analysis"*. Ophthalmology, 2014. **121**(11): pp. 2081-2090.

[10] Christakis P.G., Kalenak J.W., Tsai J.C., Zurakowski D., Kammer J.A., Harasymowycz P.J., Mura J.J., Cantor L.B., and Ahmed, II, *"The Ahmed versus Baerveldt Study: Five-Year Treatment Outcomes"*. Ophthalmology, 2016. **123**(10): pp. 2093-2102.

[11] Tsukahara S. and Sasaki T., *"Postural Change of IOP in Normal Persons and in Patients with Primary Wide Open-Angle Glaucoma and Low-Tension Glaucoma"*. British Journal of Ophthalmology, 1984. **68**(6): pp. 389-392.

[12] McLaren J.W., *"Measurement of Aqueous Humor Flow"*. Experimental Eye Research, 2009. **88**(4): pp. 641-647.

[13] Weinreb R.N., Aung T., and Medeiros F.A., *"The Pathophysiology and Treatment of Glaucoma: A Review"*. The Journal of the American Medical Association, 2014. **311**(18): pp. 1901-1911.

[14] *"Preferred Practice Pattern: Primary Open-Angle Glaucoma"*, American Academy of Ophthalmology, 2015. American Academy of Ophthalmology Preferred Practice Patterns Committee GP: Chicago, Illinois. [Cited: September 5, 2017]. Available from: https://www.aao.org/preferred-practice-pattern/primary-open-angle-glaucoma-suspect-ppp-2015.

[15] Mosaed S. and Minckler D.S., *"Aqueous Shunts in the Treatment of Glaucoma"*. Expert Review of Medical Devices, 2010. **7**(5): pp. 661-666.

[16] Rodgers C.D., Meyer A.M., and Sherwood M.B., *"Relationship between Glaucoma Drainage Device Size and Intraocular Pressure Control: Does Size Matter?"*. Journal of Current Glaucoma Practices, 2017. **11**(1): pp. 1-2.

[17] Jung K.I., Park H.Y., and Park C.K., *"The Effect of Tube Length on Postoperative Outcome after Glaucoma Drainage Implant Surgery"*. Acta Ophthalmologica, 2013. **91**(4): pp. e325-327.

[18] Gedde S.J., Schiffman J.C., Feuer W.J., Herndon L.W., Brandt J.D., and Budenz D.L., *"Treatment Outcomes in the Tube versus Trabeculectomy (TVT) Study after Five Years of Follow-Up"*. American Journal of Ophthalmology, 2012. **153**(5): pp. 789-803.

[19] Arora K.S., Robin A.L., Corcoran K.J., Corcoran S.L., and Ramulu P.Y., *"Use of Various Glaucoma Surgeries and Procedures in Medicare Beneficiaries from 1994 to 2012"*. Ophthalmology, 2015. **122**(8): pp. 1615-1624.

[20] Kaplan R.I., De Moraes C.G., Cioffi G.A., Al-Aswad L.A., and Blumberg D.M., *"Comparative Cost-Effectiveness of the Baerveldt Implant, Trabeculectomy with Mitomycin, and Medical Treatment"*. The Journal of the American Medical Association in Ophthalmology, 2015. **133**(5): pp. 560-567.

[21] Herndon L.W., Smith O.U., Khaimi M.A., Mosaed S., Greenwood M.D., Sarkisian S.R.Jr., Berlin M., Roka V., Riggs M., Giers U., Vold S.D., Töteberg-Harms M., Mertens E.L., and Barnebey H., *"Where We Are Today with MIGS"*. Glaucoma Today by Bryn Mawr Communications (BMC), March-April 2017. [Cited: September 5, 2017]. Available from: http://glaucomatoday.com/2017/04/where-we-are-today-with-migs/.

[22] Resende A.F., Patel N.S., Waisbourd M., and Katz L.J., *"iStent(R) Trabecular Microbypass Stent: An Update"*. Journal of Ophthalmology, 2016. Published online June 20, 2016. [Cited: August 20, 2017]. Available from: https://www.ncbi.nlm.nih.gov/pmc/articles/PMC4931099/.

[23] Richter G.M. and Coleman A.L., *"Minimally Invasive Glaucoma Surgery: Current Status and Future Prospects"*. Clinical Ophthalmology, 2016. **10**: pp. 189-206.

[24] Sarkisian S.R.J., *"The Ex-PRESS Mini Glaucoma Shunt: Technique and Experience"*. Middle East African Journal of Ophthalmology, 2009. **16**(3): pp. 134-137.

[25] Hillen M., *"Glaucoma Management Strategies"*. The Ophthalmologists, 2017, Texere Publishing Limited.

[26] Shaarawy T., Goldberg I., and Fechtner R., *"Ex-PRESS Glaucoma Filtration Device: Review of Clinical Experience and Comparison with Trabeculectomy"*. Survey of Ophthalmology, 2015. **60**(4): pp. 327-345.

[27] Mizoguchi T., Nishigaki S., Sato T., Wakiyama H., and Ogino N., *"Clinical Results of Trabectome Surgery for Open-Angle Glaucoma"*. Clinical Ophthalmology, 2015. **9**: pp. 1889-1894.

[28] Center M.E., *"Cataract Surgery with iStent in Patients with Glaucoma"*, 2013. [Cited: June 16, 2017]. Available from: http://melbourneeyecentre.com.au/blog/cataract-surgery-with-istent-in-patients-with-glaucoma/.

[29] Shields M.B., *"Cyclodestructive Surgery for Glaucoma: Past, Present, and Future"*. Transactions of the American Ophthalmological Society, 1985. **83**: pp. 285-303.

[30] Bietti G., *"Surgical Intervention on the Ciliary Body; New Trends for the Relief of Glaucoma"*. Journal of the American Medical Association, 1950. **142**(12): pp. 889-897.

[31] Coleman D.J., Lizzi F.L., Driller J., Rosado A.L., Burgess S.E., Torpey J.H., Smith M.E., Silverman R.H., Yablonski M.E., Chang S., and Rondeau M.J., *"Therapeutic Ultrasound in the Treatment of Glaucoma. Ii. Clinical Applications"*. Ophthalmology, 1985. **92**(3): pp. 347-353.

[32] Beckman H., Kinoshita A., Rota A.N., and Sugar H.S., *"Transscleral Ruby Laser Irradiation of the Ciliary Body in the Treatment of Intractable Glaucoma"*. Transactions - American Academy of Ophthalmology and Otolaryngology, 1972. **76**(2): pp. 423-436.

[33] Christakis P.G., Kalenak J.W., Tsai J.C., Zurakowski D., Kammer J.A., Harasymowycz P.J., Mura J.J., Cantor L.B., and Ahmed I.I., *"The Ahmed versus Baerveldt Study: Five-Year Treatment Outcomes"*. Ophthalmology, 2016. **123**(10): pp. 2093-2102.

[34] Schwartz K.S., Lee R.K., and Gedde S.J., *"Glaucoma Drainage Implants: A Critical Comparison of Types"*. Current Opinion in Ophthalmology, 2006. **17**(2): pp. 181-189.

[35] Christakis P.G., Tsai J.C., Kalenak J.W., Zurakowski D., Cantor L.B., Kammer J.A., and Ahmed I.I.K., *"The Ahmed Versus Baerveldt Study: Three-Year Treatment Outcomes"*. Ophthalmology, 2013. **120**(11): pp. 2232-2240.

[36] Christakis P.G., Zhang D., Budenz D.L., Barton K., Tsai J.C., and Ahmed I.I.K., *"Five Year Pooled Data Analysis of the Ahmed Baerveldt Comparison Study and the Ahmed versus Baerveldt Study"*. American Journal of Ophthalmology, 2017. **176**: pp. 118-126.

[37] Sherwood M.B. and Smith M.F., *"Prevention of Early Hypotony Associated with Molteno Implants by a New Occluding Stent Technique"*. Ophthalmology, 1993. **100**(1): pp. 85-90.

[38] Gilbert D.D. and Bond B., *"Intraluminal Pressure Response in Baerveldt Tube Shunts: A Comparison of Modification Techniques"*. Journal of Glaucoma, 2007. **16**(1): pp. 62-67.

[39] Breckenridge R.R., Bartholomew L.R., Crosson C.E., and Kent A.R., *"Outflow Resistance of the Baerveldt Glaucoma Drainage Implant and Modifications for Early Postoperative Intraocular Pressure Control"*. Journal of Glaucoma, 2004(13): pp. 396-399.

[40] Brooks S.E., Davey M.P., Lee M.B., and Baerveldt G., *"Modifications of the Glaucoma Drainage Implant to Prevent Early Postoperative Hypertension and Hypotony - a Laboratory Study"*. Ophthalmic Surgery, 1994. **25**(5): pp. 311-316.

[41] Munden P.M. and Boyce M. *"A Retrospective Review of Baerveldt Implants with Tubing Insert Modification to Reduce Post-Operative Hypotony"*. Poster #D0210 at *The Association for Research in Vision and Ophthalmology (ARVO) Annual Meeting*. 2016. Seattle, WA. May 1-5.

[42] Ramani A., *"Reliable Experimental Setup to Test the Pressure Modulation of Baerveldt Implant Tubes for Reducing Post-Operative Hypotony"*, Master of Science Thesis in *Mechanical Engineering*. 2015, University of Kansas.

[43] Munden P.M., Ramani A., Kieweg S.L., Dougherty R.L., and Boyce M. *"An Experimental Model of Pressure Modulation in Baerveldt Implants to Reduce Post-Operative Hypotony"*. Poster #2005 at *The Association for Research in Vision & Ophthalmology (ARVO) Annual Meeting*. 2015. Denver, CO. May 3-7.

[44] *"SS-2-HC-7-4"*, in Spare Parts and Accessories - Hose and Flexible Tubing, Swagelok Company. July. [Cited: June 28, 2017]. Available from: https://www.swagelok.com/en/catalog/Product/Detail?part=SS-2-HC-7-4.

[45] *"Fluidic Connections"*, IDEX Health & Science. 2016. [Cited: June 28, 2017]. Available from: https://www.idex-hs.com/fluidics/fluidic-connections.html#tab-2.

[46] CorSolutions, *"Pneuwave Pump"*, CorSolutions. 2016. [Cited: November 11, 2016]. Available from: http://www.mycorsolutions.com/pneuwave.html.

[47] *"KDS Legato 100 Series User's Manual"*, 2017. kdScientific. [Cited: February 20, 2017]. Available from: https://www.kdscientific.com/technical-resources/manuals.html.

[48] *"Station Archive (KSLAWRE1)"*, PWS-Station Observations for KKSLAWRE1. 2017. [Cited: September 24, 2017]. Available from: https://www.pwsweather.com/archivewx.php?id

=KKSLAWRE1&d=20170831&t=day#.

[49] Spitzer D.W., *"How Pressure Variations Affect Flow Measurement"*, September 26, 2010. [Cited: September 27, 2017]. Available from: https://www.flowcontrolnetwork.com/how-pressure-variations-affect-flow-measurement/.

[50] Munson B.R., Young D.F., Okiishi T.H., and Huebsch W.W., *"Fundamentals of Fluid Mechanics"*. Sixth ed. 2009, NJ: John Wiley and Sons.

[51] *"CRC Handbook of Chemistry and Physics"*. 98 ed. 1988, Boca Raton, Florida: CRC Press.

[52] *"Leica DM2500 M Microscope for Material Analysis"*, Leica Microsystems. 2012.

[53] *"MicroXCT-200 and MicroXCT-400 User's Guide"*, Xradia. 2010.

[54] Lim K.S., Allan B., Khaw P.T., Willis S., Lloyd A.W., Muir A., Gard P., Faragher R.G.A., Olliff C.J., Hanlon G.W., Wong L., Reed S., and Denyer S., *"Experimental Flow Studies in Glaucoma Drainage Device Development"*. British Journal of Ophthalmology, 2001. **85**: pp. 1231-1236.

[55] Porter J.M., Krawczyk C.H., and Carey R.F., *"In Vitro Flow Testing of Glaucoma Drainage Devices"*. Ophthalmology, 1997. **104**(10): pp. 1701-1707.

[56] Prata J.A.Jr., Mermoud A., LaBree L., and Minckler D.S., *"In Vitro and In Vivo Flow Characteristics of Glaucoma Drainage Implants"*. Ophthalmology, 1995. **102**(6): pp. 894-904.

[57] Lim K.S., Wells A.P., and Khaw P.T., *"Needle Perforations of Molteno Tubes"*. Journal of Glaucoma, 2002. **11**(5): pp. 434-438.

[58] *"Fused Silica (Deactivated)"*, Trajan Scientific Australia. 2016. [Cited: September 8, 2017]. Available from: http://www.sge.com/products/gc--lc-supplies/gc-supplies/gc-tubing/fused-silica-100-methyl-deactivated3.

[59] Fitz B.D. and Jamiolkowski D.D., *"Hydrolysis Profiling: An In Vitro Methodology to Predict In Vivo Absorption Time"*. Journal of Biomedical Materials Research Part B: Applied Biomaterials, 2013. **101**(6): pp. 1014-1022.

[60] Melancia D., Abegão Pinto L., and Marques-Neves C., *"Cataract Surgery and Intraocular Pressure"*. Ophthalmic Research, 2015. **53**(3): pp. 141-148.

[61] Watts P. and Austin M., *"Retained Viscoat and Intraocular Pressure after Phaceomulsification"*. Indian Journal of Ophthalmology, 1999. **47**(4): pp. 237-240.

[62] Bissen-Miyajima H., *"Ophthalmic Viscosurgical Devices"*. Current Opinion in Ophthalmology, 2008. **19**(1): pp. 50-54.

[63] Higashide T. and Sugiyama K.., *"Use of Viscoelastic Substance in Ophthalmic Surgery - Focus on Sodium Hyaluronate"*. Clinical Opthalmology, 2008. **2**(1): pp. 21-30.

[64] Rainer G., Stifter E., Luksch A., and Menapace R., *"Comparison of the Effect of Viscoat and Duovisc on Postoperative Intraocular Pressure after Small-Incision Cataract Surgery"*. Journal of Cataract Refractive Surgery, 2008. **34**(2): pp. 253-257.

[65] Mimura T., Nakashizuka T., and Mori M., *"Recent Advances and History of Vitreous Surgery"*. Journal of Healthcare Engineering, 2011. **2**(4): pp. 447-458.

[66] Castellarin A., Grigorian R., Bhagat N., Del Priore L., and Zarbin M.A., *"Vitrectomy with Silicone Oil Infusion in Severe Diabetic Retinopathy"*. British Journal of Ophthalmology, 2003. **87**(3): pp. 318-321.

[67] Jalali S., *"Retinal Detachment"*. Community Eye Health, 2003. **16**(46): pp. 25-26.

[68] Boyd K., *"Retinal Detachment: Who Is at Risk for a Torn or Detached Retina?"*, in Detached or Torn Retina, American Academy of Ophthalmology. March 1, 2016. [Cited: Aug 29, 2017]. Available from: https://www.aao.org/eye-health/diseases/detached-torn-retina-risk.

[69] *"Model FP7 - Ahmed Glaucoma Valve Surgical Procedure"*, New World Medical 2017. [Cited: August 30, 2017]. Available from: http://www.newworldmedical.com/product-fp7.

[70] Cheng J., Abolhasani M., Beltran-Agullo L., Moss E.B., Buys Y.M., and Trope G.E., *"Priming the Ahmed Glaucoma Valve: Pressure Required and Effect of Overpriming"*. Journal of Glaucoma, 2015. **24**(4): pp. e34-35.

[71] Yoshino M., Bissen-Miyajima H., and Ohki S., *"Residual Amounts of Ophthalmic Viscosurgical Devices on the Corneal Endothelium Following Phacoemulsification"*. Japanese Journal of Ophthalmology, 2009. **53**(1): pp. 62-64.

[72] Federman J.L. and Schubert H.D., *"Complications Associated with the Use of Silicone Oil in 150 Eyes after Retina-Vitreous Surgery"*. Ophthalmology, 1988. **95**(7): pp. 870-876.

[73] Lott B., *"Omegadyne Inc. Certificate of Calibration - PX429-2.5GV"*, 2010.

[74] *"BX 1500G"*, in Power Saving Back-UPS XS 1500, APC Schneider Electric. 2017. [Cited: September 1, 2017]. Available from: http://www.apc.com/shop/us/en/products/Power-Saving-Back-UPS-XS-1500/P-BX1500G.

[75] *"Miller Manufacturing Company 9300 White Digital Still Air Incubator"*, Amazon. 2017. [Cited: September 1, 2017]. Available from: https://www.amazon.com/Miller-Manufacturing-Company-9300-Incubator/dp/B00KKRDQAE.

[76] Morgan P., *"GC Column Cutting Mini Guide"*, 2013, Thermo Fisher Scientific: Cheshire, UK. [Cited: October 15, 2017]. Available from: https://tools.thermofisher.com/content/sfs/brochures/TN-GC-Column-Cutting-TN20778_E.pdf.

[77] *"KD Scientific Legato 100 Series Syringe Pump User's Manual"*, KD Scientific. [Cited: September 1, 2017]. Available from: https://www.kdscientific.com/media/manuals/KDS%20Legato%20100%20Series_5617-006REV2.0.pdf.

[78] *"1/4" MNPT Pressure Transducer, 0-15 psi, 36 in lead"*, in Pressure and Vacuum Transducers, Dwyer Instruments, 2016. Grainger. [Cited: August 10, 2017]. Available from: https://www.grainger.com/product/DWYER-INSTRUMENTS-1-4-MNPT-Pressure-Transmitter-2HLV3.

[79] *"DuoVisc"*, in OVDs, My Alcon. [Cited: August 16, 2017]. Available from: https://www.myalcon.com/products/surgical/ovds/duovisc.shtml.

[80] Glaucoma Laser Trial Research Group, *"The Glaucoma Laser Trial (GLT) and Glaucoma Laser Trial Follow-up Study: 7. Results. Glaucoma Laser Trial Research Group"*. American Journal of Ophthalmology, 1995. **120**(6): pp. 718-731.

# APPENDICES

## Appendix A: Device Specifications

### A.1. List of Components Used in this Study

The main components in Setups 1 and 2 and their specifications are listed in Table A.1.1. Table A.1.2 lists the other materials and components used in this study, as well as their respective specifications.

Table A.1.1: List of components in the setups (modified from Ref. 42)

| Component | Make - Model | Serial/Part Number | Specifications/Descriptions |
|---|---|---|---|
| 1/32 in. OD PEEK tubing | Supplied by CorSolutions | - | - PEEK material<br>- 1/32 in. OD<br>- Setup 1: 3.25 ft. long (bottle to pump), 8 in. long (pump to 1/16 in. tubing)<br>- Setup 2: 2.6 ft. long, 8 in. long (pump to 1/16 in. tubing) |
| 1/16 in. OD clear PTFE tubing | Supplied by CorSolutions | - | - PTFE material<br>- 1/16 in. OD<br>- 1 ft. long |
| 500 ml glass bottle | Sigma Aldrich: CLS13955000 | - | 500 ml |
| Connector cable for transducer | Omega: CA-329-4PC24-015 | - | 15 feet long |
| Data logger | Omega: OM-CP-VOLT101A-160MV | Setup 1 (S/N: P59725)<br>Setup 2 (S/N: P44261) | 4 readings per second<br>(1 reading per 24 hrs)<br>- Range: 90 - 160 mV<br>- ± 0.01% FSR (Calibrated accuracy) |
| Incubator | Miller Manufacturing: Little Giant Still Air Incubators - Model 9300 | P/N: 9300 | - Styrofoam material<br>- 8 in. x 17.75 in. x 17.75 in.<br>- ±1°F temperature control |

Table A.1.1: List of components in the setups (continued)

| | | | |
|---|---|---|---|
| Medical grade tubing (IV extension tubing) | Various suppliers | - | - ID: ~1/8 in.<br>- Length: ~5 in. to 12 in.<br>- Luer lock connections<br>- Material: PVC, PP, Polyethylene, or Polycarbonate |
| Medical grade three-way valves | Various suppliers | - | - Luer lock connections |
| PEEK connector for 1/16 in. tubing | IDEX Health & Science: 10-32 one-piece conical fingertight connector | P/N: F-120 | - PEEK material<br>- 10-32 conical port configuration<br>- For 1/16" OD tubing<br>- 5000 psi max pressure rating |
| PEEK connector for luer lock to three-way valve | IDEX Health & Science: 10-32 female-to-female luer adapter | P/N: P-659 | - PEEK material<br>- 10-32 conical port configuration<br>- Female-to-female luer tape configuration<br>- 45 psi max pressure<br>- 1.30 mm through-hole diameter |
| Power supply | Hewlett Packard | S/N: E3630A | 20 V DC supply |
| Pressure transducer | Omega: PX429-2.5GV | Setup 1 (S/N: 419345)<br>Setup 2 (S/N: 419411) | 0 - 2.5 psi<br>(± 0.08% best straight line;<br>± 0.2 mm Hg) |
| Pump | CorSolutions: PneuWave Micro Pump | Setup 1<br>(S/N: 20140701.3; P/N: 227494)<br>Setup 2<br>(S/N: 20141231.3; P/N: CS3900r5-1 CH) | 0 - 50 µl/min<br>(±5%, ±0.125 µl/min) |
| SS hose connector | Swagelok | P/N: SS-2-HC-7-4 | - 316 SS material<br>- 1/8 in. ID hose connector<br>- 1/4 in. female NPT connector |
| Uninterruptible power supply (UPS) | Schneider Electric: APC Back-UPS XS 1500 | P/N: BX1500G | - 10 output connectors<br>- 120V nominal output voltage<br>- Run time: 2 hrs 8 mins at minimum load (50 Watts), 13 mins at half load (432.5 Watts), 4 mins at full load (865 Watts) |

Table A.1.2: Other materials and items used in this study

| Item | Make/Model | Specifications/Use |
|---|---|---|
| 1 ml syringe | EXELINT International:<br>1 ml luer lock tip syringe<br>(Ref: 26050) | - Pyrogen free<br>- Sterile in package<br>- Luer lock tip<br>- Volume: 1 ml |
| 3 ml syringe | Henry Schein: single use syringe Luer-Lock<br>(Ref: 9004475) | - Pyrogen and latex free<br>- Sterile in package<br>- Luer lock tip<br>- Volume: 3 ml |
| 5 ml and 10 ml syringes | BD Medical:<br>- BD 5 ml syringe<br>(Ref: 309603)<br>- BD 10 ml syringe<br>(Ref: 309604) | - Latex free<br>- Sterile in package<br>- Luer lock tip<br>- Volume: 5 ml and 10 ml |
| 250 ml beaker | Pyrex: Griffin low form beaker | - Glass<br>- Volume: 250 ml |
| Centrifugation tubes | Eppendorf:<br>Eppendorf tubes<br>(D158798Q) | - 5 ml volume<br>- Used for storing used/unused test samples |
| Ceramic column cutter (wafer) | Thermo Scientific: ceramic column cutter<br>(P/N 60201-318) | - Four smooth and four serrated edges<br>- Smooth edges are situated on the rear edges of the tile (with no writing)<br>- Serrated edges are on the front (with writing)<br>- Size: 1 in. by 1 in. (25 mm by 25 mm) |
| Data logger [current input] | Omega: current data logger 20 mA (OM-CP-Process101A-20MA) | Range: -2 to 30 mA<br>(± 0.05% full scale) |
| Gloves | Curad: Nitrile exam gloves | - Non-sterile<br>- Chemical resistant<br>- Nitrile |

Table A.1.2: Other materials and items used in this study (continued)

| | | |
|---|---|---|
| Light Microscope | Bausch & Lomb | - Objective magnification: 0.7X to 3X<br>- Eyepiece magnification: 10x |
| MicroXCT Tomographic X-Ray Microscope | Xradia MicroXCT-400 | - 90 keV micro-focused source<br>- 2K x 2K charge coupled device camera<br>- 90kV and 150 kV X-ray source<br>- 20x magnification (±1.5 μm)<br>- 40x magnification (±1 μm)<br>- Maximum sample diameter: 500 μm<br>- Maximum sample height: 400 mm<br>- Maximum sample weight: 15 kg |
| Stage micrometer scale | OMAX: 0.01 mm microscope calibration slide (X00R1DZWX) | - 1 mm width<br>- 0.01 mm division |
| Surgical tweezers | Miltex Premium: SWISS jeweler style forceps (17-303) | - Antimagnetic and anti-acid<br>- Stainless steel<br>- Narrow, fine<br>- 4-3/4 in. (12.1 cm) long |
| Surgical scissors | Stephens Instruments: Westcott tenotomy stitch scissors (S7-1315) | - Stainless steel<br>- Standard blades<br>- 11 cm long |
| Syringe pump | KdScientific: KDS Legato 100 syringe pump | 1.26 pl/min to 88.404 ml/min (±0.5%) |
| Transducer (Transducer 3) [current output pressure transducer] | Dwyer Instruments (Distributed by Grainger): pressure transducer, 0 - 15 psi, 36 in. lead (626-07-GH-P1-E1-S1) | - 0 to 15 psi (± 0.25% full scale)<br>- 4 to 20 mA DC |
| Wire cutters | - | - 5 in. (13 cm cut length) |

## A.2. Pressure Transducer Voltage-to-Pressure Conversion

***OMEGA Pressure Transducers (Transducers 1 and 2)***

Table A.2.1 shows the calibration data of Transducers 1 and 2 that were provided by Omega, as well as the gradient and intercept calculated from the data points provided using the least squares method. Figure A.2.1. shows the plot of $\Delta P$ against output voltage ($V_o$) for Transducer 1 and the resulting linear equation that was used to convert $V_o$ (V) to $\Delta P$ (mm Hg). Figure A.2.2 shows the $\Delta P$ versus $V_o$ for Transducer 2 and its resulting linear equation found with the least squares method.

Table A.2.1: Transducer 1's and Transducer 2's calibration data provided by Omega [73]. Gradient and intercept values were calculated using the least squares method

| Transducer 1 | | | | Transducer 2 | | | |
|---|---|---|---|---|---|---|---|
| Output Voltage, $V_o$ | | Input Pressure, $\Delta P$ | | Output Voltage, $V_o$ | | Input Pressure, $\Delta P$ | |
| V | mV | psi | mm Hg | V | mV | psi | mm Hg |
| 0.000024 | 0.02 | 0 | 0.0 | -0.000023 | -0.02 | 0 | 0.0 |
| 0.050049 | 50.05 | 1.25 | 64.6 | 0.049977 | 49.98 | 1.25 | 64.6 |
| 0.100084 | 100.08 | 2.5 | 129.3 | 0.099981 | 99.98 | 2.5 | 129.3 |
| 0.050052 | 50.05 | 1.25 | 64.6 | 0.049974 | 49.97 | 1.25 | 64.6 |
| 0.000025 | 0.03 | 0 | 0.0 | -0.000025 | -0.03 | 0 | 0.0 |
| Gradient: 24.985 | | Intercept: -0.0006 | | Gradient: 24.999 | | Intercept: 0.0006 | |

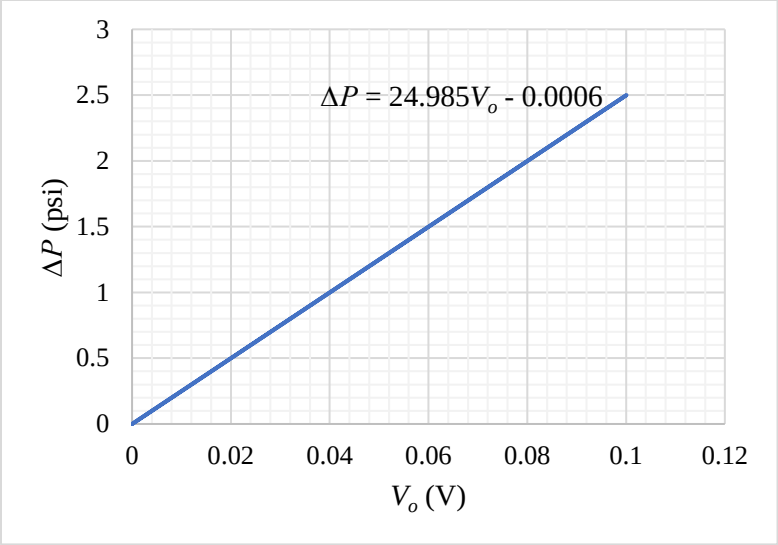


Fig. A.2.1: Plot of pressure, $\Delta P$, against output voltage, $V_o$, for Transducer 1

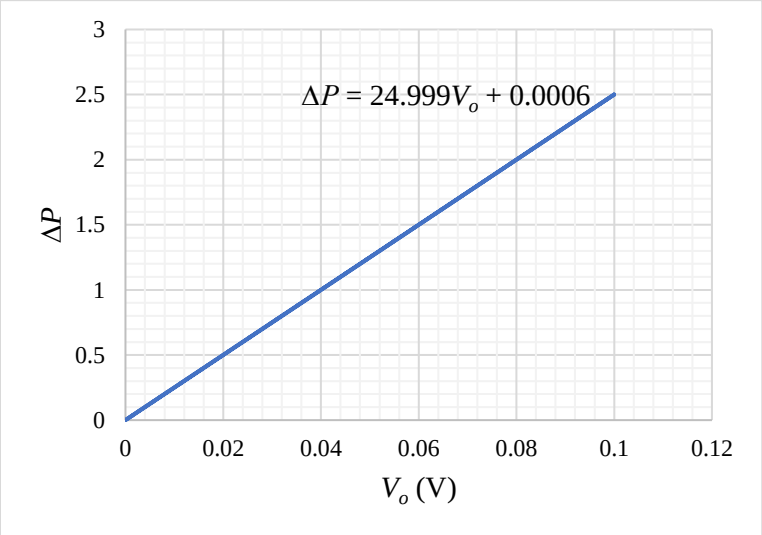


Fig. A.2.2: Plot of pressure, $\Delta P$, against output voltage, $V_o$, for Transducer 2

***Dwyer Pressure Transducer (Transducer 3)***

Unlike Transducers 1 and 2, there was no calibration sheet for Transducer 3. Therefore, the conversion from current to pressure was done using the transducer's specified minimum/maximum pressures (0 psi/15 psi), and minimum/maximum input current (4 mA/20 mA). Table A.2.3 and

Fig. A.2.3 show the calibration data and the plot of $\Delta P$ versus $I$ for Transducer 3, respectively.

Table A.2.2: Transducer 3's calibration data. Gradient and intercept values were calculated using the least squares method

| Transducer 3 | | |
|---|---|---|
| Output Current, $I$ | Input Pressure, $\Delta P$ | |
| mA | psi | mm Hg |
| 4.0 | 0.0 | 0.0 |
| 20.0 | 15.0 | 775.7 |
| Gradient: 0.9375 | Intercept: | -3.750 |

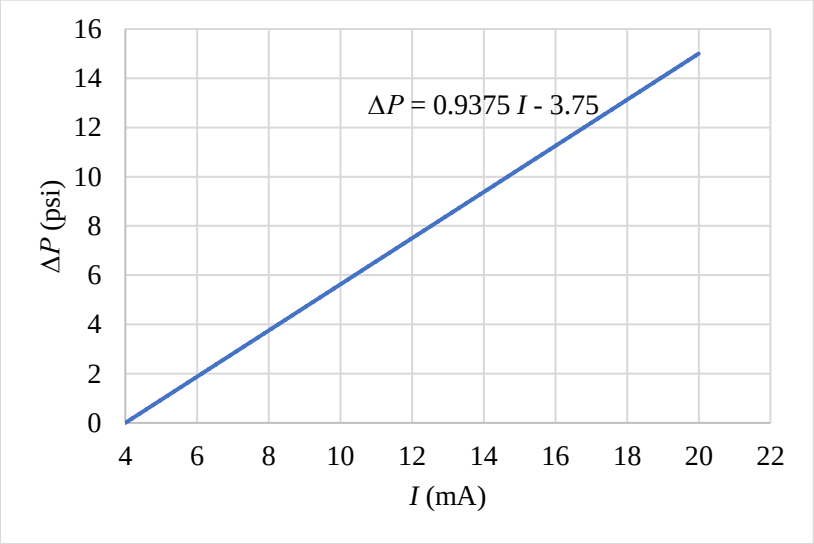


Fig. A.2.3: $\Delta P$ versus output current for Transducer 3 and its resulting linear equation found using the least squares method

***Excel Formula to Simplify Volt-to-Pressure and Current-to-Pressure Conversion (Sticky Notes)***

Figure A.2.4 shows the three Excel tables that are available in Sticky Notes on the computer Desktop. These tables are to allow easy conversion of the pressure data units from V to mm Hg for Transducers 1 and 2, and Amp to mm Hg for Transducer 3. These tables are copied and pasted

into the Excel spreadsheet exported from the Omega data logger. Instructions for using these tables are given in App. B.1 (Stage 4).

**Transducer 1**

| | | |
|---|---|---|
| baseline: | =AVERAGE(F8:F98) | |
| | | |
| hour | raw mm Hg | sample mm Hg |
| 0 | =(24.985*C8-0.0006)*51.715 | =F8 - $F$5 |
| =E8+10/3600 | =(24.985*C9-0.0006)*51.715 | =F9 - $F$5 |

**Transducer 2**

| | | |
|---|---|---|
| baseline: | =AVERAGE(F8:F98) | |
| | | |
| hour | raw mm Hg | sample mm Hg |
| 0 | =(24.999*C8+0.0006)*51.715 | =F8 - $F$5 |
| =E8+10/3600 | =(24.999*C9+0.0006)*51.715 | =F9 - $F$5 |

**Transducer 3**

| | | |
|---|---|---|
| baseline: | =AVERAGE(F8:F98) | |
| | | |
| hour | raw mm Hg | sample mm Hg |
| 0 | =(0.9375*C8-3.75)*51.715 | =F8 - $F$5 |
| =E8+10/3600 | =(0.9375*C9-3.75)*51.715 | =F9 - $F$5 |

Baseline:
Calculates the average $\Delta P$ between 0 to 15 minutes of data logging. The 0 - 15 minute period is when there is no sample in the test section (Baseline $\Delta P$).

Sample mm Hg:
Subtracts the average baseline $\Delta P$ from the measured $\Delta P$ (mm Hg)

Fig. A.2.4: Excel tables available in Sticky Notes on Desktop for conversion from V or Amp to mm Hg

## A.3. APC Backup Power Supply Unit Specifications

The following lists the specifications of the APC UPS XS 1500 unit connected to the setups [74].

Make/Model: APC UPS SX 1500 (BX1500G)

***Output***

Output Power Capacity: 865 Watts/1.5 kVA

Nominal Output Voltage: 120 V

Output Frequency: 50/60 Hz ± 3 Hz

Waveform Type: Stepped approximation to a sine wave

Output Connections: 5 x NEMA 5-15 (UPS and surge)

5 x NEMA 5-15 (battery backup)

Transfer Time: 8 ms typical (12 ms maximum)

***Input***

Nominal Input Voltage: 120V

Input Frequency: 50/60 Hz ± 3 Hz (auto sensing)

Input Connections: NEMA 5-15P

Cord Length: 6 ft. (1.83 m)

Number of Power Cords: 1

***Batteries & Runtime***

Battery Type: Maintenance free sealed lead-acid battery with suspended electrolyte

Included Battery Modules: 1

Typical Recharge Time: 16 hours

Replacement Battery: APCRBC124

Expected Battery Life: 3 - 5 years

RBC Quantity: 1

Run time: 2 hours and 8 mins at minimum load (50 Watts)

13 minutes at half load (432.5 Watts)

4 minutes at full load (865 Watts)

***Communications & Management***

Interface Port(s): USB

Control Panel: Multi-function LCD status and control console

***Surge Protection and Filtering***

Surge energy rating: 354 Joules

Data Line Protection: RJ45 10/100 Base-T Ethernet protection, Cable modem/Video protection

Filtering: Full time multi-pole noise filtering (5% IEEE surge let-through; zero clamping response time; meets UL 1449)

***Physical Description***

Maximum Height: 11.85 in. (301 mm, 30.1 cm)

Maximum Width: 4.4 in. (112 mm, 11.2 cm)

Maximum Depth: 15.04 in. (382 mm, 38.2 cm)

Net Weight: 23.76 lb (10.8 kg)

Color: Black

***Environmental***

Operating Environment: 32 - 104 °F (0 - 40 °C)

Operating Relative Humidity: 0 - 95%

Operating Elevation: 0 - 30000 ft (0 - 9000 m)

Storage Temperature: -15 to 45 °C

Storage Relative Humidity: 0 - 95%

Storage Elevation: 0 - 50000 ft. (0 - 15000 m)

## A.4. Temperature Controlled Test Section (Incubator) Specifications

The following lists the specifications of the incubator used to maintain the environment around the test sample [75].

Make/Model: Miller Manufacturing Company 9300 White Digital Still Air Incubator

Material: Styrofoam

ASIN: B00KKRDQAE

Color: White

Item Dimensions: 8 x 17.75 x 17.75 in.

Manufacture Part Number: 9300

Model Number: 9300

Shipping Weight: 3.1 lb

Included Components: Heating element

Digital control board (self-regulating, adjustable)

The LCD display with LED light (temperature and humidity readings)

Built-in digital hydrometer and moisture channels

## Appendix B: Sample Preparation, Flow Trial and Cleaning Procedures

There are four main stages to performing the flow trials.

Stage 0: Turning on the pumps

Stage 1: Measuring baseline $\Delta P$ (time span: ~ 15 minutes)

*Baseline $\Delta P$ = $\Delta P$ caused by flow resistance such as elevation, friction in the tubes, and sudden changes in tube cross-sectional area at control flow rate. For VSD tube trials, the $\Delta P$ caused by the 24G dispensing tip is assumed negligible (<0.1 mm Hg).*

Stage 2: Priming the pumps (time span: ~ 15 minutes)

*Pumps primed at a high flow rate of 10 µl/min to remove any remaining air bubbles in the flow lines from the pump to the sample tube exit.*

Stage 3: Measuring the $\Delta P$ caused by the sample (time span: chosen flow trial period)

*$\Delta P$ measured at control flow rate with sample attached to tube end at the test section.*

Stage 4: Retrieving, converting and saving collected data

*Retrieve, convert (V or Amp to mm Hg), and save the data measured and collected by the pumps and the data loggers.*

### B.1. General Testing and Data Collection Procedure

***Stage 0: Turning on the pumps and sample setup***

1. Fill the 500 ml glass bottle (reservoir) with the desired fluid [e.g., DI water, 0.04% sodium azide ($NaN_3$) solution, or balanced salt solution (BSS)] and replace the bottle cap. Ensure that the cap is screwed on tight and that the end of the PEEK tube is fully submerged in the fluid.

2. Open the PneuWave pump program on the computer by clicking on the icon shown in Fig. B.1.1. (Caution: Do NOT close the PneuWave program while trials are being run.)

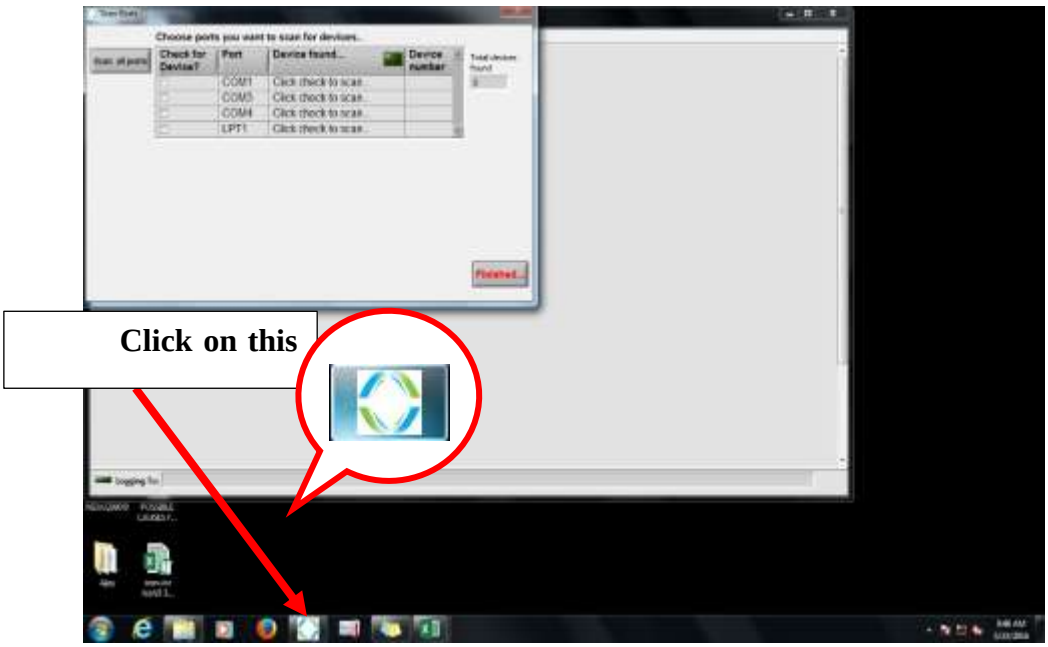


Fig. B.1.1: Location of Pneuwave program icon on desktop

3. Flip the switches on the backs of Pumps 1 and 2 to turn the pumps on.
4. On the computer, select <COM3> and <COM4> in the Pneuwave window (represents Pumps 1 and 2, respectively). Then, click <Finished…> as shown in Fig. B.1.2.
5. On the top graph (Device Number: 3), for the 'Control Mode', select <Flow> as shown in Fig. B.1.3. This will set the pump in Setup 1 to maintain a specific control flow rate.
6. In the 'Target' space, type in the desired control flow rate value and click <Set> (Fig. B.1.4). For example, if the value '2.5' is typed into the 'Target' space, the pump will be set at a fixed flow rate of 2.5 µl/min.
7. Repeat steps 5 and 6 for the bottom graph (Device Number: 4).

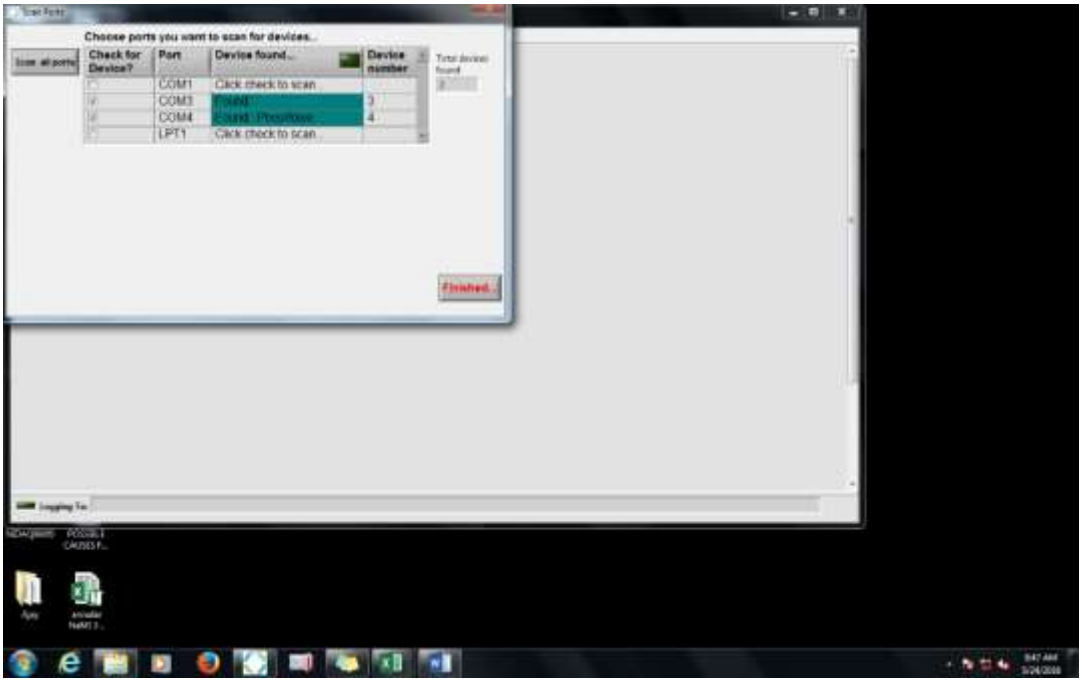


Fig. B.1.2: Selecting pump ports

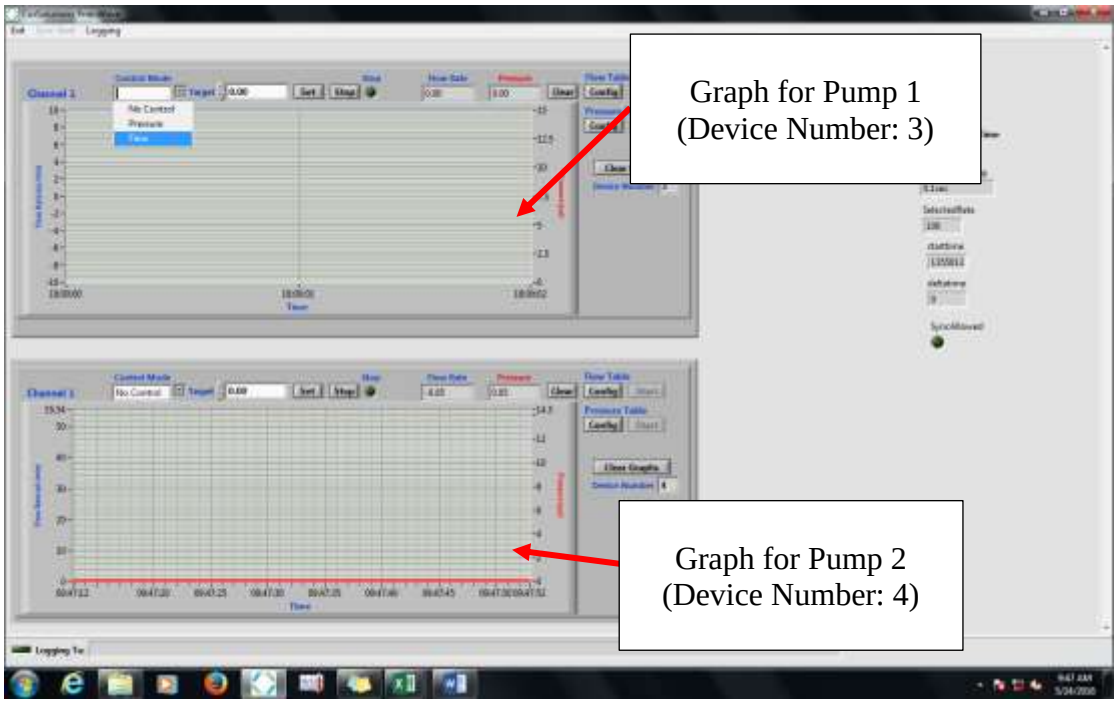


Fig. B.1.3: Selecting <Flow> from the drop down bar to set pump to flow rate control

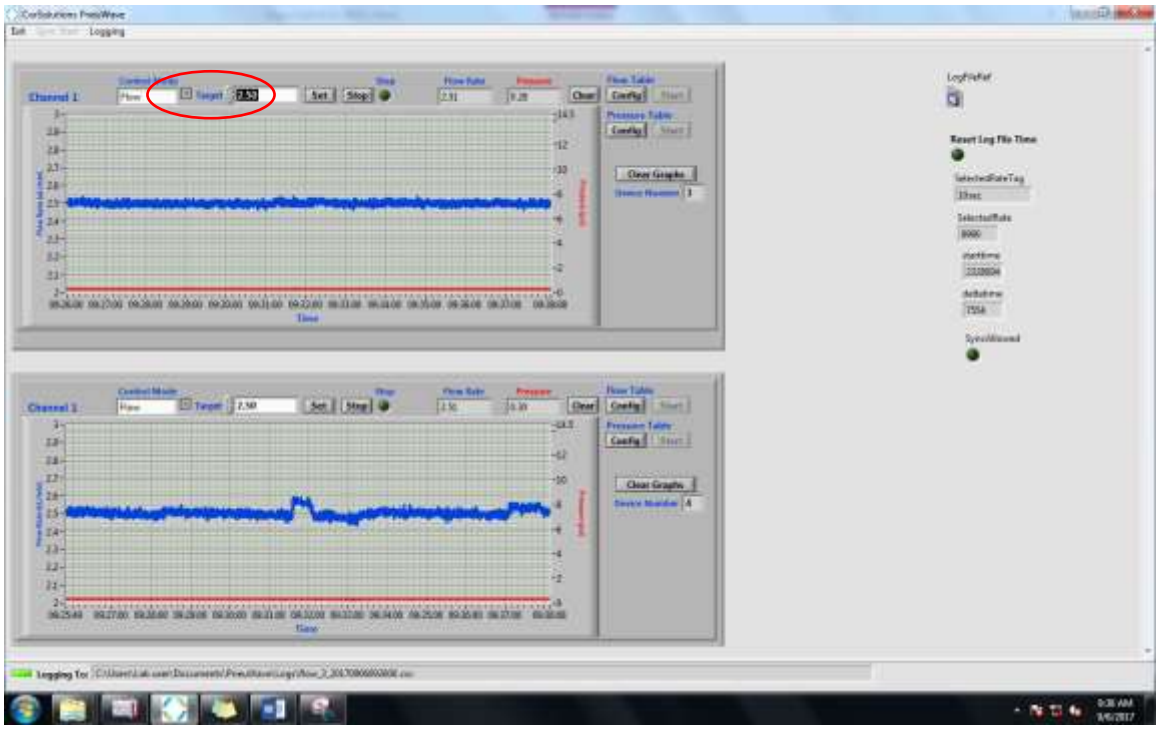

Fig. B.1.4: Setting Pump 1 flow rate to maintain at 2.5 µl/min

***Stage 1: Measuring Baseline ΔP***

1. Set the pump to the desired control flow rate (2.5 µl/min).
2. To begin data collection in **Setup 1**, ensure that the data collection cable is plugged into the Omega data logger as shown in Fig. B.1.5.
3. Check the tubes and connections between the pump and the test section to ensure that there are no visible air bubbles. Remove any trapped air bubbles by tapping the tubes and setting the pump to a high flow rate of 10 µl/min for ~15 minutes.
4. Fill the 5 middle lanes of the collection trough with DI water and place the tube-to-sample luer lock end submerged in the DI water as shown in Fig. B.1.6.
5. To select the pump's logging rate (frequency: 0.1 Hz), select <Rate>, then select <10 sec>, as shown in Fig. B.1.7. *It is important to choose 10 sec in order to reduce the data file size.*

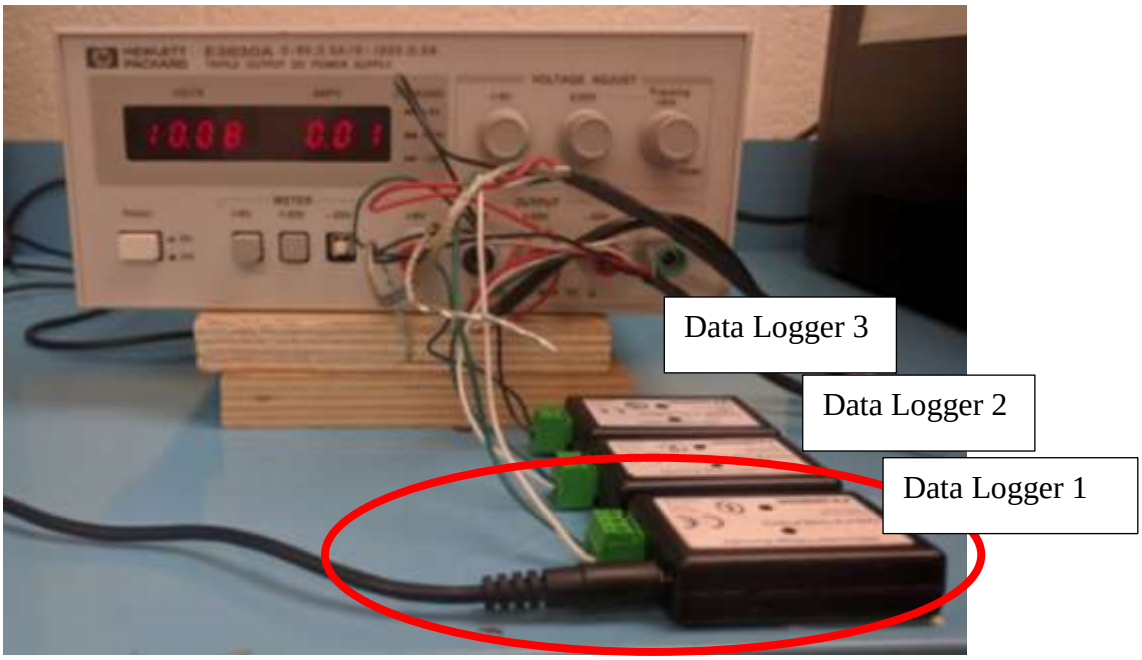


Fig. B.1.5: Data collection cable plugged into Omega data logger 1

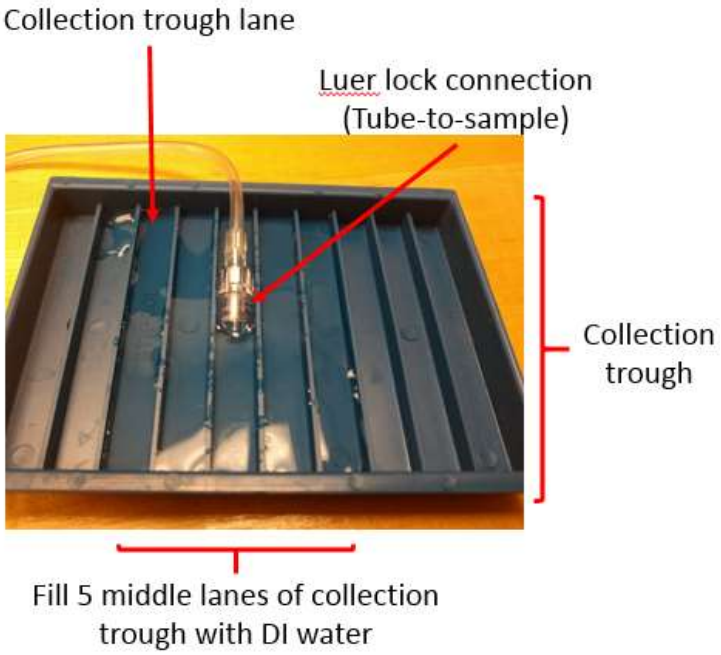


Fig. B.1.6: Submerge tube-to-sample end in DI water in collection trough

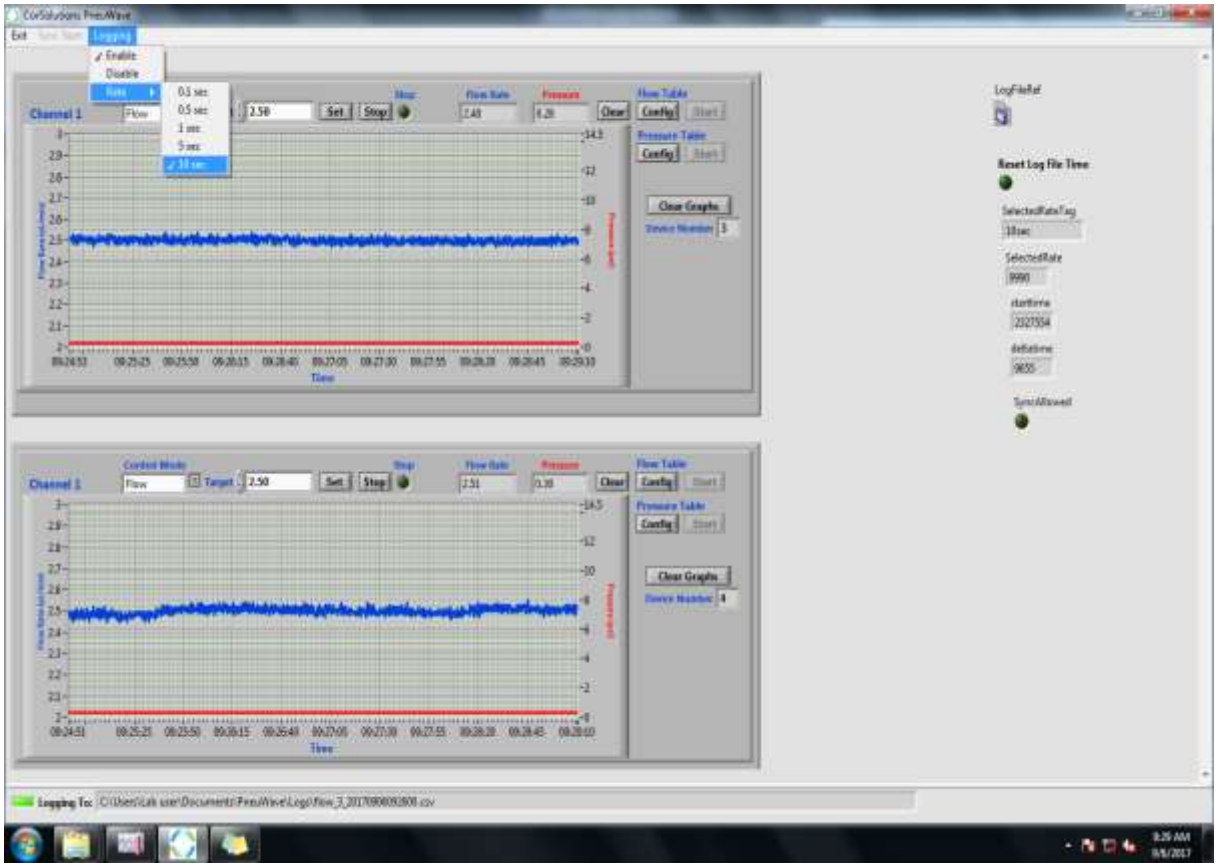


Fig. B.1.7: Setting pump data logging rate (10-second interval)

6. To log the pump data, click on the <Logging> tab, select <Enable> as shown in Fig. B.1.8.
7. Open the Omega transducer program on the computer as shown in Fig. B.1.9.
8. To begin data logging, click on the <Custom Start> icon in the top left corner of the window as shown in Fig. B.1.10.
9. A window will pop up as shown in Fig. B.1.11. Select <10 seconds> from the drop down for <Reading interval:> as shown in Fig. B.1.11, then select <Start>.
10. Record the date and time that data logging is started on the experiment log sheet (Fig. D.1.1) in the “Trial Date” and “Time-Baseline” spaces, respectively.
11. Close the Omega program. The Omega logger will still continue logging, even if the program is closed.

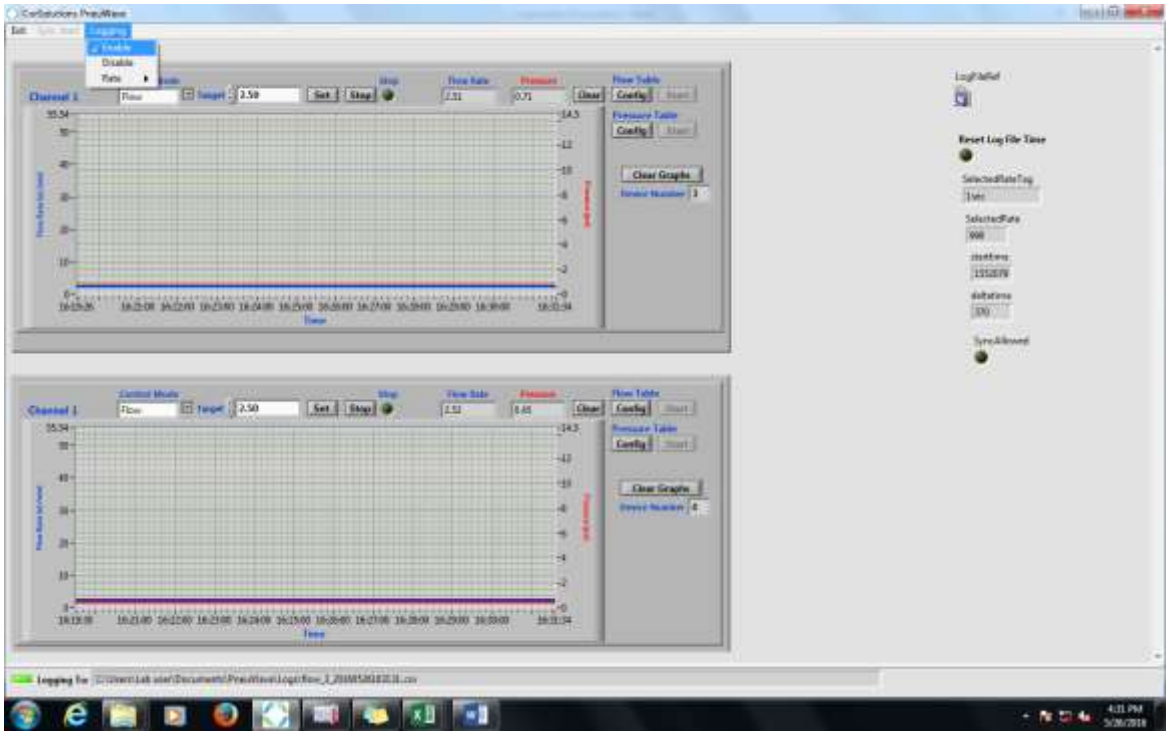

Fig. B.1.8: Enabling pump data logging for Pump 1

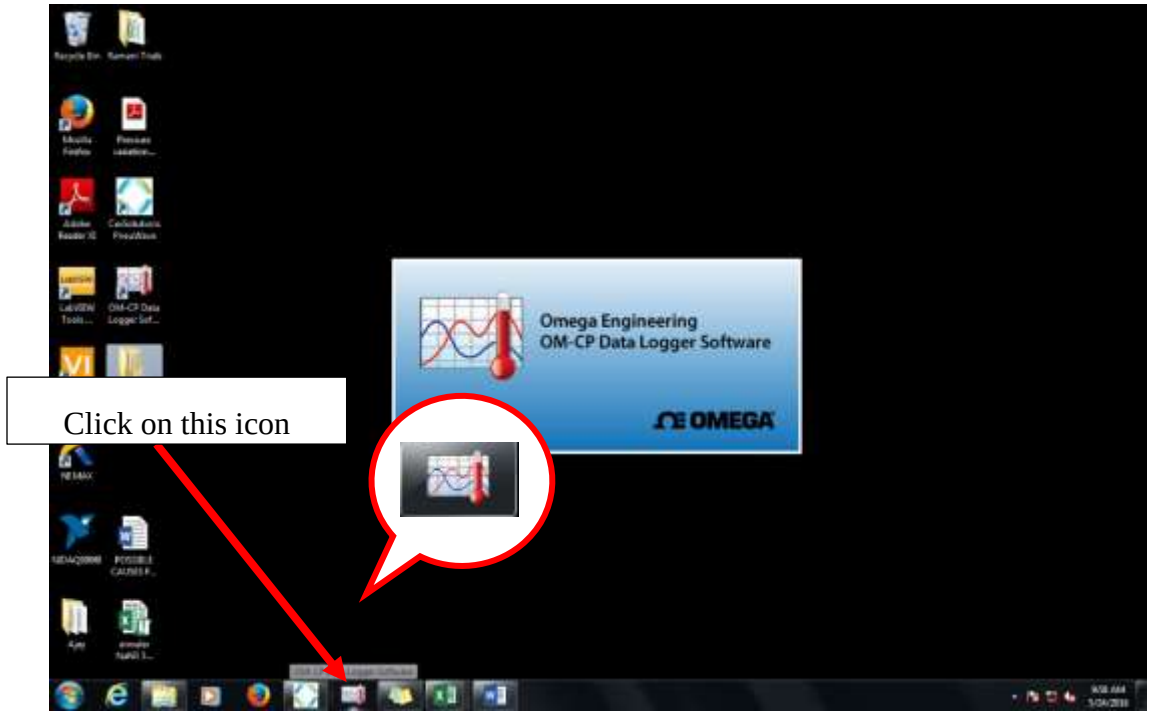


Fig. B.1.9: Opening the Omega transducer program

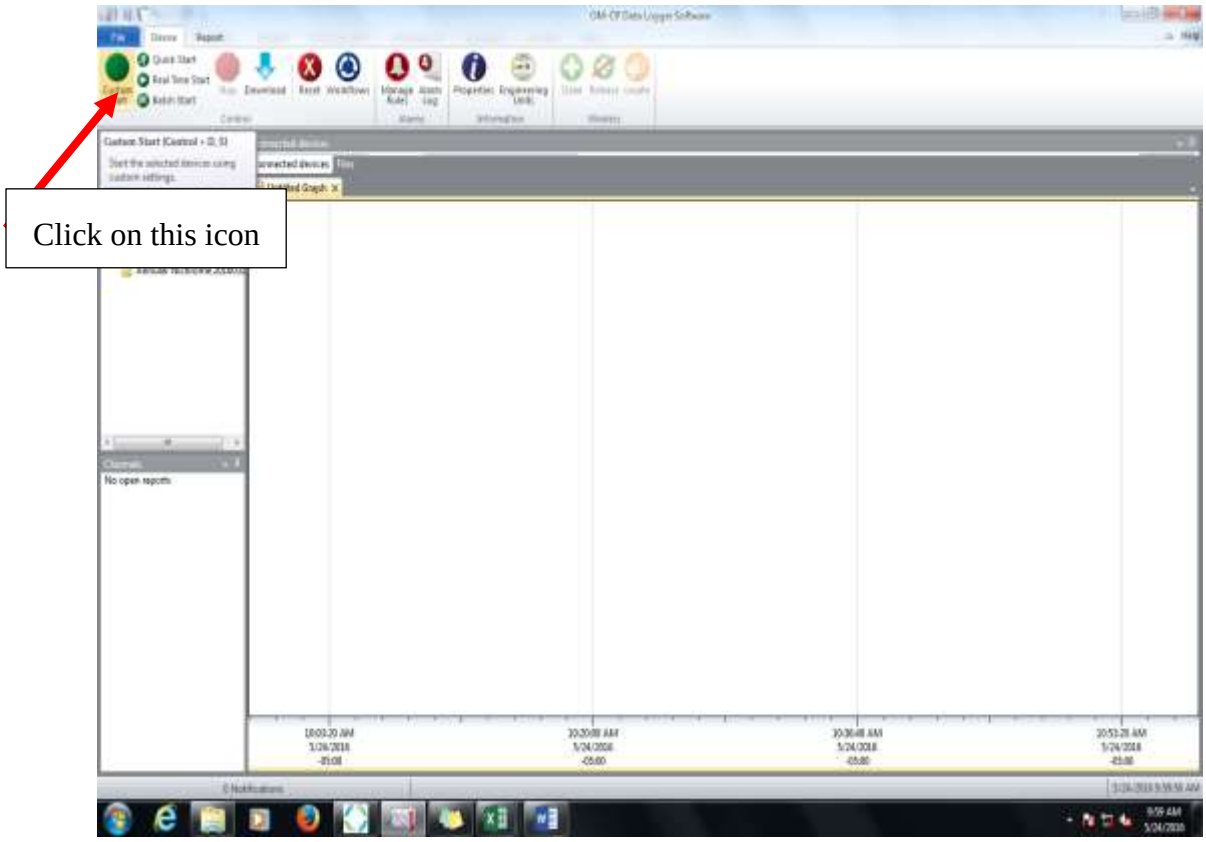


Fig. B.1.10: Starting pressure transducer data logging

Fig. B.1.11: Selecting pressure transducer data logging rate (10 seconds)

12. Begin data collection in **Setup 2** by first ensuring that the data collection cable is plugged into the Omega data logger as shown in Fig. B.1.12.
13. Repeat steps 1 - 11 of Stage 1 in Setup 2, recording the experiment details in the next section of the experiment log (App. D.1).

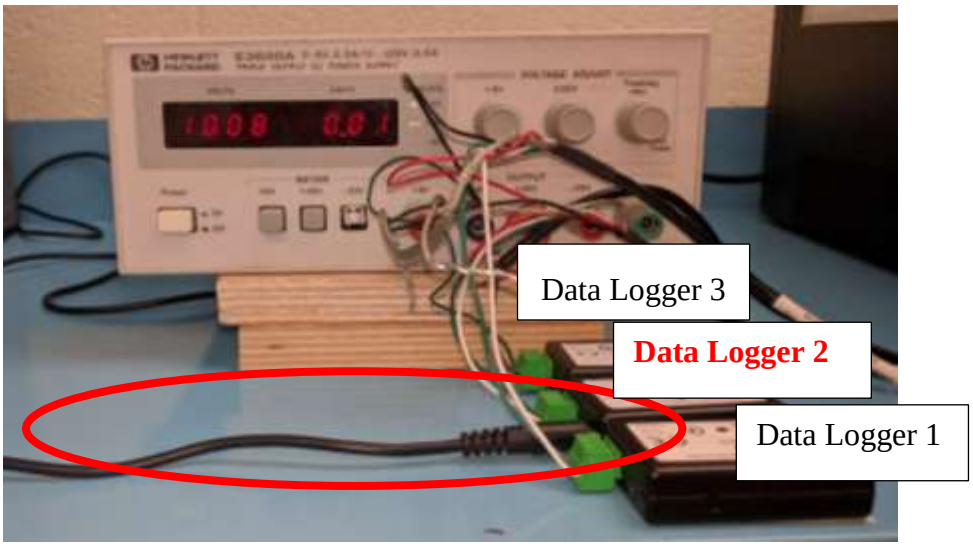


Fig. B.1.12: Data collection cable plugged into Omega data logger 2

***Stage 2: Priming the Pumps***

The Stage 2 procedures for connecting the samples are the same for both Setups 1 and 2.

1. After ~15 minutes of collecting baseline pressures at 2.5 µl/min, remove the lid of the incubator.
2. Flush the sample tip with DI water using a syringe to remove any air trapped in the sample.
3. Fill the cannula with DI water as well as the luer lock end of the tube that is to be connected to the sample. Make sure that there are no air bubbles trapped between the cannula and the luer lock end.
4. Fill the center five lanes of the blue collection trough with DI water and place the end tip of the prepared sample in the center lane as shown in Fig. B.1.13.

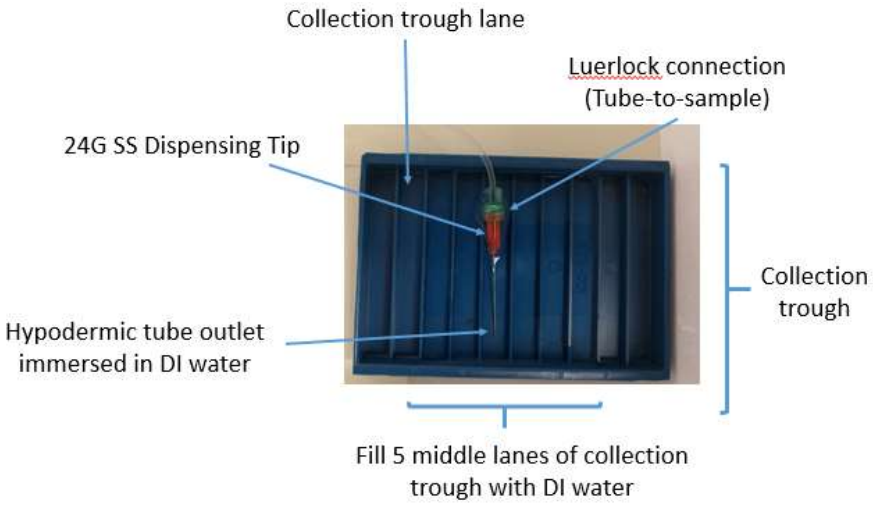


Fig. B.1.13: Positioning of sample end tip in collection trough

5. Place the incubator lid back on the incubator.
6. If the incubator is to be set to a temperature higher than room temperature (i.e., body temperature, 37°C/98.6°F), connect the incubator to a power outlet. The incubator will automatically turn on.
7. Set the incubator temperature to the desired temperature by holding the 'SET' button for 3 seconds. Then, adjust to the desired temperature by pressing either the 'UP' or 'DOWN' button.
8. Increase the flow rate for both Pumps 1 and 2 to 10 µl/min.
9. Record the time that the flow rate was set to 10 µl/min in the experiment log on the "Time-Prime/AGV" space for both pumps (Fig. D.1.1).
10. Record the set flow rate in the experiment log on the 'Flow rate: *Prime*' space for both pumps (Fig. D.1.1).

***Stage 3: Measuring ΔP Caused by Sample***

1. After ~15 minutes of priming the pumps at 10 µl/min, decrease the flow rate for both Pumps

1 and 2 back to the control flow rate (2.5 µl/min).

2. Record the time that the flow rate was set back to the control flow rate in the experiment log on the "Time-Trial" space for both pumps (Fig. D.1.1).
3. Record the set flow rate in the experiment log on the 'Flow rate: *Control*' space for both pumps (Fig. D.1.1).
4. Fill in the remaining spaces in the experiment log sheet that had not been completed according to the settings and conditions of the trial (refer to App. D.1 for further instructions on how to complete the remaining spaces).

**NOTE: DO NOT** close the pump program while running the experimental trials because this will disable pump logging. Pump flow and pressure data will no longer be logged by the pump.

***Stage 4: Retrieving, Processing and Saving Data Collected***

1. **To RETRIEVE** the pressure data from Data Logger 1 in **Setup 1,** ensure that the data collection cable is plugged into Data Logger 1 as shown in Fig. B.1.5.
2. Open the Omega transducer program on the computer screen as shown in Fig. B.1.9.
3. In the program window, click on the <Stop> icon to stop data logging as shown in Fig. B.1.14.
4. In the experiment log sheet, record the time and date on which data logging was stopped. Record the time and date in the "Time-End" and "End Date" spaces, respectively.
5. To retrieve the data, click on the <Download> icon as shown in Fig. B.1.15.
6. Rename the report on the small pop-up window in the "Untitled Report" space that is shown in Fig. B.1.16. It is suggested that the title format include: "ExperimentType"-"Date(DDMMYY)"-"Time(24hour)"-"Sample #"-"Setup #"-"Trial #" (e.g., "Nylon-BGI-26052016-1400-Smp1-Stp2-Tr4").

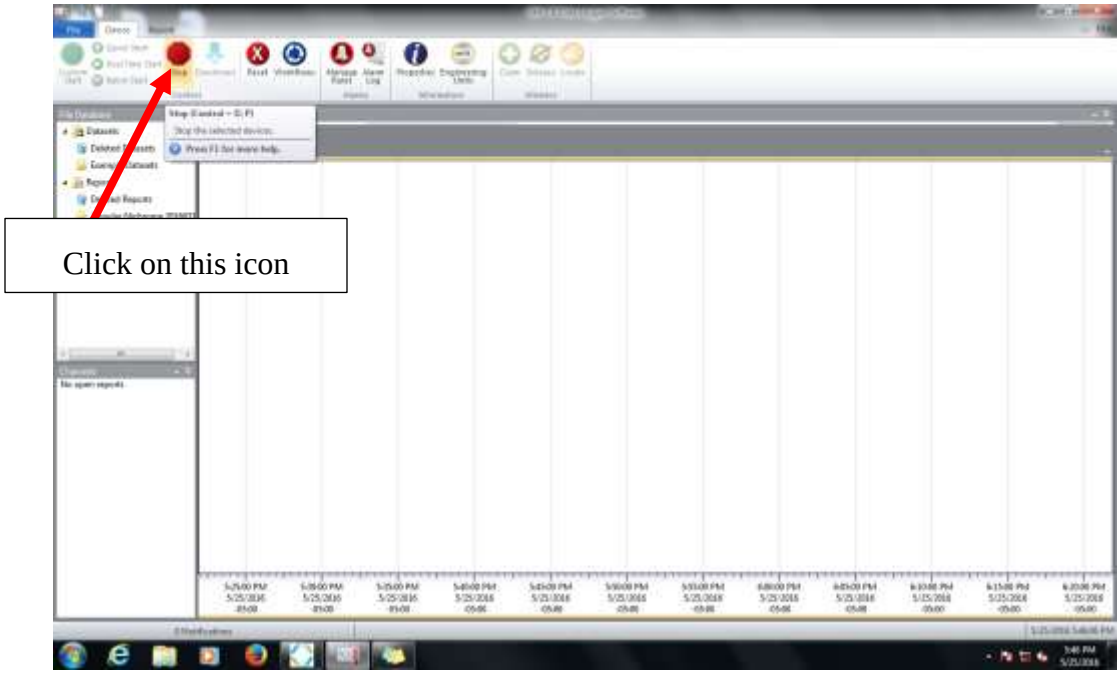


Fig. B.1.14: Stopping the transducer from continuous data logging

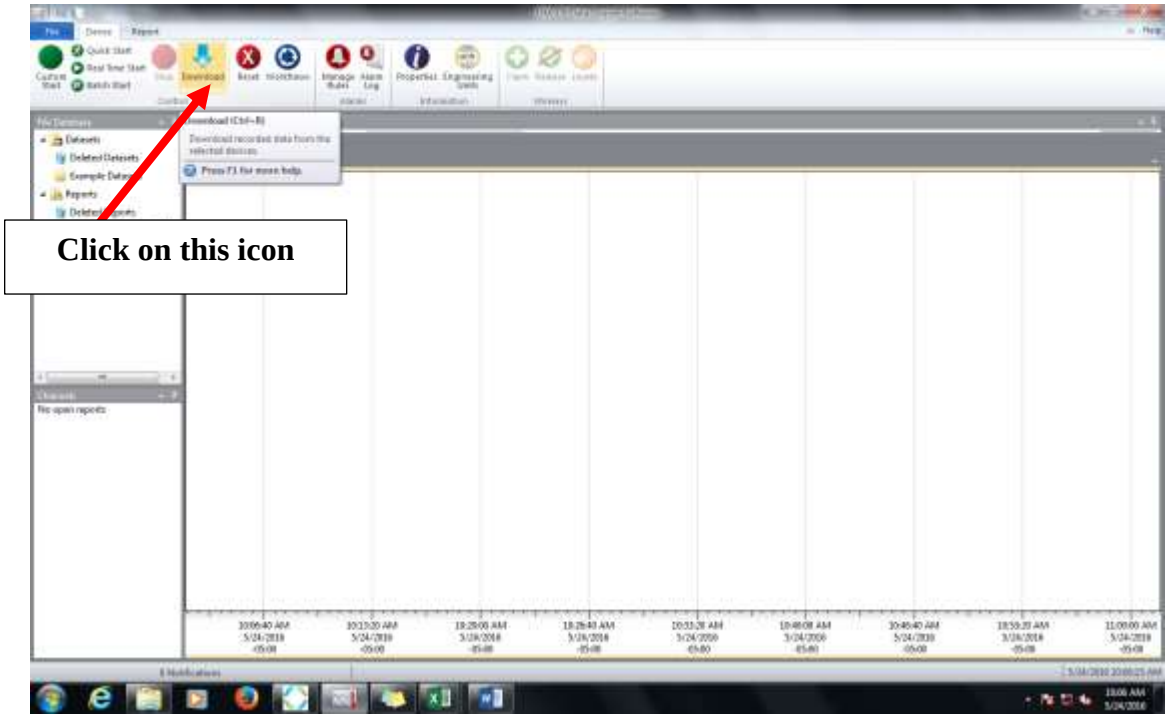


Fig. B.1.15: Downloading collected data from data logger

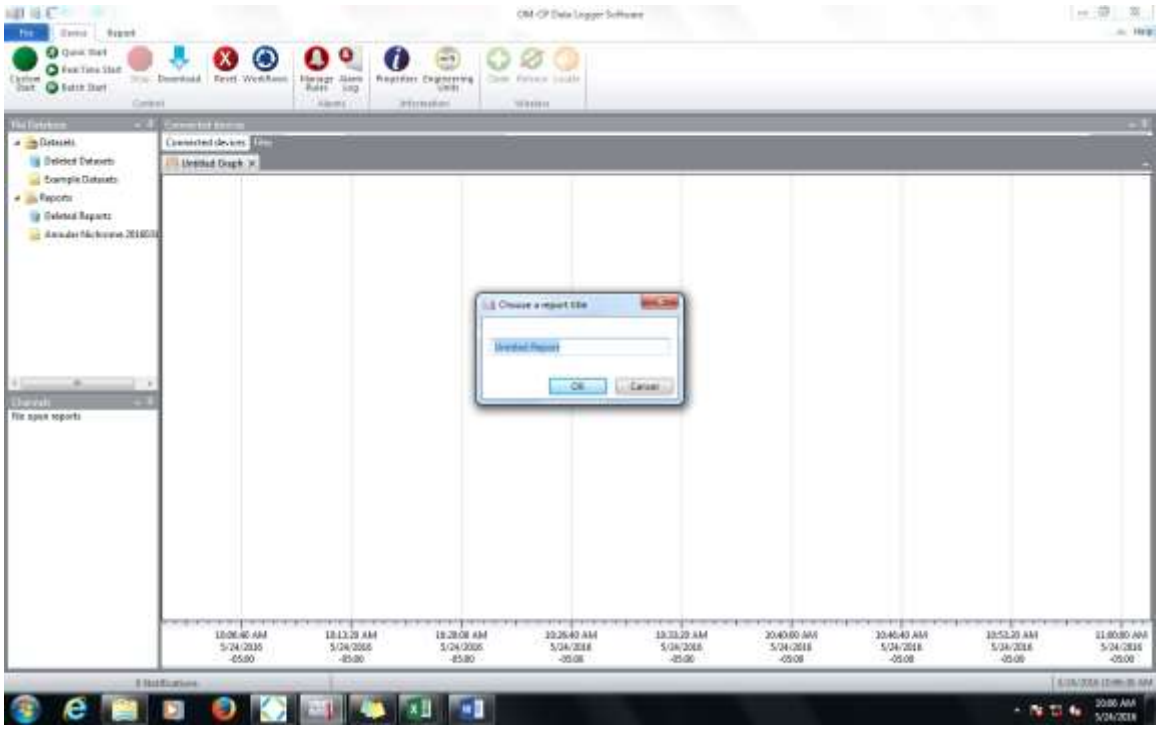

Fig. B.1.16: Naming the report file

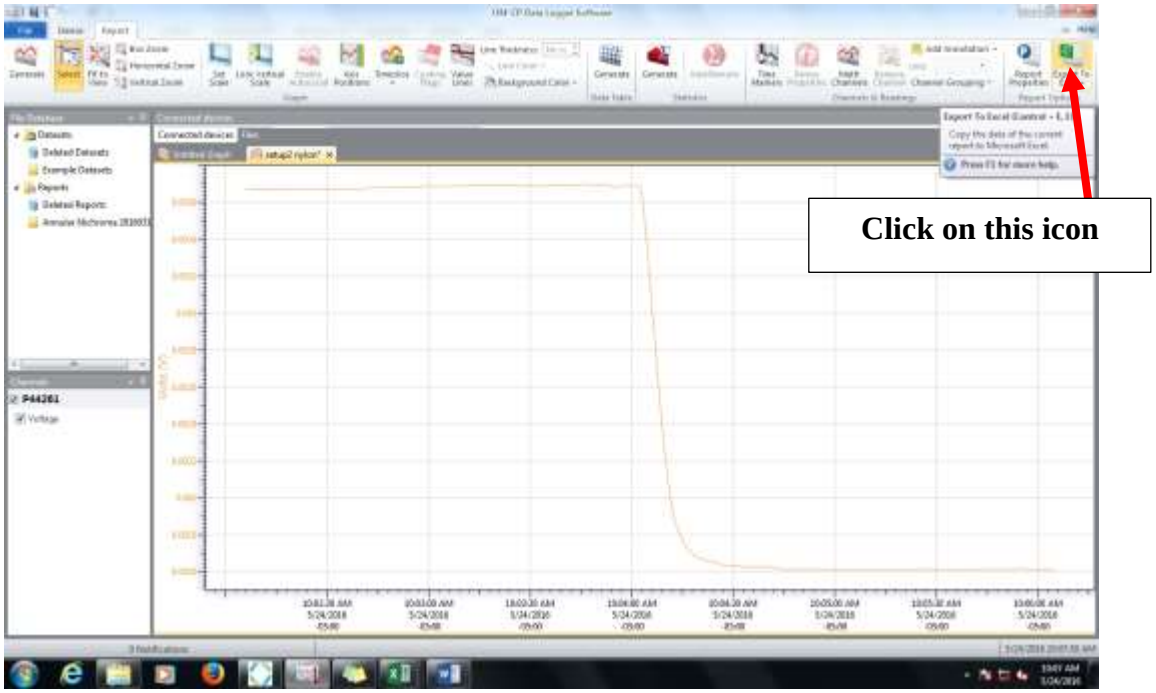


Fig. B.1.17: Exporting the file into an Excel spreadsheet

7. A plot will appear as shown in Fig. B.1.17. To export the data into Excel, click on the <Export to Excel> icon in the top right of the window as shown in Fig. B.1.17.
8. A window will pop up asking “Would you like a chart to be displayed?” as shown in Fig. B.1.18. Select <No>.
9. An Excel spreadsheet will automatically open as shown in Fig. B.1.19.

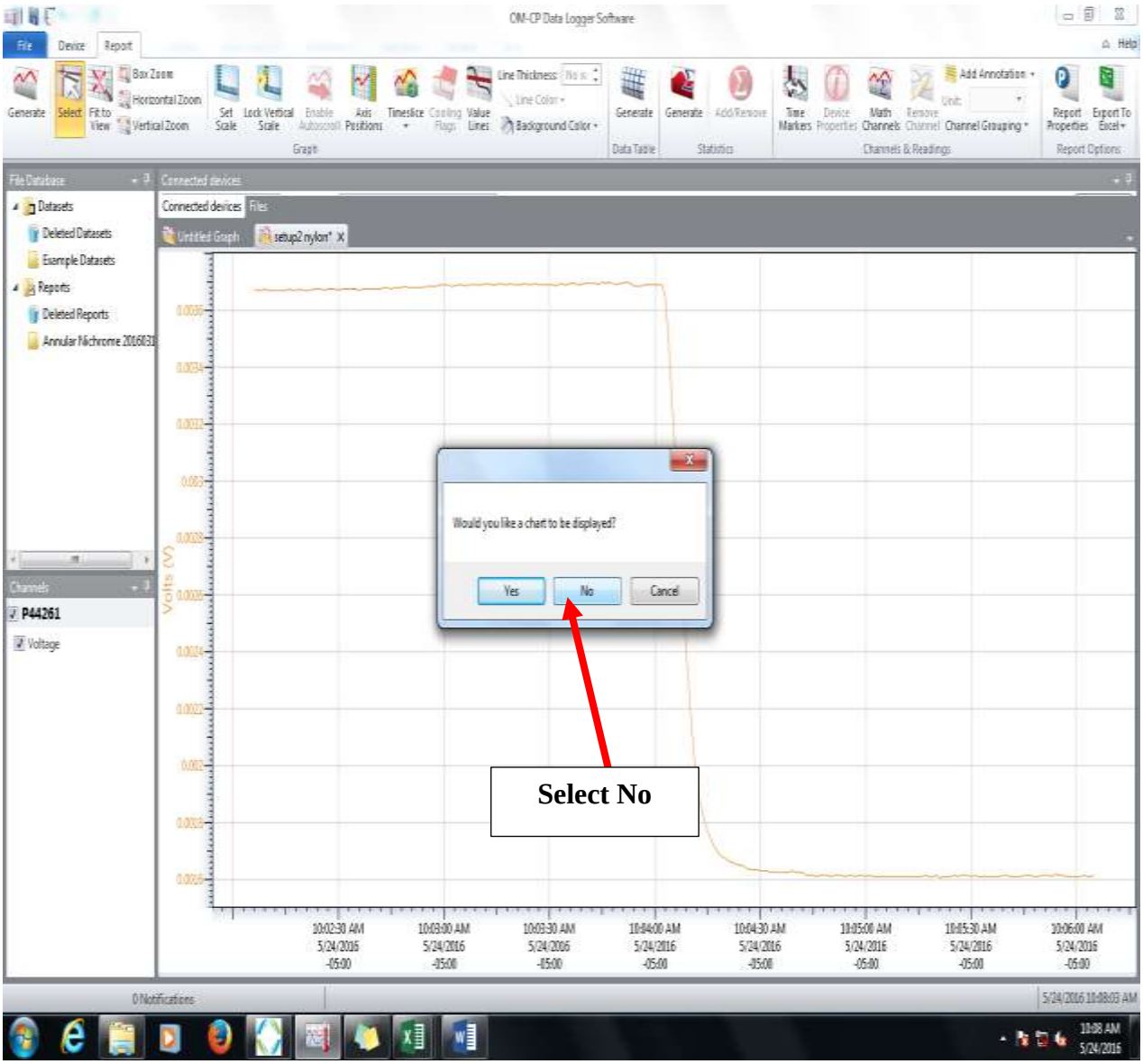


Fig. B.1.18: Selecting <No> when asked if a chart is to be displayed

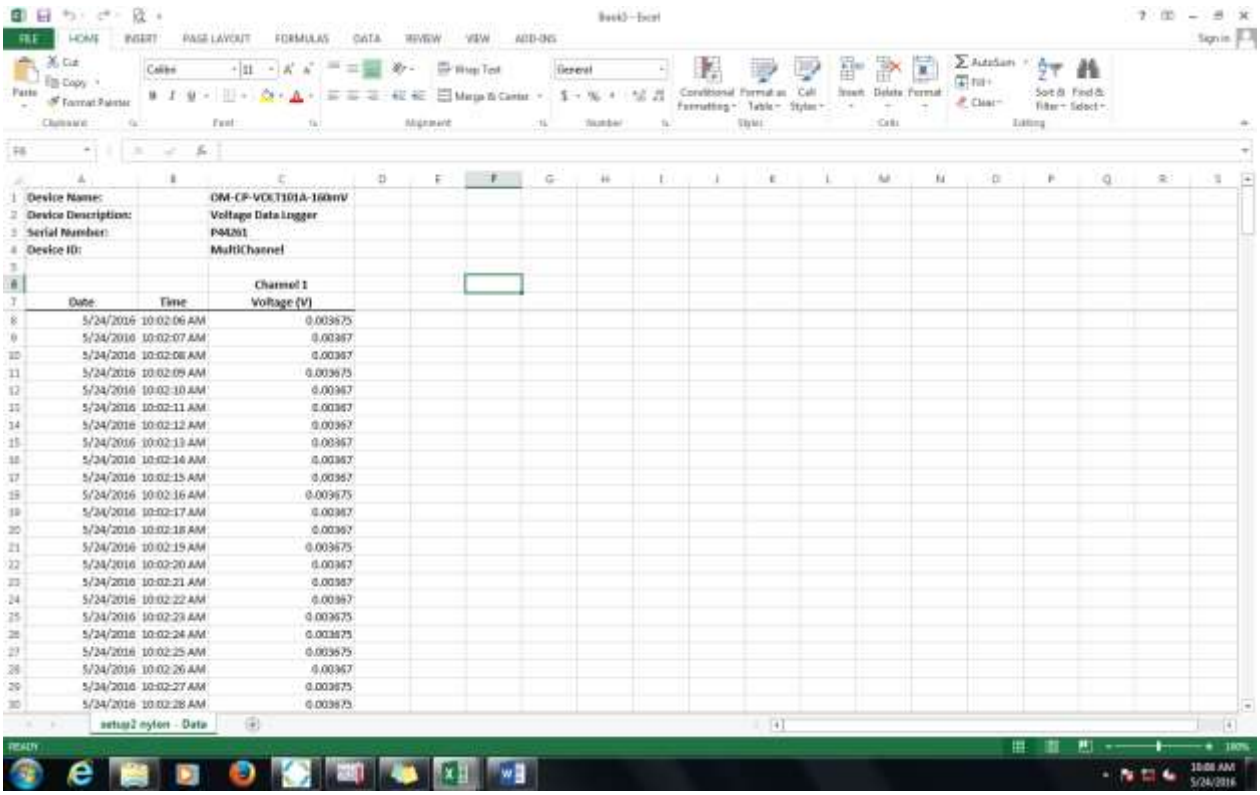

| | | |
|---|---|---|
| Device Name: | | OM-CP-VOLT101A-160mV |
| Device Description: | | Voltage Data Logger |
| Serial Number: | | P44261 |
| Device ID: | | MultiChannel |
| | | Channel 1 |
| Date | Time | Voltage (V) |
| 5/24/2016 | 10:02:06 AM | 0.003675 |
| 5/24/2016 | 10:02:07 AM | 0.00367 |
| 5/24/2016 | 10:02:08 AM | 0.00367 |
| 5/24/2016 | 10:02:09 AM | 0.003675 |
| 5/24/2016 | 10:02:10 AM | 0.00367 |
| 5/24/2016 | 10:02:11 AM | 0.00367 |
| 5/24/2016 | 10:02:12 AM | 0.00367 |
| 5/24/2016 | 10:02:13 AM | 0.00367 |
| 5/24/2016 | 10:02:14 AM | 0.00367 |
| 5/24/2016 | 10:02:15 AM | 0.00367 |
| 5/24/2016 | 10:02:16 AM | 0.003675 |
| 5/24/2016 | 10:02:17 AM | 0.00367 |
| 5/24/2016 | 10:02:18 AM | 0.00367 |
| 5/24/2016 | 10:02:19 AM | 0.003675 |
| 5/24/2016 | 10:02:20 AM | 0.00367 |
| 5/24/2016 | 10:02:21 AM | 0.00367 |
| 5/24/2016 | 10:02:22 AM | 0.00367 |
| 5/24/2016 | 10:02:23 AM | 0.003675 |
| 5/24/2016 | 10:02:24 AM | 0.003675 |
| 5/24/2016 | 10:02:25 AM | 0.003675 |
| 5/24/2016 | 10:02:26 AM | 0.00367 |
| 5/24/2016 | 10:02:27 AM | 0.003675 |
| 5/24/2016 | 10:02:28 AM | 0.003675 |

Fig. B.1.19: Excel spreadsheet that opens

The next steps are to **CONVERT** the voltage (V) or amperage (Amp) data to pressure (mm Hg) and to **FILTER** the baseline $\Delta P$ (due to residual flow resistance) from the desired $\Delta P$ data ($\Delta P$ at sample section).

10. Go to Sticky Notes by clicking on the icon shown in Fig. B.1.20.
11. Highlight the table labelled “Transducer 1” in the Sticky Notes as shown in Fig. B.1.21. Then copy the table by holding <Ctrl> and <C> on the keyboard. (The formulas in the tables are based on the voltage- or amperage-to-pressure conversion in App. A.2.)
12. In the Excel spreadsheet, select cell E4 and paste the copied table in that cell by holding <Ctrl> and <V>. The table will be copied in the Excel spreadsheet as shown in Fig. B.1.22. (*Make certain that the table is pasted in cells E5 to G9 as shown in Fig. B.1.22*).

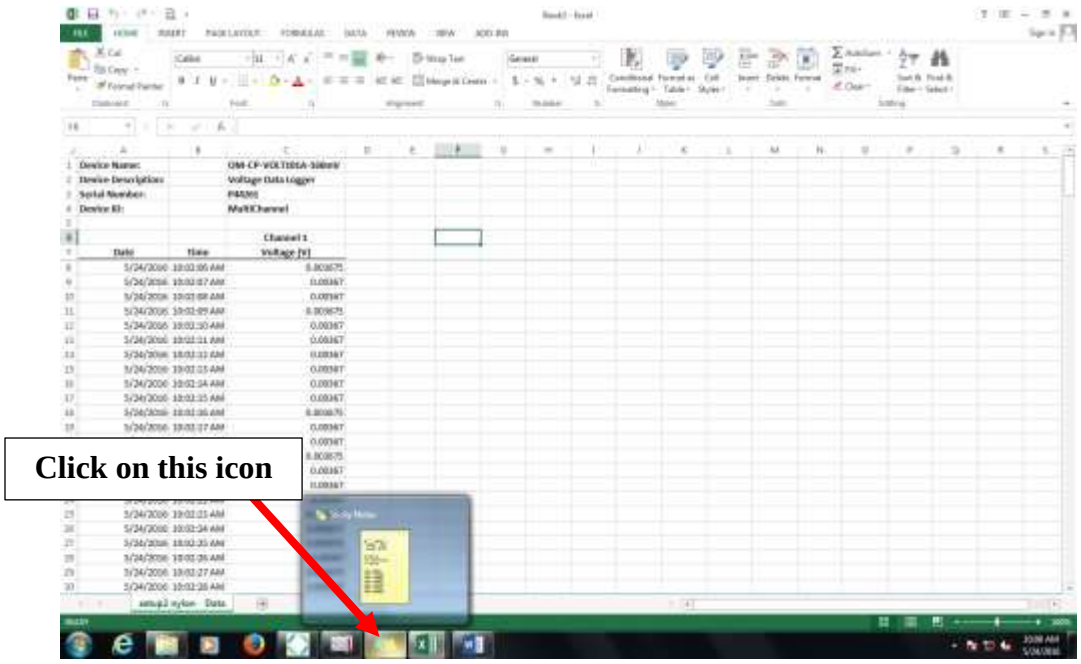


Fig. B.1.20: Clicking on the Sticky Notes icon

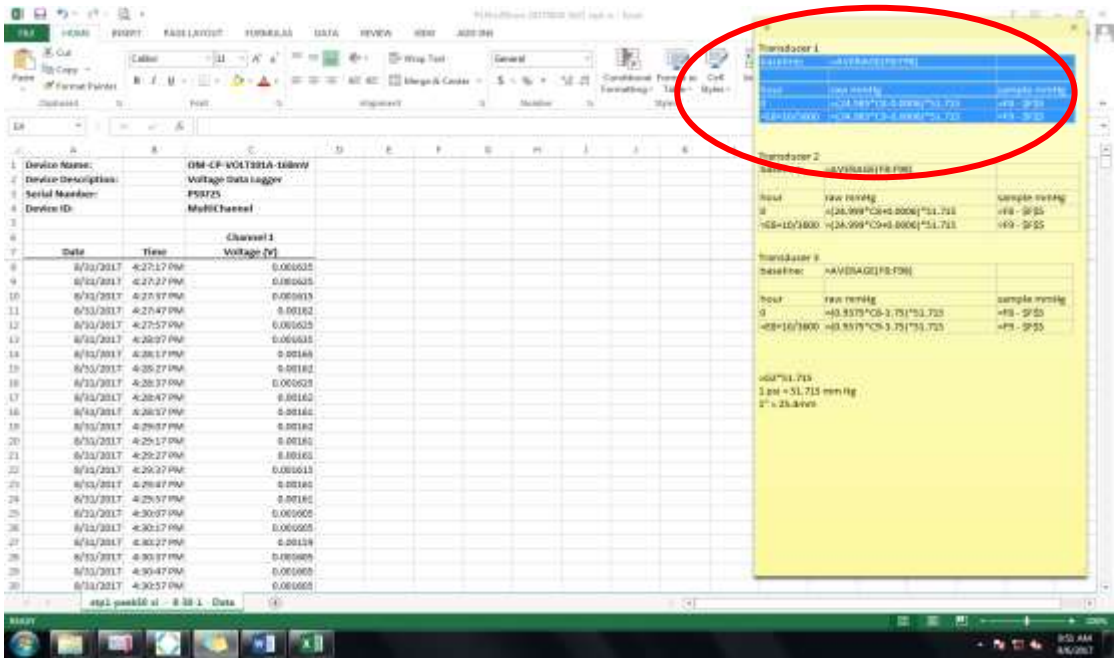

Fig. B.1.21: Highlighting and copying the top table in the Sticky Notes (conversion table for Transducer 1)

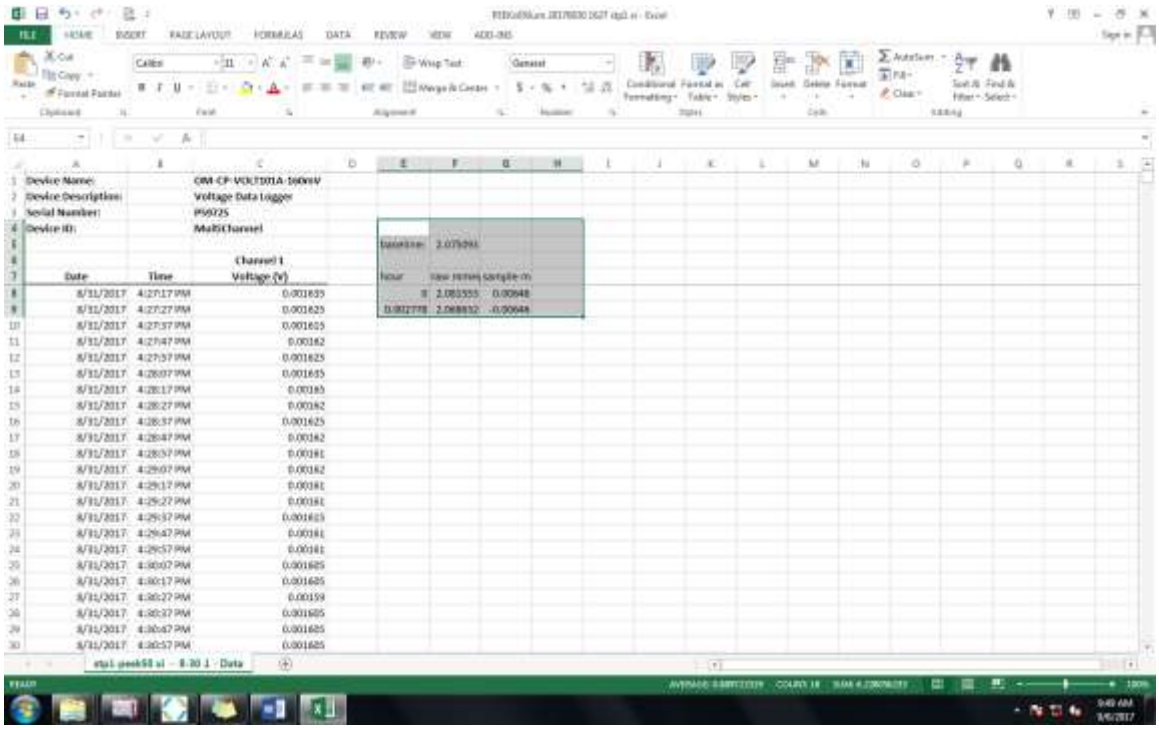


Fig. B.1.22: Table copied from Sticky Notes and pasted in the Excel spreadsheet

13. Highlight cells E9, F9 and G9, then hold <Ctrl>, <Alt> and <End> to highlight the rest of the cells below these cells. Then hold <Ctrl> and <D> to copy the formula in cells E9, F9 and G9 to all highlighted cells.
14. **To PLOT** the data, highlight the cells from E8 and F8 down to the last row of data as shown in Fig. B.1.23 by highlighting cell E8 and F8, then holding <Ctrl>, <Alt> and <↓>. Select the <INSERT> tab and click on the icon as shown in Fig. B.1.23.
15. **SAVE** the Excel spreadsheet. It is suggested that the saved file format should include: "Experiment Type"-"Date (DDMMYY)"-"Time (24hour)"-"Sample #"-"Setup #"-"Trial #" (e.g., "Nylon-BGI-26052016-1400-Smp1-Stp2-Tr4").
16. **To SAVE** the Omega data logger plot, return to the Omega program. Select the <File> tab on the top left corner, select <Save To> from the drop down on the left as shown in Fig. B.1.24, and select the desired file in which the file is to be saved.

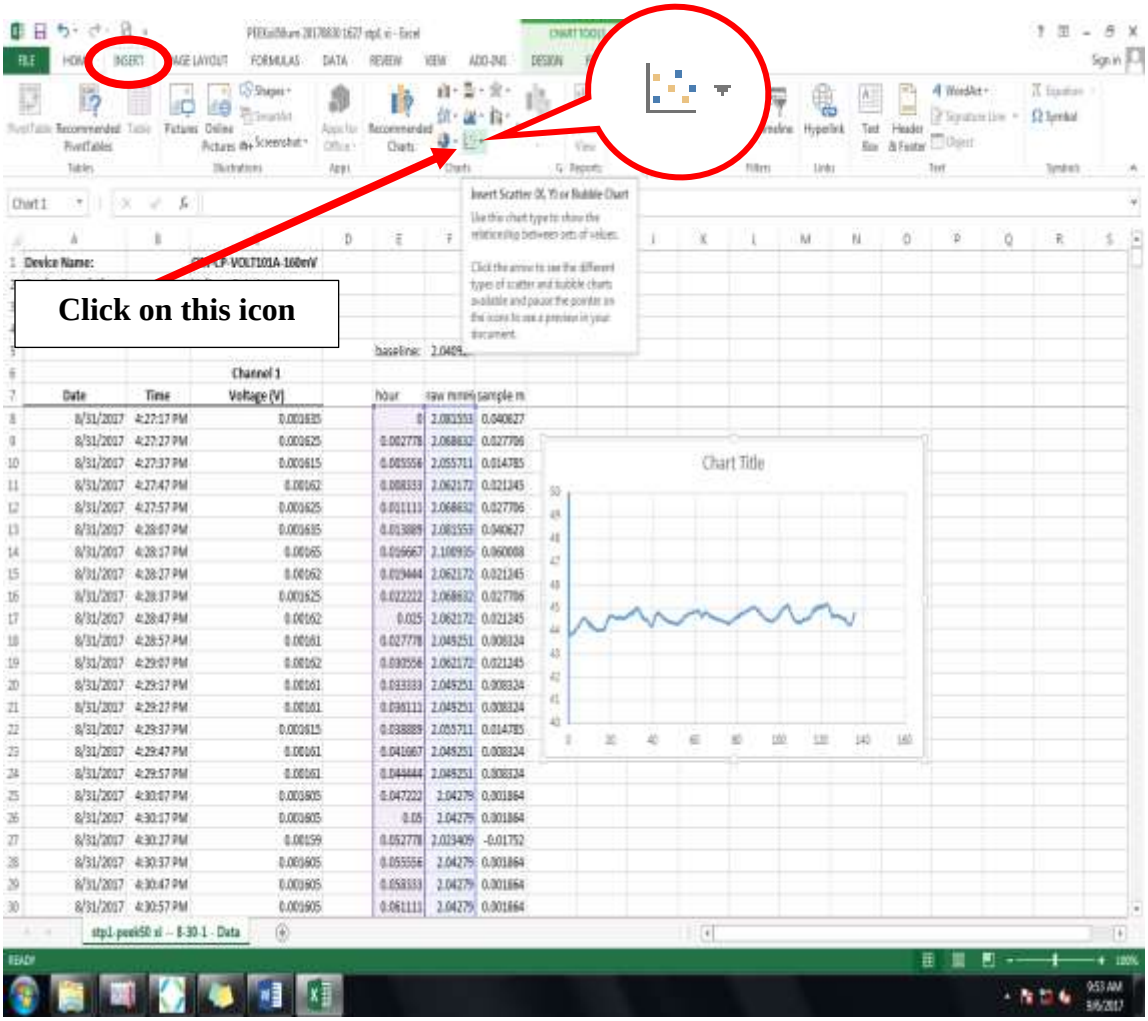


Fig. B.1.23: Creating a plot from the highlighted data

17. **To retrieve** the data from **Data Logger 2,** first close the Omega program.
18. Ensure that the data collection cable is plugged into Data Logger 2 as shown in Fig. B.1.12.
19. Open the Omega program again. Repeat steps 1 to 16. For Step 11 (converting from V to mm Hg), highlight the table labelled “Transducer 2” in the Sticky Notes instead of the table for Transducer 1.
20. Turn off logging for the pump. Go to the PneuWave pump window, select the <Logging> tab, then select <Disable> from the drop down list as shown in Fig. B.1.25. This will disable logging of both pumps.

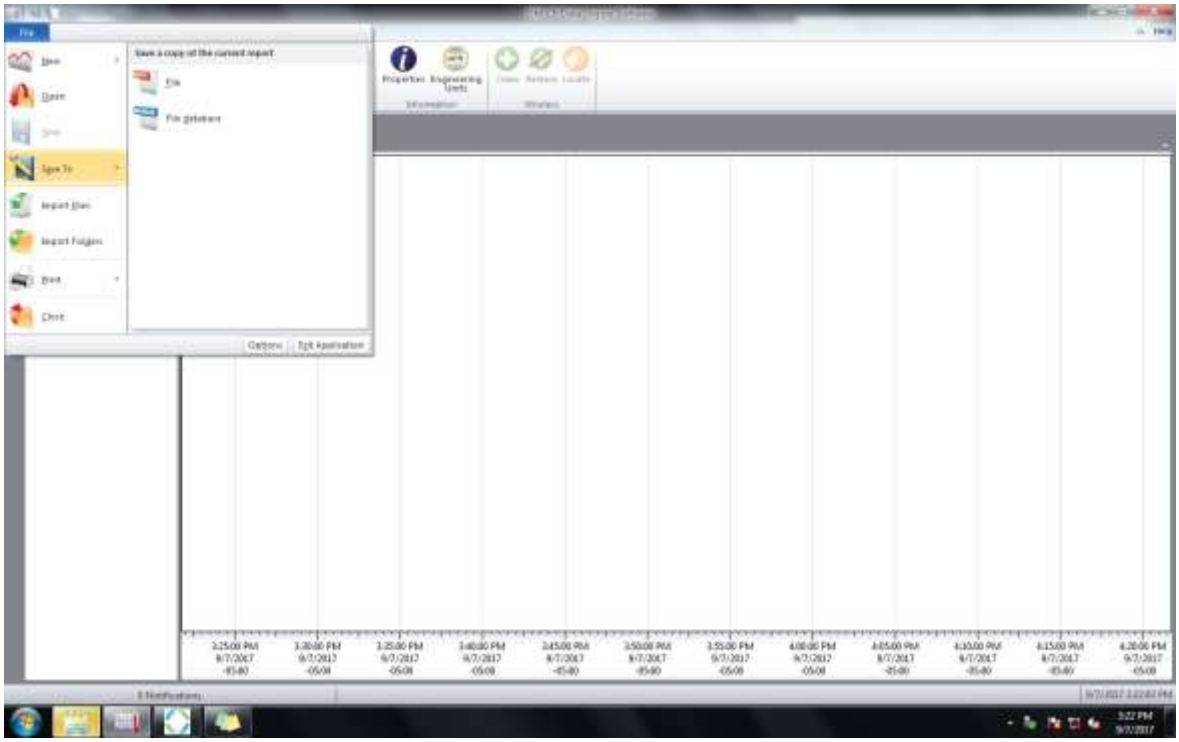

Fig. B.1.24: Saving Omega data logger plot

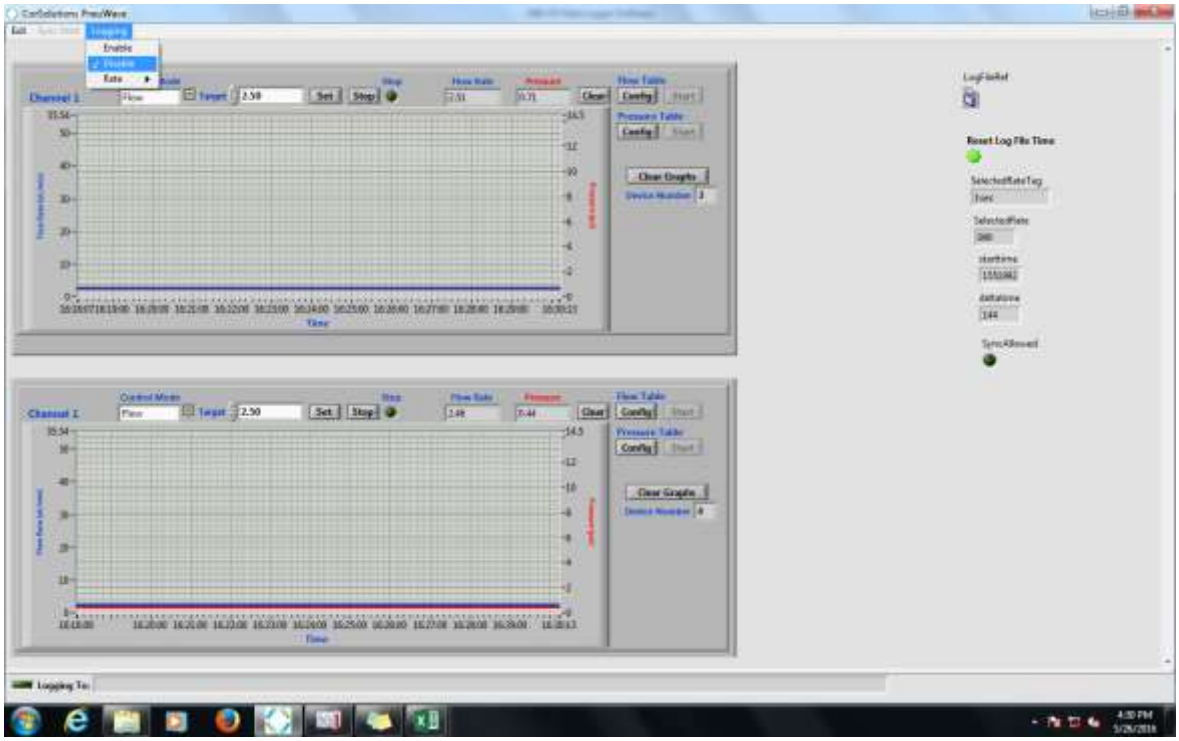

Fig. B.1.25: Disabling pump logging

21. To retrieve the pump data logs, perform the following steps:

    a. Open Windows Explorer by clicking on the icon shown in Fig. B.1.26.

    b. Open the <Documents> folder (Fig. B.1.26).

    c. Open the <PneuWave> folder (Fig. B.1.26).

    d. Open the <Logs> folder (Fig. B.1.27).

22. Open the desired log from the file list as shown in Fig. B.1.28. The logs are named as follows:

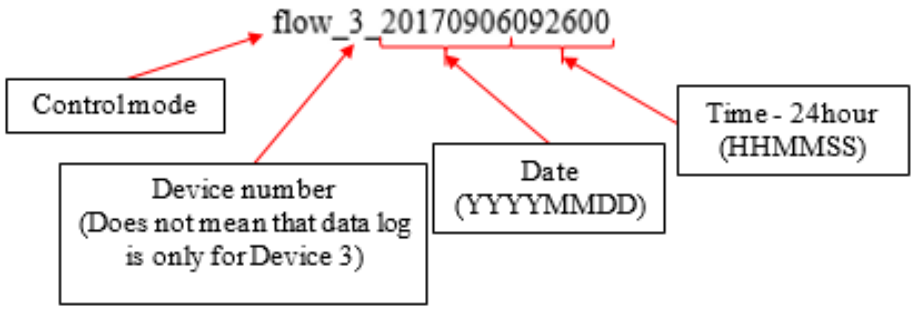


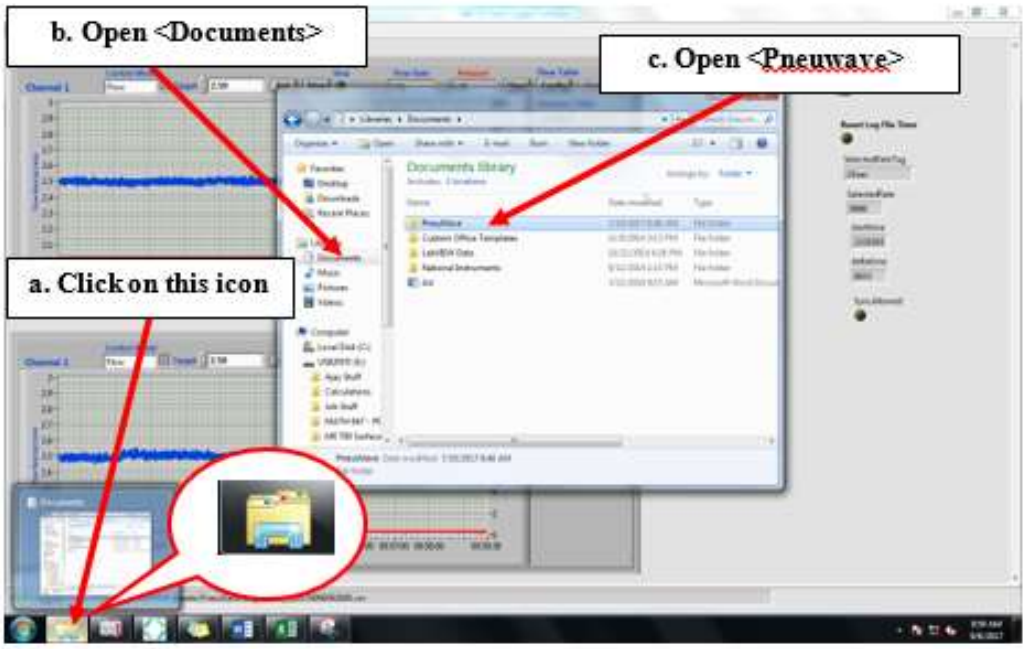


Fig. B.1.26: Retrieving pump data logs


Fig. B.1.27: Opening the <Logs> data folder

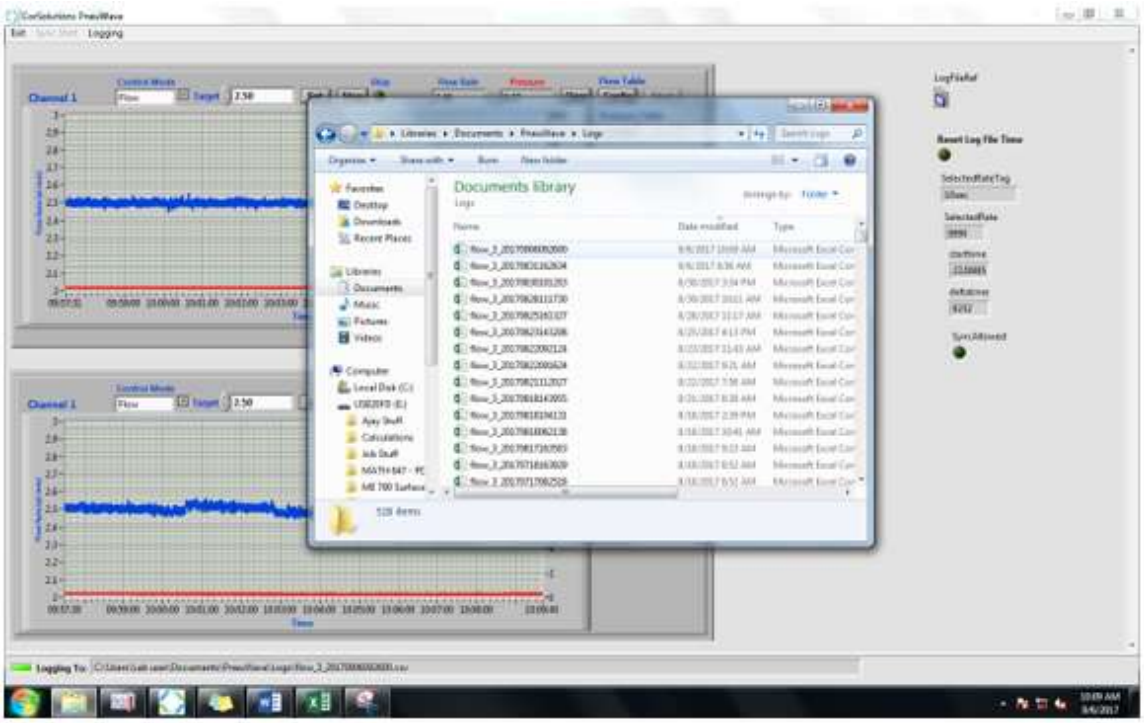

Fig. B.1.28: Pump data log files

23. After opening the desired log file, an Excel spreadsheet (.csv) will display as shown in Fig. B.1.29. Notice that the data logs are organized according to time. Figure B.1.30 explains the column labels.

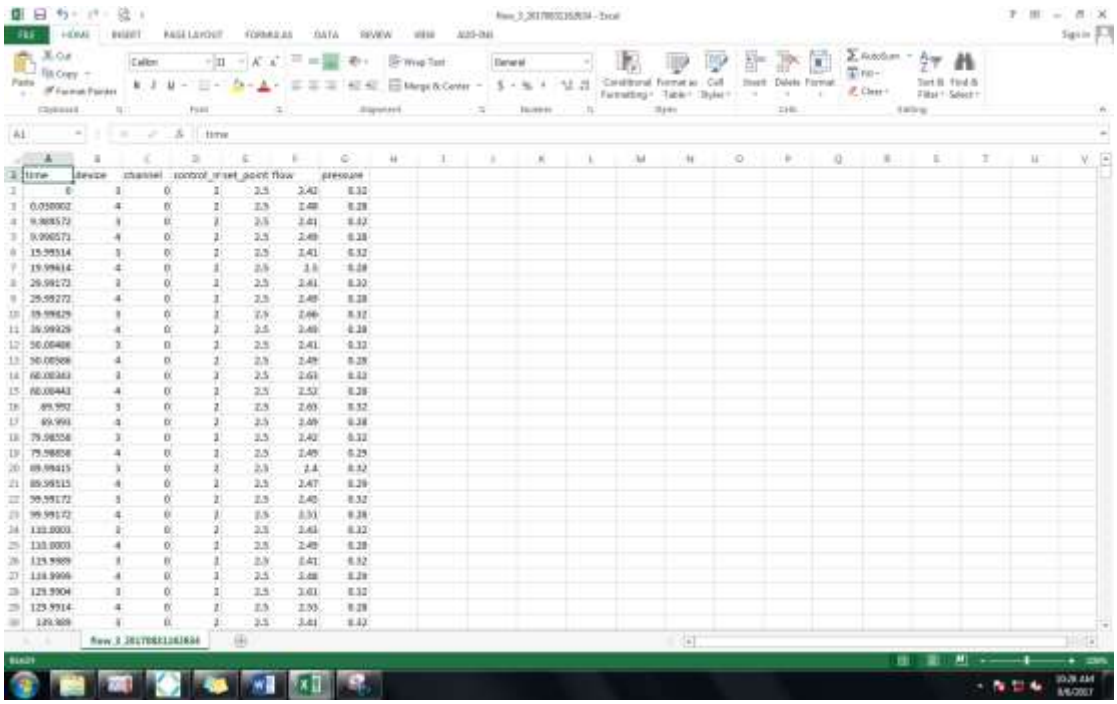

Fig. B.1.29: Raw pump log data that is sorted according to time

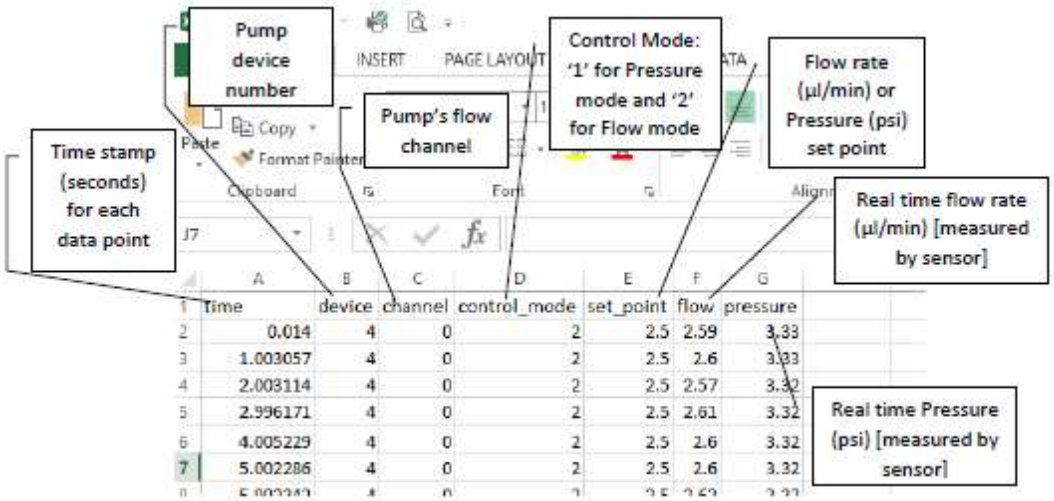


Fig. B.1.30: Column labels of the pump log data (reproduced from Ref. 42)

24. To sort the data logs according to Device, highlight all of the data values as shown in Fig. B.1.31. Then, click on the <Sort & Filter> icon in the <Home> tab and select <Custom Sort…> from the drop down menu (Fig. B.1.31).

25. A window will pop up as shown in Fig. B.1.32. Select <device> from the <Sort by> drop down selection then click <OK>.

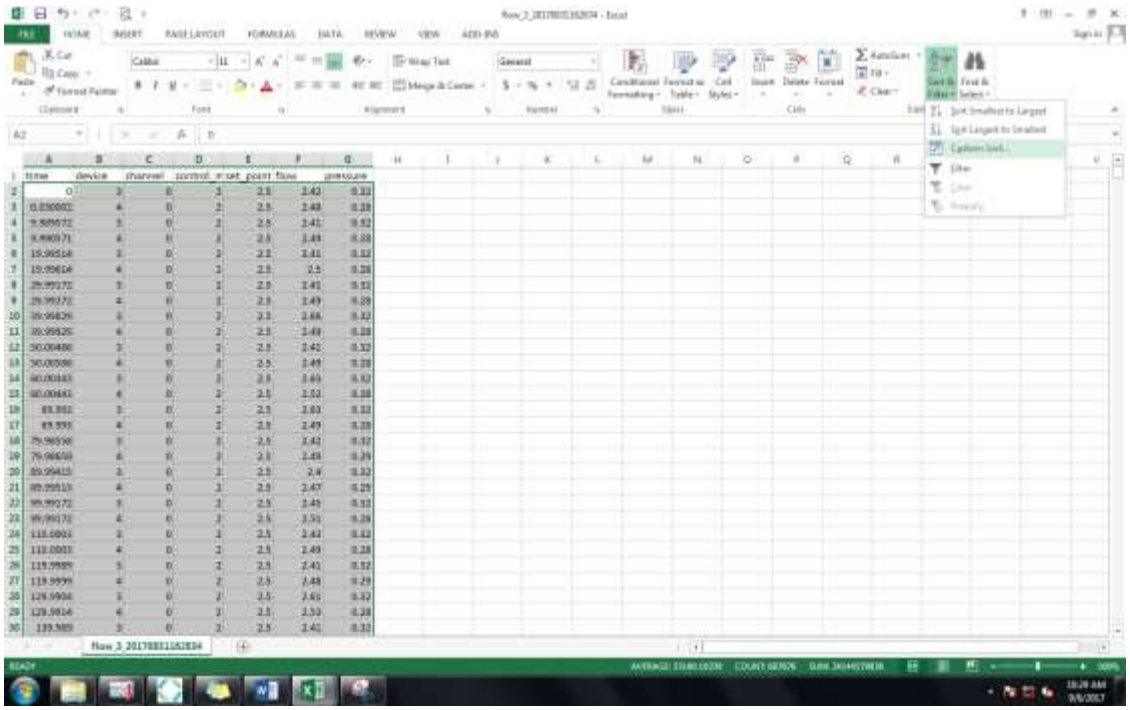

Fig. B.1.31: Highlighting and custom sorting the pump data

26. The values will be sorted according to Device number as shown in Fig. B.1.33.

27. Note that the pump pressure data are recorded in units of psi. To convert the pressure data to mm Hg, multiply the pressure data by 51.715 mm Hg/psi as shown in Fig. B.1.33, and drag the formula down to the final desired cell.

28. Save the file in the desired folder. It is recommended that the file format be changed from a comma delimited (.csv) file to an Excel workbook (.xlsx) file when saving in order to enable plots and the formulas that were created in the file to be saved.

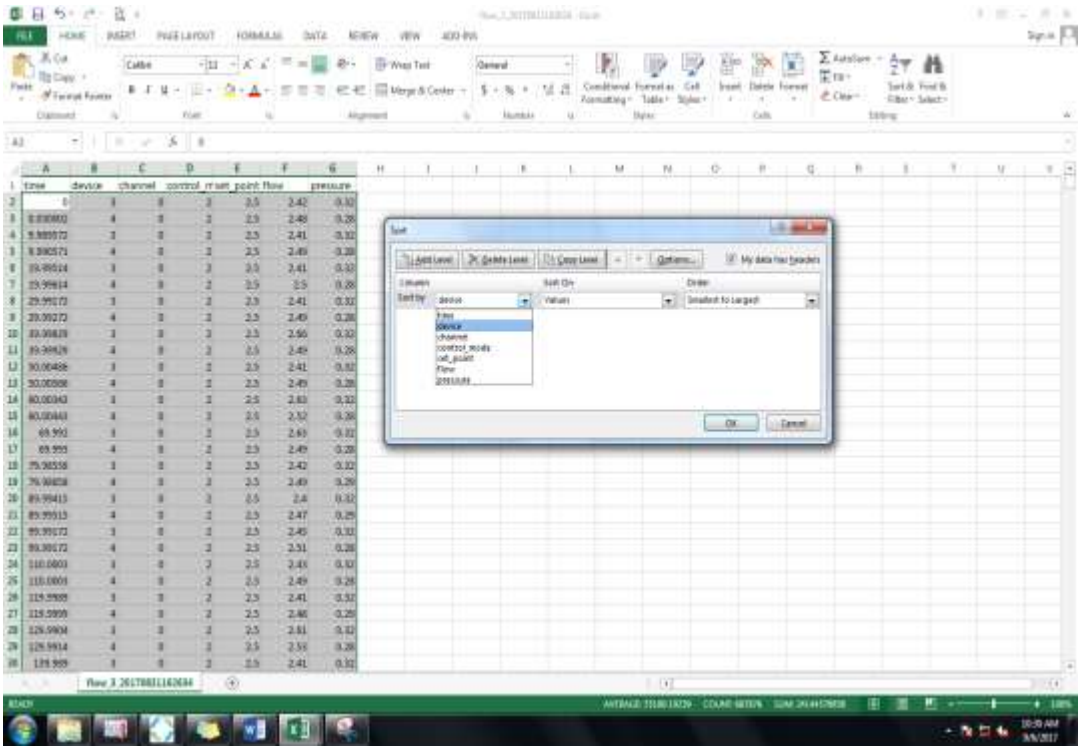

Fig. B.1.32: Sorting the pump data by Device number

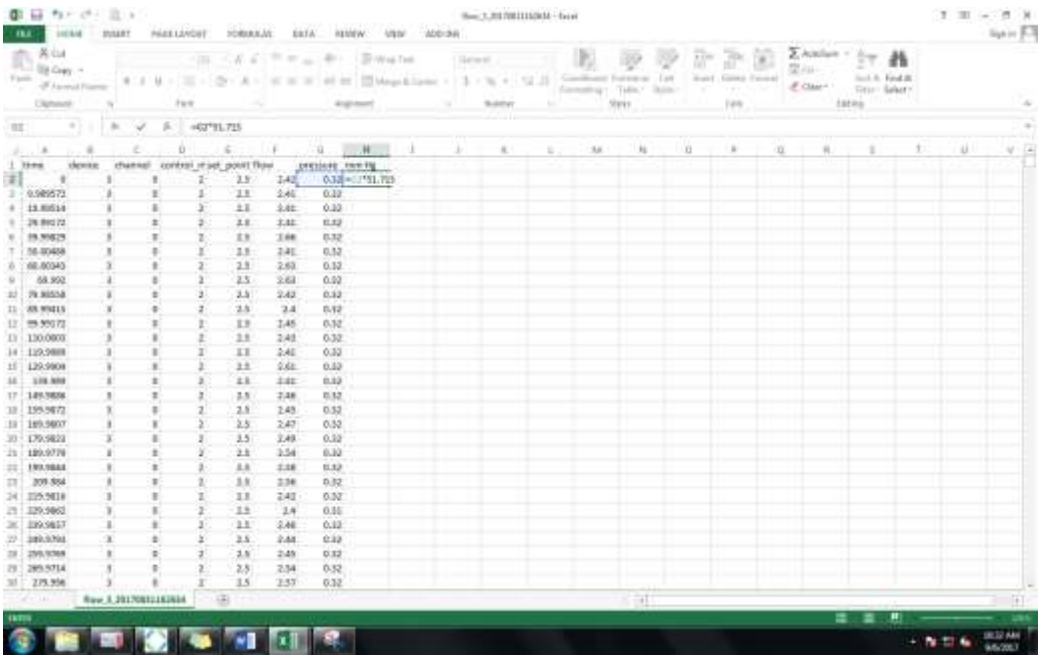

Fig. B.1.33: Converting pressure from psi to mm Hg (multiplying by 51.715 mm Hg/psi)

## B.2. When Transducer 3 or Data Logger 3 Is Used

Transducer 3 is a current-output pressure transducer. It is connected to Data Logger 3 which is an Omega current-input data logger. When Transducer 3 is to be used to measure pressure in the experiment, ensure that the data collection cable is connected to Data Logger 3 as shown in Fig. B.2.1. Remember to connect the data collection cable at the beginning of the trial to start logging transducer pressure data (Stage 1) and when retrieving pressure data at the end of the trial (Stage 4). For converting the data from Amp to mm Hg, copy the table from Sticky Note labelled "Transducer 3".

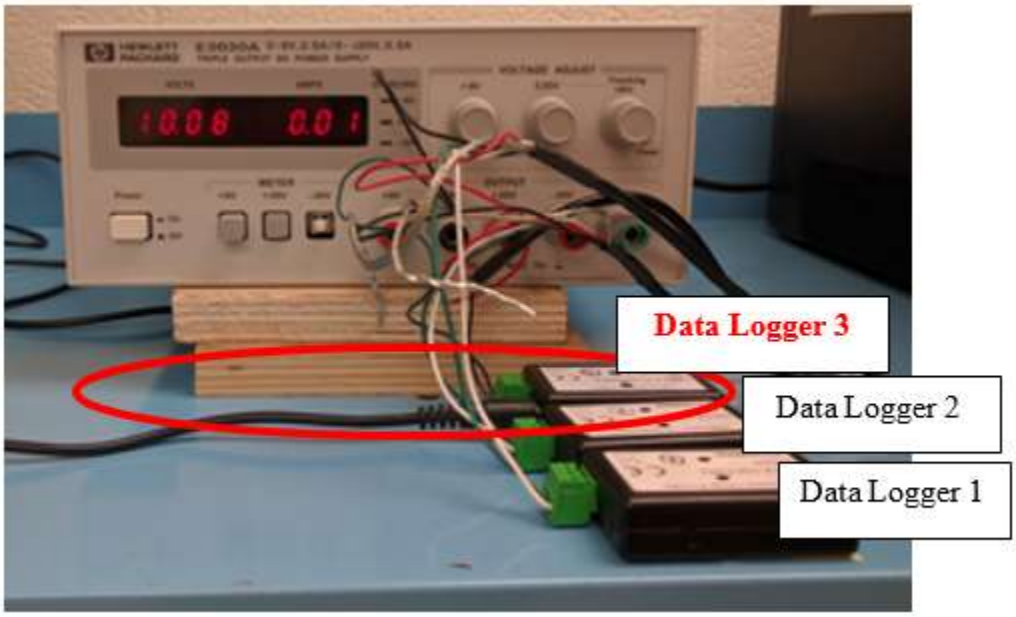


Fig. B.2.1: Connecting data collection cable to Data Logger 3

## B.3. Tubular Flow Trial with VSD Tube Sample Preparation

The following are the materials, tools and procedures for preparing the VSD microtubes samples for single tube flow trials.

***Materials and Tools***

50 µm or 75 µm ID VSD tube (SGE Analytical Science), 24G SS dispensing tip (Jensen Global), gel super glue (Loctite), ceramic capillary cutter/wafer (Thermo Scientific), ruler (1 mm), microscope (Bausch & Lomb; 3X magnification)

***Procedures***

1. Measure 25 mm of the 50 µm or 75 µm VSD tubing using a ruler and place the tip of your thumb at the 25 mm point that is to be cut.
2. Pinch the VSD tubing between the finger and thumb of one hand.

*Note that the ceramic wafer has four smooth edges and four serrated edges. The smooth edges are on the rear edges of the wafer (with no writing) and the serrated edges are on the front edges (with writing) [76].*

3. With the other hand, use the smooth edge of the ceramic wafer (edge with no writing) to score across the point on the VSD tubing that is to be cut, applying light pressure as shown in Fig. B.3.1 [76]. Hold the wafer approximately 45° to the VSD tubing as shown in Fig. B.3.1 and ensure that the uncut side of the tubing is supported against the finger during scoring [76].

Fig. B.3.1: Cutting VSD tubing with a ceramic cutter

4. Using the wafer, flick the tubing just above the cut while supporting the tubing by pinching it between the finger and thumb below the cut [76]. This will break the tubing.

   *If the break is successful, the break should be clean leaving no fragments or burrs. If necessary, check the end of the cut VSD tube under the microscope.*

5. Re-measure the tube that was cut to ensure that it is 25 mm long and record the actual length measured on the experiment log sheet in the 'Tube: Length' space.
6. Slide the cut 25 mm VSD tube into the 24G SS dispensing tip and super glue at the location shown in Fig. B.3.2. (*Ensure that the super glue is the gel type super glue*)

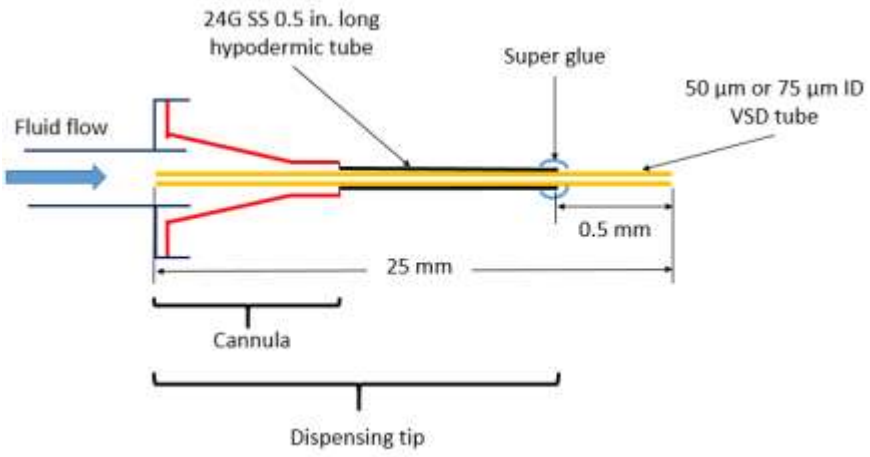


Fig. B.3.2: Configuration of tubular flow trial test sample

7. Let the sample dry overnight.
8. After the sample has dried, flush the sample tip with DI water using a syringe. Check for leaks at the super glue connection and check if water flows from the VSD tube end.

## B.4. Annular Flow Trial with SS Hypodermic Tube Sample Preparation

The following are the materials, tools and procedures for preparing the stiff annular test samples for annular flow trials.

***Materials and Tools***

23G/24G/30G SS dispensing tip (Jensen Global; refer to App. B.6), 26G/28G/30G/36G nichrome wire (AWG; refer to App. B.6), wire cutter (5 in. or 13 cm cutting area), ruler (1 mm), emery paper (grade 80 - 100)

***Procedures***

1. Measure, then cut, an 8 mm long nichrome wire sample (26G, 28G, 30G or 36G) using a wire cutter. Be sure to avoid bending the sample during cutting and handling.
2. Re-measure the cut wire in order to ensure it is 8 mm long and record the actual length measured on the experiment log sheet in the 'Tube: Length' space (Fig. D.1.1). Inspect the ends of the 8 mm wire sample in order to ensure that there are no significant deformations or burrs.
3. If there are significant burrs or deformations, either sand the end of the sample with emery paper or cut a new sample. Be careful not to bend the wire sample during sanding.
4. Place the cut wire sample into the tube end of the desired dispensing tip (23G, 24G or 30G) as shown in Fig. B.2.4, being careful not to bend the wire sample.

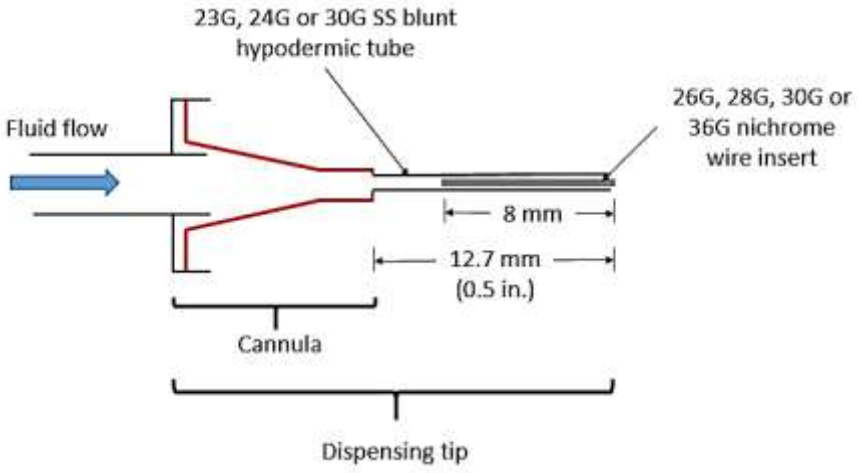


Fig. B.4.1: Configuration of annular flow trial test sample with SS hypodermic tube

## B.5. Annular Flow Trial with BGI Tube Sample Preparation

The following are the materials, tools and procedures for preparing BGI tube samples for annular flow trials with degradable/non-degradable inserts.

***Materials and Tools***

30G SS dispensing tip (Jensen Global), BGI tubing (300 μm ID), degradable/non-degradable insert sample (refer to App. B.6), gel super glue (Loctite), ruler (1 mm), microscope (Bausch & Lomb; 3X magnification), surgical scissors (11 cm long)

***Procedures***

1. Measure then cut a 12 mm long sample of BGI tubing using the surgical scissors as shown in Fig. B.5.1.
2. Re-measure the cut sample in order to ensure it is 12 mm long and record the actual length measured on the experiment log sheet in the 'Tube: Length' space (Fig. D.1.1).

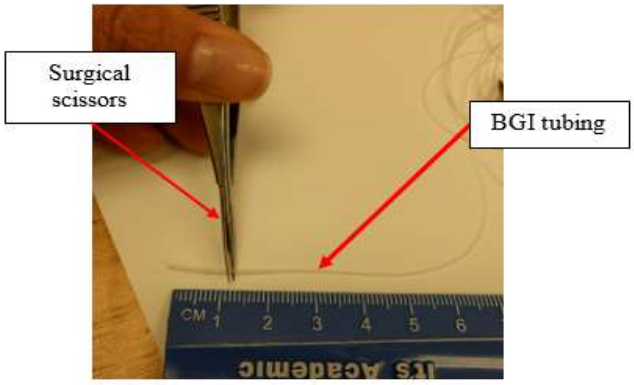


Fig. B.5.1: Cutting the BGI tube with surgical scissors

3. Slide the cut BGI tube over the 30G dispensing tip, making sure that a 10 mm length of the BGI tube sample is not in contact with the hypodermic tube as shown in Fig. B.5.2.
4. Super glue at the connection between the BGI tube and the hypodermic tube as shown in Fig. B.5.2. Ensure that no glue enters the BGI tube or the hypodermic tube.

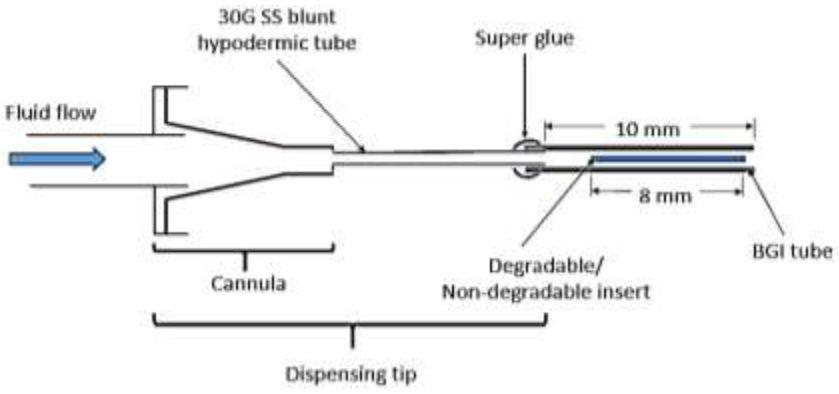


Fig. B.5.2: Configuration of annular flow trial test sample with BGI tube

5. Leave the sample to dry overnight.
6. Just before the trial, cut the 8 mm degradable/non-degradable insert and place it into the BGI tube as shown in Fig. B.5.2. If the insert is a degradable insert, use gloves during handling to prevent transfer of moisture from the hand to the insert.
7. Re-measure the cut sample in order to ensure it is 8 mm long and record the actual length measured on the experiment log sheet in the 'Tube: Length' space (Fig. D.1.1).

## B.6. List of Tubes and Inserts Used in the Study

Table B.6.1 lists the types of tubes and inserts used for preparation of the test samples, as well as the range of actual IDs/ODs of the tubes/inserts used.

Table B.6.1: List of tubes and inserts used to prepare test samples

| Tube/Insert | Make/Model/Part Number | Specifications as Provided by Supplier | Range of Measured ID |
|---|---|---|---|
| 24G SS hypodermic tube (0.5 in. and 1.5 in.) | Jensen Global:<br>JG24-0.5X (0.5 in. long);<br>JG24-1.5X (1.5 in. long) | - Luer Lock hub<br>- 24G blunt tip<br>- Color: Red<br>- ID: 0.015 in. (0.381 mm)<br>- OD: 0.022 in. (0.559 mm)<br>- Polypropylene hub<br>- UV-bonded 304 SS cannula | ID: 0.347 mm - 0.362 mm (Measured with micro-CT) |

Table B.6.1: List of tubes and inserts used to prepare test samples (continued)

| Tube/Insert | Make/Model/Part Number | Specifications as Provided by Supplier | Range of Measured ID |
|---|---|---|---|
| 23G SS hypodermic tube | Jensen Global: JG23-0.5X | - Luer Lock hub<br>- 23G blunt tip<br>- Color: Sky Blue<br>- ID: 0.016 in. (0.406 mm)<br>- OD: 0.025 in. (0.635 mm)<br>- Polypropylene hub<br>- UV-bonded 304 SS cannula | ID: 0.433 mm - 0.439 mm (measured with micro-CT) |
| 30G SS hypodermic tube | Jensen Global: JG30-0.5X | - Luer Lock hub<br>- 30G blunt tip<br>- Color: Sky Blue<br>- ID: 0.006 in. (0.152 mm)<br>- OD: 0.012 in. (0.305 mm)<br>- Polypropylene hub<br>- UV-bonded 304 SS cannula | ID: 0.163 mm - 0.167 mm (measured with micro-CT) |
| 50 µm VSD tubing | SGE Analytical Science (by TRAJAN):<br>2 m x 50 µm/220 µm VSD Tubing (P/N: 062444, S/N: 1207105B) | - Methyl deactivated fused silica tubing<br>- Chemically inert<br>- Thermally stable up to 380 °C<br>- ID: 50 µm<br>- OD: 220 µm<br>- Length: 2 m | ID: 49.3 µm - 52.8 µm |
| 75 µm VSD tubing | SGE Analytical Science (by TRAJAN):<br>2 m x 75 µm / 190 µm VSD Tubing (P/N: 0624450, S/N: 1108894) | - Methyl deactivated fused silica tubing<br>- Chemically inert<br>- Thermally stable up to 380 °C<br>- ID: 75 µm<br>- OD: 190 µm<br>- Length: 2 m | ID: 75.3 µm - 76.9 µm |
| BGI tubing | Silastic (Dow Corning):<br>Laboratory tubing;<br>CAT #: 508-001;<br>Lot #: 0007637304 | - ID: 0.30 mm<br>- OD: 0.64 mm | ID: 0.344 mm - 0.352 mm (measured with Leica microscope) |
| 26G nichrome wire | Master of Clouds:<br>26G Nichrome 80 wire (787421218725) | - 26 AWG nichrome wire<br>- OD: 0.405 mm<br>- Spool length: 25 ft. | OD: 0.411 mm - 0.412 mm (measured with micro-CT) |

Table B.6.1: List of tubes and inserts used to prepare test samples (continued)

| Tube/Insert | Make/Model/Part Number | Specifications as Provided by Supplier | Range of Measured ID |
|---|---|---|---|
| 28G nichrome wire [*Used in the micro-CT trials in Chapter 3*] | Master of Clouds: 28G Nichrome 80 wire (787421218732) | - 28 AWG nichrome wire<br>- OD: 0.321 mm<br>- Spool length: 25 ft. | OD: 0.328 mm - 0.333 mm (measured with micro-CT) |
| 30G nichrome wire | Master of Clouds: 30G Nichrome 80 wire (787421218749) | - 30 AWG nichrome wire<br>- OD: 0.254 mm<br>- Spool length: 25 ft. | OD: 0.263 mm - 0.269 mm (measured with micro-CT) |
| 36G nichrome wire | Master of Clouds: 36G Nichrome 80 wire (605930535907) | - 36 AWG nichrome wire<br>- OD: 0.127 mm<br>- Spool length: 25 ft. | OD: 0.134 mm - 0.139 mm (measured with micro-CT) |
| 28G nichrome wire [*Used for all 28G insert annular trials except for the micro-CT trials in Chapter 3*] | Lightning Vapes: Nichrome 80 resistance wire | - 28 AWG nichrome wire<br>- OD: 0.32 mm<br>- Spool length: 25 ft. | OD: 0.315 mm - 0.323 mm (measured with micrometer) |
| 29G kanthal wire | TemCo: Kanthal A-1 annealed round resistance wire (RW01690) | - 29 AWG kanthal wire<br>- OD: 0.286 mm<br>- Spool length: 50 ft. | OD: 0.279 mm - 0.292 mm (measured with micrometer) |
| 28G SS wire | Artistic Wire: SS wire (3592610905) | - 28 AWG SS wire<br>- OD: 0.32 mm<br>- Spool length: 117 ft. | OD: 0.320 mm - 0.328 mm (measured with micrometer) |
| 28G SS wire | Cousin: Steel Elegance SS wire (29505125) | - 28 AWG SS wire<br>- OD: 0.32 mm<br>- Spool length: 20 ft. | OD: 0.386 mm - 0.391 mm (measured with micrometer) |
| Nylon monofilament | Beadalon Supplemax: Monofilament illusion cord (JN0.30W-F) | - OD: 0.30 mm<br>- Spool length: 164 ft. | OD: 0.300 mm - 0.305 mm (measured with micrometer) |

Table B.6.1: List of tubes and inserts used to prepare test samples (continued)

| Tube/Insert | Make/Model/Part Number | Specifications as Provided by Supplier | Range of Measured ID |
|---|---|---|---|
| 3-0 prolene suture | Ethicon:<br>3-0 prolene blue monofilament (8665) | - OD: 0.20 mm<br>- Non-absorbable medical grade suture<br>- Color: Blue (undyed)<br>- Suture type: Monofilament<br>- Material: Polypropylene<br>- Spool length: 18 in. | OD: 0.241 mm - 0.246 mm (measured with micrometer) |
| 3-0 monocryl suture | Ethicon: 3-0 monocryl undyed monofilament (Y215) | - OD: 0.20 mm<br>- Absorbable medical grade suture<br>- Color: Clear (undyed)<br>- Suture type: Monofilament<br>- Material: Poliglecaprone 25<br>- Spool length: 27 in. | OD: 0.269 mm - 0.282 mm (measured with micrometer) |
| PLGA monofilament | Fabricated at the Berkland Lab in KU: PLGA monofilament (AP-045) | - OD: ~0.25 mm<br>- Absorbable monofilament<br>- Material: Poly(lactic-co-glycolic acid) acid endcap (AP-045)<br>- LA to GA ratio: 50:50 | OD: 0.258 mm - 0.300 mm (measured with micrometer) |

## Appendix C: Specifications of Devices Purchased for Setup Validation

### C.1. kdScientific Syringe Pump

The following lists the specifications of the kdScientific syringe pump [77].

| | |
|---|---|
| Model: | KDS Legato 100 |
| Accuracy: | ± 0.5% |
| Reproducibility: | ± 0.05% |
| Syringe volume (min./max.): | 0.5 µl/60 ml |
| Flow rate: | 1.26 pl/min (Min. 0.5 µl syringe) |
| | 26.017 ml/min (Max. 10 ml syringe) |
| | 88.404 ml/min (Max. 60 ml syringe) |
| Linear force (max.): | 13.6 kg (30 lbs) at 100% force selection |
| Drive motor: | 0.9° stepper motor |
| Motor drive control: | Microprocessor with 1/16 microstepping |
| Step resolution: | 0.069 µm/step |
| Input power: | 12-30 VDC |
| Input power connection: | 2.5 mm ID x 5.5 mm OD male plug |
| Power supply: | 100-240 VAC, 50 - 60 Hz, 9 Watts Universal Power Supply |
| Dimensions: | 22.6 cm x 19.05 cm x 15 cm (9 in. x 7.5 in. x 5 in.) |
| Weight: | 2.66 kg (5.9 lbs) |
| Operating temperature: | 4°C to 40°C (40°F - 104°F) |
| Storage temperature: | -10°C to 70°C (14°F - 158°F) |
| Storage humidity: | 20% - 80% relative humidity, non-condensing |

## C.2. Dwyer Current Output Pressure Transducer

The following lists the specifications of the Dwyer pressure transducer (Transducer 3) used to verify the pressure readings of Transducers 1 and 2 [78].

| | |
|---|---|
| Model number: | 626-07-GH-P1-E1-S1 |
| Item number: | 2HLR2 |
| Housing: | Stainless steel |
| NEMA rating: | 4X |
| Loop resistance: | 0 to 1300 Ω |
| Max. pressure: | 30 psi |
| Thermal error: | ± 0.02 % of full scale per 1°F |
| Compatible with: | Liquids and gas |

***Transmitter***

| | |
|---|---|
| Transmitter type: | Pressure transmitter |
| Wetted materials: | 316 stainless steel, 316L stainless steel |
| Pressure range: | 0 to 15 psi |
| Accuracy: | ± 0.25% of full scale |
| Output range: | 4 mA to 20 mA DC |
| Power required: | 13 to 30 VDC |
| Process connection: | 1/4 in. male NPT |
| Lead length: | 36 in. |
| Operating temperature: | 0°F to 200°F |

## C.3. Omega Current Input Data Logger

Following are the specifications of the Omega current input data logger (Data Logger 3) used to log the pressure readings of Transducer 3 [44].

*Note that unlike Data Loggers 1 and 2, this data logger was not purchased with a NIST calibration certificate. To obtain a NIST calibration certificate with the data logger, order using the model number OM-CP-PROCESS101A-20MA-CERT.*

| | |
|---|---|
| Model number: | OM-CP-PROCESS101A-20MA |
| Nominal input range: | 20 mA |
| Measurement range: | -2 to 30 mA |
| Input voltage range: | 0 to 2.5 V |
| Resolution: | 0.5 µA |
| Accuracy: | ± 0.05% of full scale |
| Input impedance: | 10 Ω ± 1 Ω |
| Input connection: | Removable screw terminal |
| Analog conversion time: | 133 ms nominal |
| Frequency rejection: | 50 to 60 Hz |
| Reading rate: | 4 Hz to 1 reading every 24 hours |
| Memory: | 1,000,000 readings |
| Wrap around: | Yes |
| Battery type: | 3.6 V lithium battery (OM-CP-BAT105) |
| Battery life: | 10 year battery life, typical at 15 min reading rate |
| Time accuracy: | ± 1 minute/month (stand-alone data logging) |
| Computer interface: | USB interface cable (115,200 baud) |

| | |
|---|---|
| Software: | XP SP3/Vista/7 and 8 (32 and 64-bit) |
| Operating temperature: | -40°C to 80°C (-40°F to 176°F) |
| Operating humidity: | 0 to 95% relative humidity, non-condensing |
| Dimensions: | 36 mm x 56 mm x 16 mm (1.4 in. x 2.2 in. 0.6 in.) |
| Weight: | 24 g (0.9 oz) |
| Material: | ABS plastic |

## Appendix D: Experiment Logs

### D.1. Template for Logging Flow Trial Characteristics

In order to keep track of the critical characteristics of a trial, all necessary information required to completely identify and repeat the trial are recorded in an experiment log sheet. Record the following information on the log sheet (Fig. D.1.1) as follows:

1. **Trial Type**: Type of trial (single open tube flow, annular flow, AGV, etc.)
2. **Sample**: Type of sample (23G/24G/30G SS tube, BGI tube, 26G/28G/30G/36G wire inserts, degradable inserts, sutures, etc.)
3. **Setup-Pump-Transducer**: The setup, pump and transducer combination (e.g., for Setup 1, Pump 1 and Transducer 1, write "1-1-1")
4. **Trial #**: The number of repetitions ($1^{st}$, $2^{nd}$, $3^{rd}$, etc.)
5. **Solution**: The type of fluid solution (e.g., DI water, DI + 0.04% $NaN_3$, BSS + 0.04% $NaN_3$, etc.)
6. **Tube (Length and ID)**: Measured length and inner diameter of the tube sample used
7. **Insert (Length and OD)**: Measured length and outer diameter of the insert placed in the tube sample
8. **Trial Date**: Date the trial was started (e.g., 8/2/2017)
9. **Time-Baseline**: Time at which the baseline $\Delta P$ was logged. This is when the sample was not connected at test section and flow rate was set at control flow rate (typically 2.5 µl/min)
10. **Time-Prime/AGV**: For single tube and annular flow trials, this space is for recording the time at which the pump was primed (high flow rate). For an AGV trial, this space is for recording the time at which the AGV sample was connected to the test section.

11. **Time-Trial**: Time at which $\Delta P$ was logged after the sample was connected at test section and flow rate was set at the control flow rate (2.5µl/min)
12. **Time-End**: Time at which data logging was stopped
13. **End Date**: Date on which data logging was stopped
14. **Flow rate (Prime and Control)**: Prime = flow rate value used to prime the pumps (e.g., 10 µl/min); Control = control flow rate for flow trial (e.g., 2.5 µl/min)
15. **Disconnected luer lock**: Check the box if the sample cannula was removed from the luer lock of the tube end at test section before the new trial
16. **Changed trough water**: Check the box if the fluid in the trough was changed before the new trial
17. **Incubator**: Check the box if incubator was used, and fill in the set temperature of the incubator
18. **Reset pump**: Check the box if the pump was manually reset (switched off then on again) immediately before starting the new trial
19. **Flushed sample w. syringe**: Check the box if the test sample was flushed manually with a syringe filled with DI water prior to the new trial
20. ***Empty check box***: Check and fill in the space if there was a new or regular procedure done that was not otherwise noted
21. **Notes**: Fill in any additional observations or special procedures taken for the trial

**EXPERIMENT LOG**

Trial Type: _____ **Trial Date:** _____

Sample: _____ Time-Baseline: _____

Setup-Pump-Transducer: _____ Time-Prime/AGV: _____

Trial #: _____ Time-Trial: _____

Solution: _____ Time-End: _____

Tube: *Length* _____ *ID* _____ **End Date:** _____

Insert: *Length* _____ *OD* _____ Flow rate: *Prime* _____ *Control* _____

□ Disconnected luer lock □ Changed trough water □ Incubator _____ °F/°C

□ Reset pump □ Flushed sample w. syringe □ _____

Notes: _____

_____

_____

_____

**EXPERIMENT LOG**

Trial Type: _____ **Trial Date:** _____

Sample: _____ Time-Baseline: _____

Setup-Pump-Transducer: _____ Time-Prime/AGV: _____

Trial #: _____ Time-Trial: _____

Solution: _____ Time-End: _____

Tube: *Length* _____ *ID* _____ **End Date:** _____

Insert: *Length* _____ *OD* _____ Flow rate: *Prime* _____ *Control* _____

□ Disconnected luer lock □ Changed trough water □ Incubator _____ °F/°C

□ Reset pump □ Flushed sample w. syringe □ _____

Notes: _____

_____

_____

_____

Fig. D.1.1: Experiment log sheet template

## D.2. Log for Pneumatic Pump vs. Syringe Pump Check

Tables D.2.1 (a) and (b), and D.2.2 (a) and (b) are the experimental logs of the input and output parameters during the pneumatic vs. syringe pump flow rate check.

Table D.2.1 (a): Log of input parameters for cross-check testing between pneumatic pump and syringe pump (first part)

| INPUT PARAMETERS | | | | |
|---|---|---|---|---|
| **Syringe Setting** | **Trial Number** | **Date (MM/DD/YY)** | **Force Setting** | **Input Syringe Volume (ml)** |
| Custom syringe, 2 ml (8.91 mm ID) | 1 | 12/06/16 | 100% | 2 |
| | 2 | 12/06/16 | 100% | 2 |
| | 3 | 12/07/16 | 100% | 2 |
| KDS glass, 5 ml | 4 | 12/07/16 | 30% | 5 |
| KDS glass, 2 ml | 5 | 12/07/16 | 20% | 2 |
| Cadence glass, 2 ml | 6 | 12/08/16 | 20% | 2 |
| Cadence glass, 5 ml | 7 | 12/08/16 | 20% | 5 |
| KDS glass, 5 ml | 8 | 12/08/16 | 20% | 5 |
| | 9 | 12/08/16 | 20% | 5 |
| BD plasti-pak | 10 | 12/08/16 | 50% | 5 |
| | 11 | 12/12/16 | 50% | 5 |
| | 12 | 12/12/16 | 50% | 5 |
| | 13 | 12/12/16 | 50% | 5 |
| | 14 | 12/13/16 | 50% | 5 |
| | 15 | 12/14/16 | 50% | 5 |
| | 16 | 12/16/16 | 50% | 5 |

Table D.2.1 (b): Log of input parameters for cross-check testing between pneumatic pump and syringe pump (second part)

| INPUT PARAMETERS | | | | | | |
|---|---|---|---|---|---|---|
| **Syringe Setting** | **Trial Number** | **Fluid Volume in Syringe (ml)** | **Input Flow Rate (µl/min)** | **Target Set (Time or Volume)** | **Time Start (HH:MM)** | **Transducer valve** |
| Custom syringe, 2 ml (8.91 mm ID as labelled on syringe) | 1 | 2 | 30 | 1:06:30 | 12:14 PM | Open |
| | 2 | 2 | 30 | 1:06:30 | 3:15 PM | Open |
| | 3 | 2 | 30 | 1:06:30 | 9:46 AM | Open |
| KDS glass, 5 ml | 4 | 5 | 30 | 2 ml | 12:37 PM | Closed |
| KDS glass, 2 ml | 5 | 2 | 30 | 2 ml | 3:48 PM | Open |
| Cadence glass, 2 ml | 6 | 2 | 30 | 2 ml | 10:54 AM | Open |
| Cadence glass, 5 ml | 7 | 5 | 30 | 2 ml | 12:22 PM | Open |
| KDS glass, 5 ml | 8 | 5 | 30 | 2 ml | 3:26 PM | Open |
| | 9 | 5 | 30 | 2 ml | 8:30 PM | Open |
| BD plasti-pak | 10 | 5 | 30 | 2 ml | 2:52 PM | Open |
| | 11 | 5 | 30 | 2 ml | 10:27 AM | Open |
| | 12 | 5 | 30 | 2 ml | 12:20 PM | Open |
| | 13 | 5 | 30 | 2 ml | 3:24 PM | Open |
| | 14 | 5 | 15 | 2 ml | 4:06 PM | Open |
| | 15 | 5 | 15 | 2 ml | 10:10 AM | Open |
| | 16 | 5 | 15 | 2 ml | 8:52 AM | Open |

Table D.2.2 (a): Log of output parameters for cross-check testing between pneumatic pump and syringe pump (first part)

| OUTPUT PARAMETERS | | | | | | | |
|---|---|---|---|---|---|---|---|
| **Syringe Setting** | **Trial Number** | **Time Elapsed (Time Taken to Empty Syringe)** | | **Time Remaining** | **Recorded Infused Volume[a]** | **Volume Left in Syringe[b]** | **Measured Output Volume[c]** |
| | | **HH:MM:SS** | **minutes** | **HH:MM:SS** | **(ml)** | **(ml)** | **(ml)** |
| Custom syringe, 2 ml (8.91mm ID) | 1 | 1:05:22 | 65 | 0:01:08 | 1.96 | 0.0 | 1.2 |
| | 2 | 1:03:11 | 63 | 0:03:19 | 1.89 | 0.0 | 0.9 |
| | 3 | 1:06:30 | 66 | 0:00:00 | 2.00 | 0.2 | 0.9 |
| KDS glass, 5 ml | 4 | 1:06:40 | 66 | 0:00:00 | 2.05 | 3.0 | 0.9 |
| KDS glass, 2 ml | 5 | 0:32:40 | 32 | 0:34:00 | 0.98 | 0.0 | 0.9 |
| Cadence glass, 2 ml | 6 | 1:04:40 | 64 | 0:02:00 | 2.92 | 0.0 | 0.8 |
| Cadence glass, 5 ml | 7 | 1:06:40 | 66 | 0:00:00 | 2.00 | 3.4 | 0.3 |
| KDS glass, 5 ml | 8 | 1:06:40 | 66 | 0:00:00 | 2.00 | 3.4 | 0.2 |
| | 9 | 1:06:40 | 66 | 0:00:00 | 2.00 | 2.8 | 0.2 |
| BD plasti-pak | 10 | 1:06:40 | 66 | 0:00:00 | 2.00 | 3.0 | 1.4 |
| | 11 | 1:06:40 | 66 | 0:00:00 | 2.00 | 1.0 | 1.9 |
| | 12 | 1:06:40 | 66 | 0:00:00 | 2.00 | 2.9 | 1.9 |
| | 13 | 1:06:40 | 66 | 0:00:00 | 2.00 | 3.0 | 1.9 |
| | 14 | 2:13:20 | 133 | 0:00:00 | 2.00 | 3.0 | 1.9 |
| | 15 | 2:13:20 | 133 | 0:00:00 | 2.00 | 3.0 | 1.9 |
| | 16 | 2:13:20 | 133 | 0:00:00 | 2.00 | 3.0 | 1.9 |

[a] Volume of fluid infused as shown on the syringe pump display (estimated by the pump)

[b] Volume of fluid that was not pumped out of the syringe by the syringe pump

[c] Volume of fluid that was pumped out of the pump (output fluid was collected in a 3 ml syringe)

[b, c] These volumes were compared with the recorded infused volume[a] to verify that the volume of fluid dispensed as displayed on the syringe pump matched the actual volume of fluid dispensed

Table D.2.2 (b): Log of output parameters for cross-check testing between pneumatic pump and syringe pump (second part)

| OUTPUT PARAMETERS | | | | | |
|---|---|---|---|---|---|
| **Syringe setting** | **Trial number** | **Calculated flow rate based on flow rate output Volume (µl/min)[a]** | **Average flow rate measured by flow meter (µl/min)[b]** | **Measured versus calculated flow rate error[c]** | **Comments/Pump status** |
| Custom syringe, 2 ml (8.91mm ID) | 1 | 18.46 | 18.93 | 3% | Motor stalled (error 217) - No more fluid left in syringe |
| | 2 | 14.29 | 18.79 | 32% | Motor stalled (error 217) - No more fluid left in syringe |
| | 3 | 13.64 | 17.49 | 28% | Infusion complete |
| KDS glass, 5 ml | 4 | 13.64 | 12.80 | 6% | Infusion complete |
| KDS glass, 2 ml | 5 | 28.13 | 35.67 | 27% | Motor stalled (error 217) - No more fluid left in syringe |
| Cadence glass, 2 ml | 6 | 12.50 | 16.84 | 35% | Motor stalled (error 217) - No more fluid left in syringe |
| Cadence glass, 5 ml | 7 | 4.55 | 16.84 | 271% | Infusion complete |
| KDS glass, 5 ml | 8 | 3.03 | 7.44 | 146% | Infusion complete |
| | 9 | 3.03 | 7.67 | 153% | Infusion complete |
| BD plasti-pak | 10 | 21.21 | 27.39 | 29% | Infusion complete, volume measurement not accurate. Collection syringe faulty. |
| | 11 | 28.79 | 28.15 | 2% | Infusion complete |
| | 12 | 28.79 | 28.58 | 1% | Infusion complete |
| | 13 | 28.79 | 28.53 | 1% | Infusion complete |

Table D.2.2 (b): Log of output parameters for cross-check testing between pneumatic pump and syringe pump (second part) [continued]

| OUTPUT PARAMETERS | | | | | |
|---|---|---|---|---|---|
| **Syringe setting** | **Trial number** | **Calculated flow rate based on flow rate output volume (µl/min)[a]** | **Average flow rate measured by flow meter (µl/min)[b]** | **Measured versus calculated flow rate error[c]** | **Comments/Pump status** |
| BD plasti-pak | 14 | 14.29 | 14.60 | 2% | Infusion complete |
| | 15 | 14.29 | 14.55 | 2% | Infusion complete |
| | 16 | 13.91 | 14.54 | 5% | Infusion complete |

[a] Calculated flow rate (µl/min) = Measured output volume (µl)/Time elapsed (min)

[b] Average flow rate measured by the pneumatic pump over the length of the trial

[c] Flow rate error = (Measured flow rate/Calculate flow rate – 1) x 100

## Appendix E: MicroXCT Tomographical Microscope

### E.1. Using the Xradia MicroXCT Tomographic X-Ray Microscope

Before using the Xradia MicroXCT microscope, training under Dr. Ye (IBER lab) is required. Training for this author took approximately three weeks. However, the length of training is highly dependent on the learning speed of the trainee, the availability of the microXCT microscope (machine is sometimes used by other students), and the time it takes for the microXCT microscope to produce micro-CT scans of the sample (dependent on the size and material of the sample). During training, Dr. Ye shows the trainee how to use the microXCT microscope and demonstrates how to obtain micro-CT scans of the sample. After approximately two to three demonstrations (two to three samples), the trainee operates the microXCT microscope by himself/herself under the supervision of Dr. Ye. Dr. Ye will no longer supervise the trainee after both Dr. Ye and the trainee are confident that the trainee is able to operate the microXCT without supervision.

#### *Internal Cost Rate*

The cost of using the microXCT microscope is as follows:

| | |
|---|---|
| Sample Setup/Operation | $45.00/hr |
| Tomography Acquisition | $10.00/hr |
| Reconstruction/Processing | $45.00/hr |
| Staff Time | $50.00/hr |

#### *Overview of Procedure*

Figure E.1.1 is a chart that shows the main processes and programs involved in taking a micro-CT scan using the microXCT. Take note that this is merely an overview, and training prior to using the microXCT is mandatory.

There are three main programs (XMController, XMReconstructor, XM3DViewer) and four main processes for obtaining a micro-CT image using the microXCT microscope. The four processes for obtaining a micro-CT image include (a) setup, (b) data acquisition, (c) reconstruction, and (d) 3D-viewing.

(a) Setup

Prepare the sample for the micro-CT scan by securing it on the pin vise with mounting putty as shown in Fig. E.1.2. Slowly rotate the sample 360° and visually inspect it to ensure that it remains as perpendicular to the table surface as possible at every rotation angle. Then, place the pin vise with the sample on the mounting platform in the microXCT chamber. This process takes approximately 0.5 hour.

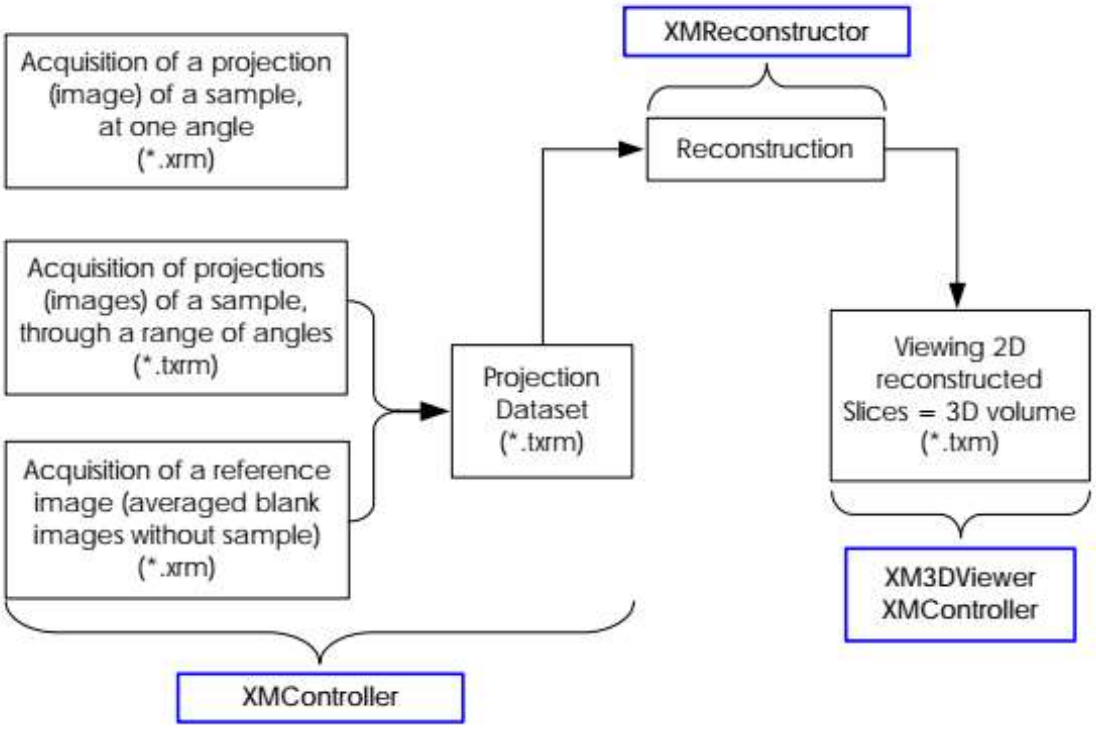


Fig. E.1.1: MicroXCT data, processes and files (reproduced from Ref. 53)

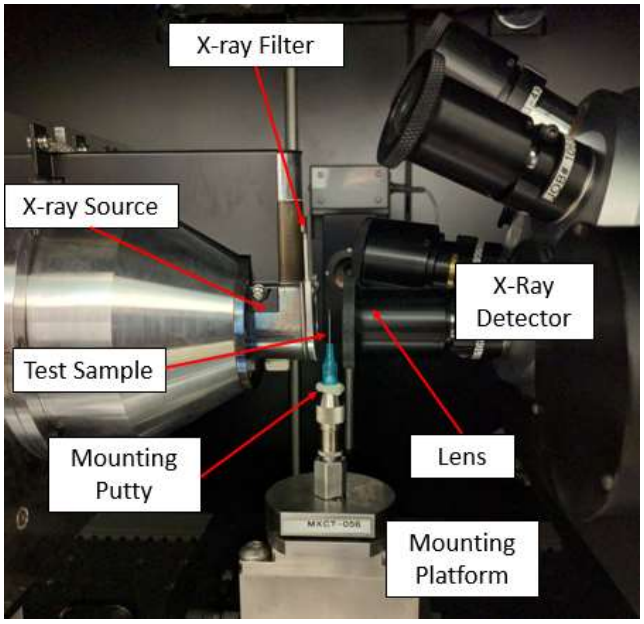


Fig. E.1.2: Setup of sample inside micro-CT

(b) Data acquisition

Data acquisition (a.k.a. tomography acquisition) involves taking multiple images of the sample at different angles of rotation. Data acquisition is performed using the XMController program. Before data acquisition, the reference rotation axis must be set up, making the X and Z axis at the center of the sample for all degrees of rotation. The X and Z axes location is checked at 0° and 90° rotations. The process of setting up the reference rotation axis for data acquisition takes approximately 15 to 30 minutes. After setting up the rotation, the user selects the settings for data acquisition (e.g., number of images, number of reference images, and angle of rotation), then starts the data acquisition process. Data acquisition is an automated process. Therefore, the user does not need to be present after data acquisition begins.

For these samples, the 20x and 40x magnification lenses are used. The measurement accuracy for the 20x and 40x lenses are ± 1.5 μm and 1.0 μm, respectively. It is suggested that data acquisition for an annular sample with SS hypodermic tube and nichrome insert be performed at

20x magnification. Analysis of an annular sample that is composed of SS hypodermic tube and nichrome insert at 20x magnification will take a total data acquisition time of approximately 22 hours. For a VSD tube sample, data acquisition can be done at 20x or 40x magnification. 20x will provide a larger imaging area but less tomography detail, and measurements would be less precise. The total data acquisition time for a VSD tube sample at 20x magnification will take approximately 6 hours. At 40x, the total data acquisition time for a VSD sample should take approximately 15 hours. 40x magnification is recommended for taking micro-CT images of VSD tube samples. 20x magnification is recommended for the SS tube samples.

(c) Reconstruction

After data acquisition is complete, reconstruction of the images taken during data acquisition is done. The user has to manually open the XMReconstructor program to begin reconstruction. Reconstruction is done in order to create a 3D image from the acquired data/images and takes approximately 20 minutes.

(d) 3D-Viewing

Once reconstruction is done, the 3D image of the sample is available to be viewed using the XM3DViewer program. Open the XM3DViewer program to view, analyze, measure and save the sample images. The user can label the images, change the color contrast of the images and select different viewing options. The user can chose the desired images and export them as a report document in Microsoft Word. This process can take approximately 15 minutes to 1 hour, depending on the types of images and the clarity of the micro-CT images that were taken.

## E.2. Tubular Flow Trial Sample Micro-CT Images

Figures E.2.1, E.2.2 and E.2.3 are the micro-CT images of the 50 μm ID VSD tube samples

(Samples 1, 2 and 3) that were used for the 10-day trials described in Section 3.6.1, whose $\Delta P$ results are shown in Fig. 3.7 and Table 3.3 (±1.5 μm accuracy).

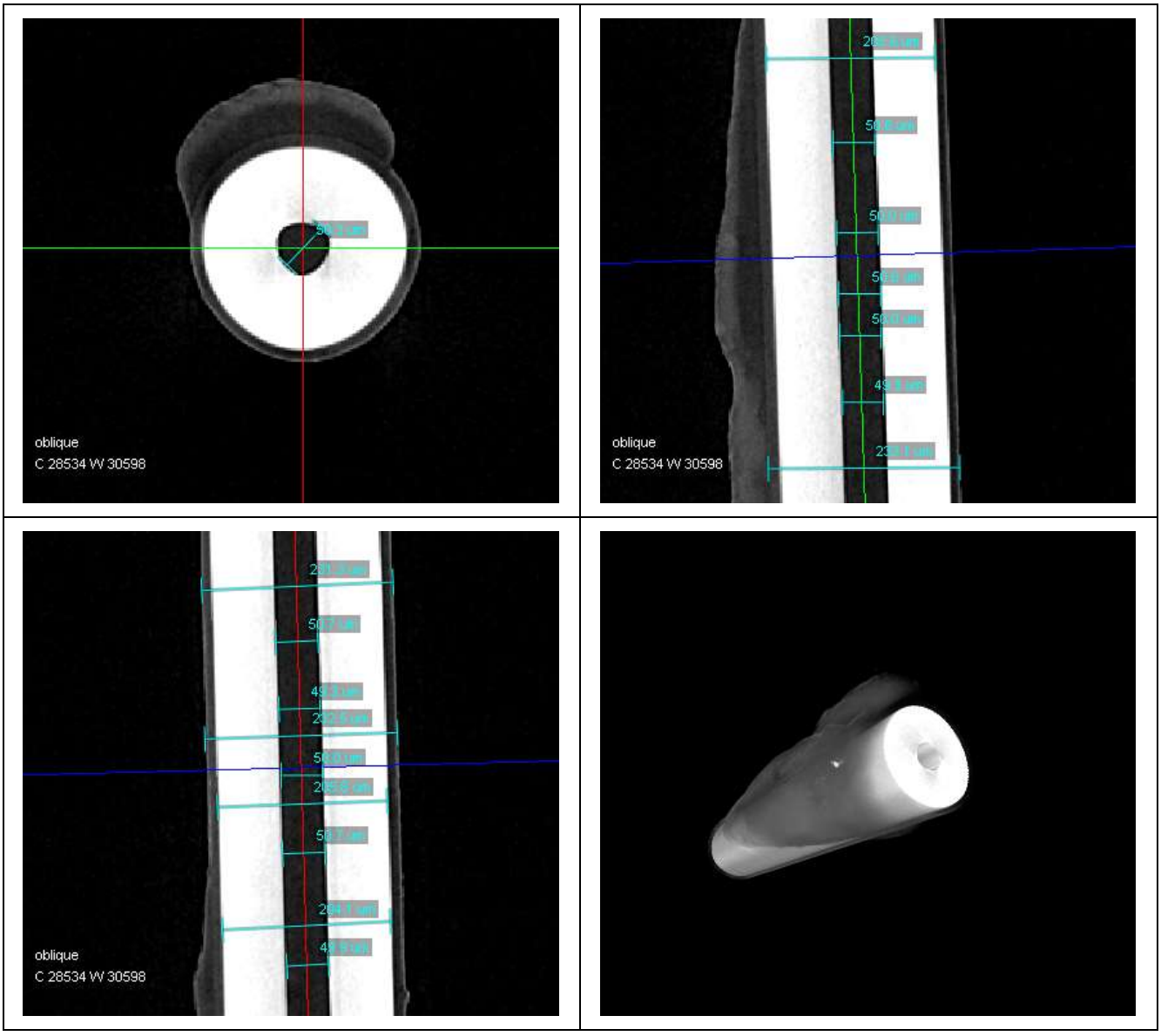


Fig. E.2.1: Micro-CT images of the 50 μm ID VSD tube Sample 1 after a 10-day trial. Views shown are: X-Y plane [top left], Y-Z plane [top right], X-Z plane [bottom left] and 3D view [bottom right] (magnification: 20x) [March 3, 2017]

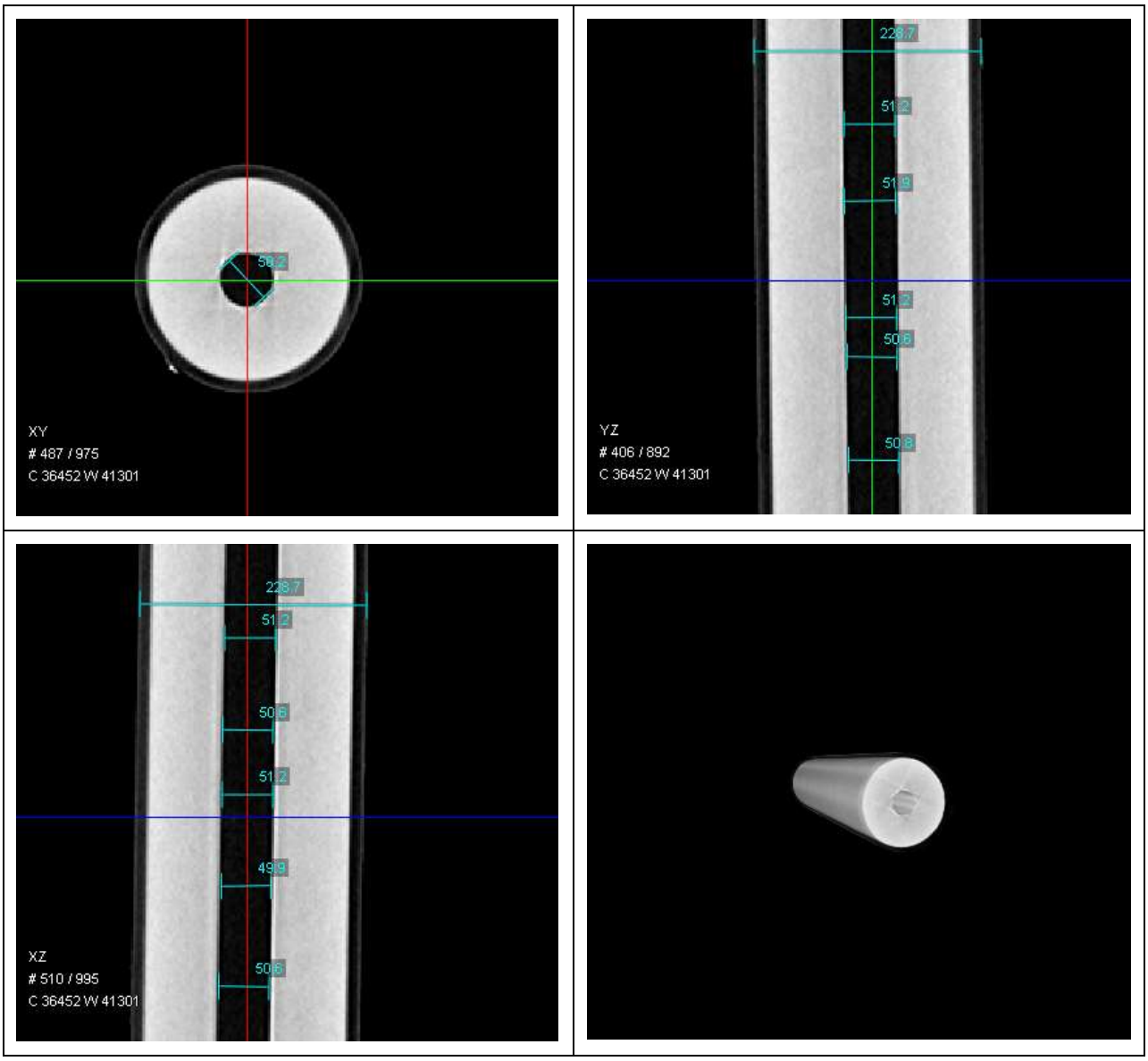


Fig. E.2.2: Micro-CT images of the 50 µm ID VSD tube Sample 2 after a 10-day trial. Views shown are: X-Y plane [top left], Y-Z plane [top right], X-Z plane [bottom left] and 3D view [bottom right] (magnification: 20x) [March 29, 2017]

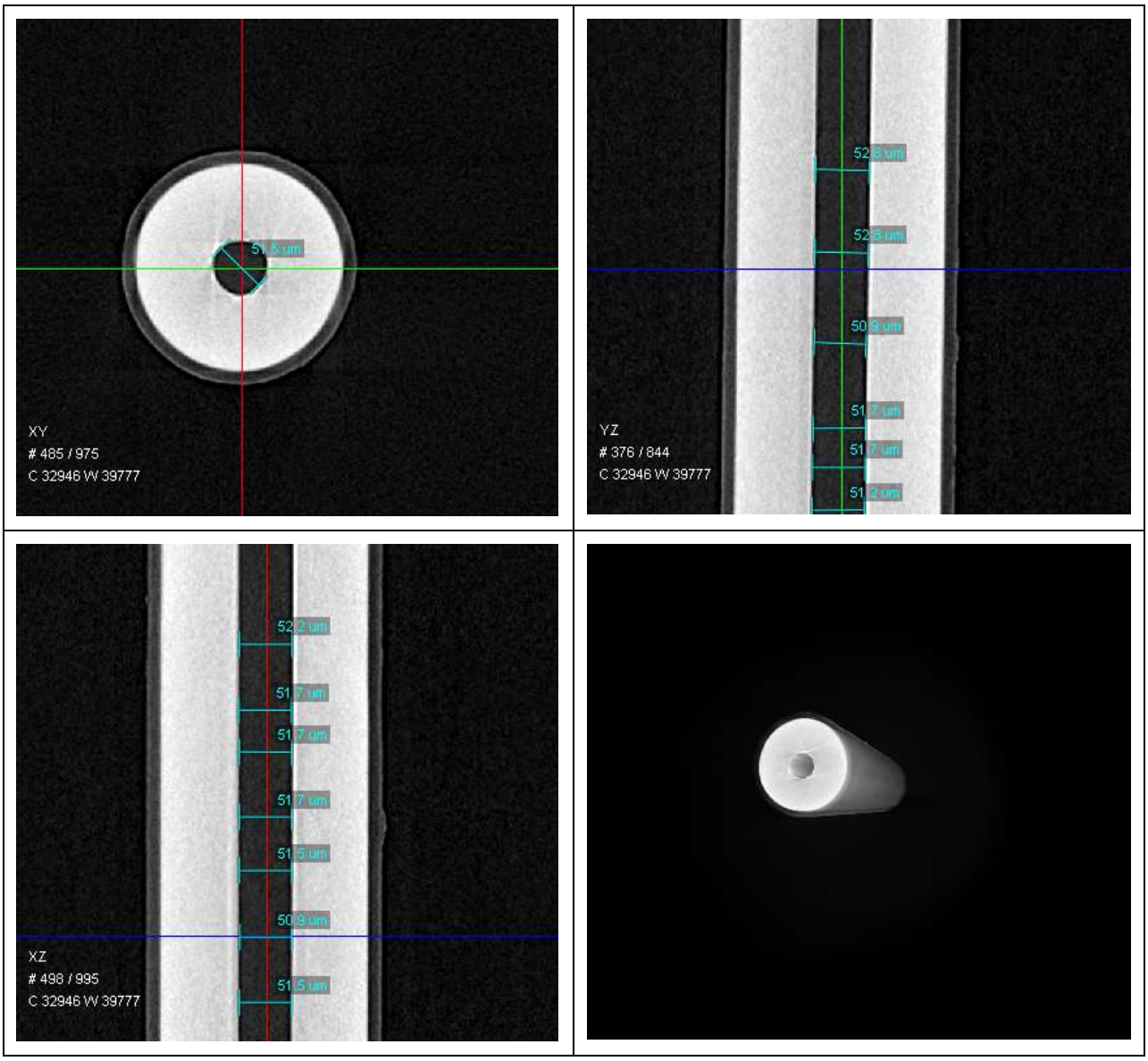


Fig. E.2.3: Micro-CT images of the 50 µm ID VSD tube Sample 3 after a 10-day trial. Views shown are: X-Y plane [top left], Y-Z plane [top right], X-Z plane [bottom left] and 3D view [bottom right] (magnification: 20x) [April 6, 2017]

The micro-CT images taken of the 75 µm ID VSD tube sample used for the 2-day trial described in Section 3.6.1 are shown in Fig. E.2.4 ($\Delta P$ results are shown in Fig. 3.7 and Table 3.3).

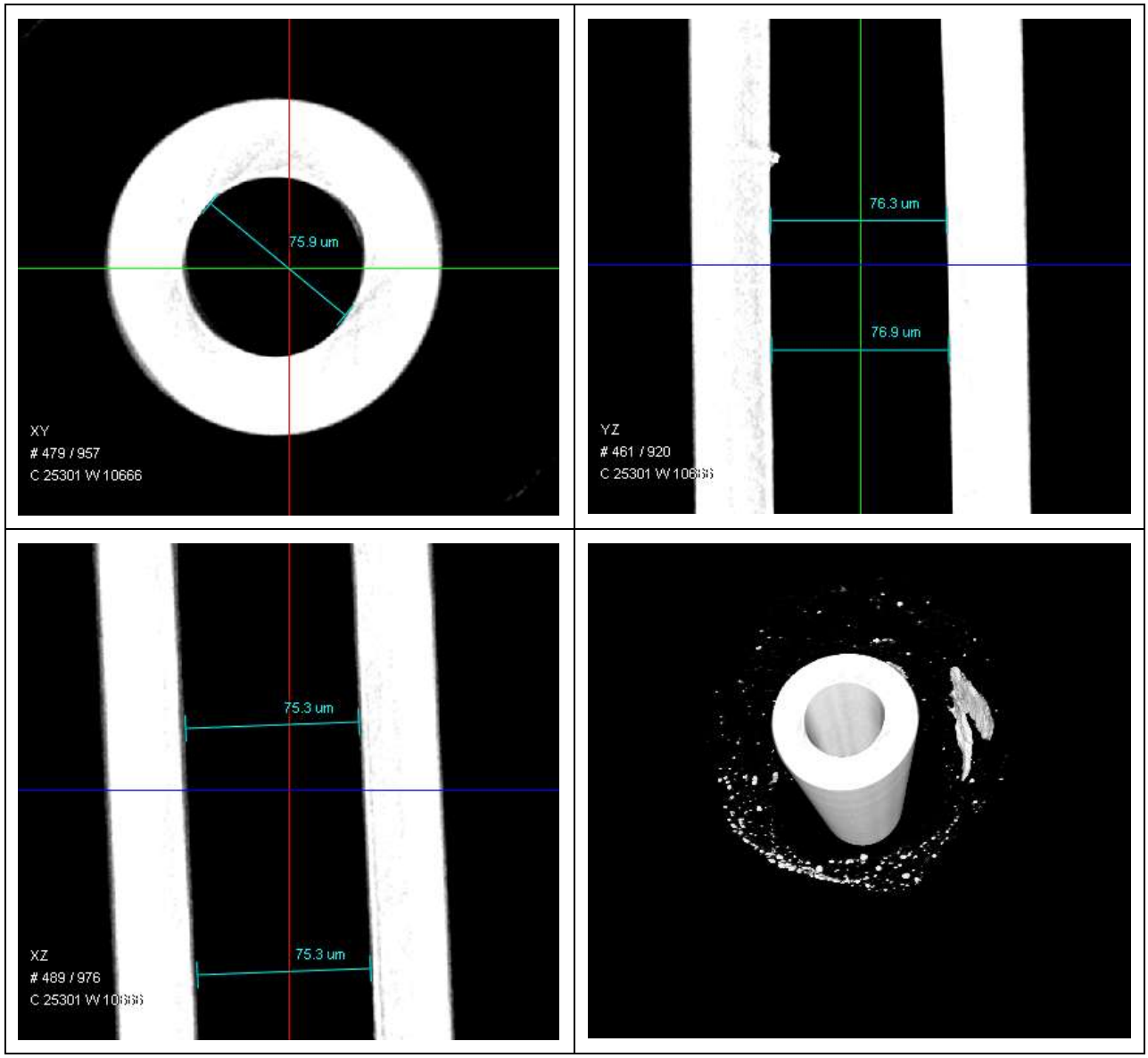


Fig. E.2.4: Micro-CT images of the 75 µm ID VSD tube sample after a 2-day trial. Views shown are: X-Y plane [top left], Y-Z plane [top right], X-Z plane [bottom left] and 3D view [bottom right] (magnification: 40x) [January 30, 2017]

## E.3. Annular Flow Trial Sample Micro-CT Images

Figures E.3.1 to E.3.5 are micro-CT scans of the samples used in the annular flow trials described in the submitted paper (Sections 3.1 to 3.7). Figures E.3.6 and E.3.7 are the micro-CT scans of the samples that were not discussed in the submitted paper (Section 3.8). The figures are sorted in the same order as for Table 3.4, according to $D_{eff}$, from the lowest to the highest.

Note that Fig. E.3.1 is different from Figs. E.3.2 to E.3.7. This was because these measurements were taken from the non-reconstructed images. During the time that the scans for Fig. E.3.1 were taken, there was a technical issue with the microXCT microscope, causing it to not be able to reconstruct a clear image after data acquisition. A reconstructed image would show the cross-sectional view of the sample, as well as showing more clearly the walls of the tube and the insert.

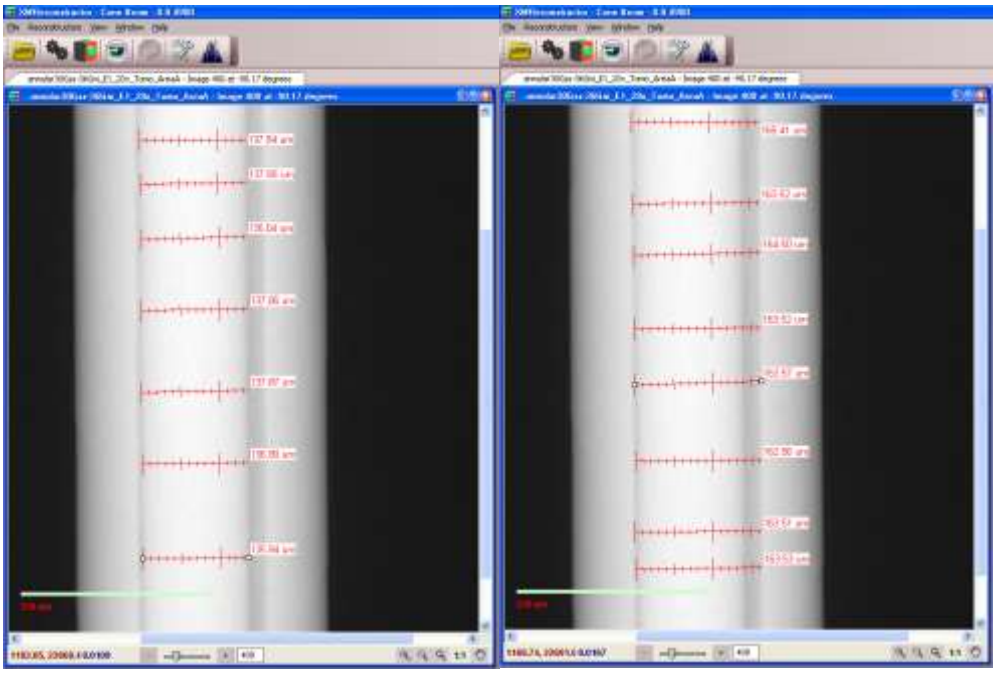

Fig. E.3.1: Micro-CT images of annular 30G SS hypodermic tube with 36G nichrome insert, Sample E1, without reconstruction with $D_i$ measurements [left] and $D_o$ measurements [right] (magnification: 20x) [April 25, 2017]

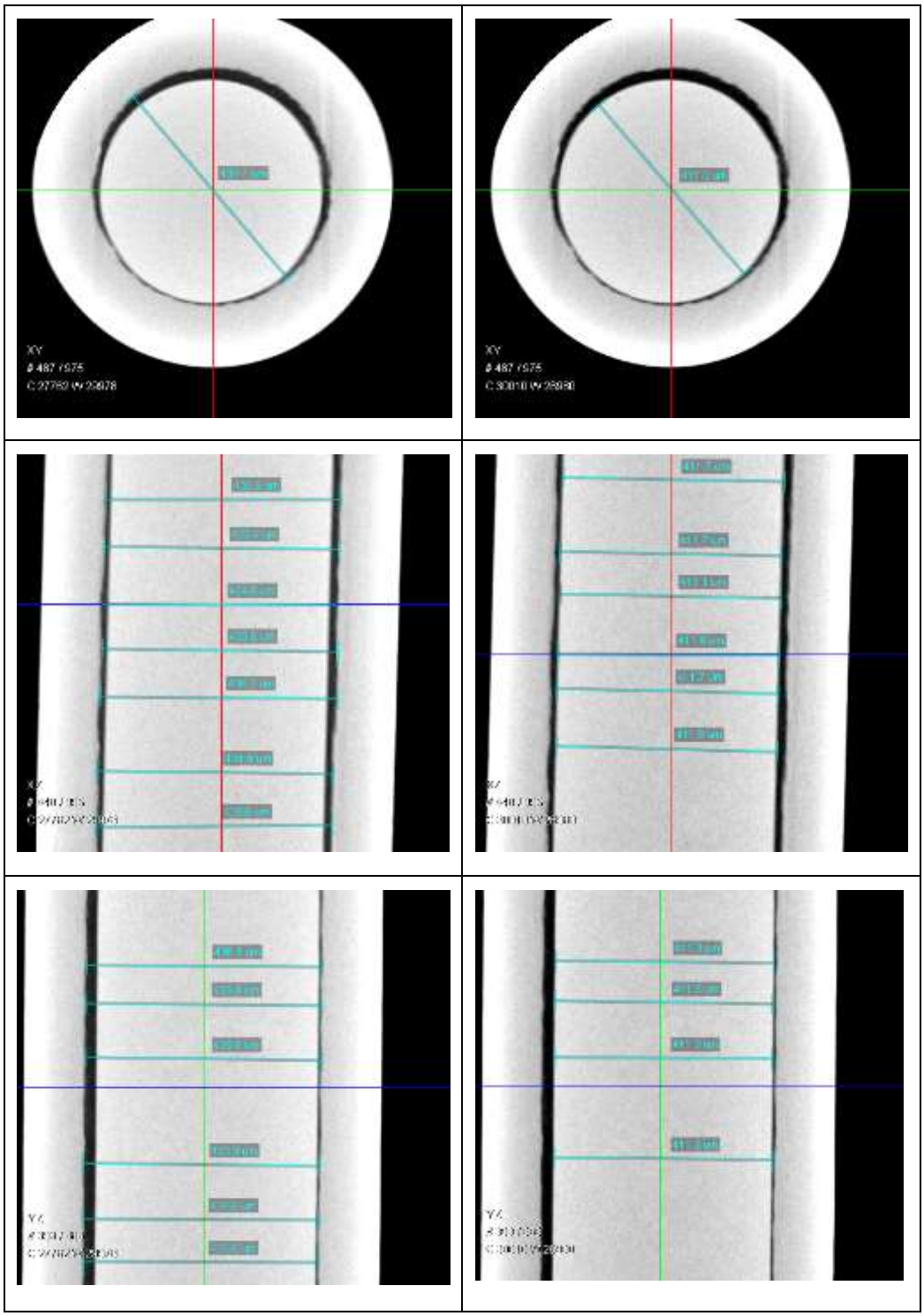

Fig. E.3.2: Micro-CT images of annular 23G SS hypodermic tube with 26G nichrome insert, Sample B1, with $D_o$ measurements in the X-Y plane [top left], X-Z plane [center left] and Y-Z plane [bottom left]; and with $D_i$ measurements in the X-Y plane [top right], X-Z plane [center right] and Y-Z plane [bottom right] (magnification: 20x) [April 11, 2017]

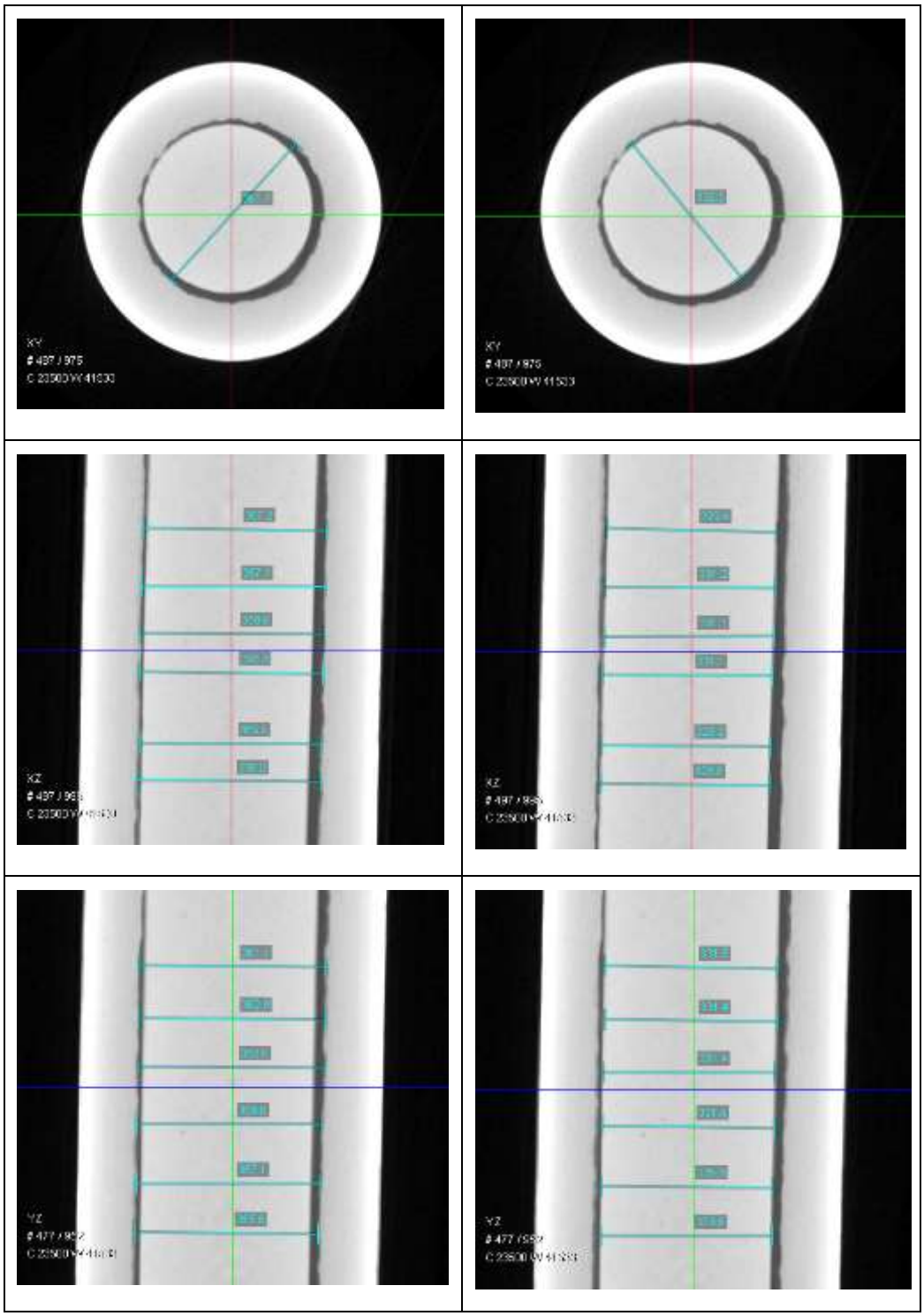

Fig. E.3.3: Micro-CT images of annular 24G SS hypodermic tube with 28G nichrome insert, Sample C01, with $D_o$ measurements in the X-Y plane [top left], X-Z plane [center left] and Y-Z plane [bottom left]; and with $D_i$ measurements in the X-Y plane [top right], X-Z plane [center right] and Y-Z plane [bottom right] (magnification: 20x) [April 24, 2017]

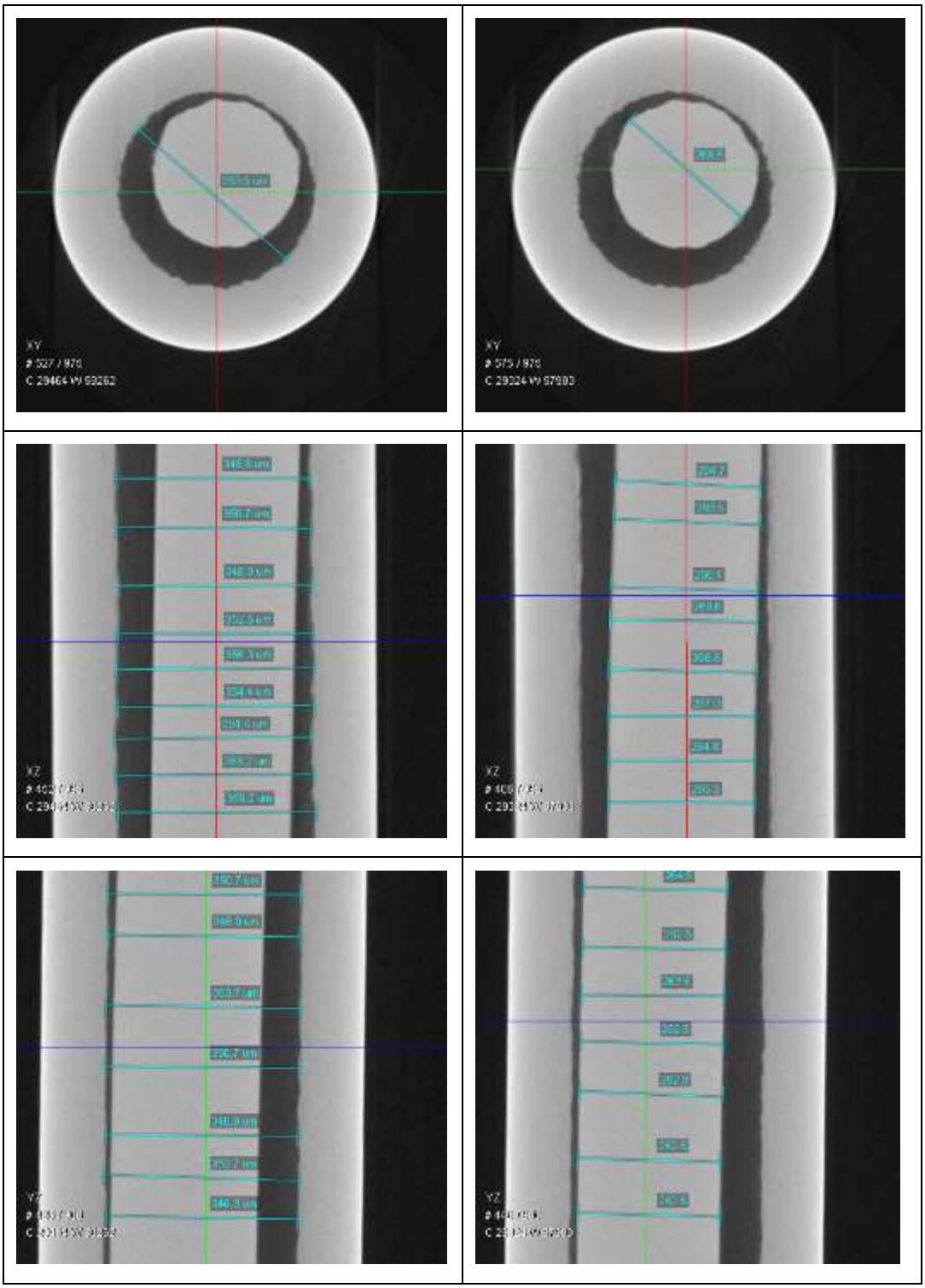

Fig. E.3.4: Micro-CT images of annular 24G SS hypodermic tube with 30G nichrome insert, Sample D1, with $D_o$ measurements in the X-Y plane [top left], X-Z plane [center left] and Y-Z plane [bottom left]; and with $D_i$ measurements in the X-Y plane [top right], X-Z plane [center right] and Y-Z plane [bottom right] (magnification: 20x) [April 14, 2017]

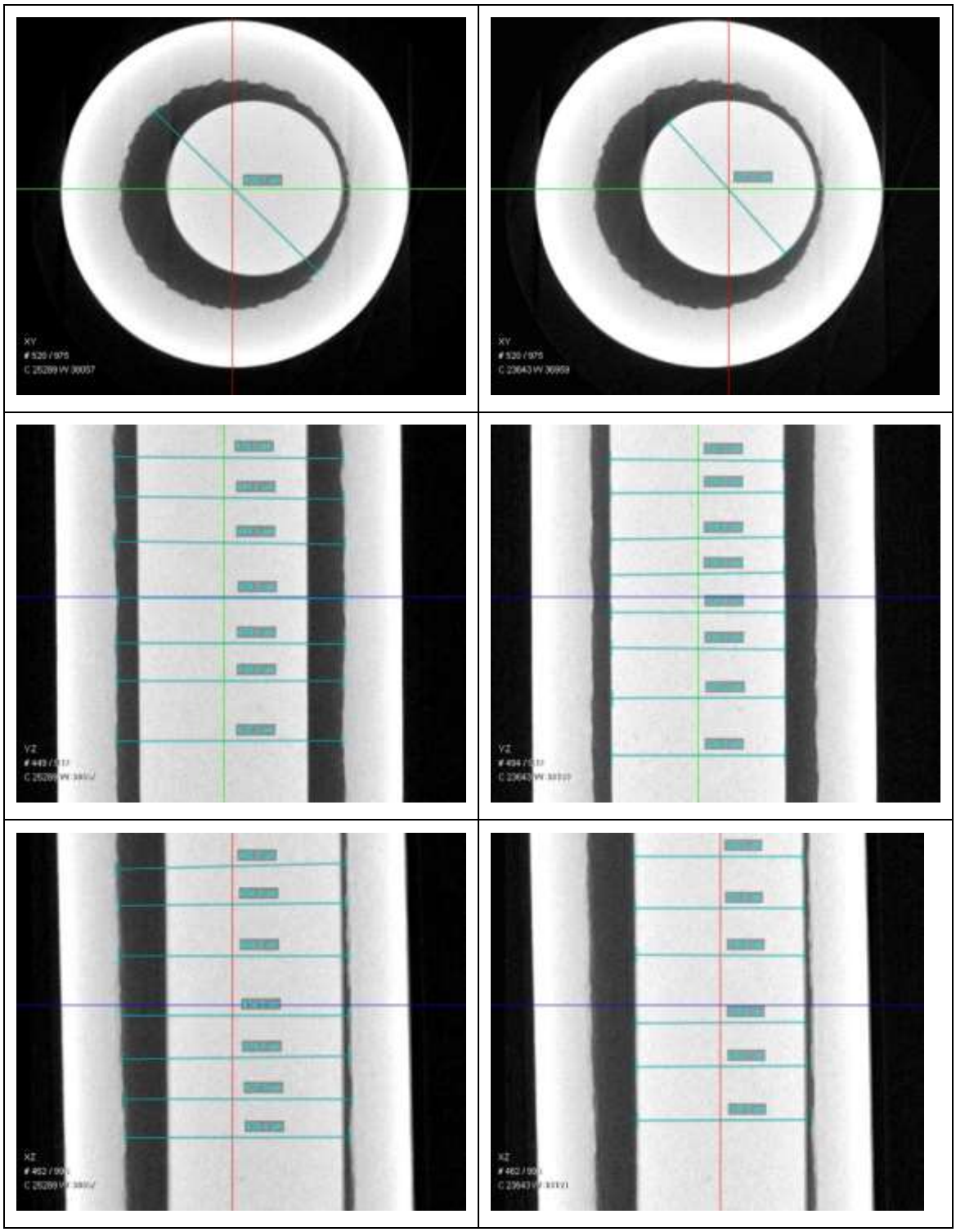

Fig. E.3.5: Micro-CT images of annular 23G SS hypodermic tube with 28G nichrome insert, Sample A1, with $D_o$ measurements in the X-Y plane [top left], X-Z plane [center left] and Y-Z plane [bottom left]; and with $D_i$ measurements in the X-Y plane [top right], X-Z plane [center right] and Y-Z plane [bottom right] (magnification: 20x) [April 26, 2017]

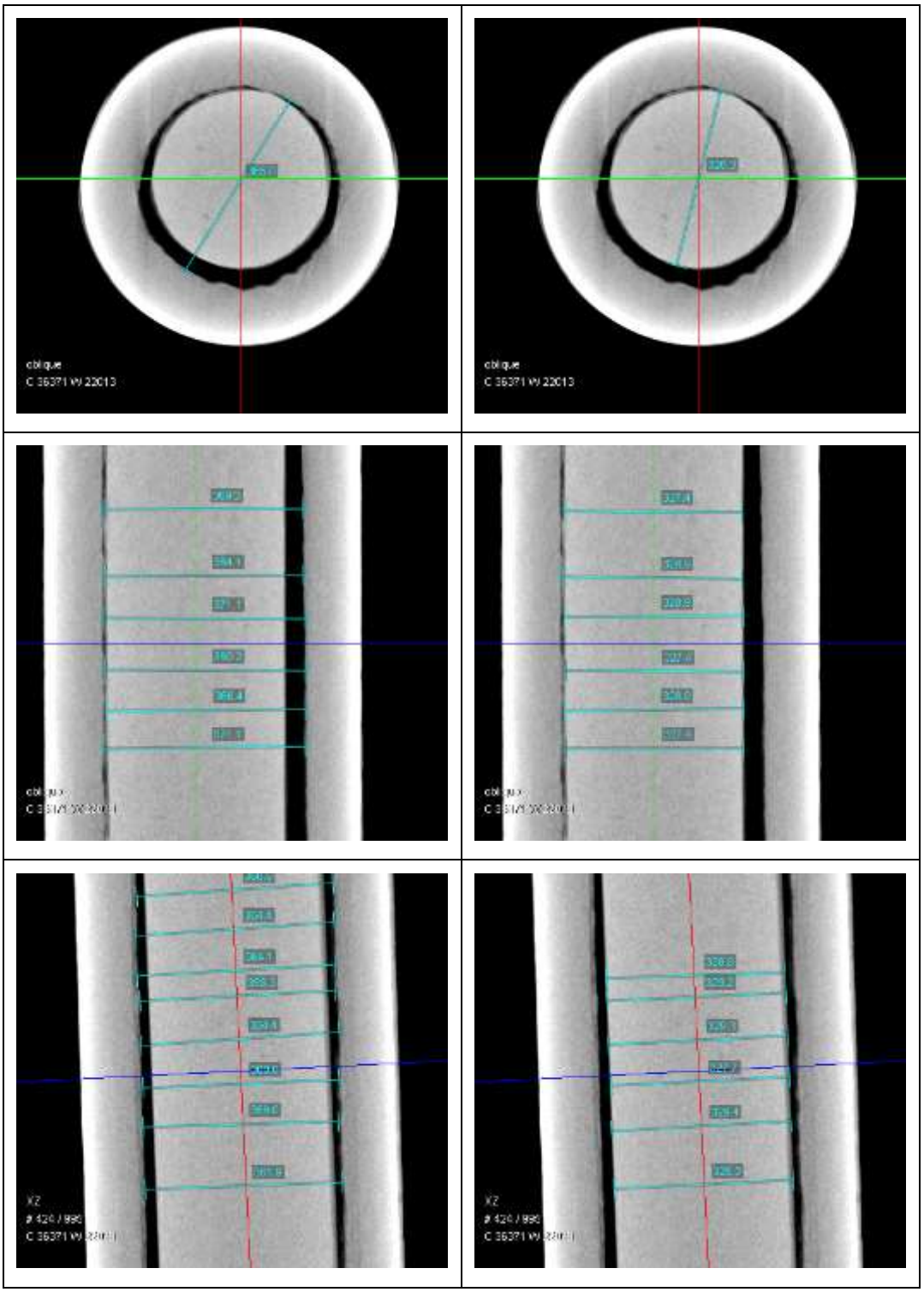

Fig. E.3.6: Micro-CT images of annular 24G SS hypodermic tube with 28G nichrome insert, Sample C02, with $D_o$ measurements in the X-Y plane [top left], X-Z plane [center left] and Y-Z plane [bottom left]; and with $D_i$ measurements in the X-Y plane [top right], X-Z plane [center right] and Y-Z plane [bottom right] (magnification: 20x) [May 1, 2017]

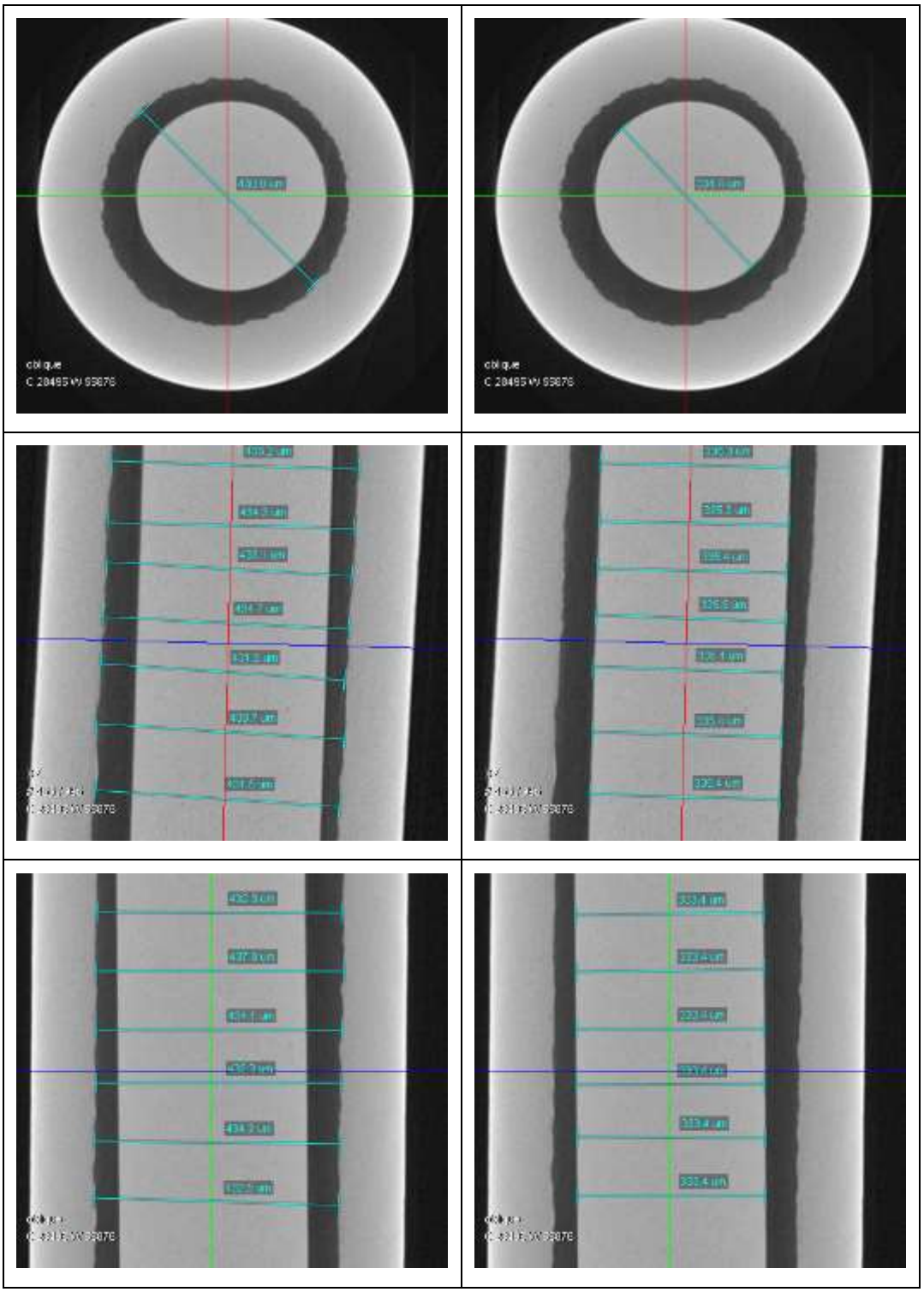

Fig. E.3.7: Micro-CT images of annular 23G SS hypodermic tube with 28G nichrome insert, Sample A2, with $D_o$ measurements in the X-Y plane [top left], X-Z plane [center left] and Y-Z plane [bottom left]; and with $D_i$ measurements in the X-Y plane [top right], X-Z plane [center right] and Y-Z plane [bottom right] (magnification: 20x) [May 1, 2017]

## Appendix F: Resolving Continuously Increasing $\Delta P$ and General Troubleshooting

### F.1. Preparing Bleach Solution and Sodium Azide Solution

Materials and equipment: bleach, deionized (DI) water, sodium azide ($NaN_3$) powder, 200 ml and 800 ml beakers, precision weighing scale (0.0001 g), nitrile gloves, poncho/lab coat

Access to materials and equipment: $NaN_3$ powder can be obtained from Qian (post-doc student in Berkland lab). Qian can also prepare the solution. These procedures are given in case Qian is unable to prepare the solution (Qian's email address: jianqian@ku.edu). A precision weighing scale is available in the IBER lab. Contact Dr. Ye for access (Dr. Ye's email address: yeq@ku.edu).

#### *a. Preparing 10% Bleach Solution*

Solution concentration (volume/volume): 10%

Volume of solvent (DI water): 250 ml

Volume of solute (bleach): 25 ml

***Caution***: DO NOT allow contact of bleach with body or clothes. Wear gloves and a protective layer over clothes during handling (poncho is available in the lab).

***Disposal***: Discard down the drain and dilute with running water.

***Procedure*:**

1. Rinse out the 200 ml and 800 ml beakers with DI water.
2. Measure 25 ml of bleach using the 200 ml beaker.
3. Fill the 800 ml beaker with 250 ml of DI water.
4. Pour the 25 ml of bleach into the 800 ml beaker of DI water and mix thoroughly.

***b. Preparing 0.04% $NaN_3$ Solution***

Solution concentration (mass/volume in units of g/ml x 100): 0.04%

Volume of solvent (DI water): 3785 ml (1 gallon)

Mass of solute ($NaN_3$ powder): 1.514 g

***Caution***: DO NOT allow any contact of $NaN_3$ powder with metal because $NaN_3$ powder explodes when in contact with metal. Use gloves during handling. READ $NaN_3$ safety data sheet (SDS) before use. The SDS for $NaN_3$ can be found at the link below:

https://www.sigmaaldrich.com/catalog/product/sial/s2002?lang=en&region=US

***Disposal***: DO NOT discard $NaN_3$ powder or $NaN_3$ solution down the drain. Pour solution in plastic/glass waste container and send for disposal through KU-EHS. DO NOT mix solution with acidic substances. Print the hazardous material waste container label available from the KU-EHS website, fill out the label and paste it on the waste container. The label can also be found from the link below:

https://ehs.ku.edu/sites/ehs.ku.edu/files/docs/hmep/hazmatlabel.pdf

Submit a request for waste disposal pickup using the link below:

https://ehs.ku.edu/hazardous-materialswaste-pickup-request

Remember to write the date on which the request was submitted on the waste container label.

***Procedure*:**

1. Rinse and fill a 1 gallon plastic container with DI water.
2. To zero the precision weighing scale, place an empty anti-static weighing boat (small light

polystyrene containers for weighing liquid or powdered samples) on the balance and press the <Tare> or <Zero> button (varies depending on scale).

*A precision weighing scale is available in the IBER lab. Contact Dr. Ye for access (yeq@ku.edu).*

3. Pour the powder into the weighing boat and place it on the balance. Remove or add more powder from/to the weighing boat until there is 1.514 g of $NaN_3$ powder in the boat.
4. Carefully pour the 1.514 g of $NaN_3$ powder into the 1 gallon container containing DI water, then shake the bottle to thoroughly mix the solution.

## F.2. Cleaning and Sterilization Protocol

The anti-microbial cleaning and sterilization protocol is to be performed once every one or two months.

***Materials Required***

10% bleach solution [see App. F.1(a) for preparation], isopropyl alcohol (IPA), deionized (DI) water, 0.04% sodium azide ($NaN_3$) solution [see App. F.1(b) for preparation], Tuttnauer Brinkmann 2340EA Autoclave (available in the IBER lab, contact Dr. Ye for access)

***Procedure***

10% bleach solution flush

1. Rinse out the glass bottle from the setup with DI water (refer to Figs. 2.1 and 2.2, which show the location of the glass bottle in the setup).
2. Pour approximately 100 ml of 10% bleach solution into the glass bottle before closing the cap.

3. Turn on the pump and set the pump to a flow rate of 15 μl/min. Ensure that there is no sample at the end of the test section.
4. Allow the pump to run over night (~12 hours).

DI water flush

5. Immediately after the 10% bleach flush is complete, stop the pump, remove the bottle's cap and discard the leftover bleach solution.
6. Rinse out the glass bottle and pour approximately 100 ml of DI water into the bottle.
7. Replace the bottle cap and start the pump at a flow rate of 15 μl/min.
8. Allow the pump to run for at least 5 hours.
9. Stop the pump, remove the bottle cap and discard the leftover DI water from the bottle.

IPA flush

10. Immediately after the DI water flush is complete, pour approximately 50 ml of IPA into the glass bottle.
11. Replace the bottle cap and start the pump at a flow rate of 15 μl/min.
12. Allow the pump to run over night (~12 hours).

DI water flush

13. Immediately after the IPA flush is completed, stop the pump, rinse out the glass bottle and pour approximately 100 ml of DI water into the bottle.
14. Replace the bottle cap and start the pump at a flow rate of 15 μl/min.
15. Allow the pump to run for at least 5 hours.

Bottle autoclave

16. Stop the pump and remove the glass bottle from the setup.
17. Pour out the contents of the glass bottle and rinse with DI water.
18. Autoclave the glass bottle. DO NOT autoclave the cap. Two glass bottles can be autoclaved at one time. Press the "Unwrapped instrument" program key on the autoclave control panel. [refer to user manual placed on top of the autoclave]
19. After autoclaving, carefully remove the glass bottle from the autoclave chamber. Be sure to cover the mouth of the glass bottle with a clean paper towel during transport to prevent any impurities from entering the bottle.
20. Pour approximately 200 ml of 0.04% $NaN_3$ solution into the autoclaved glass bottle and replace the bottle cap.
21. Turn on the pump and start the pump at 15 μl/min for approximately 5 hours before performing any trials.
22. At this point, the system should be ready for trials, without concern for microbial growth (for at least one to two months). If the pressure continuously increases during future single tube flow trials or annular non-degradable insert trials, repeat the cleaning process even if one month has not passed since the last cleaning.

## F.3. Potential Issues and Troubleshooting Steps

Table F.3.1 lists the potential problems that may arise during trials and the recommended steps for resolving them.

Table F.3.1: List of potential issues and the procedures recommended for troubleshooting

| Potential Issue | Recommended Troubleshooting Steps |
|---|---|
| The pump does not maintain the set flow rate | 1. Turn the pumps off and on again.<br>2. Reset the computer.<br>3. Disconnect the 1/32 in. PEEK tubing from the 1/16 in. clear tubing. For at least 5 hours, purge pump at high flow rate of 30 μl/min to remove possible air bubbles trapped in the pump tubing.<br>4. As a precautionary step to prevent damage to the transducers when the flow rate is high, close the inlet of the three-way valve connected to the transducer. *Do not forget to reopen the three-way valve before performing flow trials.*<br>5. Perform cleaning and sterilization procedure. |
| Δ*P* continuously increases with time during a flow trial with inserts that should not change in size, or with an open tube | 1. Check for air bubbles in the tube lines.<br>2. Remove any sample and purge the pump at high flow rate of 15 μl/min.<br>3. Replace current sample with a new sample.<br>4. Perform cleaning and sterilization procedure. |
| Δ*P* decreases drastically in a short time, or Δ*P* is very much lower than expected (especially for single tube VSD flow trials) | 1. Tubing at test section is leaking fluid. Check for leaks and replace tubing.<br>2. Test sample is leaking at super glue connection (mainly for VSD and BGI samples). Replace test sample. |
| Δ*P* is consistently too low or is below zero | 1. Three-way valve is closed. May have forgotten to reopen three-way valve at inlet connected to transducer. |

## Appendix G: AGV Trial Procedures and Test Fluid Specifications

The following sections describe the procedures for performing trials with AGVs as well as the steps for preparing the AGV samples. The following sections also describe the specifications for the ophthalmic surgical fluid devices (OVDs and silicone oil) that were used in the AGV trials discussed in Sections 4.2.2 and 4.2.3.

### G.1. AGV Sample Preparation

1. Remove a new AGV from its sealed package.
2. Connect the AGV to a 30G SS dispensing tip as shown in Fig. G.1.1.

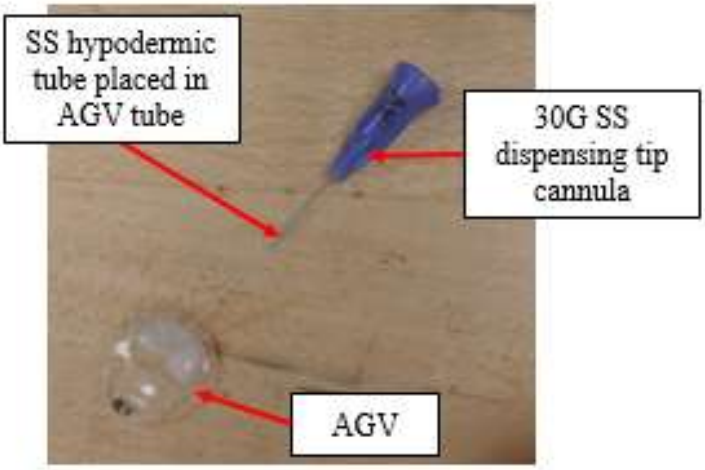


Fig. G.1.1: AGV sample configuration

3. If the sample is to be manually primed before the flow trial, fill a syringe with DI water and connect the syringe to the 30G SS cannula. Push on the syringe piston, flushing DI water through the AGV. A stream of water should shoot out of the AGV without much resistance.

If a stream of water does not shoot out of the AGV (only droplets forming at the AGV plate), the AGV is defective. Discard the AGV and use a non-defective AGV for the trial.

## G.2. Experimental Setup with Sample Attached

1. Place a 200 ml beaker at the end of the tube end as shown in Fig. G.2.1.

*If the 1/8 in. ID medical grade tubing is not long enough to ensure that the three-way valve does not lift off the test section surface, connect more 1/8 in. tubing as shown in Fig. G.2.1.*

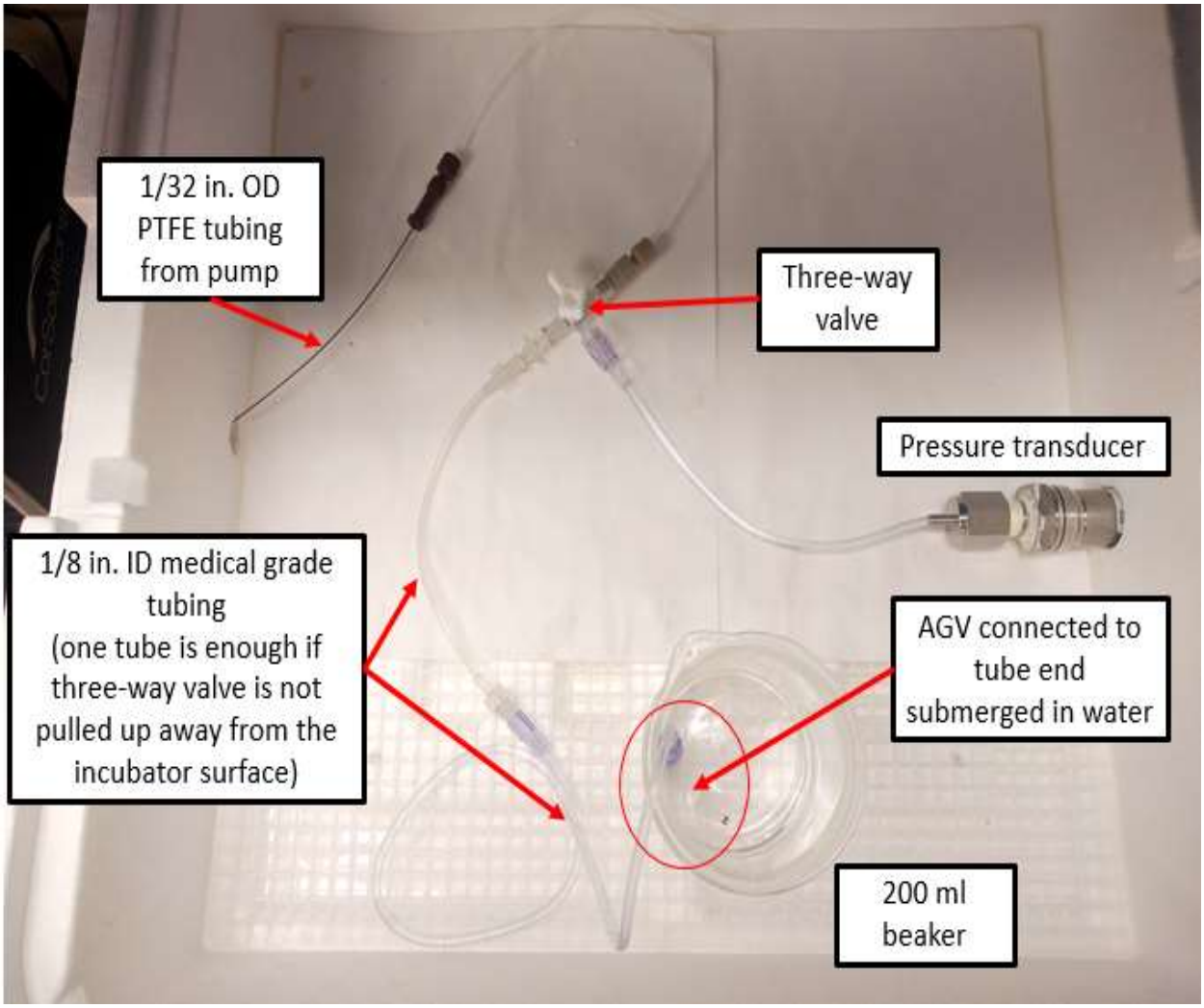


Fig. G.2.1: Configuration of AGV trial experimental setup

2. Fill the beaker with DI water up to the 50 ml mark.
3. Place the prepared AGV sample in the beaker filled with DI water, ensuring that the AGV is submerged entirely in water as shown in Fig. G.2.2.

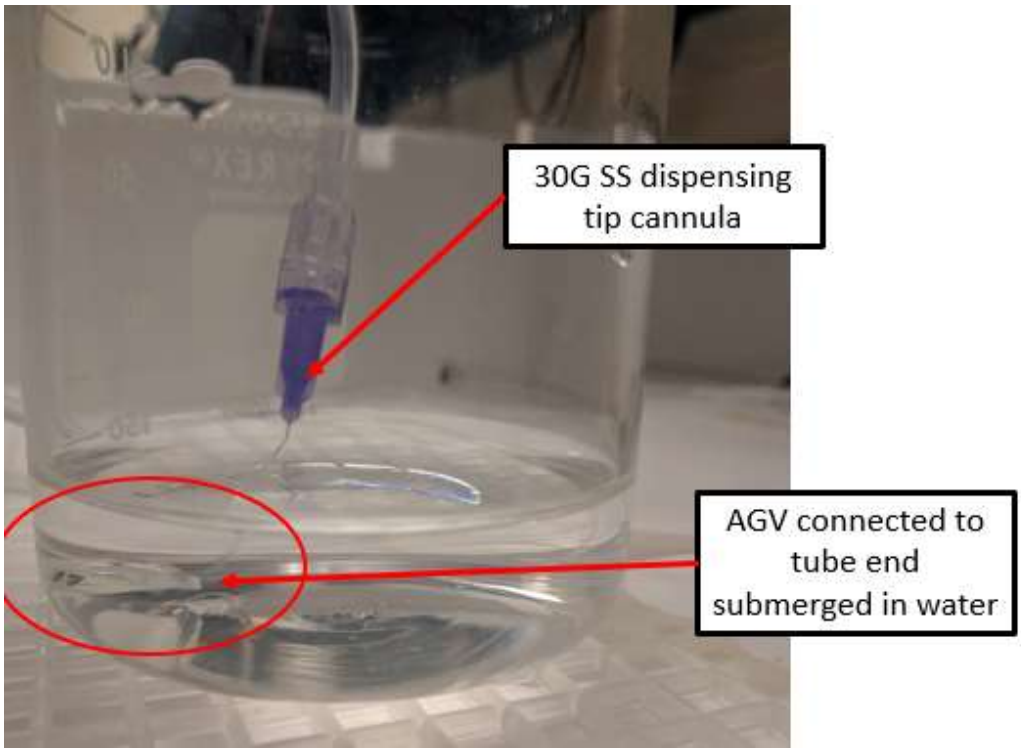


Fig. G.2.2: AGV trial sample placed in beaker

## G.3. Experimental Procedure

Stages 0, 1 and 4 of the general testing and data collection procedures described in App. B.1 can be applied to the AGV trials with the setup configured as shown in Fig. G.2.1. However, for the AGV flow trials, Stages 2 and 3 are different from the general procedures in App. B.1.

***Stage 0: Turning on the Pumps***

All Stage 0 procedures are the same as the general procedures for Stage 0 in App. B.1 except that the sample is configured as shown in Fig. G.2.1.

***Stage 1: Measuring Baseline $\Delta P$***

The Stage 1 procedure is the same as the general procedures for Stage 1 in App. B.1. In this stage, the AGV is not connected to the tube-to-sample luer lock connection. Only the 30G SS cannula is connected to the tube end of the test section and submerged in water in the beaker.

***Stage 2: Measuring ΔP Caused by AGV***

1. After measuring the baseline Δ*P* in Stage 1, attach the AGV sample to the 30G SS cannula that was secured to the tube-to-sample connection.
2. On the experiment log sheet, record the time that the AGV sample was attached in the "Time-Prime/AGV" space (Fig. D.1.1).

3a. If the purpose of the trial is to measure the Δ*P* modulation caused by the AGV, proceed to Stage 4 (Skip Stage 3).

3b. If purpose of the trial is to study the Δ*P* modulation when OVDs or silicone oil flows through the AGV, proceed to Stage 3.

***Stage 3: Measuring ΔP Caused by OVD or Silicone Oil in AGV***

1. After ~20 minutes of logging baseline Δ*P* with the AGV sample attached to the tube-to-sample connection, remove the AGV sample from the 30G SS dispensing tip. Record the time that the AGV was removed on the Experiment Log sheet in the "Time-Trial" space (Fig. D.1.1).

If using OVD (Viscoat or ProVisc):

2. Remove the desired OVD (Viscoat or ProVisc) syringe from the DuoVisc box. The box contains two syringes (one with Viscoat and the other with ProVisc), two 27G angled cannulas (dispensing tips), and two cannula locking rings.
3. Place the provided 27G dispensing tip over the mouth of the syringe and lock the dispensing tip to the syringe with the cannula locking ring as shown in Fig. G.3.1.
4. Insert the end of the 27G dispensing tip into the tube of the AGV sample as shown in Fig. G.3.1.

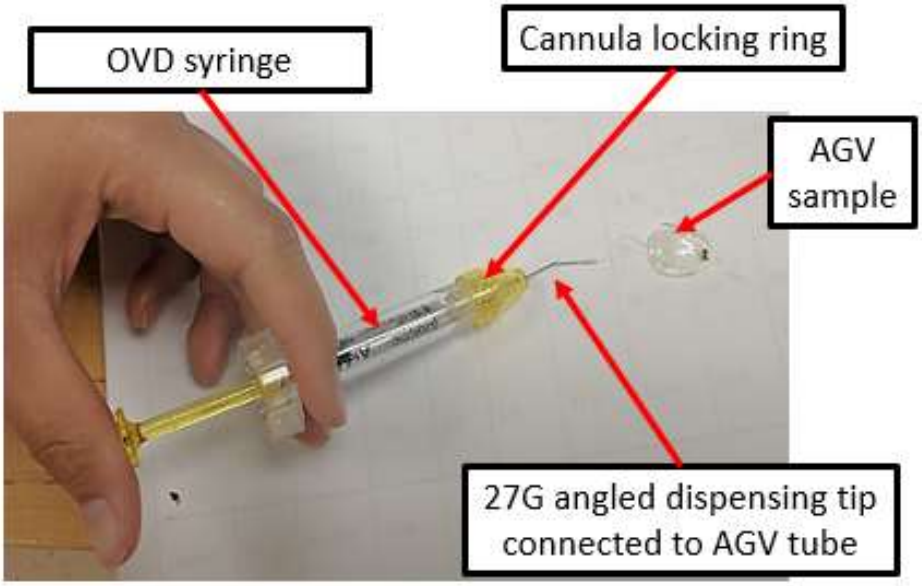


Fig. G.3.1: Injecting OVD into the AGV tube

5. Push the syringe piston in order to dispense the OVD from the syringe into the AGV tube. Ensure that the OVD does not pass through the valve of the AGV sample. (Allow an air bubble into the AGV tube when inserting the 27G dispensing tip in order to clearly see the OVD enter the AGV tube)
6. Disconnect the AGV sample from the OVD syringe's 27G dispensing tip and return it to the tube-to-sample connection at the test section as shown in Fig. G.2.2.
7. Record the time that the AGV sample is reconnected to the tube-to-sample connector on the Experiment Log in the "Time-Trial" space (Fig. D.1.1).

If using silicone oil (pure or emulsified):

2. Draw 1 ml of silicone oil from the Alcon silicone oil bottle using a clean syringe (without a dispensing tip). If using pure silicone oil for the flow trial, skip to Step 5. If using emulsified silicone oil, continue to Step 3.

3. Dispense the 1 ml of silicone oil into a 5 ml centrifuge tube. Draw 1 ml of DI water into the syringe, and dispense the DI water into the 5 ml centrifuge tube containing the silicone oil. Shake vigorously for approximately 1 minute in order to properly prepare the emulsified silicone oil solution.
4. Draw approximately 1 ml of the emulsified silicone oil from the centrifuge tube into the syringe.
5. Place a 30G dispensing tip over the mouth of the syringe, then insert the 30G dispensing tip into the AGV tube, similar to that shown in Fig. G.3.1.
6. Push the syringe piston in order to dispense the silicone oil (pure or emulsified) from the syringe into the AGV tube. Ensure that the silicone oil does not pass through the valve of the AGV sample. (Allow an air bubble into the AGV tube when inserting the 30G dispensing tip in order to clearly see the silicone oil enter the AGV tube)
7. Disconnect the AGV sample from the silicone oil syringe's 30G dispensing tip and reconnect it to the tube-to-sample connector at the test section as shown in Fig. G.2.2.
8. Record the time that the AGV sample is reconnected to the tube-to-sample connector on the Experiment Log sheet in the "Time-Trial" space (Fig. D.1.1).

***Stage 4: Retrieving, Processing and Saving Data Collected***

All Stage 4 procedures here are the same as the Stage 4 procedures in App. B.1.

## G.4. Viscoat, ProVisc and Silicone Oil Specifications

The following lists the properties and specifications of Viscoat, ProVisc [79] and Silikon 1000 [80].

***VISCOAT OVD***

| | |
|---|---|
| Volume: | 0.35 or 0.50 ml |
| Components: | 3% Sodium Hyaluronate, 4% Chondroitin Sulfate |
| Molecular Weight: | 600,000 Daltons |
| Dynamic Viscosity: | 40,000 cps |
| CDI:[a] | 3.5 |
| Classification: | Medium Viscosity Dispersive |
| Osmolality: | 325 Osm |
| Specialty: | 1. Better endothelial cell protection |
| | 2. Superior clarity and visualization |
| | 3. Superior retention during lens removal |

***ProVisc OVD***

| | |
|---|---|
| Size: | 0.40 or 0.55 ml |
| Components: | 1% Sodium Hyaluronate |
| Molecular Weight: | 2,400,000 Daltons |
| Dynamic Viscosity: | 39,000 cps |
| CDI:[a] | 43 |
| Classification: | Viscosity Cohesive |
| Osmolality: | 310 Osm |
| Specialty: | 1. Superior anterior capsule dome maintenance |
| | 2. Proven mechanical protection of space maintenance |
| | 3. Easy to remove after procedure |

[a] *CDI = Cohesion/Dispersion Index (percent of viscoelastic solution aspirated per 100 mm Hg applied)*

***SILIKON 1000***

Chemical name: Purified polydimethylsiloxane

Specific gravity: 0.97 (lower than water and AH)

Dynamic viscosity: 1000 cps (at 25°C)

Refractive index: 1.40

Supply information: 10 ml glass vial filled with 8.5 ml of sterile silicone oil

## Appendix H: NIH R03 Grant Proposal Submitted

The following is the Specific Aims and Research Strategy sections of the National Institute of Health (NIH) R03 grant proposal that was submitted to the National Institute of Arthritis and Musculoskeletal and Skin Diseases (NIAMS) on June 16th, 2017. The authors for this grant were: this author, Dr. Ronald Dougherty and Dr. Sara Wilson. The proposal was declined after approximately three months. The main reason for being declined was because there were insufficient publications regarding this research to support the feasibility of the proposed research. Therefore, it is recommended that a paper on the topic of this research be published prior to resubmission of this proposal. Note that the references for the proposal are at the end of the proposal on pages 260 - 263.

### I. Specific Aims

Glaucoma is a class of eye diseases that damages the optic nerve, leading to the progressive loss of vision. In 2011, it was reported that 2.71 million people in the US (44.77 million worldwide) had primary open angle glaucoma (POAG), and it is anticipated that by 2050, US POAG cases will increase to 7.32 million.[1] In severe glaucoma cases where the patient's intraocular pressure (IOP) levels cannot be controlled via laser trabeculoplasty and pharmocological treatments, glaucoma drainage implant surgery involving the insertion of a tube shunt into the eye is performed.[2] This type of glaucoma surgery has increased by ~300% over the past 25 years, while trabeculoplasty has decreased by ~15%.[3,4] The implanted tube allows for the drainage of excess fluid out of the eye, lowering the IOP to a safe level. Two commonly used glaucoma drainage devices are the valved Ahmed Glaucoma Valve (AGV) and the non-valved Baerveldt Glaucoma Implant (BGI).

BGIs have been reported to have higher and longer-term success rates in reducing and maintaining IOP levels, requiring less medication for IOP control as compared to AGVs; however, BGIs provide little to no aqueous humor (AH) flow resistance at the early post-operative (post-op) stages (4-6 weeks after surgery), causing vision-threatening hypotony-related complications (dangerously low IOP levels).[5,6] IOP control with BGIs is highly dependent on scar tissues forming around the episcleral plate of the BGI to provide sufficient post-op AH flow resistance. In efforts to provide initial post-op AH resistance, many intra-operative (intra-op) modifications to BGIs have been developed. These methods include a two-stage surgical method,[7] tube occlusion with a non-absorbable stent suture,[8,9] injection of viscoelatic solution into the anterior chamber of the eye,[10] and external ligation of the tube with an absorbable suture followed by tube fenestrations.[2,11,12] Although these methods provide relatively adequate early post-op IOP control, they are unable to lower IOP immediately after surgery (only lowers IOP after one week) nor provide consistent IOP control during the early post-op weeks (IOP increases again after approximately one month).[13,14] These intra-op methods have not been able to substantially reduce the rate of hypotony-related complications that range from 19% to 71.8%.[7,8,10,13,14]

We propose to study a novel method that has been shown through a preliminary study to provide good IOP control during the early post-op period, and avoid hypotony-related post-op complications. This method involves the preoperative placement of a degradable insert of appropriate diameter and length in the tubing of a BGI to provide sufficient resistance to AH outflow in the early post-op period.[15,16] ***The overall hypothesis is that the ideal insert design would provide sufficient initial post-op AH outflow resistance, providing stable immediate post-op IOP control without the need for intra-op modifications.*** Our team has developed two precision micro-flow-pressure-measuring setups that will enable the efficient and accurate

undertaking of the following aims.

1. Develop a mathematical model, utilizing computational fluid dynamics (CFD), to predict the pressure effects of placing an insert in a BGI tube. *Hypothesis:* The major design parameters that will affect the pressure in the tube are the insert's outer diameter, length, and surface roughness.
2. Validate the mathematically predicted versus experimentally measured pressure modulations caused by annular flow when an insert is placed in a BGI-like tube. Provide experimental pressure data through BGI-like tubes containing inserts to check and validate the mathematical model. *Hypothesis:* The pressure variations caused by annular flow when an insert is placed in a BGI-like tube will match the mathematical model predictions.
3. Obtain preliminary data on the effects of placing a degradable insert in a BGI tube and make initial modifications of the mathematical model to account for these effects. Experimentally measure the pressure and flow rate resulting from a degradable suture being placed in BGI tubing. Compare the measured pressures with those of the mathematical model and systematically explore relevant modifications that could allow improved predictions. *Hypothesis:* The experimental pressures will first increase as the insert swells [to some degree], then will decrease as the insert degrades, finally returning to the baseline pressure of the hollow tube after the insert has completely disappeared. The original mathematical model's predictions may not match this type of variation perfectly, but can be carefully modified to behave similarly to the experimental results for a specific type of degradable suture.

With the success of these aims, this research will provide the framework for the design and development of the ideal insert which, when placed in a BGI tube, would provide immediate post-op IOP control. Therefore, the need for surgeon-dependent intra-op BGI modification techniques

will be substantially reduced. This research is in line with the National Eye Institute's (NEI) vision strategy in preventing and treating glaucoma and in line with the National Institute of Biomedical Imaging and Bioengineering's (NIBIB) mission to improve health through the development of biomedical technologies.

## II. Research Strategy

### *A. Significance*

Glaucoma is one of the leading causes of irreversible blindness in the world.[17] Studies have shown that the projected number of glaucoma patients worldwide will reach 111.8 million by 2040.[18] Among the common treatments for glaucoma, glaucoma drainage devices are becoming more popular as compared to medication and trabeculectomy or laser trabeculoplasty.[19,20] A glaucoma drainage device is fundamentally made of a silicone tube connected to a silicone plate that is sutured on the eye. The silicone tube shunts AH out of the eye to lower IOP levels. Figure H.1 shows a valved (AGV) and non-valved (BGI) glaucoma drainage device. Studies such as the Tube vs. Trabeculectomy (TVT) study[21] and the study on cost-effectiveness of BGIs versus medication and trabeculectomy[19] have demonstrated the superiority of glaucoma drainage devices over the other two commonly used treatments. This is due to its greater long-term success of reducing IOP levels compared to the other treatment methods, as well as its greater overall cost-effectiveness despite costing up to $3904 more than medical treatment and $2203 more than trabeculectomy.[19]

Despite their lower failure rates, BGI drainage devices have the issue of providing little to no flow resistance when shunting AH out of the eye in the early post-op stage, before scar tissue forms on the BGI's end plate. Only approximately four to six weeks after surgery will fibrous scar

tissue form over the BGI plate to create sufficient AH flow resistance, providing "natural" IOP control. During the immediate post-op period when flow resistance is low, the IOP falls below nominal ranges, causing hypotony-related complications such as choroidal detachment, choroidal hemorrhage, and flat anterior chamber, which can also lead to blindness.[22] It is therefore, vital to ensure IOP control in the early post-op stages after glaucoma drainage surgery.

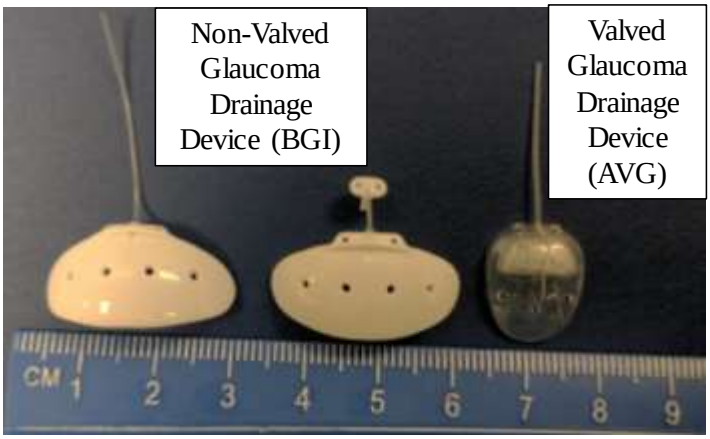


Fig. H.1: Example of non-valved and valved glaucoma drainage devices

In efforts to solve this issue, valved glaucoma drainage devices were developed, the most popular being the AGV, which is essentially a glaucoma drainage device with a butterfly valve attached to the end plate of the tube shunt. The design of this AGV provides the AH flow resistance that the BGI fails to provide in the early post-op stages. Despite this advantage that the AGV has over the BGI, the AGV has been reported to fail to reduce patient IOP levels more often than the BGI.[5,23] A five-year study by Christakis *et al.* comparing the performance of the BGI and the AGV reported that BGIs provided better IOP control, despite causing more-hypotony related post-op complications than AGVs.[6] This failure of AVGs to reduce long-term IOP levels is often due to the device's inability to reduce flow resistance as resistance created by scar tissue growth takes over. The combination of both the flow resistance created by the valve and that created by scar tissue growth causes excessive flow resistance, leading to an increased IOP. For this reason, BGIs

are still very popular among ophthalmologists.

Since BGIs provide better and more long-term IOP control overall, intra-op BGI modifications have been developed in attempts to overcome its early post-op hypotony issues. These techniques include a two-stage surgical method,[7] tube occlusion with a non-absorbable stent suture that is often removed after about four weeks,[8,9] injection of viscoelatic solution into the anterior chamber of the eye,[10] and external ligation of the tube with an absorbable suture followed by tube fenestrations.[2,11,12] The technique that is more commonly used is the external tube ligation with an absorbable suture followed by tube fenestrations. This technique provides relatively adequate IOP control and does not require a second surgery. However, it does not provide immediate or consistent IOP control, nor does it eliminate the occurrence of hypotony.

A study by Emerick *et al.* evaluating the efficacy of this technique of tube ligation followed by tube fenestrations reported that IOP levels only reduced below 20 mm Hg at the end of one week after surgery, and increased the third and fourth weeks after surgery before decreasing again the fifth week.[13] Approximately 6% of the subjects experienced hypotony and 25% of the subjects experienced ocular hypertension (IOP greater than 30 mm Hg) one day after surgery.[13] *In vivo* trials evaluating other intra-op methods also report the occurrence of hypotony-related complications in up to 71.8% of glaucoma patients with BGI implants.[7-10] These show that the standard intra-op modification technique and other intra-op methods that are currently used cannot provide consistent immediate IOP control and eliminate early post-op hypotony complications.

Several *in vitro* studies have investigated the effectiveness of intra-op modifications made to BGIs; however, none have reported pressure-data that last longer than 15 minutes.[2,11,12,24] To our knowledge, there has not been a study that investigates tube pressure modulations caused by these BGI modifications over the clinically relevant period of 4-6 weeks. There is therefore, a lack of

pressure control understanding during this immediate post-op stage, when it is vital to prevent hypotony complications.

***B. Innovation***

We propose to systematically study an improved BGI design with a degradable insert placed into the BGI prior to implantation that will provide temporary resistance in the early post-op stages (Fig. H.2). We hypothesize that this degradable insert, when designed appropriately with the design parameters predicted using the mathematical model, will provide the proper temporary AH flow resistance through the BGI tube.

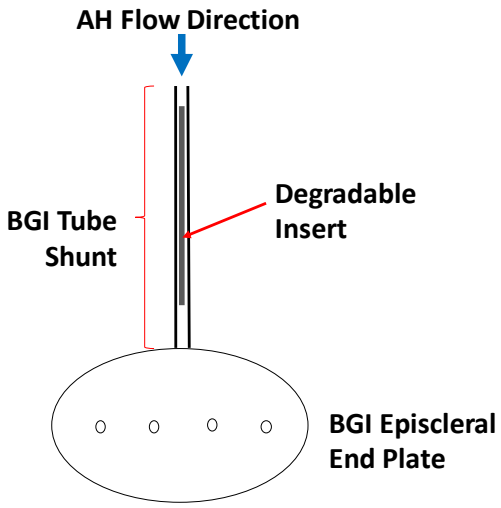


Fig. H.2: Configuration of degradable insert in BGI tube

As the insert degrades, reducing in size, the tube flow resistance would decrease in time. As this resistance decreases, scar tissue would form over the BGI plate, creating "natural" resistance. Unlike current intra-op modifications, this pre-designed insert would be placed inside the BGI tube prior to surgery, and reduce the need for intra-op interventions.

A preliminary study has demonstrated that this degradable insert technique can provide the desired IOP control during the immediate post-op period and decreases the occurrence of

hypotony-related complications, unlike current intra-op modifications.[25] In this preliminary study with 20 glaucoma patients, a degradable monofilament suture (poliglecaprone-25) was placed in the BGI tubing lumen and implanted in the eye. The study reported lowered IOP levels within the desired range one day after surgery and maintenance of good IOP control after 11 months with zero occurrence of hypotony-related complications.[25] With the ability to provide consistent immediate post-op IOP control, this proposed method would yield reduced occurrence of hypotony-related complications.

Our research will also provide an in-depth understanding of how this proposed technique affects flow and pressure in the BGI tube throughout the clinically relevant period of 4-6 weeks. The *in vitro* pressure-flow-measurement setup that we have developed is capable of measuring micro-flow and pressures for at least 10-days [projected to handle 30 days], which is longer than any data reported by prior *in vitro* studies that investigated the efficacy of intra-op modifications.[2,11,12,24] Additionally, our research will be able to monitor the degradation process of the BGI tube insert and determine the effects of this process on the resulting intraluminal pressure-flow relationship. This can be achieved with the availability of an on-site micro-CT that we will utilize to take accurate 3-D imaging measurements of the insert inside the tube at different time intervals, without destroying the insert.

With the success of these proposed aims, we will be able to provide a strong mathematical model that gives the necessary design parameters for the design of degradable inserts in these applications. After demonstrating *in vitro* that this proposed method provides the necessary fluid resistance for the clinically relevant period, we propose future comparisons of this method with current intraoperative modification techniques. This future research would require a thorough *in vivo* study because current intraoperative methods are highly dependent on scar tissue growth.

With this future study in mind, a successful *in vitro* study and properly designed insert must be accomplished in order to justify the next step of performing an *in vivo* study.

***C. Approach***

Specific Aims 1 and 2 will be completed in parallel. The mathematical model developed in Specific Aim 1 will be validated with experimental testing done in Specific Aim 2. The two main variables that we will be examining are insert diameter and length. In Specific Aim 3, we will investigate the pressure-flow effects of placing a commercially available degradable suture in a BGI tube. The timeline for these aims is shown in Table H.1.

Table H.1: Timeline

| | Year 1 | | | | Year 2 | | | |
|---|---|---|---|---|---|---|---|---|
| Task | Q1 | Q2 | Q3 | Q4 | Q1 | Q2 | Q3 | Q4 |
| Specific Aim 1 | | | | | | | | |
| Specific Aim 2 | | | | | | | | |
| Specific Aim 3 | | | | | | | | |

Specific Aim 1. Develop a mathematical model, utilizing computational fluid dynamics (CFD), to predict the pressure effects of placing an insert in a BGI tube

*Justification for Specific Aims 1 and 2*

The developed mathematical model will provide systematic insight into predicting the pressure and flow modulations when the insert's design parameters are changed. The experimental testing will allow us to check and validate the mathematical model's predictions. We will study the effects of the two most important design parameters for this insert; flow area [$(A_f = \pi(D_o^2 - D_i^2)/4)$ for cases considered herein; where $D_o$ = inner diameter of hollow tube and $D_i$ = outer diameter of insert] and insert length ($L$) on tube pressure ($\Delta P$). We have selected these variables because they are the most reasonable to manipulate in order to provide the target tube [and physiologic]

pressures when developing and designing future inserts. Based on the laminar flow Hagen-Poiseuille (H-P) relationship ($\Delta P = 128\mu LQ/\pi/D_{ef}^4$),[26] the other variables that largely affect tube pressure are flow rate ($Q$) and viscosity ($\mu$), which are influenced by human body conditions and not as reasonable to manipulate *in vivo*. Note that $D_{ef}^4 = [(D_o^4 - D_i^4) - (D_o^2 - D_i^2)^2/\ln(D_o/D_i)]$. We will use ANSYS FLUENT for CFD analysis. CFD analysis will provide a more accurate mathematical model [than H-P] for predicting the effects of an insert's outer diameter and length change on intraluminal pressure.

*1.1. Mathematical Framework, Assumptions and Conditions*

The hollow tube ($D_o$) and the insert ($D_i$) are considered to be the same length ($L$). The relative roughness of the walls will be set at 2.3%.[27] The fluid will be modeled as pure water, with constant viscosity and density at body temperature (37°C). Fluid flow will be considered to be a constant flow rate of 2.5 µl/min, which is approximately the average rate of AH production in the eye.[28]

*1.2. CFD Analysis and Post-Processing*

To investigate the effect of flow area ($A_f$) on tube pressure ($\Delta P$), CFD analysis will be done for a range of $A_f$ from ~5000 $\mu m^2$ to ~35000 $\mu m^2$. Tube $D_o$ will be kept constant at 300 µm, which is the approximate inner diameter of BGI tubing. The resulting $\Delta P$ calculated will be plotted against $A_f$, in order to explore the possibility of a straightforward relationship, like that of H-P.

*1.3. Feasibility, Expected Outcomes, Potential Problems, Alternative Strategies*

This specific aim is feasible given that we have the necessary computer equipment and the necessary FLUENT licenses already available at the University of Kansas. We expect that an increase in $D_i$ will cause the resulting tube pressure ($\Delta P$) to increase by around a power of four (see H-P equation above). We also anticipate that $\Delta P$ will increase as $L$ increases. $A_f$ has a larger

influence on $\Delta P$ compared to $L$. A plot of $\Delta P$, hydraulic Reynolds number ($Re_h$), and flow velocity ($V_f$) against $A_f$ should resemble that of Fig. H.3 which is produced based on the fundamental H-P equation.[26] In order to verify that the CFD analysis accurately matches the physical model, we will perform Specific Aims 1 and 2 in parallel.

Greater accuracy of the mathematical model is insured by cross-checking the predicted $\Delta P$ obtained from the mathematical model with the experimental $\Delta$P measured in Specific Aim 2. The mathematical model can be adjusted to account for significant discrepancies between the theoretical and experimental $\Delta$P. More details regarding factors that may affect $\Delta$P are provided in Section 2.6.

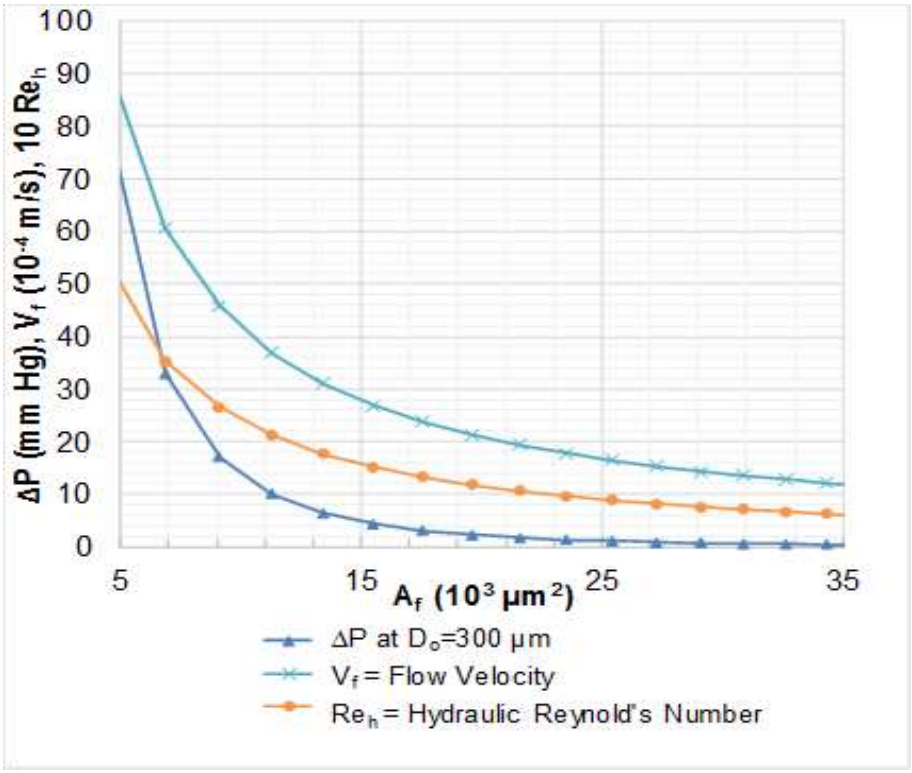


Fig. H.3: Plot of pressure, velocity and Reynolds number versus flow area for $D_o$ = 300 µm, $L$ = 8 mm, and $Q$ = 2.5 µl/min

Specific Aim 2. Validate the mathematically predicted versus experimentally measured pressure

modulations caused by annular flow when an insert is placed in a BGI-like tube

Two duplicate microflow pressure-measurement setups have been developed at the University of Kansas. With funds from this NIH grant, we plan to purchase a third setup in order to have the equipment needed to perform the proposed number of trials in a timely manner during this grant's timeframe. These setups can provide fluid flow rates between 0.5 - 50 µl/min and measure pressures between 0 - 130 mm Hg. Each setup consists of a precision pneumatic pump (CorSolutions, ±0.125 µl/min), a glass bottle as the fluid reservoir, microfluidic tubing and connections, a pressure transducer (Omega, ±0.2 mm Hg), a data logger (Omega), and a test section.[16,29] The test sample is located in a temperature-controlled incubator (± 2°F) (Fig. H.4).

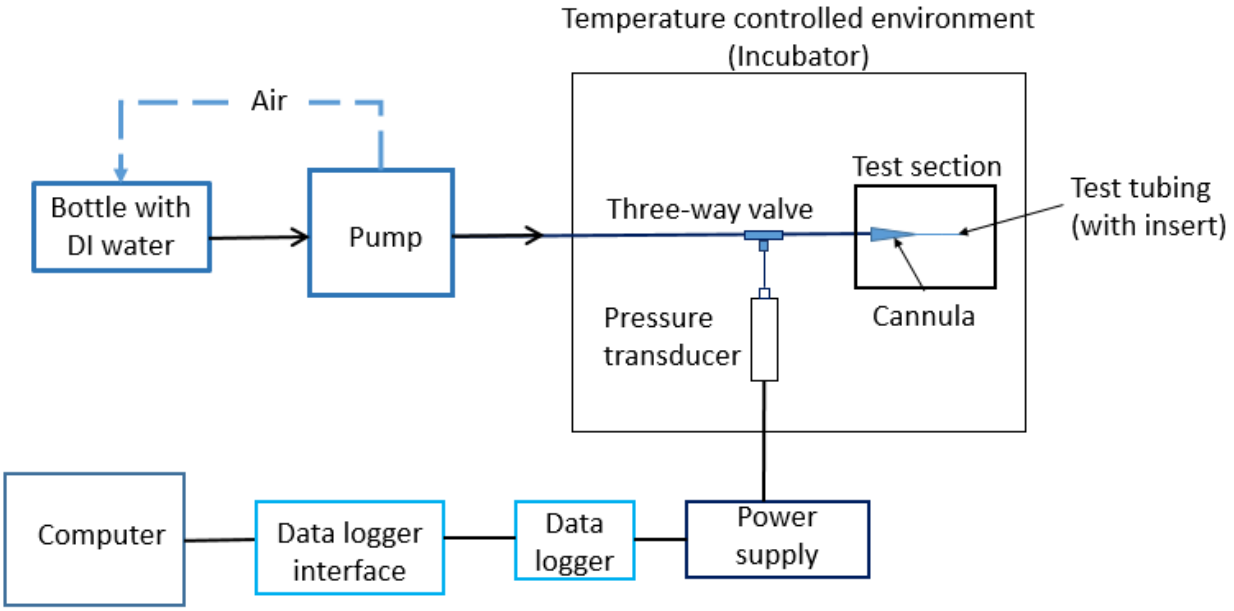


Fig. H.4: Microflow pressure-and-flow measurement setup configuration

*2.1. Experimental Setup Cleaning and Sterilization*

In order to remove impurities from the fluids and tubing, the system will be periodically cleaned and sterilized with a combination of bleach, isopropyl alcohol, DI water, and 0.04% sodium azide ($NaN_3$) solution; then flushed completely with DI water. The glass bottles will also

be sterilized and filled with balanced salt solution (BSS) (Alcon) containing 0.04% $NaN_3$ in order to prevent bacteria growth. BSS will be used because it has similar chemical composition and properties as the eye's AH.[30]

*2.2. Test Sample Preparation*

A power analysis with $\alpha$=0.05 and $\beta$=0.80 (1-sample, 2-sided equality test) based on the mean and standard deviation obtained from preliminary short-term microtube experimental trials indicated that we need a sample size of five for each combination of $A_f$ and $L$. This makes a total of 100 samples for tests to be performed as shown in Table H.2 (10 samples per annular configuration).

Table H.2: Diameter, length and flow area of annular tube combinations

| Stainless Steel Tube | | Nichrome Wire | | Flow Area, $A_f$ ($\mu m^2$) | Number of Trials per Insert ($L$) | |
|---|---|---|---|---|---|---|
| Gauge | $D_o$ (µm) | Gauge | $D_i$ (µm) | | 4 mm | 8 mm |
| 23G | 406 | 26G | 404 | 1336 | 5 | 5 |
| 30G | 152 | 36G | 127 | 5478 | 5 | 5 |
| 25G | 305 | 29G | 287 | 8369 | 5 | 5 |
| 27G | 229 | 32G | 203 | 8758 | 5 | 5 |
| 26G | 279 | 30G | 254 | 10465 | 5 | 5 |
| 24G | 381 | 27G | 361 | 11655 | 5 | 5 |
| 27G | 229 | 34G | 160 | 21076 | 5 | 5 |
| 25G | 305 | 30G | 254 | 22391 | 5 | 5 |
| 26G | 279 | 32G | 203 | 28707 | 5 | 5 |
| 24G | 381 | 28G | 320 | 33584 | 5 | 5 |

Note that Table H.2 information indicates that there may be pairs of combinations which are close enough to each other so as not to need both test combinations. However, Table H.2 diameters are nominal manufacturer's values;[31-33] and may not be actual diameters. For example, the 406/404 µm combination should not allow insert placement, if the diameters are completely accurate; but the nominal values may be "off" enough to allow wire insertion. In addition, Fig. H.3

indicates that the $A_f$ of the 381/320 μm combination may yield too low of a pressure, if the manufacturer's diameters are correct. So, some combinations will not be run, but the micro-CT scans will be able to differentiate sufficiently to make those decisions. We expect to have 7 combinations that are in an appropriate range.

A sample will consist of a hypodermic stainless-steel dispensing tip (Jensen Global, Inc.) containing a nichrome wire insert (Master of Clouds). The nichrome inserts will be inserted into the hypodermic tips after acquiring baseline pressure measurements for the tips alone. Average baseline pressure will be subtracted from the pressure data acquired after the nichrome insert is placed in the hypodermic tip.

*2.3. Experimental Flow Trials*

It is important that the tip of the test sample be submerged in a shallow collection trough filled with DI water in order to eliminate surface tension effects on the microtubular flow. The incubator of Fig. H.4 will be set to 37°C to simulate body conditions. After collecting baseline pressure data, the nichrome wire will be inserted and the pump will be set to 10 μl/min for ~15 minutes in order to remove any undetected air bubbles in the tube-insert combination. Then the pump will be set to the 2.5 μl/min flow rate and left for ~10 minutes for the pressure to stabilize after the change in flow rate. Pressure data will be logged for 5 hours at 0.1 Hz. The same experimental procedure will be repeated for all 10 trials of each of the ~7 annular combinations in Table H.2 finally used.

*2.4. Micro-CT Imaging and Measurements*

Because a one micron change in $D_o$ or $D_i$ can strongly affect the resulting tube pressure, it is important to obtain accurate measurements of these diameters (± 0.2 μm). We will be using a

Tomographic X-ray microscope, Xradia MicroXCT (Carl Zeiss X-ray Microscopy, CA) to take non-destructive micro-CT images of the samples (Fig. H.5) at ± 0.2 µm.

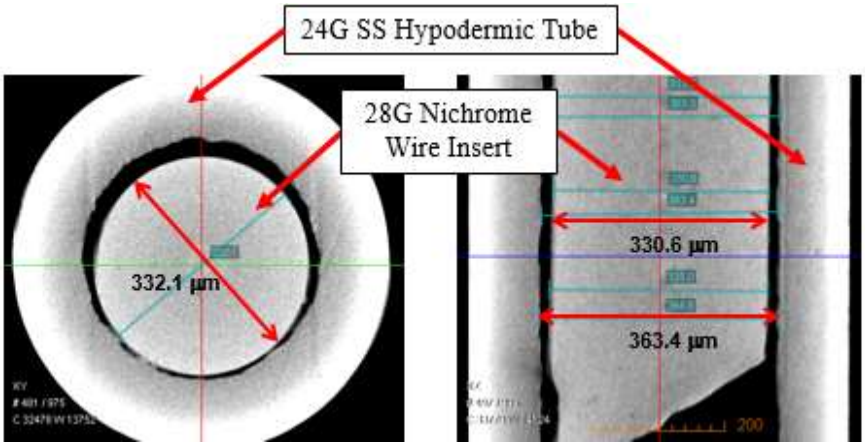


Fig. H.5: Example of a micro-CT image of a 24G stainless steel hypodermic tube containing a 28G nichrome wire insert

*2.5. Post-processing and Analysis*

The average pressure will be calculated, beginning at the point of pressure stabilization (deviation < ±2 mm Hg), and ending at the final collected data point. $D_o$ and $D_i$ of each sample will be measured from the micro-CT images and will be used in the mathematical model to calculate the theoretical pressure that is then compared to the experimental results.

*2.6. Feasibility, Expected Outcomes, Potential Problems, Alternative Strategies*

Our preliminary trials have demonstrated that we are capable of, and equipped to, successfully perform these tasks.[15,16,29,37] Again, accuracy is ensured by cross-checking the experimental data with the theoretically predictions in Specific Aim 1. We expect the experimental pressure data to correspond to the pressure-diameter and pressure-length relationships determined in Specific Aim 1. However, the experimental pressure data may be consistently higher than the mathematically predicted pressures. We expect that this discrepancy might occur, and be caused by factors such as surface roughness and electro-viscous effects.[34] These factors are not considered in conventional

fluid dynamics equations due to their negligible effects in flow through relatively larger tubes; but may be magnified in this situation because the tube flow area is significantly smaller [$A_f$ < 17671 μm$^2$, since ($D_o - D_i$) < 150 μm].[35,36] Another factor that can affect ΔP is non-concentricity of the insert within the tube. Alternatives: Should the CFD and experimental results not agree well enough, the CFD model's tube surface roughness and fluid viscosity can be adjusted as well as adjustments for non-concentricity. These potential adjustments should allow enough flexibility for the production of a theoretical model that can reasonably match experimental results, without violating the physics involved.

Specific Aim 3. Obtain preliminary data on the effects of placing a degradable insert in a BGI tube and make initial modifications of the mathematical model to account for these effects

*Justification for Specific Aim 3*

It is important to determine how pressure varies when a degradable insert is used. It is also important to investigate how actual BGI tubes behave (e.g., expansion due to increased pressure). For eventual use in humans, it is necessary that the inserts be carefully chosen to maintain IOP within the physiologic range. Since degradable sutures have quite a bit of diameter variability, and may swell, initial testing will help to select the best suture size(s). Aim 2's results will help in making these selections. Aim 3's preliminary data will provide solid indicators as to future research direction with degradable inserts in real BGI tubes. This Aim will also give strong indications as to the changes needed in the mathematical model so that it can replicate degrading insert results, and thus be used in the future to predict the effects of wider variation in these inserts than examined by experiment.

*3.1. Test Sample Preparation*

The degradable insert used will be a commercially available poliglecaprone-25

monofilament suture that is known as Monocryl (Ethicon Inc., Sommerville, NJ). These come in sizes of 2-0, 3-0, 4-0, and 5-0 (nominally 0.30 mm, 0.20 mm, 0.15 mm, and 0.10 mm diameters, respectively). With these diameters potentially varying ±0.05 mm,[38] some initial tests will be used to determine the best selection(s) for Aim 3. A power analysis with $\alpha$=0.05 and $\beta$=0.80 (1-sample, 2-sided equality test) based on the mean and standard deviation obtained from the long-term microtube preliminary experimental trial indicated that we need a sample size of five.[29] A 10 mm long BGI tube will be fitted on a 30G stainless steel hypodermic dispensing tip (Jensen Global, Inc.). Superglue will be used to securely fasten the BGI tube on the hypodermic tip. The insert (L) will be carefully placed in the BGI tube immediately after baseline $\Delta$P measurements in order to minimize exposure to moisture for a prolonged time period before the trial. One L of 8 mm will be investigated (ten samples).

*3.2. Experimental Flow Trial*

The experiment will be carried out using the three microflow pressure-measuring setups. Section 2.1's setup cleaning procedure will be carried out prior to experimental trials. Section 2.3's baseline pressure measurements and priming/initialization of the pump will be performed. Pressure data will be logged at 0.1 Hz, and retrieved daily to allow periodic inspection of results. For the first trial, logging will be stopped when pressure returns approximately to the baseline measurements. The total time ($t$) of this first trial will then be divided roughly equally among the following four trials ($t$ is expected to be 3 to 6 weeks, per manufacturer estimates of 25% strength in that period and complete degradation in 12 to 16 weeks[38,39,40,41]). Then, each of those trials will be stopped at $\tau/4$, $\tau/2$, $3\tau/4$ and $\tau$, respectively, in order to make micro-CT measurements and have insert sizes/shapes at each time interval. With this information, the measured and mathematical

model pressures will be compared. As with Aim 2, physically relevant mathematical model modifications will be investigated for improving the comparison.

*3.3. Micro-CT Imaging, Post-processing and Analysis*

Micro-CT images of the samples will be taken before and after each trial. A typical micro-CT scan for this specimen size takes approximately 7-8 hours. Micro-CT imaging is important in this specific aim because it will allow us to accurately measure the change in insert diameter without destroying or removing the insert from the tube. The degradation rate of the insert will be calculated as $\Delta V/\Delta\tau$ where V is the cylindrical insert's volume in $\mu m^3$ and $\tau$ is time in hours.

*3.4 Feasibility, Expected Outcomes, Potential Problems, Alternative Strategies*

These tasks are feasible given that we have access to an in-house Tomographic X-ray microscope. We expect the insert diameter to initially increase due to swelling (with accompanying $\Delta P$ increase), then decrease as the insert degrades. The decreasing diameter of the insert will cause decreasing $\Delta P$. It is expected that the mathematical model can be reasonably modified to match experimental tube $\Delta P$ variation; and needed modifications will be made to achieve this goal. Should the first trial's insert not behave as expected (i.e., $\Delta P$ not within the desired/expected physiologically relevant range), we will substitute a larger or smaller diameter suture and repeat the first trial before running the following trials. If needed, we will continue to modify the insert diameter until $\Delta P$ behaves as desired. If the BGI tubing causes issues with expansion or contraction, we will substitute the stainless steel metal tubing used in Aim 2 testing. Thus, these suture and tubing options should allow production of sufficient preliminary data to facilitate planning/direction for eventually performing future in vivo studies beyond this grant. In addition, if needed, suture diameter in the CFD model can be set to change as a function of time - - in order to produce improved model/experiment agreement.

## Preliminary Studies

### *Validation of Microflow Setup Using Hollow Microtubular Trials*[29, 37]

To validate the pressure and flow measurement capabilities of our current microflow setups, we performed experimental flow trials using hollow microtubes.[29] Five flow trials per setup were made using 35 mm long polyether-ether-ketone-sheathed fused silica (PEEKsil) microtubes with ~50 μm inner diameter.[29] The flow trial procedures of *Section 2.3* were followed. The five-trial average showed a repeatable ±0.02% difference in pressures ($\Delta P$) measured between the two setups (Table H.3).

Table H.3: Comparison of measured pressures in Setups 1 and 2 for 3-hr flow trials in 50 μm microtubes

| Trial Number | Experimental ΔP (mm Hg) | |
|---|---|---|
| | Setup 1 | Setup 2 |
| Average | 57.6 | 58.8 |
| Standard Deviation | 12.8 | 9.3 |

The large standard deviations in Table H.3 are due mainly to small changes in the 50 μm diameter tubes causing large (fourth power) effects on $\Delta P$, per H-P theory. We also performed three separate 10-day trials with 50 μm PEEKsil tubes and found that the maximum standard deviation of measured ΔP data was only 1.6 mm Hg. To our knowledge, there are not published comparable long-term (e.g., 5 to 30 days) studies.

### *Preliminary Annular Trials with Stainless Steel Tubes and Nichrome Inserts.*[29]

To verify the validity of the experimental setups in measuring $\Delta P$ and $Q$ through annular tubes with inserts, preliminary three-hour flow trials were performed using combinations of 23G, 24G and 30G SS hypodermic tubes, and 26G, 28G, 30G and 36G nichrome wire inserts.[29] The flow trial procedures were those of Section 2.3. Micro-CT scans were taken of the tube-insert

samples after each trial. Table H.4's summary of results shows that average measured steady-state $\Delta P$s were relatively close to the theoretical $\Delta P$s and within the theoretical range, accounting for variation in $L$, $Q$, $D_o$ and $D_i$.

Table H.4: Annular flow pressure results

| Sample | $A_f$ (μm$^2$) | $\Delta P$ (mm Hg) | | |
|---|---|---|---|---|
| | | Theory (Range) | Experiment | Difference |
| 30-36G | 6706 | 19.9 (10.2 to 39.5) | 15 | 33% |
| 24-28G | 15217 | 8.9 (4.2 - 19.2) | 9.6 | -7% |
| 23-26G | 17199 | 9.3 (6.3 - 20.3) | 8.8 | 6% |
| 24-30G | 42007 | 0.34 (0.21 - 0.54) | 0.24 | 41% |
| 23-28G | 61472 | 0.17 (0.11 - 0.31) | 0.37 | -54% |

Larger variation from theory was seen with higher $A_f$ because the pressures were low and more susceptible to measurement error (Omega pressure transducer, ±0.2 mm Hg). At small $A_f$, more variability in theory predictions were observed due to diameter measurement variability (XRadian MicroXCT, ± 0.2 μm).

***Preliminary Study: Modified Surgical Technique of Placing a Degradable Suture in BGI Tubes[25]***

A preliminary study was performed with 20 glaucoma patients.[25] These 20 glaucoma patients underwent a modified procedure involving the insertion of an 8 mm PGC suture into the BGI tube during surgery. At least one month of post-surgical follow-up was carried out.[25] The mean IOP before surgery was 37.1 mm Hg.[25] After surgery the mean IOP fell to 13.9 mm Hg at a day after surgery, 15.7 mm Hg at one week after surgery, and 17.0 mm Hg at the last follow-up (average = 149 days; range: 1 - 11 months).[25] There were zero occurrences of hypotony-related complications and only one patient required a return to surgery for a tube revision.[25]

**REFERENCE**


1. Vajaranant TS, Wu S, Torres M, Varma R. The Changing Face of Primary Open-Angle Glaucoma in the United States: Demographic and Geographic Changes from 2011 to 2050. *Am J Ophthalmol*. 2012;154(2):303-314.

2. Gilbert DD, Bond B. Intraluminal Pressure Response in Baerveldt Tube Shunts: A Comparison of Modification Techniques. *J Glaucoma*. 2007;16(1):62-67.

3. Arora KS, Robin AL, Corcoran KJ, Corcoran SL, Ramulu PY. Use of Various Glaucoma Surgeries and Procedures in Medicare Beneficiaries from 1994 to 2012. *Ophthalmology*. 2015;122(8):1615-1624.

4. Young M. Laser Trabeculoplasty Is Back in Force. *Eye World*. Eye World News Services. March 2012. [Accessed on June 4, 2017]. Available from: https://www.eyeworld.org/article-laser-trabeculoplasty-is-back-in-.

5. Christakis PG, Tsai JC, Kalenak JW, Zurakowski D, Cantor LB, Kammer JA, Ahmed IIK. The Ahmed Versus Baerveldt Study: Three-Year Treatment Outcomes. *Ophthalmology*. 2013;120(11):2232-2240.

6. Christakis PG, Zhang D, Budenz DL, Barton K, Tsai JC, Ahmed IIK. Five Year Pooled Data Analysis of the Ahmed Baerveldt Comparison Study and the Ahmed Versus Baerveldt Study. *Am J Ophthalmol*. 2017;176:118-126.

7. Tong L, Frazao K, LaBree L, Varma R. Intraocular Pressure Control and Complications with Two-Stage Insertion of the Baerveldt Implant. *Ophthalmology*. 2003;110(2):353-358.

8. Kansal S, Moster MR, Kim D, Schmidt CM, Jr., Wilson RP, Katz LJ. Effectiveness of Nonocclusive Ligature and Fenestration Used in Baerveldt Aqueous Shunts for Early Postoperative Intraocular Pressure Control. *J Glaucoma*. 2002;11(1):65-70.

9. Sherwood MB, Smith MF. Prevention of Early Hypotony Associated with Molteno Implants by a New Occluding Stent Technique. *Ophthalmology*. 1993;100(1):85-90.

10. Marchini G, Ceruti P, Vizzari G, Toscani M, Amantea C, Tosi R, Marchetti P. Long-Term Outcomes of a Modified Technique Using the Baerveldt Glaucoma Implant for the Treatment of Refractory Glaucoma. *J Glaucoma*. 2016;25(12):952-958.

11. Breckenridge RR, Bartholomew LR, Crosson CE, Kent AR. Outflow Resistance of the Baerveldt Glaucoma Drainage Implant and Modifications for Early Postoperative Intraocular Pressure Control. *J Glaucoma*. 2004(13):396-399.

12. Brooks SE, Davey MP, Lee MB, Baerveldt G. Modifications of the Glaucoma Drainage Implant to Prevent Early Postoperative Hypertension and Hypotony - a Laboratory Study. *Ophthalmic Surg*. 1994;25(5):311-316.

13. Emerick GT, Gedde SJ, Budenz DL. Tube Fenestrations in Baerveldt Glaucoma Implant Surgery: 1-Year Results Compared with Standard Implant Surgery. *J Glaucoma*.11(4):340-346.

14. Trible JR, Brown DB. Occlusive Ligature and Standardized Fenestration of a Baerveldt Tube with and without Antimetabolites for Early Postoperative Intraocular Pressure Control. *Ophthalmology*. 1998;105(12):2243-2250.

15. Munden PM, Ramani A, Kieweg SL, Dougherty RL, Boyce M. An Experimental Model of Pressure Modulation in Baerveldt Implants to Reduce Post-Operative Hypotony. The Association for Research in Vision & Ophthalmology (ARVO) Annual Meeting; May 3-7, 2015; Denver, CO.

16. Ramani A. Reliable Experimental Setup to Test the Pressure Modulation of Baerveldt Implant Tubes for Reducing Post-Operative Hypotony [Master of Science Thesis]: University of Kansas; 2015.

17. Susanna RJ, De Moraes CG, Cioffi GA, Ritch R. Why Do People (Still) Go Blind from Glaucoma? *Transl Vis Sci Technol*. 2015;4(2):1.

18. Tham YC, Li X, Wong TY, Quigley HA, Aung T, Cheng CY. Global Prevalence of Glaucoma and Projections of Glaucoma Burden through 2040: A Systematic Review and Meta-Analysis. *Ophthalmology*. 2014;121(11):2081-2090.

19. Kaplan RI, De Moraes CG, Cioffi GA, Al-Aswad LA, Blumberg DM. Comparative Cost-Effectiveness of the Baerveldt Implant, Trabeculectomy with Mitomycin, and Medical Treatment. *JAMA Ophthalmol*. 2015;133(5):560-567.

20. Ramulu PY, Corcoran KJ, Corcoran SL, Robin AL. Utilization of Various Glaucoma Surgeries and Procedures in Medicare Beneficiaries from 1995 to 2004. *Ophthalmology*. 2007;114(12):2265-2270.

21. Gedde SJ, Schiffman JC, Feuer WJ, Herndon LW, Brandt JD, Budenz DL. Treatment Outcomes in the Tube Versus Trabeculectomy (Tvt) Study after Five Years of Follow-Up. *Am J Ophthalmol*. 2012;153(5):789-803.

22. Bailey AK, Sarkisian SR, Jr. Complications of Tube Implants and Their Management. *Curr Opin Ophthalmol*. 2014;25(2):148-153.

23. Christakis PG, Kalenak JW, Zurakowski D, Tsai JC, Kammer JA, Harasymowycz PJ, Ahmed, II. The Ahmed Versus Baerveldt Study: One-Year Treatment Outcomes. *Ophthalmology*. 2011;118(11):2180-2189.

24. Porter JM, Krawczyk CH, Carey RF. In Vitro Flow Testing of Glaucoma Drainage Devices. *Ophthalmology*. 1997;104(10):1701-1707.

25. Munden PM, Boyce M. A Retrospective Review of Baerveldt Implants with Tubing Insert Modification to Reduce Post-Operative Hypotony. The Association for Research in Vision and Ophthalmology (ARVO) Annual Meeting; May 1-5, 2016; Seattle, WA.

26. Munson BR, Young DF, Okiishi TH, Huebsch WW. Fundamentals of Fluid Mechanics. Sixth ed. NJ: *John Wiley and Sons*; 2009.

27. Tang GH, Li Z, He YL, Zhao CY, Tao WQ. Experimental Observations and Lattice Boltzmann Method Study of the Electroviscous Effect for Liquid Flow in Microchannels. *J Micromech Microeng*. 2007;17:539-550.

28. Goel M, Picciani RG, Lee RK, Bhattacharya SK. Aqueous Humor Dynamics: A Review. *Open Ophthalmol J*. 2010;4:52-59.

29. Teo THT, Ramani A, Munden PM, Wilson SE, Kieweg SL, Dougherty RL. Validation of an Experimental Setup to Reliably Simulate Flow through Non-Valved Glaucoma Drainage Devices. *J Med Device*. [Under review].

30. Ross A, Blake RC, Ayyala RS. Surface Tension of Aqueous Humor. *J Glaucoma*. 2010;19(7):456-459.

31. Flumatic Liquid Control Equipment Co.,Limited; "Tip Syringes and Accessory," accessed June 2017; www.flumatic.com

32. Fisnar, "Stainless Steel Dispensing Tips," accessed June 2017; http://www.fisnar.com/products/dispensing-tips/stainless-steel-dispensing-tips

33. Jacobs Online, "Nichrome 60 Wire," accessed June 2017; http://jacobs-online.biz/nichrome_wire.htm

34. Jiang RJ, Song FQ, Li HM. Flow Characteristics of Deionized Water in Microtubes. *China Physics Letter*. 2006;23(12):3305-3308.

35. Xu SL, Yue XA, Hou JR. Experimental Investigation on Flow Characteristics of Deionized Water in Microtubes. *Chinese Sci Bull*. 2007;52(6):849-854.

36. Mala GM, Li DQ. Flow Characteristics of Water in Microtubes. *Int J Heat Fluid Fl*. 1999;20(2):142-148.

37. Teo THT, Wilson SE, Munden PM, Dougherty RL. Validation of Experimental Setup to Simulate and Model Non-Valved Glaucoma Drainage Devices. 2017 Summer Biomechanics, Bioengineering and Biotransport Conference (SB3C2017), 2017; Tucson, AZ.

38. Ethicon, "Monocryl (Poligelcaproe 25) Monofilament Suture", accessed June 2017, www.ethicon.com/healthcare-professionals/products/wound-closure/absorbable-sutures/monocryl-poliglecaprone-25#!description-and-specs

39. Surgical Suture Guide; accessed June 2017; http://www.surgical-instrument-pictures.com/suture.html

40. Absorbable Suture Chart; accessed June 2017; http://academicdepartments.musc.edu/surgery/education/resident_info/supplement/suture_manuals/absorbable_suture_chart.pdf

41. Serag Wiessner, "Suture Materials: Techniques and Knots", accessed June 2017; http://fmdental.pl/uploads/20110107131642.pdf